

DTIC FILE COPY

HSD-TR-90-021



AD-A225 029

EVALUATION OF POTENTIAL DAMAGE TO UNCONVENTIONAL STRUCTURES BY SONIC BOOMS

**Louis C. Sutherland
Ron Brown
Dawn Goerner**

**Wyle Laboratories
128 Maryland Street
El Segundo, CA 90245**

**DTIC
ELECTE
AUG 07 1990**
S D

April 1990

Final Report for Period November 1988 - January 1990

Approved for public release; distribution is unlimited.

**Noise and Sonic Boom Impact Technology
Human Systems
Human Systems Division
Air Force Systems Command
Brooks Air Force Base, Texas 78235-5000**

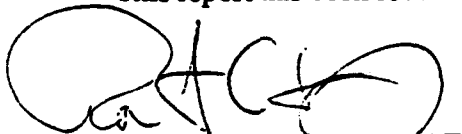
90 08 06 044

NOTICE

When Government drawings, specifications, or other data are used for any purpose other than in connection with a definitely Government-related procurement, the United States Government incurs no responsibility nor any obligation whatsoever. The fact that the Government may have formulated or in any way supplied the said drawings, specifications, or other data, is not to be regarded by implication, or otherwise as in any manner construed, as licensing the holder, or any other person or corporation; or conveying any rights or permission to manufacture, use, or sell any patented invention that may in any way be related thereto.

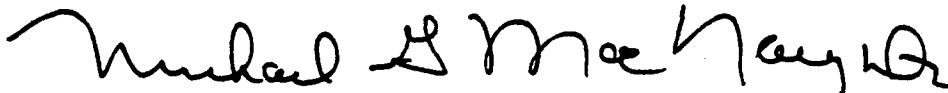
This report has been reviewed and it is releasable to the National Technical Information Service (NTIS), where it will be available to the general public, including foreign nationals.

This report has been reviewed and is approved for publication.



ROBERT C. KULL, Capt., USAF
NSBIT Program Manager

FOR THE COMMANDER



MICHAEL G. MACNAUGHTON, Col, USAF, BSC
Program Director
Human Systems

Please do not request copies of this report from the Human Systems Division. Copies may be obtained from DTIC. Address your request for additional copies to:

Defense Technical Information Center
Cameron Station
Alexandria VA 22304-6145

If your address has changed, if you wish to be removed from our mailing list, or if your organization no longer employs the addressee, please notify HSD/XART, Brooks AFB TX 78235-5000 to help us maintain a current mailing list.

Copies of this report should not be returned unless return is required by security considerations, contractual obligations, or notice on a specific document.

REPORT DOCUMENTATION PAGE

Form Approved
OPM No. 0704-0188

Public reporting burden for this collection of information is estimated to average 1 hour per response, including the time for reviewing instructions, searching existing data sources, gathering and maintaining the data needed, and reviewing the collection of information. Send comments regarding this burden estimate or any other aspect of this collection of information, including suggestions for reducing this burden, to Washington Headquarters Services, Directorate for Information Operations and Reports, 1215 Jefferson Davis Highway, Suite 1204, Arlington, VA 22202-4302, and to the Office of Information and Regulatory Affairs, Office of Management and Budget, Washington, DC 20503.

1. AGENCY USE ONLY (Leave Blank)		2. REPORT DATE May 1990		3. REPORT TYPE AND DATES COVERED Final Report (11/88 to 1/90)	
4. TITLE AND SUBTITLE Evaluation of Potential Damage to Unconventional Structures by Sonic Booms				5. FUNDING NUMBERS Procurement Instrument ID No.: F08635-89-C-0044 Program Element No.: 63723F Project No.: 3037 Task No.: 05 Work Unit Accession No.: 01	
6. AUTHOR(S) Sutherland, Louis C.; Brown, Ron; Goerner, Dawn					
7. PERFORMING ORGANIZATION NAME(S) AND ADDRESS(ES) Wyle Laboratories 128 Maryland St. El Segundo, California 90245				8. PERFORMING ORGANIZATION REPORT NUMBER WR 89-14	
9. SPONSORING/MONITORING AGENCY NAME(S) AND ADDRESS(ES) Human Systems Division, Noise & Sonic Boom Impact Technology (NSBIT) Program OL-AC HSD/YA-NSBIT Wright-Patterson AFB, OH 45433-6573				10. SPONSORING/MONITORING AGENCY REPORT NUMBER	
11. SUPPLEMENTARY NOTES					
12a. DISTRIBUTION/AVAILABILITY STATEMENT Approved for public release; distribution unlimited				12b. DISTRIBUTION CODE	
13. ABSTRACT (Maximum 200 words) Supersonic operations of U.S. Air Force aircraft cause sonic booms which may be the source of damage to unconventional structures. This problem is addressed in this report by (1) a literature survey of damage prediction and damage assessment techniques for such structures; (2) development of a statistical model for sonic boom overpressures with emphasis on supersonic operating areas (SOAs) employed for air combat maneuver training; (3) development of an analytical model to predict the probability of damage; (4) execution of a limited experimental program at White Sands Missile Range to evaluate response and potential damage of two unconventional structures in support of the prediction model; and finally (5) definition of algorithms for use in the Air Force ASAN computer program for evaluation of the probability of damage to unconventional structures from sonic booms.					
14. SUBJECT TERMS Sonic Booms, Analytical Model, Damage Assessment, Unconventional Structures, Archaeology, Historic Buildings, Adobe, Indian Dwellings, Noise Assessment, Prediction Model, National Monuments				15. NUMBER OF PAGES 273	
				16. PRICE CODE	
17. SECURITY CLASSIFICATION OF REPORT Unclassified	18. SECURITY CLASSIFICATION OF THIS PAGE Unclassified	19. SECURITY CLASSIFICATION OF ABSTRACT Unclassified	20. LIMITATION OF ABSTRACT Unlimited		

TABLE OF CONTENTS

	Page
1.0 INTRODUCTION.....	1-1
2.0 UNCONVENTIONAL STRUCTURES.....	2-1
2.1 Selection of Unconventional Structures.....	2-1
2.2 Basis for Prediction of Damage to Unconventional Structures from Sonic Booms	2-6
2.2.1 Framework for an Excitation-Response-Damage Prediction Model	2-8
2.2.2 Framework for Statistical Models for Excitation-Response- Damage Prediction	2-8
2.2.3 Details of Statistical Model for Damage Assessment.....	2-9
2.3 Field Inspection Techniques to Assess Potential Damage to Unconventional Structures.....	2-12
2.3.1 Field Techniques Selected.....	2-15
2.3.2 Summary of Sonic Boom and Blast Damage Inspection Techniques from Previous Studies.....	2-16
3.0 SONIC BOOM ENVIRONMENT	3-1
3.1 Sonic Boom Environment for ACM Activity	3-2
3.1.1 WSMR Test Data.....	3-3
3.1.2 Spatial Variation of Peak Pressure from WSMR Data.....	3-10
3.1.3 Model for Statistical Variation of Sonic Boom Peak Pressures in WSMR SOA.....	3-15
3.1.4 Possible Variations in ACM Model for Other SOAs.....	3-21
3.2 Sonic Boom Pressures for Other Types of Supersonic Flight Activity	3-22
3.2.1 Sonic Boom Environments Under Level Flight Supersonic Corridors at Varying Altitudes.....	3-24
3.2.2 Sonic Booms for Flight at Low Altitude Not Restricted to Steady Flight.....	3-29
3.3. Correction from Free Field to Effective Pressure on Structure	3-31
3.3.1 Correction Due to Angle of Incidence of Sonic Boom Wave	3-31
3.3.2 Effective Acoustic Pressure on Various Types of Structure	3-31
3.4 Time Histories and Frequency Spectra for Sonic Booms	3-33
3.4.1 Time Histories of Sonic Booms.....	3-33
3.4.2 Frequency Spectra of Sonic Booms	3-35
4.0 MODELS FOR STRUCTURAL RESPONSE AND DAMAGE FROM SONIC BOOM.....	4-1
4.1 Vibration Response of Single Degree of Freedom Systems to Sonic Boom	4-1
4.1.1 Correction for Multi-Modal Response.....	4-10
4.1.2 Vibration Response of Non-Structural (Terrain) Elements.....	4-10
4.1.3 Vibration Response of Radio Telescopes to Sonic Boom.....	4-11
4.2 Stress Response to Vibration Induced by Sonic Booms	4-12
4.2.1 Stress Response of Building Elements	4-13
4.2.2 Response of Non-Structural Elements.....	4-16

TABLE OF CONTENTS - Continued

	Page
4.3 Experiment-Based (Empirical) Models for Response to Sonic Boom	4-18
4.3.1 Experimental Data on Structural Response to Noise	4-18
4.3.2 Experimental Data on Seismic/Structural Response to Noise	4-23
4.4 Damage Threshold Stress Criteria for Unconventional Structures	4-28
4.4.1 Fatigue Considerations in Damage Assessments	4-28
4.4.2 Material Strength Data Applicable to Damage Prediction	4-29
4.4.3 Material Strength Estimates for Wood Frame Buildings	4-38
4.4.4 Material Strength Estimates for Metal Frame Buildings	4-45
4.4.5 Estimated Damage Stresses for Seismically Sensitive Structures	4-46
4.4.6 Avalanche Sites and Landslide Areas	4-47
4.4.7 Summary, Damage Stress Criteria	4-54
 5.0 EXPERIMENTAL EVALUATION OF DYNAMIC RESPONSE OF UNCONVENTIONAL STRUCTURES	 5-1
5.1 Structure Description	5-1
5.1.1 Structure A Description	5-3
5.1.2 Structure B Description	5-3
5.2 Structural Response and Acoustic Measurement Systems	5-3
5.2.1 Acoustic and Structural Vibration Measurement Instrumentation ...	5-7
5.2.2 System Operation	5-12
5.2.3 Transducer Mounting	5-12
5.2.4 Mechanical Impedance Measurements	5-16
5.2.5 Structural Response Measurements	5-18
5.3 Test Results	5-24
5.3.1 Photographic Examination	5-24
5.3.2 Mechanical Impedance Measurements	5-27
5.3.3 Structural Response Tests	5-36
5.4 Evaluation of Test Results	5-41
5.5 Recommendations for Future Photographic Documentation	5-46
 6.0 STRUCTURAL DAMAGE ASSESSMENT FOR UNCONVENTIONAL STRUCTURES	 6-1
6.1 Step 1 - Selection of Structures	6-1
6.2 Step 2 - Definition of Free Field Sonic Boom Pressures	6-1
6.2.1 Air Combat Maneuver (ACM) Training	6-2
6.2.2 Other Supersonic Flight Activity	6-3
6.3 Step 3 - Definition of Effective Sonic Boom Pressures	6-4
6.4 Step 4 - Define Peak Stress Response	6-6
6.5 Step 5 - Computation of Probability of Damage for One Sonic Boom	6-8
6.6 Step 6 - Computation of Weighted Probability of Damage According to Estimated Frequency of Booms	6-10
6.6.1 Weighted Probability of Damage for SOA Used for ACM Training	6-10
6.6.2 Sensitivity Analysis	6-14
6.6.3 Damage Estimates for Other Types of Supersonic Activity	6-16

TABLE OF CONTENTS - Continued

	Page
6.7 Step 7 - Calculation of a Global Measure of Damage Potential	6-16
6.8 Summary	6-18
REFERENCES	R-1
APPENDIX A Bibliography for Response of Unconventional Structures to Sonic Boom	A-1
APPENDIX B Metric Conversion Tables and Physical Properties of Various Basic Building Construction Materials	B-1
APPENDIX C Analytical Background	C-1
C.1 Relationship Between Various Spectral Measures of Sonic Booms	C-2
C.2 Multimodal Response of Simply Supported Panel to Normally Incident Sonic Boom	C-6
APPENDIX D Photographs of Structure A Walls Before and After Tests	D-1
APPENDIX E Time Histories of Sonic Boom Pressure and Structural Response of Structures A and B	E-1
APPENDIX F Compilation of Weather Data from White Sands Missile Range for the Period of February 20, 1989 to April 12, 1989	F-1



Accession For	
NTIS GRA&I	<input checked="" type="checkbox"/>
DTIC TAB	<input type="checkbox"/>
Unannounced	<input type="checkbox"/>
Justification	
By	
Distribution /	
Availability Codes	
Dist	Avail and/or Special
A-1	

LIST OF TABLES

Table	Page
2-1 Relative Frequency of Public Comments in Draft EIS's About Potential Damage to Unconventional Structures from Sonic Boom	2-2
2-2 Location and Type of Buildings Considered as Candidate "Unconventional" Structures	2-4
2-3 Reduced List of Candidate Unconventional Structures from Table 2-2 Sorted According to Type of Construction	2-5
2-4 Final List of Unconventional Structures to Be Considered in This Study	2-5
2-5 Maximum Safe Predicted or Recorded Peak Sonic Boom Overpressure for Representative Building Materials on Interior Walls and Ceilings	2-19
3-1 Summary of WSMR Measurements and Coordinates of Measurement Points in Terms of Actual and Transformed Coordinates Which Define the Ellipse Describing the Spatial Variation in Peak Pressure	3-13
3-2 Standard Deviations of Log-Normal Distribution of Sonic Boom Peak Pressures from Controlled and ACM Supersonic Flights	3-19
3-3 Predicted Long Time Average CSEL ₀ and DNCL ₀ at the Center of the ACM Noise Ellipse According to the Flight Track Data and Noise Estimation Procedures in Galloway, 1983	3-23
3-4 Carpet Boom Characteristics Estimated for a Variety of Low Level Supersonic Flight Operations	3-30
4-1 Stress Factors K_S , E , C_L , and E/C_L Used in Eq. (4-7) to Relate Peak Velocity to Stress for Various Aspect Ratios of Simply Supported Plates Made from Different Materials Vibrating in the Fundamental Mode	4-14
4-2 Typical Fundamental Resonance Frequencies, f_0 , Dynamic Magnification Factors, Q and Surface Weights, w (lb/ft ²) for Some Building Walls	4-24
4-3 Summary of Average Measured Values for the Vertical Peak Ground Velocity, V_{pk} Relative to the Local Peak Acoustic Pressure, P_{pk}	4-25
4-4 Comparison of Failure Load and Estimated Failure Stress of Old vs. New Glass Window Panes of Thickness h and Side Dimensions a , b	4-31
4-5 Size Categories and Associated Parameters Used in Evaluation of Potential Window Damage	4-33
4-6 Summary of Estimated Failure or Damage Stress Values for Various Types of Masonry Walls Based on (a) Blast Damage Criteria and (b) Static Test Data	4-34

LIST OF TABLES - Continued

Table	Page
4-7 Criteria for Maximum Structural Displacement and Velocities to Avoid Damage to Prehistoric, Historic, Sensitive and Conventional Structures	4-41
4-8 Static and Dynamic Properties of Soils and Snow	4-51
5-1 Instrumentation Characteristics (Set-Up in Structure A)	5-11
5-2 Summary of Impedance Tests Performed on Structures A and B.....	5-28
5-3 Summary of Tyndall Test Data Listing Peak Sonic Boom Pressures on Channel 0 and Peak Structural Responses and Ratios of Peak Acceleration or Displacement to Peak Pressure.....	5-37
6-1 Four Major Categories and Subcategories of Unconventional Structures Evaluated for Potential Damage by Sonic Boom.....	6-2
6-2 Estimated Default Values for Ratio P_e/P_f of Effective to Free Field Sonic Boom Pressure and Corresponding Values of σ_L	6-5
6-3 Summary of Structural Response Prediction Model Parameters	6-7
6-4 Summary of Damage Probability Estimate for Unconventional Structure Located at Center of SOA Ellipse	6-9
6-5 Probability of Damage Per Day for Unconventional Structures Located at One of Four Different Elliptical Radii Under an SOA Ellipse With an Average of 500 ACM Sorties Per Month	6-11
6-6 Evaluation of Sensitivity of Damage Predictions for SOAs by Comparing POD_n Values	6-15
6-7 Estimates of the Probability of Damage Per Boom for a Range of Sonic Boom Pressures from Supersonic Corridor (Level) Flights.....	6-17

LIST OF FIGURES

Figure	Page
2-1 Conceptual Illustration of Difference in Stress-Strain Characteristics of (a) Ductile, and (b) Brittle Materials.	2-7
2-2 Probability Density Function of the Effective Factor of Safety for the (a) Linear and (b) Log-Normal Cases.....	2-10
2-3 Examples of Cracking Damage in Structures from Natural Causes.....	2-22
3-1 Speed and Altitude Limits for Booms to Reach Ground for Standard Atmosphere and Level Flight Conditions	3-4
3-2 Contours of Measured Values and Gaussian Distribution Models Fitted for DNCL and Number of Sonic Booms per Day from WSMR Tests (Based on 550 ACM Sorties per Day).....	3-6
3-3 Computed C-Weighted Response of Sound Level Meter with Cut-Off Frequency of 0.5 Hz and 2 Hz for the Microphone and Pre-Amplifier Respectively to 0.2 Second N-Wave	3-9
3-4 Relationship Between Energy, Arithmetic and Log Mean Values for Any Variable with a Log-Normal Distribution as a Function of the Standard Deviation of the Log of the Variable.....	3-14
3-5 Comparison of Measured and Predicted Long Time Average Peak Pressures (Adjusted to Log Mean Values) as a Function of the Elliptical Radius	3-14
3-6 Cumulative Probability Distribution of Relative Peak Sonic Boom Pressures from Oklahoma City Test for Airplane A and Relative C-Weighted Sound Exposure from Reserve SOA Test	3-17
3-7 Cumulative Probability Distribution of Ratios of Measured to Long Time Average Overpressures for the XB-70 Aircraft for Measuring Stations on the Track and at a Lateral Distance of 13 Miles.....	3-18
3-8 Cumulative Probability Distribution of Pooled Data of Individual Values of Peak Overpressures from WSMR Test	3-20
3-9 Comparison Between Theory, Flight Test, and Wind Tunnel Measurements for a Supersonic Bomber	3-25
3-10 Comparison Between Full-Signature Boom Model, Carlson Far-Field Model, and Current Model.....	3-27
3-11 Lateral Spread of Sonic Boom Carpet Pattern for Very Low (a) and (b) and High (c) and (d) Altitudes.....	3-28

LIST OF FIGURES - Continued

Figure	Page
3-12 Schematic Diagrams Showing Relative Frequency of Occurrence of Categories of 1152 Waveforms Measured at Ground Level During Sonic Boom Tests on Four Airplanes	3-34
3-13 Converging Rays for Small and Large Acceleration, Low and High Altitude and Associated Nominal Sonic Boom Wave Forms	3-36
3-14 Sound Exposure Spectrum Levels for Sonic Booms	3-38
4-1 Typical Transient Acceleration Response of Structure to Sonic Boom; Response Measured on 18" Adobe Wall for Event MR 081 for This Program	4-2
4-2 Normalized Shock Spectra for Excitation of (a) Undamped and (b) and (c) Damped System by Ideal N-Wave.....	4-4
4-3 Summary of DAF Values Measured on Ground Microphones from Ninety F104 and Fifteen B58 Sonic Boom Records from White Sands FAA Test Program in 1965	4-7
4-4 Normalized Residual Velocity Shock Spectrum for Predicting Peak Velocity Response of Structures with a Surface Weight w (psf) to a Sonic Boom with an Effective Peak Pressure P_e (psf)	4-9
4-5 Measured and Predicted Peak Sonic Boom-Induced Stresses in Various Building Elements	4-19
4-6 Distribution of Logarithm of Modulus of Rupture for 58 Tests of Adobe Bricks from Various Manufacturers Compared to Theoretical Log-Normal Distribution	4-37
4-7 Safe Levels of Blasting Vibration for Houses Using a Combination of Velocity and Displacement.....	4-42
4-8 Probability Damage Analysis of Nine Sets of Data for Typical Residential Walls Exposed to Vibration from Surface Mine Blasting or Mechanical Shaker Tests.....	4-44
4-9 Number of Slab Avalanches Versus Bed-Surface Inclination θ	4-50
4-10 Shear Stress at Bed Surface Versus Bed-Surface Density	4-50
4-11 Diagram Showing Gradual Decrease of Shearing Resistance of Stiff, Fissured London Clay.....	4-53

LIST OF FIGURES - Continued

Figure	Page
5-1a Measured ACM Day-Night Average C-Weighted Sound Level in Lava/Mesa Airspace	5-2
5-1b Measured ACM Booms Per Day in Lava/Mesa Airspace	5-2
5-2 WSMR Lava/Mesa Airspace and Coordinates.....	5-4
5-3 George McDonald Ranch House (Structure A)	5-5
5-4 McDonald Brothers Ranch House (Structure B).....	5-6
5-5 Structural Response Measurement System Block Diagram.....	5-8
5-6 Data Acquisition Hardware and Computer.....	5-9
5-7 Acoustic Instruments - Bear, SBM-1 and Microphones.....	5-9
5-8 Front Porch Area of Structure A	5-13
5-9 Plaster and Adobe on Inside Wall of Structure B	5-14
5-10 Side View of Mounted Accelerometer.....	5-15
5-11 Top View of Mounted LVDT.....	5-15
5-12 Frequency Response Variations Between Driver and Accelerometer Mounting Configurations	5-17
5-13 Impedance Hammer	5-19
5-14 Accelerometer Mounted on Wall	5-19
5-15 Floor Plan of Structure A	5-21
5-16 Floor Plan of Structure B	5-23
5-17 Typical Sonic Boom Event with Selected Response Channels.....	5-25
5-18 Typical Wall Surface of Structure A.....	5-26
5-19 Impedance Test on Wall 101E - Repeat Tests.....	5-30
5-20 Impedance Test on Wall 101E - Before and After Boom Mounting.....	5-31
5-21 Wall Driver Force Input (Test FS 101E1)	5-33
5-22 Wall Acceleration 2 inches from Driver (Test FS 101E1).....	5-34

LIST OF FIGURES - Continued

Figure	Page
5-23 Wall Acceleration 12 inches from Driver (Test FS 101E1)	5-35
5-24 Typical Time History Curves of Acoustic Pressure and Response for Boom #MR 081, Room 101 - Structure A	5-39
5-25 Displacement of Crack in Wall 101S of Structure A.....	5-40
5-26 Comparison of Measured and Predicted Ratio of Peak Velocity Response, at Center of Three Outside Walls and in Ceiling, to Peak Sonic Boom Pressure on Nearby Ground Microphones for Structure A.....	5-43
5-27 Velocity to Pressure Transfer Function Spectra Measured from Seven Different Sonic Boom Tests at the Center of Three Different Walls in Structure A	5-44
6-1 Graphic Summary of Predicted Probability of Damage Events Per Day for Unconventional Structures Located at the Center and 40 Miles (On Major Axis of Ellipse) from Center of an SOA with an Average of 500 ACM Sorties Per Month	6-13

1.0 INTRODUCTION

This report presents a method for the evaluation of potential damage to unconventional structures by sonic booms. There is a substantial body of data and information available on sonic boom damage to conventional structures such as windows, plaster, etc. (e.g., Hershey and Higgins, 1976, Haber and Nakaki, 1989), but very little comparable information is available on the potential damage to unconventional structures such as historical buildings of various types using both conventional and unconventional architecture. These involve colonial structures in the eastern part of the U.S., early American stone or adobe buildings, prehistoric archaeological monuments, especially in the western part of the U.S. (some dating back over 900 years), water wells or water tanks, other atypical structures such as large radio antennas, and areas subject to landslides or snow avalanches. This report is intended to provide a method for prediction of potential damage from sonic boom to such structures on a generic basis for potential use in site-specific environmental impact evaluations relating to supersonic training areas.

The report is also designed to provide the definition of the input data and algorithms required to carry out this damage assessment with the use of a new computer program called ASAN (Assessment System for Aircraft Noise) under development for the Noise and Sonic Boom Impact Technology (NSBIT) program (Haber and Nakaki, 1989).

The Environmental Impact Assessment process carried out for proposed supersonic training operations must include consideration of damage potential for unconventional structures in order to respond to the public about their oft-expressed concerns regarding such potential damage. Up to now, very few data have been available which could be used to objectively demonstrate the degree of damage, if any, that may occur to such unconventional structures (Battis, 1983).

Thus, the primary purpose of this report is to fill this need for the U.S. Air Force (USAF) to support the environmental assessment process for supersonic training areas. A secondary purpose is to support the USAF in the evaluation of claims for any damage that may, or is purported to have, occurred for unconventional structures exposed to sonic boom.

This report includes the following.

- Review of types of unconventional structures, critical material properties needed to assess potential damage to such structures from sonic boom, and a brief review of

applicable field inspection techniques for assessing damage on the basis of changes between the pre- and post-exposure conditions of the unconventional structure (Section 2).

- Definition of a statistical model for sonic boom exposure in supersonic flight training areas (Section 3).
- Development of analytical models for predicting potential damage to unconventional structures from such exposure (Section 4).
- Results of a series of measurements of the structural response of unconventional structures during or after exposure to sonic booms (Section 5).
- Summary of a generic damage prediction model to assist environmental planners in preparation of environmental impact assessments or environmental impact statements about potential damage to unconventional structures (Section 6).
- A series of supporting appendixes, including:

Appendix A – Bibliography on Sonic Boom, Structural Response and Damage

Appendix B – Materials Property Data on a Wide Range of Building Materials

Appendix C – Analytical Background

C.1 Relationship Between Various Spectral Measures of Sonic Booms

C.2 Multimodal Response of Simply Supported Panel to Normally Incident Sonic Boom

Appendix D – Photographs of Wall Cracks Before and After 2 Months of Sonic Boom Exposure

Appendix E – Time Histories of Sonic Boom Pressures and Structural Responses for Structures A and B

Appendix F – Summary Tables of Weather Data During the Test Period

A list of abbreviations and symbols used in the report follows.

List of Abbreviations and Symbols

ABBREVIATION DEFINITION

ACM	Air Combat Maneuver (Training)
ASAN	Assessment System for Aircraft Noise
BLM	Bureau of Land Management
CSEL	C-Weighted Sound Exposure Level
CSEL ₀	Long Time Average Value of CSEL
DAF	Dynamic Amplification Factor
DNCL	Average Day-Night C-Weighted Sound Level
EIS	Environmental Impact Statement
MOA	Military Operating Area
NASA	National Aeronautics and Space Administration
NDT	Non-Destructive Testing
NSBIT	Noise and Sonic Boom Technology
POD	Probability of Damage
SDOF	Single Degree of Freedom System
SOA	Supersonic Operating Area
WSMR	White Sands Missile Range

SYMBOL DEFINITION

A	Area of structural panel or cross-sectional area of beam, in ²
A'	Cross-sectional area of unit width strip of plate, in ²
C _D	Speed of dilatational (compressional) waves in ground, ft/sec
C _L	Longitudinal speed of sound in structural material, in/sec
C _m	Constant in Eq. (4-10b) for resonance frequency of wall, with units Hz · inches
C _S	Speed of shear waves in earth material, in/sec
D	Ratio, P _e /P _f of effective to true free field peak sonic boom pressure
DAF(f)	Dynamic amplification factor at frequency f, dimensionless
D _R (f)	Residual Pressure Shock Spectrum at frequency f, psf
E	Modulus of Elasticity of structural material, psi
E(f)	Energy Spectral Density of Sonic Boom = P(f) ² , (psf · sec) ²
F _s	Factor of safety = σ_y/σ_{pk}
G	Shear Modulus of earth material, psi
H	Effective altitude of aircraft in Eq. (3-11), ft
I	Area moment of inertia of cross section of uniform beam, in ⁴

List of Abbreviations and Symbols - Continued

SYMBOL	DEFINITION
I'	Area moment of inertia of cross section of unit strip of uniform plate, in^4
K	Constant in Eq. (4-11) relating stress in plate to static pressure load, dimensionless
K_a	Atmospheric-dependent parameter in Equation (3-11) for nominal sonic boom peak pressure, psf
K_b	Constant in Eq. (4-12) and (4-13) for stress vs static load on built-up panel, dimensionless
K_S	Shape/vibration mode factor in Eq. (4-7) relating peak velocity, V_{pk} to peak strain, ϵ_{pk} , dimensionless
L	Length of aircraft in Eq. (3-11), ft
L_{CDN}	Average day-night C-weighted sound level, dB re: $20\mu\text{Pa}$
L_{CE}	C-weighted sound exposure level, dB re: $(20\mu\text{Pa})^2 \cdot \text{sec}$
$L_E(f)$	Sound exposure spectrum level of sonic boom, dB re: $(20\mu\text{Pa})^2 \cdot \text{sec}/\text{Hz}$
$L_{VE}(f)$	Velocity exposure spectrum level, dB re: $(1 \text{ in}/\text{sec})^2 \cdot \text{sec}/\text{Hz}$
L_{pk}	Peak flat (unweighted) sound level, dB re: $20\mu\text{Pa}$
M	Mach number, Eq. (3-11) .
M	Bending moment for lateral load on wall, $\text{in} \cdot \text{lb}$
M_{mn}	Generalized mass for plate in $m\text{nth}$ mode
N	Number of ACM sorties per month in a given SOA
P	Static pressure load on structure, psi or psf
P_e	Effective peak sonic boom pressure, psf
P_f	Actual free field peak sonic boom pressure, psf
$P(f)$	Fourier spectra of sonic boom pressure time history, $\text{psf} \cdot \text{sec}$
$P^*(f)$	Complex conjugate of $P(f)$
$P(t)$	Pressure as a function of time, psf
P_o	Nominal (long time average) peak free field sonic boom pressure, psf
P_{pk}	Peak pressure of sonic boom or any other transient pressure, psf
$P(x)$	Probability density function of x where $x = \sigma_s, \sigma_{pk}, P_e$, etc.
POD	Probability of Damage for one sonic boom
POD_n	Probability of Damage for n booms per day at a given site
Q	Dynamic magnification factor (Table 4-2)
S_b	Non-dimensional non-linear bending stress response of windows to static pressure loads (see Table 4-4)
SE	Sound exposure, $(\text{psf})^2 \cdot \text{sec}$
$SE(f)$	Sound exposure spectral density of sonic boom = $2 E(f)$, $(\text{psf} \cdot \text{sec})^2$
T	Duration of ideal N-wave sonic boom time history, sec

List of Abbreviations and Symbols - Continued

SYMBOL	DEFINITION
V_{pk}	Peak velocity response of structure to sonic boom, in/sec
$V(f)$	Fourier spectra of velocity response to sonic boom, units of (in/sec) · sec
$V_{mn}(t)$	Velocity response of plate in mnth mode at time t, in/sec
$V_R(f)$	Residual velocity shock response spectra at frequency f (same as V_{pk}), in/sec
$V_T(t)$	Total multimodal velocity response of plate at time t, in/sec
W	Weight of structural panel, lb
X	Distance from center of ellipse along minor axis, miles
X'	$X/(a/b)$
X_{min}	Minimum (negative) deflection response to transient excitation during time excitation is present, in.
X_{max}	Maximum (positive) deflection response to transient excitation during time excitation is present, in.
$X_{rmax,min}$	Maximum and minimum deflection response to transient excitation after excitation ceases, in.
X_{pk}	Peak deflection response of structure to sonic boom, in.
X_s	Deflection response of structure to static pressure with same magnitude as peak pressure of sonic boom, in.
Y	Distance from center of ellipse along major axis, miles
Y'	Quantity having a log normal distribution
$\langle Y' \rangle$	Energy mean value of Y'
Y'_L	Log mean value of Y'
Y'_m	Arithmetic mean value of Y'
Z	Dimensionless distance, $[(X/\sigma_x)^2 + (Y/\sigma_y)^2]^{1/2}$
a	1/2 length of minor axis of SOA maneuvering ellipse, miles
a	Length of short side of panel, in.
a_{pk}	Peak acceleration response of structure to sonic boom, g's
b	1/2 length of major axis of SOA maneuvering ellipse, miles
b	Length of long side of panel, in.
c	Speed of sound in air ≈ 1117 ft/s
c'	Distance between neutral and outer-most fiber of beam, in.
d	Diameter of radio antenna, ft
e	a/b , eccentricity parameter for ellipse
$\text{erfc}(z)$	Complementary error function of z
f	Frequency, Hz
f_c	Characteristic frequency, in Hz, for acoustic loading of radio antenna
f_{max}	Frequency ($= \sqrt{3/\pi T}$) at peak of envelope of Residual Velocity Shock Response Spectrum, $V_R(f)$, Hz
f_0	Fundamental resonance frequency of structure, Hz

List of Abbreviations and Symbols - Continued

SYMBOL	DEFINITION
g	Acceleration of gravity, 386 in ² /sec
$g_{mn}(X,Y)$	Mode shape of plate at coordinates X,Y
h	Thickness of plate, in.
j	$\sqrt{-1}$
k	Spring constant for SDOF model of structure, lb/in
k_s	Shape factor in Eq. (3-11) for sonic boom peak pressure, dimensionless
p_0	Reference pressure = 20 μ Pa
q	Non-dimensional pressure load in expression for non-linear response of windows to static load (Table 4-4)
m,n	Mode numbers for bending vibration of plate with sides a,b
n	Number of sonic booms per day at a given position, X,Y
r	Elliptical radius, $[(X')^2 + (Y')^2]^{1/2}$, miles
t	Thickness of inner or outer surface of built-up panel, in.
t_0	Reference time = 1 sec
w	Surface density of panel, psi or psf
w'	Width of stud in built-up wall, in. (Eq. 4-13 & 4-15)
x	Log, to the base 10, of the factor of safety, F_s
\bar{x}	Mean value of x
z	$\bar{x}/\sqrt{2} \sigma_L$, the argument in $\text{erfc}(z)$
Δf	Reference bandwidth = 1 Hz
$\epsilon_{mn}(t)$	Generalized displacement of plate at time t, in.
ϵ_{pk}	Peak strain, dimensionless
ω	Angular resonance frequency of plate at mnth mode, radians/sec
μ	Poisson's ratio
ρ	Mass density of material, lb sec ² /in ⁴ (or kg/m ³)
$\sigma_L(x)$	Standard deviation of log ₁₀ of x where $x = \sigma_s, P_e, F_s$, etc.
σ_{pk}	Peak dynamic stress, psi
σ_s	Stress response to static pressure which has same magnitude as peak pressure of sonic boom, psi (also equal to damage threshold stress)
σ_x	Standard deviation of DNCL pattern along minor axis of ellipse
σ_y	Standard deviation of DNCL pattern along major axis of ellipse
σ_x'	Standard deviation of pattern for n along minor axis of ellipse
σ_y'	Standard deviation of pattern for n along major axis of ellipse
θ	Angle, projected onto ground, between normal to vertical wall surface and flight track of supersonic aircraft, degrees

2.0 UNCONVENTIONAL STRUCTURES

The initial task in this study was to establish a reasonable list of unconventional structures to be considered throughout the remainder of the program. Since the purpose of this study is to provide generic guidelines, it would be desirable that this list include as wide a range as practical of unconventional types of structures that may be encountered in supersonic training areas. Furthermore, in order that potential damage to these structures from sonic boom can be assessed, a logical basis for assessing the probability of damage to these structures must be established in terms of a statistical model. Finally, for field evaluation of the possible occurrence of any actual sonic boom damage, systematic inspection techniques need to be examined which would allow comparison of pre- and post-sonic boom exposure. This section addresses these three issues: (1) the types of unconventional structures to be considered, (2) the statistical basis for assessing the probability of damage and (3) a review of pre- and post-exposure field inspection techniques to assist in establishing the potential occurrence of damage to unconventional structures.

2.1 Selection of Unconventional Structures

Unconventional structures are defined, for this report, as all types of structures that are not normally inhabited or used for routine commerce and which may exist under a supersonic operating area (SOA) for military aircraft. Thus, all types of inhabited dwellings and standard commercial buildings normally found under such areas are excluded.

The selection of the types of unconventional structures to be considered is based on two considerations.

- The relative frequency for which such structures are identified in transcripts of public hearings conducted during the preparation of Environmental Impact Statements (EIS's) for several SOAs.
- Logical evaluation of the types and locations of various categories of structures in areas likely to lie under SOAs.

The first source of information is summarized in Table 2-1.

For the second consideration defined above, the selection process started with an enumeration of all the locations and types of structures which would logically be encountered near supersonic military training areas. From this initial, global list, a reduced catalogue of

unique types of structures was developed, which was then narrowed to a list of individual types of construction selected.

This list, coupled with the information from Table 2-1, formed the basis for a single generic list of structures to be considered. The final list was not restricted to those types identified in Table 2-1 from the previous EIS's reviewed since these represented only a sample based on public reaction to five specific military programs and were not considered sufficiently general to provide a completely valid selection criteria for this study.

Table 2-1
Relative Frequency of Public Comments in Draft EIS's
About Potential Damage to Unconventional Structures from Sonic Boom

MOA No.(1)	Structural Type Description	Rank	Comments %(2)
1,3,4,5	Archaeological Sites	1	32.9
1,2,5	Adobe House	2	17.9
2,5	Historic Indian Sites	3	14.3
1	Water Storage Tanks	4	9.3
4	Electrical Power Plant	5	8.5
4	Ground Water	6	5.7
4,5	Open Pit Mine Slopes/Rock Slides	7	2.8
1,5	Water Wells	8	2.4
1,5	Rock Shelters/Caves	9	2.4
4	Settling - Level Fields	10	2.9
4	Oil-Gas Production	11	1.0
5	Sensitive Manufacturing Process	12	1.0
Total			100.0%

Notes:

- (1) 1 = Valentine SOA, 2 = Gandy SOA, 3 = Nellis MOA, 4 = Fallon SOA, 5 = Reserve SOA
- (2) Percent comments weighted by total number of comments per site out of a total of 115 public comments on potential damage to unconventional structures in Final Environmental Impact Statements for five different Supersonic Operating Areas (SOAs).

Table 2-2 provides a listing of anticipated types of locations and types of buildings in these locations which may fall under or near SOAs. Also listed in the table are the general types of construction for each building type.

Table 2-3, which is simply Table 2-2 resorted by type of construction with location omitted and duplications eliminated, defines the unique types of buildings and their construction. The acoustically-induced response of the various types of buildings listed is not expected to vary, in terms of basic physical characteristics, for the same type of building construction. Based on this rationale, the categories in Table 2-3 were reduced to generic types of structure to be considered, and combined with the additional types of structures in Table 2-1 to establish a final list shown in Table 2-4. The sequence of structures listed in Table 2-4 was chosen to approximate the relative frequency of public comments about various types of structure listed by Table 2-1.

The distinctions in Table 2-4 between "masonry, adobe" or "wood frame" construction have been made anticipating different criteria for potential damage effects and potential differences in details of the analytical models employed to predict the effects of acoustic loading from sonic booms. The distinction between historic buildings with or without an intact roof reflects the need to consider the difference in the effective pressure loading on the walls for these two cases.

Table 2-1 indicates the relative frequency for which public comments were made about potential damage from sonic booms for each of the types of structures listed. Comparison of Tables 2-1 and 2-4 indicates that the latter does, in fact, cover most of the types in Table 2-1. The possible exceptions are: (1) settling in open fields, (2) open pit mine slopes/rock slides, (3) electric power plants, (4) oil and gas production and (5) sensitive manufacturing processes. The first two exceptions should be covered under the topic of earth slides included in Table 2-4. The next two exceptions are not explicitly included in Table 2-4 but should be effectively included under the category of masonry, adobe, wood or metal frame buildings listed in the table. The last exception, sensitive manufacturing processes may be a legitimate concern relating to structured response from sonic boom, but is not considered pertinent to this study since it pertains to an unsatisfactory commercial building vibration environment and not structural damage. However, data contained in this report may be useful to help evaluate this type of problem.

Table 2-2

Location and Type of Buildings Considered as Candidate "Unconventional Structures"

Location	Type of Building or Site	Type of Construction
BLM Land	Archaeological Sites	Natural Stone
BLM Land	Historic Structures	Wood Frame, Masonry, Adobe
BLM Land	Utility Buildings	Wood/Metal Frame, Masonry, Adobe
Cattle Range Land	Water Tanks	Metal/Stone Tank
Cattle Range Land	Wells	Masonry Wells
Farmland	Barns	Wood Frame
Farmland	Utility Buildings	Wood/Metal Frame, Concrete Block
Indian Reservations	Archaeological Sites	Natural Stone
Indian Reservations	Old Dwellings	Masonry, Adobe
Indian Reservations	Fragile Geol. Structures	Natural Stone
Indian Reservations	Indian Petroglyphs	Natural Stone
Mountainous Areas	Avalanche Areas	Snow on Steep Slopes
Mountainous Areas	Earth Slide Areas	Soil on Steep Slopes
National Monuments	Colonial Structures	Wood
National Monuments	Colonial Structures	Stone, Brick
National Monuments	Indian Petroglyphs	Natural Stone
National Monuments	Natural Geol. Structures	Natural Stone
National Monuments	Prehistoric Structures	Adobe, Stone
National Parks	Early American Bldgs	Masonry, Adobe
National Parks	Historic Colonial Bldgs	Wood Frame, Masonry, Adobe
Any Area	Radio Telescopes	Metal Frame Construction

Table 2-3

Reduced List of Candidate Unconventional Structures from Table 2-2 Sorted According to Type of Construction.

Type of Structure	Type of Construction
Prehistoric Structures	Adobe, Stone
Wells	Masonry
Water Tanks	Metal/Stone
Archaeological Sites	Natural Stone
Fragile Geological Structures	Natural Stone
Indian Petroglyphs	Natural Stone
Avalanche Areas	Snow on Steep Slope
Earth Slide Areas	Soil on Steep Slope
Colonial Dwellings	Masonry, Wood Frame
Early American Structures	Masonry, Adobe
Barn, Covered Bridge	Wood Frame
Utility Buildings	Wood/Metal Frame/Concrete Block

Table 2-4

Final List of Unconventional Structures to be Considered in This Study

No.	Type of Structure	Type of Construction
1	Historic Buildings (1)	Masonry, Stone
2	Historic Buildings (1)	Brick
3	Historic Buildings (1)	Adobe
4	Historic Buildings (1)	Wood Frame, Plaster Interior
5	Historic Buildings (1)	Wood Frame, Wood Interior
6	Historic Buildings	Covered Wood Bridge
7	Prehistoric Structures (2)	Masonry, Stone
8	Prehistoric Structures (2)	Adobe
9	Geological/Archaeological Sites (3)	Stone Caves/Rock Formations
10	Water Tanks	Metal/Stone (above ground)
11	Wells	Masonry (below ground)
12	Slide Areas - Avalanche	Snow on Steep Slope
13	Slide Areas - Soil	Soil on Steep Slope
14	Utility Buildings of All Types	Concrete Block
15	Utility Buildings of All Types	Wood Frame
16	Utility Buildings of All Types	Metal Frame
17	Radio Telescopes	Metal Frame

- (1) More than 50-100 years old (roof intact)
- (2) Early American habitation/ceremonial sites (roof missing)
- (3) May contain petroglyphs or other Early American art

It should be emphasized that the large number of different types of structure listed in Table 2-4 is not necessarily consistent with the amount of data available on structural strength of the various materials involved. Nevertheless, while the strength data on materials used for some of these unconventional types of structure are limited, they are believed to be adequate to allow a reasonable assessments of potential damage to be made for purposes of this report.

2.2 Basis For Prediction of Damage to Unconventional Structures from Sonic Booms

Damage to an unconventional structure from sonic booms is assumed to occur whenever the peak stress induced by the sonic boom loading exceeds the strength (i.e., yield or ultimate stress) of the particular material involved. This will ordinarily be an interior wall or ceiling which tend to have the greatest response to sonic booms as well as the lowest strength.

Stress response of materials to static loads varies drastically depending upon the type of material (McClintock and Argon, 1966). Figure 2-1 illustrates, schematically, the stress-strain behavior of two basic types of building construction material - ductile and brittle - as a typical sample of each type is increasingly stressed. Most metals and woods fall in the category of ductile materials. For such materials, the stress-strain relationship is linear up to the yield stress, at which point the strain (i.e., elongation or deflection per unit dimension) begins to increase much more rapidly with an increase in stress until failure occurs at the ultimate stress. For this report, damage to buildings constructed of ductile materials, such as steel or wood frame/wall utility buildings, will be assumed to occur when the imposed stress reaches the yield stress.

The other building materials such as masonry, stone, brick, concrete, plaster and adobe (or non-structural materials such as soil or snow embankments) can be considered as brittle materials in which case damage is assumed to occur when the imposed stress reaches the ultimate (failure) stress.

An extensive collection of physical properties of a wide range of building construction materials is provided in Appendix A. These data represent a collection of materials properties data from over 50 references that was compiled for an extensive manual on sonic loads for ground facilities (Sutherland, 1968a). These data are augmented, for this report, by additional and more recent information on strength properties of glass (utilized as a model for brittle materials in terms of statistical characteristics of the strength values), adobe, masonry walls, and non-structural materials (i.e., soils and snow).

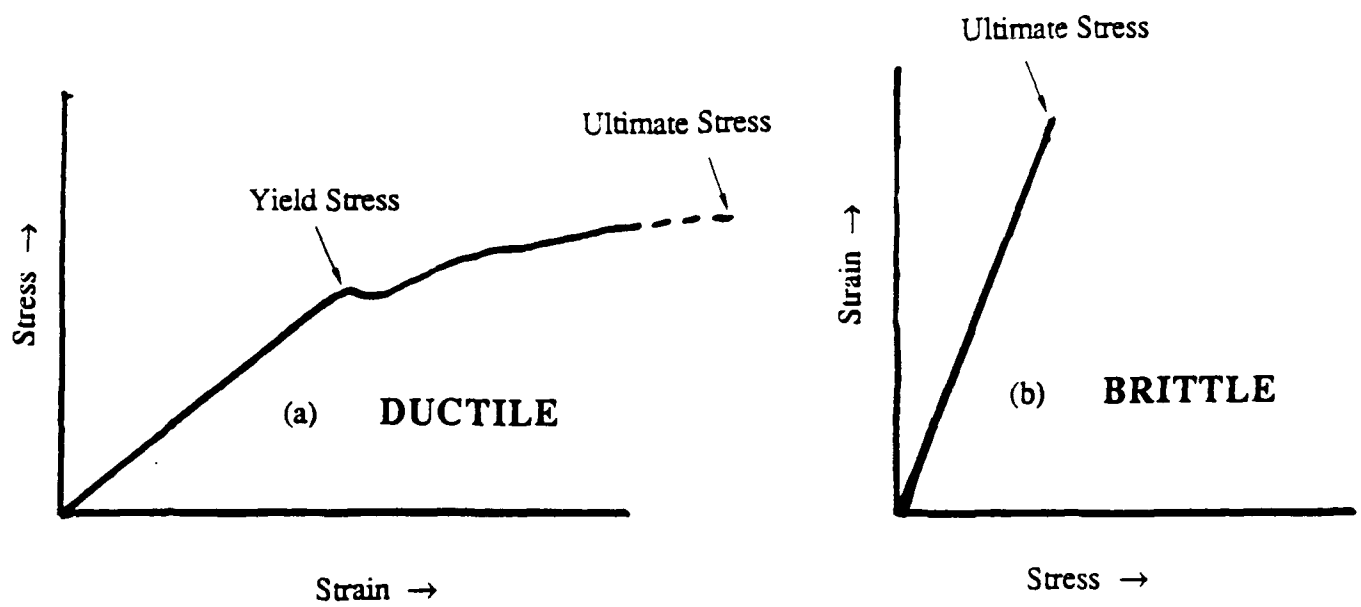


Figure 2-1. Conceptual Illustration of Difference in Stress-Strain Characteristics of (a) Ductile, and (b) Brittle Materials.

2.2.1 Framework for an Excitation-Response-Damage Prediction Model

The development of a prediction model for structural damage from any acoustic loading can be illustrated conceptually in the following simplified form. It follows the same general approach similar to that used in a previous study on the analysis of damage to structure from sonic booms (Hershey and Higgins, 1976). In that work, the peak dynamic stress σ_{pk} in a structure due to acoustic loading by a nominal free field incident acoustic pressure P_0 is given by:

$$\sigma_{pk} = P_0 \cdot (P_e/P_0) \cdot (\sigma_s/P_e) \cdot (\sigma_{pk}/\sigma_s) \quad (2-1)$$

where (P_e/P_0) is the ratio of effective acoustic pressure load to the nominal acoustic load. This factor accounts for: (a) the relationship between the orientation of the structure relative to the incident sound pressure wave, (b) the rigidity (or acoustical impedance) of the structural surface, and (c) the relationship between the wavelength of the acoustic field and the bending wavelength of the structural vibration response to the acoustic field. (σ_s/P_e) is the ratio of the maximum static stress in the structure to a static pressure load equal in magnitude to the effective acoustic pressure, P_e .

(σ_{pk}/σ_s) is the ratio of the peak dynamic stress in the structure to the static stress for dynamic and static pressure loads which have the same magnitude. This is called the *Dynamic Amplification Factor* in the Hershey and Higgins model, and it depends essentially on the product of the resonance frequency of the structure and a characteristic duration for a sonic boom.

An alternate model is also useful by replacing the last two terms in Eq. (2-1) above with a single term, (σ_{pk}/P_e) which is the ratio of the peak stress in the structure to the effective applied pressure. This term will be shown to depend on the peak structural velocity response which in turn depends on the dynamic response characteristics of a structure to a transient load. Thus, Eq. (2-1) will be modified for this report where appropriate to read:

$$\sigma_{pk} = P_0 \cdot (P_e/P_0) \cdot (\sigma_{pk}/P_e) \quad (2-2)$$

2.2.2 Framework for Statistical Models for Excitation-Response-Damage Prediction

The preceding has defined the various factors that are required to predict the occurrence of structural damage. However, the terms in Eq. (2-1) or (2-2) are really only known in a statistical sense when one considers a broad variety of conditions restricted to just one general

type of structure. Thus, following the approach of Hershey and Higgins, it is necessary to define statistical models for each of the terms in Eq. (2-1) or (2-2) in order to define a probability distribution for the peak stress, (σ_{pk}) in the structure. In addition, it is necessary to define a corresponding statistical model for the static stress, σ_s , which corresponds to a damage threshold stress.

2.2.3 Details of Statistical Model for Damage Assessment

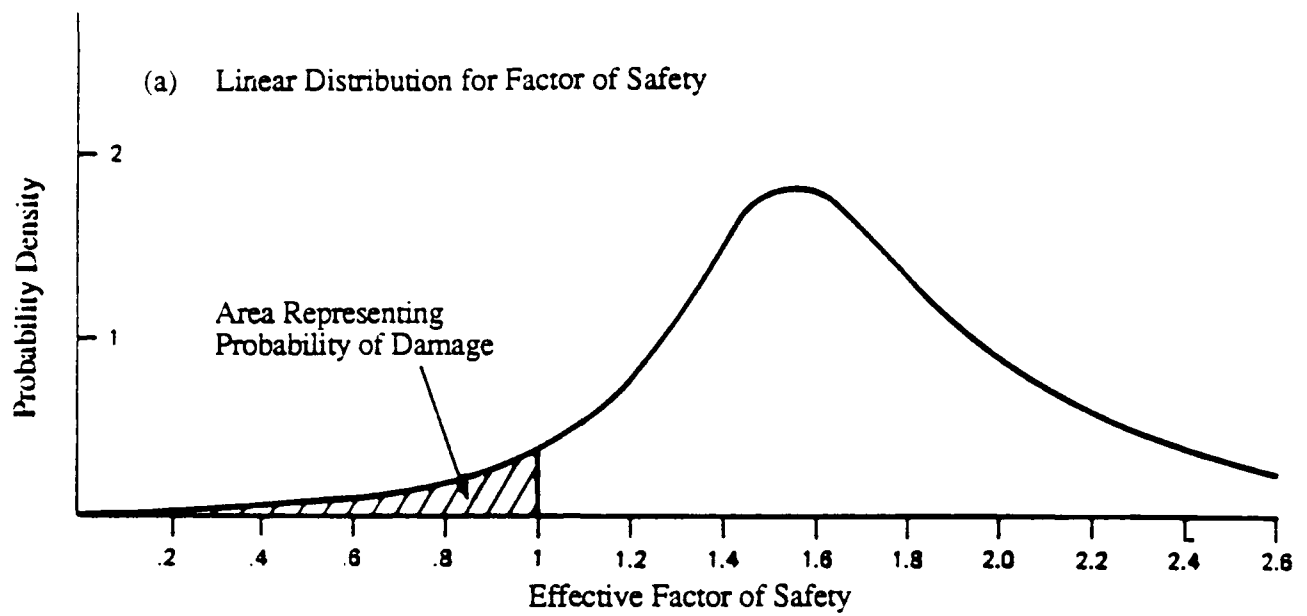
The statistical model for damage assessment is based primarily on the concepts developed by Hershey and Higgins (1976). Given a probability distribution or, more precisely, a probability density function, $P(\sigma_{pk})$ of the peak stress imposed on a structure, and a corresponding probability density function, $P(\sigma_s)$ for the strength or damage threshold stress for a structure, the total probability of failure is the integral of that part of the probability density function, $P(F_s)$ for the factor of safety F_s that lies between 0 and 1 as illustrated in Figure 2-2a. This factor of safety is given, for the i_{th} imposed stress σ_{pki} and the j_{th} damage stress σ_{sj} , by the ratio:

$$F_s = \sigma_{sj}/\sigma_{pki} \quad (2-3)$$

When both of these stress variables have a log-normal distribution, that is, the logarithms of their variables have a normal (i.e., Gaussian) distribution, then the logarithm of the factor of safety is also normally distributed. That is, from Eq. (2-3), $\text{Log}(F_s) = \text{Log}(\sigma_s) - \text{Log}(\sigma_{pk})$.* Since the *sum* or *difference* of two normally distributed statistically independent variables also has a normal distribution, the factor of safety has a log-normal distribution if both the imposed stress and failure stress variables have log-normal distribution. Note that this would not necessarily be so if the stress variables themselves instead of their logarithms were normally distributed, since the *quotient* of two normally distributed variables is not necessarily normally distributed. This is the basic reason for taking advantage of a log-normal distribution of the stress variables. It is much easier to compute the probability of failure by evaluating the integral of this log-normal distribution since this involves defining the integral of the normal distribution curve, and this integral is well tabulated or can be easily computed by closed-form numerical approximations.

Since damage is presumed to occur when the Factor of Safety F_s is less than 1 (and $\text{Log}(1) = 0$), the above approach can be used to calculate the basic probability of damage (POD). This probability, POD, is the area under that portion of the distribution of $\text{Log}(F_s)$

* Throughout this report, $\text{Log}(X)$ will denote logarithm to the base 10.



(b) Log-Normal Distribution for Factor of Safety

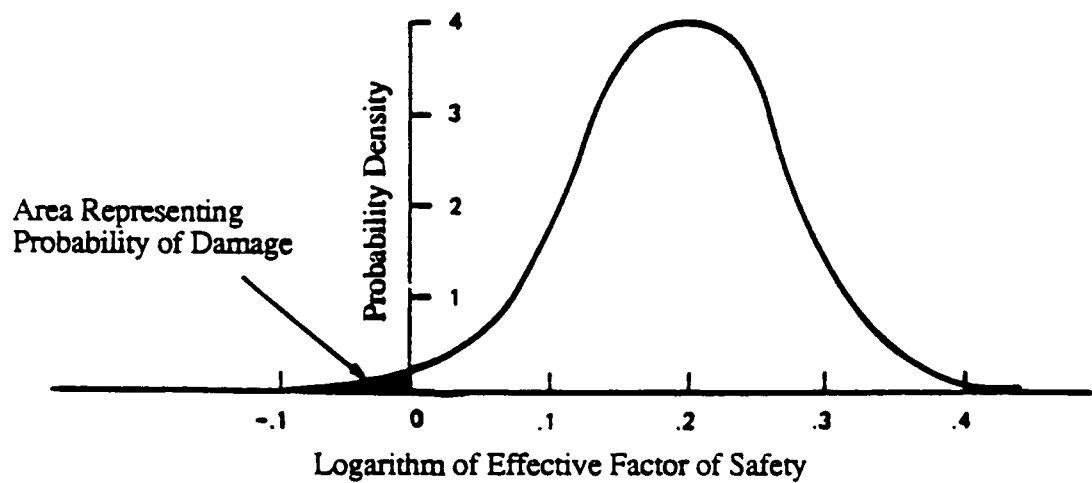


Figure 2-2. Probability Density Function of the Effective Factor of Safety for the (a) Linear and (b) Log-Normal Cases (from Hershey and Higgins, 1976).

which is less than 0 as illustrated in Figure 2-2b. That is, POD is equal to the integral for the normal distribution curve from $-\infty$ to 0 or:

$$\text{POD} = (1/\sigma_L\sqrt{2\pi}) \int_{-\infty}^0 \exp [-(x - \bar{x})^2 / 2\sigma_L^2] dx \quad (2-4)$$

where x is any value of the log of the factor of safety, \bar{x} is its mean value and σ_L is the standard deviation of this logarithm. From Eq. (2-3) the denominator σ_{pk} of the factor of safety is equal to the product of the free field sonic boom pressure P_f , the ratio P_e/P_f of the effective to the free field pressure, and the ratio σ_{pk}/P_e of the peak stress to the effective pressure. As was done by Hershey and Higgins, it would be possible to employ the rule that the logarithm of the product of several variables is equal to the sum of their logarithms. However, this is not really necessary at this point and it is desirable to retain the physical identity of each variable for now, and only convert to their logarithms in the computations.

The standard deviation σ_L of the log of the factor of safety needed to evaluate Eq. (2-4) is found by taking the square root of the sum of the variances (i.e., the square of the standard deviation of the logs) of each constituent term in the factor of safety. That is:

$$\sigma_L = \sqrt{\sigma_L(P_f)^2 + \sigma_L(P_e/P_f)^2 + \sigma_L(\sigma_{pk}/P_e)^2 + \sigma_L(\sigma_s)^2} \quad (2-5)$$

where the first three terms under the square root sign signify the square of the standard deviation of the log of each of the factors required to define the effective value of the imposed peak stress, and the last term denotes the square of the standard deviation of the log of the failure stress or strength. For purposes of tabulation of these latter quantities, it was convenient to express them in terms of decibels. This is simply equal to 20 times their value. For example, 20(Standard Deviation of Log of Pressure) has the same physical meaning as the standard deviation of a sound level in decibels (20Log [Pressure]) and can be more readily interpreted in that manner. Of course, for final computations of POD, the required form indicated by Eq. (2-5) is recovered.

For the cases of concern for this report, the probability of damage is less than 50 percent and the integral in Eq. (2-4) can be conveniently expressed in terms of the complementary error function $\text{erfc}(z)$ (Abramowitz and Stegun, 1972). Thus the probability of damage, POD, is:

$$\text{POD} = (1/2) \cdot \text{erfc}(z) \quad (2-7)$$

where $z = \bar{x}/\sigma_L\sqrt{2}$, \bar{x} is the mean value of x , which is the log of the factor of safety, (σ_s/σ_{pk}) .

The following algorithms, based on fitting polynomials to tabulated values for $\text{erfc}(z)$ (Abramowitz and Stegun, 1972), were used for computing the probability of failure for this report. Although more complex algorithms are also available, the following expressions are accurate within less than 0.7 percent for the applicable range of z .

$$\text{For } z < 1.5, \quad \text{erfc}(z) \cong 1.002873 - 1.23413 \cdot z + 0.389448 \cdot z^2 \quad (2-8a)$$

or, for $z \geq 1.5$,

$$\text{erfc}(z) \cong [\exp(-z^2)/z] [0.56417 - 0.27884 z^{-2} + 0.34498 z^{-4} - 0.33579 z^{-6}] \quad (2-8b)$$

While some of the data utilized to estimate the stress response of a structure were found to have an approximate log-normal distribution, it was usually not possible to validate such an assumption with the limited data available. Thus, when necessary, the required values of the standard deviations of the log of the quantities involved were estimated from information on the statistical variation of the variable (i.e., its own standard deviation or its range of extreme values). In the latter case, for example, it was assumed that σ_L was equal to one-fourth of the log of the ratio of the maximum to minimum value, corresponding to an estimate of the ± 2 sigma range of the log of the variable.

2.3 Field Inspection Techniques to Assess Potential Damage to Unconventional Structures

One key objective of this program was to explore experimental methods for assessing the *pre- and post-sonic boom exposure condition* of unconventional structures. Such techniques should provide a reasonable basis for comparing the existing condition of a structure before exposure relative to the type of normally minor damage that *may* result from exposure to sonic booms generated by air combat training flight activity of supersonic fighter aircraft. Potential damage from any low altitude supersonic flight activity is likely to be much more obvious so that validation of any damage is not as likely to be dependent on the more precise methods that are required to assess potential damage from sonic boom exposure from supersonic Air Combat Maneuver (ACM) flight activity.

Although the pre- and post-exposure measurement techniques are ideally required for all of the generic categories of unconventional structure, the relative ease with which such field inspection techniques can be applied will vary markedly with the type of structure. One

problem, of course, is that the pre-exposure condition of some structures can never be evaluated since they have already been exposed to sonic boom environments for a long time.

In many cases, the effect of age will also be very difficult to deal with when making any pre-exposure examination of old unconventional structures, since over time minor or even major structural damage will often result from natural phenomena (e.g., earthquakes, wind storms, lightning strikes, etc.).

Four basic types of physical parameters were considered for evaluating pre- and post-exposure conditions of unconventional structures. Selection of these parameters involved definition of the unique structural or topographical features of unconventional structures which would be subject to potential damage.

- (1) Surface topography (i.e., the presence of visible surface cracks)
- (2) Internal structural integrity (i.e., presence or absence of flaws or breaks in the structure)
- (3) "Inventory" of previous "failures" of the structural surface. This would be indicated, for example, by the presence of broken-off pieces of rock at the base of an Indian petroglyph carved on a rock wall. It was anticipated that this measure would only be qualitative at best. However, for critical prehistoric structures, simple field monitoring stations could be established to collect the natural accumulation of surface fracture material over a period of several months. These surface failures of the material would be expected to accumulate over time due to natural causes such as extreme changes in weather (especially temperature and moisture), thunder, or normal microseismic activity. Significant changes in the rate of accumulation of this material coincident with exposure to sonic booms could conceivably provide indirect evidence of the potential for sonic boom-induced damage, or, more likely, of the lack thereof. (Due to the expected long monitoring time required to establish a valid data base for such a technique, it was rejected without further study as not being practical for this program.)
- (4) Dynamic and static properties of the basic material. These material properties are really expected to be invariant with respect to exposure conditions since they will be considered to be dependent only upon the basic material itself and not on its condition. That is, the compression strength of a sample of an adobe wall will

condition. That is, the compression strength of a sample of an adobe wall will apply to the adobe material itself in an undamaged state and not to an adobe element, such as a block, which may have a crack in it. Nevertheless, these properties are included here as one of the basic types of material properties that might be evaluated with nondestructive testing (NDT) techniques for application to damage assessment of unconventional structures.

While the latter parameter may be appropriate in almost all cases, only one or two of the first three parameters will be appropriate for many unconventional building materials. For example, for an adobe building, it was anticipated that the key parameters, in addition to the material properties, would be the surface topography and the presence or absence of internal flaws.

Large variations in the values of these parameters would be expected as a function of where they are measured on a given structure. Too large a variance will make it difficult, if not impossible, to reliably distinguish between the existence of damage and the normal variance in the parameter selected for evaluation.

Although there is a large body of literature available on nondestructive testing (see Kamm and Kraska, 1971; Selner and Tracy, 1972, and Schroeder, 1971) for representative examples), no significant information is available which illustrates a direct application of NDT methods to the problems of concern for this program.

The selection of the most practical pre- and post-exposure parameters to measure obviously required consideration of which suitable measurement techniques were available. For example, it was felt that mechanical impedance could not be used reliably to evaluate pre- and post-exposure conditions for the walls of archaeological monuments where the thickness of the wall and hence the impedance, would tend to vary over a very large range. On the other hand, this technique was expected to be potentially useful for assessment of the condition of adobe buildings which have fairly uniform wall thicknesses.

Potential candidate field inspection methods considered were:

- Visual and photographic recording of surface condition, including identification and measurement of surface cracks.
- Ultrasonic NDT techniques employing steady state or impulse signals to probe the surface or near-surface layer of the material for structural faults.

- Mechanical impedance techniques to probe deeper into the material for structural faults using steady state or impulse signal processing techniques. For example, the shape of a compression wave reflected from the interface of a structural fault in a solid material may be able to provide an indication of structural damage in much the same way that seismic signals are used in the geological exploration for oil deposits.
- Measurements of the mechanical surface impedance. This technique involves the measurement of structural velocity which is convenient due to the direct relationship that exists between structural velocity and strain or stress (Hunt, 1960). Some consideration was given to the possibility of using a laser velocimeter for taking such impedance measurements. The major advantage is that the technique allows very small velocities to be measured directly with the use of a laser doppler technique. However, due to the cost of the equipment and the potential difficulty of operating such a unit in the field, further exploration was dropped. Subsequent discussions with research personnel involved in utilizing a laser velocimeter for field measurements of velocity response of the ground to acoustic excitation also indicated that there are, indeed, difficulties associated with the effective use of such an instrument in the field due to its extreme sensitivity (Sebatier, 1988).
- For metallic building materials, the use of surface penetrating dies may be suitable to explore for surface faults (Bailey and Kraska, 1970).
- Mechanical or low power laser profilometers or photographic techniques for evaluation of surface conditions on material such as old adobe or Indian petroglyphs.
- Other NDT testing techniques, such as X-ray photogrammetry or magnetic flux measurements are not expected to prove useful in this program due either to their relative complexity (e.g., X-ray systems) or their lack of suitability for evaluating potential damage to the type of non-metallic materials that are of primary concern for this program.

2.3.1 Field Techniques Selected

After considering all of the practical aspects of applying the above techniques in the field, the following were selected as suitable for this program for trial evaluation.

- Pre- and post-exposure photographic records of the surface defects (i.e., cracks). This was considered to be the simplest way to obtain and document objective data on surface conditions of brittle materials. The technique has been frequently employed in the past in studies of building damage from sonic boom (e.g., Wiggins, 1969) and blast (Siskind, et al., 1980a, b).
- Pre- and post-exposure measurements of mechanical impedance using impulsive and sine-sweep techniques were utilized with limited success. An impedance hammer to measure force and acceleration simultaneously was utilized for impulse measurements. An electrodynamic wall-driver provided a means of obtaining frequency response information for small wall areas.

The results of this exploratory effort have provided a brief evaluation of possible experimental measurement methods for evaluating pre- and post-exposure conditions of unconventional structures.

Measurements of each of the unconventional structures were taken before and after the exposure to actual sonic boom loading. In all cases, the key objective of these measurements was to determine whether or not the application of the real sonic boom loading showed consistent and demonstrable evidence of damage. A secondary objective was to provide a valid demonstration of the feasibility of carrying out such measurements in the future, with the photographic and mechanical impedance techniques evaluated. Results of applying these methods are given in Section 5.

2.3.2 Summary of Sonic Boom and Blast Damage Inspection Techniques from Previous Studies

A brief review of techniques used in previous studies of structural damage from exposure to sonic booms or air blast overpressures is helpful, at this point, to understand the basis for the techniques selected for this study. The techniques employed in the past have generally involved the luxury of labor-intensive procedures and a long observation period, neither of which were feasible for this program.

2.3.2.1 Evaluation of Structural Damage from Sonic Booms

While many programs have been conducted which involved the measurement of structural response to sonic boom (see Appendix A and Hubbard, et al., 1986), only two

programs have included any significant amount of objective examination of structural damage over a substantial period of time and for a large number of sonic boom exposures.

These were the NASA/USAF tests near Indian Springs, Nevada (Maglieri, et al., 1966) and the White Sands Missile Range tests (Wiggins, 1965). Only glass damage was recorded at the Indian Springs test. Glass, plaster and bric-a-brac damage was recorded during the White Sands test program. Two other test programs, Oklahoma City (Andrews, et al., 1965), and Edwards Air Force Base (Kryter, et al., 1966) have been conducted which involved direct measurement of structural response, but no damage occurred in the test structures.

In the Indian Springs tests, the window test specimens were carefully constructed and located on one side of small closed boxes which served as test jigs (Maglieri, et al., 1966). This mounting does not correspond to a real window configuration in a building. The only substantial window damage from the White Sands tests, involving some specially built test buildings and existing buildings, occurred during one unscheduled flight where the overpressure reached 38 psf (Wiggins, 1965).

In neither test was there any observation of glass fragments being propelled beyond the window frame as was observed in a low altitude supersonic flight test when the peak sonic boom overpressures were as high as 120 psf (Nixon, et al., 1968). A unique window damage pattern occurred for this test that has not been reported anywhere else. The structural damage reports from these tests, while qualitative, deserve more careful examination.

The Indian Springs test program (Maglieri, et al., 1966 and Nixon, et al., 1968) is the only controlled sonic boom test program conducted in the United States which exposed any normal structure to sonic boom above 30 psf overpressure. The structure consisted of "very old frame and brick buildings in poor states of repair and both old and new campers and trailers." No building response measurements were obtained at the two building sites (the towns of Belmont and Stone Cabin, Nevada). The principle findings from these tests were:

- At the nearly abandoned town of Belmont, the maximum overpressures measured were 24 and 33 psf for the two overflights which passed about 2,600 feet from the town center (2,000 feet from the nearest building).
- At Stone Cabin ranch, the maximum overpressure was 50 psf (at 6 ft above the ground at 1 mile from the track) for the one overflight at an altitude of 210 ft.

- Damage was confined to glass breakage, plaster cracking, and furnishings (bric-a-brac) falling from shelves.
- Usually glass breakage (at these buildings) occurred for the window facing the on-coming aircraft and, in some instances, glass fragments were propelled up to 12 ft.
- A small side window of a camper parked 100 ft from the track (where overpressure would have been of the order of 50 to 100 psf) was also broken and glass (fragments) flew as far as 12 ft in the direction of the aircraft approach.

For the White Sands tests the damage ranged, in a rough scale of increasing damage, from (a) spalling of old cracks, to (b) hairline extension of existing cracks to (c) falling plaster, for damage threshold overpressures ranging from 3.3 psf to 16 psf (Wiggins, 1965). Specific values for damage threshold reported from the White Sands Tests for interior walls and ceilings are given in Table 2-5. These damage threshold levels proposed in Wiggins, 1965 are useful for perspective for this program but do not necessarily apply to the categories of unconventional structures listed in Table 2-4.

2.3.2.2 Identification of Sonic Boom Damage

The most common form of structural damage from sonic boom other than window breakage, consists of cracks in interior surfaces. A number of guidelines have been developed for the identification and quantification of such damage due to both sonic boom and other causes and some of these guidelines are considered here.

From Mayes and Edge, 1964: "Discoloration, dirt penetration, and cracked edges are the basis of determining the age of cracks (e.g., old cracks may not be due to sonic boom)."

From Wiggins, 1965: "Damage to plaster and gypsum board caused by sonic boom is broken down into three categories of increasing severity of damage.

- "Slight spalling of old cracks. A little dust will fall from an existing crack that can be seen by a very observant person or a trained observer.
- "Fine or hairline cracks will extend from old ones. Extension is usually less than about 4 inches and can be detected only upon very close examination.

Table 2-5

Maximum Safe⁽¹⁾ Predicted or Recorded Peak Sonic Boom Overpressure for
Representative Building Materials on Interior Walls and Ceilings
(Adapted from Wiggins, 1965)

	Material	P _f , Peak Pressure, psf	
		Minor ⁽²⁾	Major ⁽³⁾
1.	Plaster on wood lath	3.3	5.6
2.	Plaster on gyplath	7.5	16
3.	Plaster on expanded metal lath	16	16
4.	Plaster on concrete block	16	16
5.	Gypsum board (new)	16	16
6.	Gypsum board (old)	4.5	16
7.	Nail popping (new)	5.4	16
8.	Bathroom tile (old)	4.5	8.5
9.	Damaged suspended ceiling (new)	4.0	16
10.	Stucco (new)	5.0	16

- (1) Less than one chance in 10,000 when within five miles of flight track. This corresponds to a 99.99 percent confidence that damage will not occur.
- (2) Small (less than three inches) hairline crack extensions or pre-damaged paint chipping or spalling.
- (3) Falling plaster or tile, etc.

- "Plaster falls, part of a ceiling or a loose piece of wall plaster may fall to the floor."

This semi-quantitative scale of crack damage is consistent with a very similar scale defined by the U.S. Bureau of Mines for crack damage from blasting operations (Thoenen and Windes, 1942).

2.3.2.3 Parameters Influencing the Occurrence and Detection of Cracking

Considerable knowledge exists on natural forces and mechanisms that cause structural damage (e.g., "differential settlement" of soils, lumber shrinkage and swelling from humidity changes, etc.), and is useful for damage claim investigations and support of damage claims litigation. Comprehensive summaries are given in Wiggins (1969, 1965) for experience in the U.S., and in Wilhelmsen and Larsson (1973) for experience in Sweden. This knowledge can provide strong support for preexistence of the damage or to show it was obviously caused by something other than sonic booms.

Thus, structures exposed to sonic booms can crack for a variety of reasons which have nothing to do with the sonic booms for a variety of reasons including (Wiggins, 1965):

- (1) Ratio of inside to outside surface and air temperatures
- (2) Range of inside and outside humidity (i.e., temperature and humidity influence the amount of shrinking of wood frame members which is a major source of cracking of interior surfaces).
- (3) Intensity, duration and direction of wind
- (4) Differential settlement of building foundation
- (5) Room volume, wall and ceiling area
- (6) Orientation of walls to solar heat input
- (7) Type of skin, frame, exterior materials and interior finish
- (8) History of patching
- (9) Presence of water leaking from pipes onto building structure

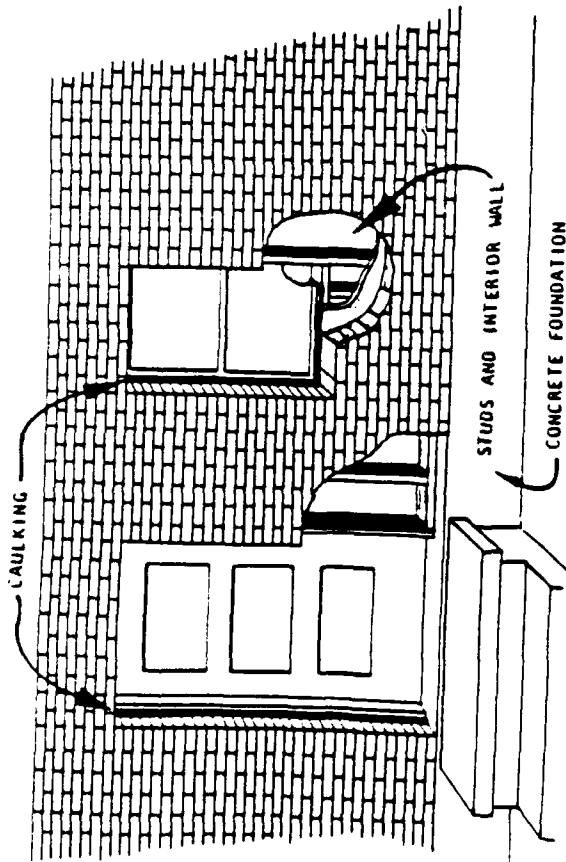
Most of these factors apply to unconventional structures just as well as they apply to conventional structures. Figure 2-3 illustrates more graphically some of these natural causes for cracking.

The factors which influence the magnitude of the dynamic loading and stress response of structures and hence influence the occurrence of cracking from sonic boom include (Sutherland, 1968a):

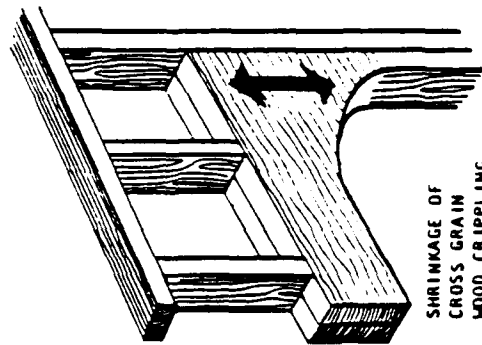
- (1) Magnitude of peak pressure of sonic boom
- (2) Wave form and duration of pressure pulse from sonic boom.
- (3) Direction of arrival of sonic boom relative to building surface.
- (4) Relative rigidity (or impedance) of surface exposed to sonic boom.
- (5) Presence and position of nearby reflecting surfaces, including the ground.
- (6) The total number of booms experienced (i.e., the effect of cumulative exposure).
- (7) The dynamic response characteristics of the structure, including its resonant frequencies, mode shape, damping, location of walls on outside or inside of structure, and presence of windows or doors.
- (8) The structural strength of the material at the time of exposure to the sonic boom.

The factors which influence the ability to observe and record cracks in structures are (Wiggins, 1965):

- (1) Frequency of observation
- (2) Objectivity of observers
- (3) Maintenance of the same observers throughout the program
- (4) Rotation of observers to randomize their effect
- (5) Application of positive crack recording methods
- (6) Analysis of data on crack length times number of cracks

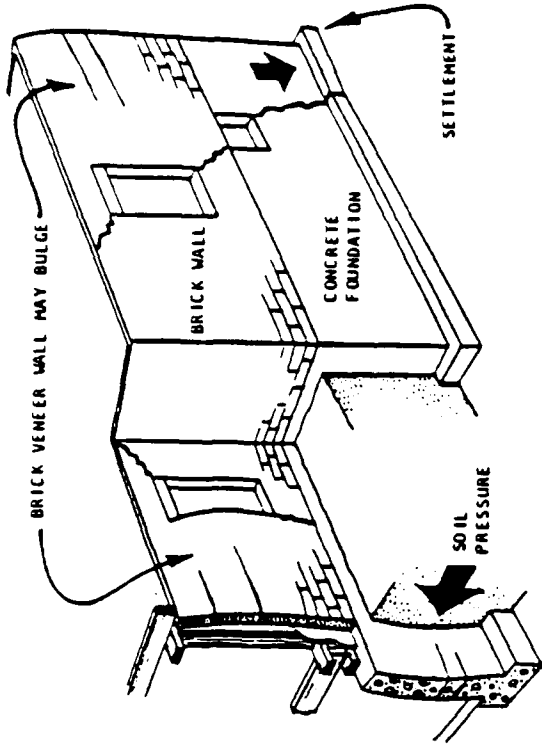


(a) Receding of Doors and Windows in Veneer Structures

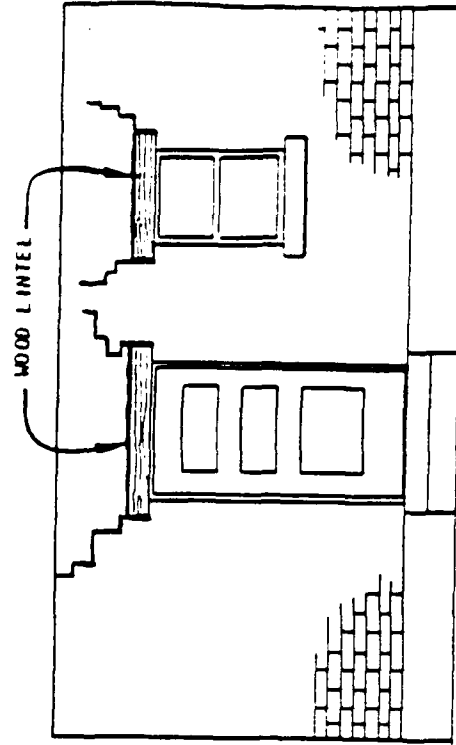


TYPICAL CRACKS AT
PLASTERED ARCH

(c) Cracks Over Interior Plastered Arches



(b) Cracks Resulting from Foundation Failure



(d) Masonry Cracks Resulting from Use of Wood Lintels

Figure 2-3. Examples of Cracking Damage in Structures from Natural Causes (Adapted from Wiggins, 1969).

- (7) Correlation between cracking data from sonic boom exposure and pre-exposure time periods (i.e., it is best to use the same position on the same structure for each of the two observation periods).

In summary, methods of damage assessment employed in the past have stressed techniques that, with the exception of crack length measurements and analysis, are often difficult to quantify objectively. The technique depends to a very large extent on the skill and experience of the inspector in applying consistent methods to achieve reliable results. Photographic records of crack damage, carefully and systematically obtained, seem to offer one of the best methods which should maximize objectivity of results and, except for experience in skilled interpretation, minimize the experience requirements for acquisition in the field. This technique would seem to be a very suitable one for use by the USAF for damage assessment.

3.0 SONIC BOOM ENVIRONMENT

This section addresses the definition of the sonic boom environment. Practical statistical models are required for the magnitude of the sonic boom overpressures for different types of supersonic flight training operations which are, or may be, carried out by the USAF. The following three items exemplify the diversity of these operations.

- Air Combat Maneuver Training (ACM) carried out within an elliptically shaped area about 35 by 60 miles at altitudes from 5000 to 40,000 ft at Mach numbers primarily from 1 to 1.1 with some small amount at Mach numbers to 1.3 (Galloway, 1983; Plotkin, et al., 1989).
- Supersonic Corridor flight activity. Usually carried out at high altitudes but occasionally below 5000 ft, along a straight flight track (Plotkin, 1985b).
- Low altitude supersonic flight. Although not currently carried out, at least not outside Federally-controlled land, such low altitude supersonic flight activity might potentially consist of a number of short level flight sections initiated and terminated by short periods of acceleration and deceleration respectively and/or abbreviated maneuver sections (i.e., turns); all at altitudes from about 100 to 1000 ft (Plotkin, 1989b).

A useful model for predicting potential structural damage from sonic booms of any magnitude can be established without defining the actual sonic boom pressures for all types of supersonic flight operations. However, it was felt that a practical approach for ACM-generated sonic booms requires that some minimum definition of actual sonic boom environments be provided, so that within one report, the overall assessment of damage potential can be accomplished for this dominant type of supersonic flight activity without a separate evaluation of the sonic boom environment itself. The inherently random, unpredictable nature of ACM operations dictates the necessity of relying on actual measured sonic boom data to validate conceptual models for predicting their sonic boom environments. Fortunately, the results of a recent comprehensive study, summarized in the following section, are available for this purpose.

For the second and third types of supersonic flight activity identified above, the flight operations are more deterministic, and well-validated theoretical models for predicting sonic boom environments can be safely utilized (Plotkin, 1989a). No attempt is made to generalize the many types of supersonic flight operations possible for these two categories of supersonic

flight. However, representative theoretically predicted and experimentally validated values for sonic boom overpressures are presented in a following section for the convenience of the reader and to make it possible to provide preliminary predictions of possible damage for such flight operations.

In all cases, following the procedure adopted in Hershey and Higgins, 1976, the basic sonic boom environment will first be defined in terms of a nominal "free-field" pressure P_0 , that is, by convention for sonic boom prediction, the pressure that actually exists at the surface of a reasonably hard reflecting ground. Thus P_0 inherently includes a pressure increase, due to reflection, normally taken as approximately 2, over the truly free field pressure that would exist in the absence of any reflecting surface (Plotkin, 1989a).

Next the actual sonic boom pressure P_f that exists under field conditions is defined in terms of the statistics for the ratio between the nominal value P_0 and the actual value P_f that differs from P_0 due to variations in weather and in the actual flight speed and altitude of the supersonic aircraft compared to the nominal or average values for that flight condition.

Finally, the effective sonic boom pressure loading on a structure is defined in terms of the ratio between the effective pressure P_e and the actual incident (free field) pressure P_f . The ratio reflects the change in effective pressure loading on a structure as a result of the direction of arrival of the sonic boom relative to the surface it strikes, the effective "acoustic impedance" of the surface (restricted to consideration of the relative solidity of the surface, i.e., the amount of openings), and the effect of differences in pressure time history on the effective loading.

3.1 Sonic Boom Environment for ACM Activity

ACM flight activity represents the most common of the three types of supersonic flight activity identified above and will be emphasized in this report. A previous study of 21 supersonic F-15 flight tracks in the Oceana ACM area predicted that the general geographical structure of the sonic boom environment under such an area would have an elliptical pattern (Galloway, 1980). Aerial combat training is carried out within a Supersonic Operating Area (SOA) by two (or more) adversary aircraft who initiate their engagement at opposite ends of a basic engagement line (i.e., the major axis of the ellipse). Using measured flight track data and a simple "carpet boom" predictive model for the sonic boom pressures, the spatial distribution of predicted noise levels were found to exhibit an elliptical pattern due to the basic nature of aerial combat training maneuvers. Examination of an expanded flight track data base for 78 sorties from Luke AFB and 18 from Nellis AFB (about 50% of the total were F-15s) tended to

confirm this ellipse concept for modeling the noise (Galloway, 1983). As discussed later, the remaining quantitative aspects of the improved model appeared to have overestimated the actual cumulative noise environments within an SOA by as much as 10 dB. Nevertheless, these initial studies provided useful preliminary information for application to a general ACM noise model that had to evolve from actual noise measurements.

Although every supersonic flight generates a sonic shock wave, some of the shock waves are refracted by the atmosphere and never reach the ground, as illustrated in Figure 3-1 by the boundary of aircraft speed and altitude (Carlson, 1978). However, this figure only applies to straight and level flight; booms generated by aircraft accelerating in a dive can reach the ground at lower speeds and altitudes than indicated by these boundaries (Galloway, 1983; Plotkin, 1989a). The first opportunity to validate these concepts for ACM sonic boom environments by actual acoustic measurements of the sonic boom pattern on the ground captured only 11 booms over an array of 17 monitors deployed in the Reserve, New Mexico Supersonic Operating Area (Brown, et al., 1985). Although limited, these data were basically consistent with the elliptical shape of the concepts original model but indicated that the number of sonic booms per sortie according to the earlier model (Galloway, 1980) was overestimated.

3.1.1 WSMR Test Data

A vastly expanded validation program was completed in January 1989 at the White Sands Missile Range (WSMR) (Plotkin, et al., 1989). The key parameters which indicate the scope of the program are:

- Duration – 6 months
- Total number of sorties – 7019
- Number of sorties involving Air Combat Maneuver (ACM) Training – 4600
- Number of sorties involving other supersonic flight training – 2419
- Number of (ACM) sonic booms recorded – 506, equivalent to 0.11 booms occurring somewhere within the SOA per ACM sortie
- Number of sonic boom monitors deployed in monitor array – 35
- Ground area covered by monitor array – 2757 square miles
- Average spacing between 22 monitors concentrated in the southwest quadrant of test area – about 6 miles

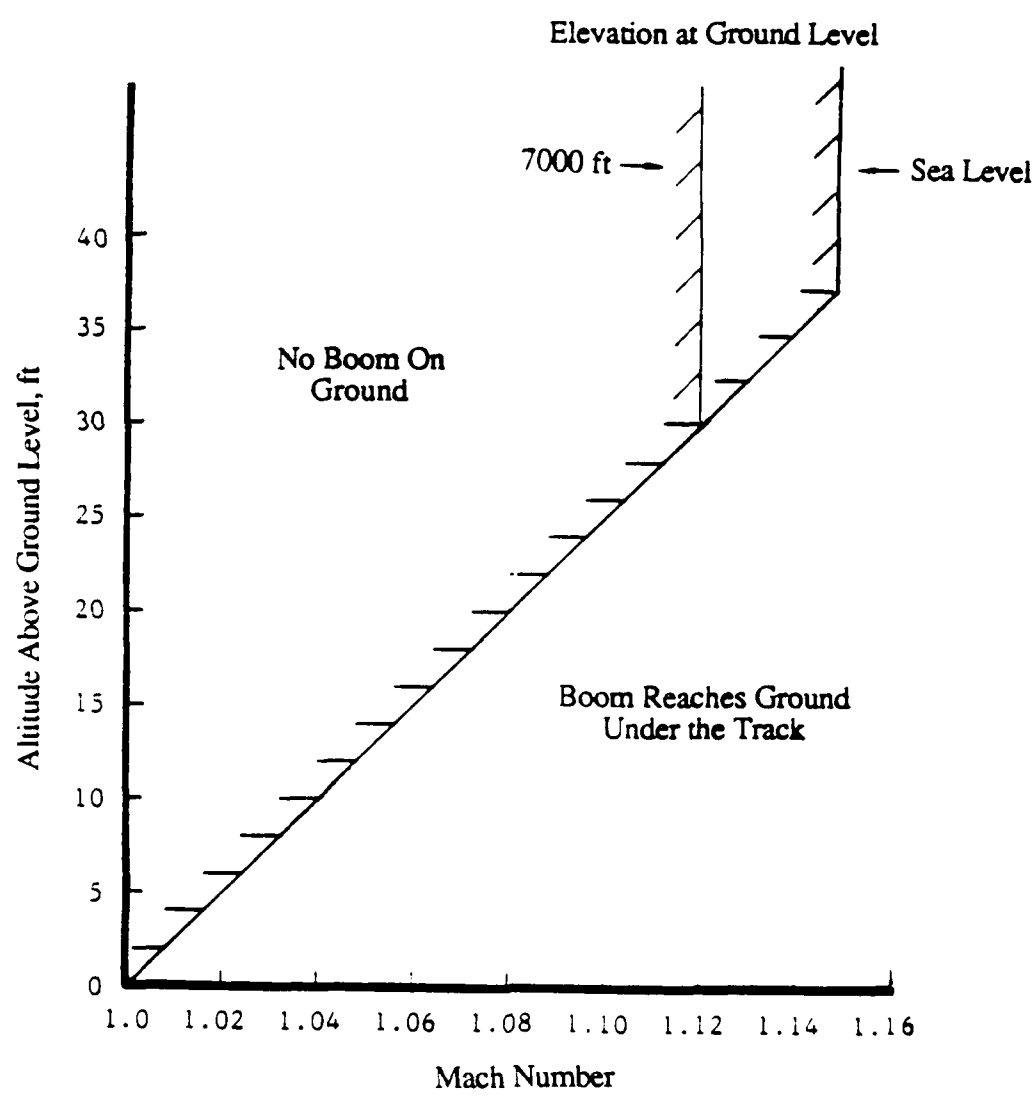
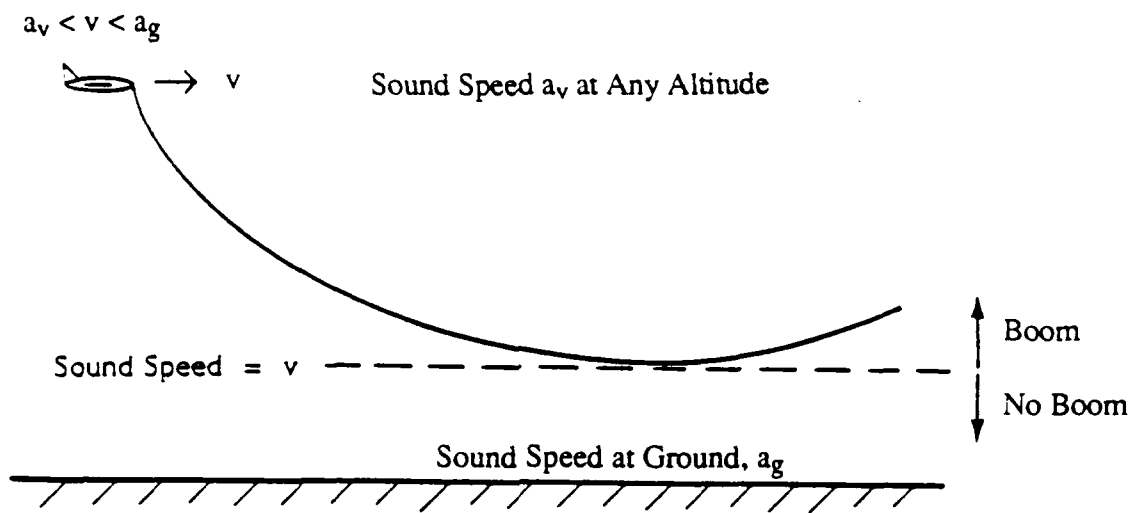


Figure 3-1. Speed and Altitude Limits for Booms to Reach Ground for Standard Atmosphere and Level Flight Conditions (from Carlson, 1978).

- Number of sonic boom records – 2246 (Each boom registered on an average of 3.8 separate monitors. In all cases, the sonic boom monitors measured the actual "free field" pressure at the ground and thus included the pressure doubling factor mentioned earlier.)
- Number of sonic booms recorded on each monitor – 8 to 112 with an average of about 64 over the 6 month test period.
- Average number of days of active measurement per monitor – 158
- Number of supersonic ACM sorties evaluated in detail through computerized analysis of Air Combat Maneuvering Instrumentation (ACMI) records – 502

The aircraft employed for ACM training during this period were 71% F-15, 13% AT-38, 10% F-16, and 6% F-5. While the results can strictly be applied only to types of ACM activity very similar to that occurring during the WSMR test and dominated by the flight procedures employed for F-15 aircraft operating out of Holloman Air Force Base, the basic agreement between the results of this study and the previous studies insures that the geometric pattern of the sonic boom environment under an SOA is now well defined.

The key results of this program can be summarized in the form of two basic expressions which were selected on the basis of a careful mathematical analysis to establish a reasonable model to define the spatial variation in the Average Day-Night C-Weighted Sound Level in decibels (abbreviated as DNCL and symbolized by L_{CDN} in equations), and the spatial variation in the number of sonic booms, n , occurring on the ground per day (Plotkin, et al., 1989). These patterns, shown in Figures 3-2a and 3-2b in terms of the mathematically smoothed two-dimensional normal (Gaussian) distribution fit to the measured data, are described by:

$$L_{CDN} = 25 + 10 \cdot \text{Log}(N) + 10 \cdot \text{Log} \left\{ \exp \left(-\frac{1}{2} [(X/\sigma_x)^2 + (Y/\sigma_y)^2] \right) \right\}, \text{ dB} \quad (3-1)$$

$$n = 0.0012 \cdot N \cdot \exp \left\{ -\frac{1}{2} [(X/\sigma'_x)^2 + (Y/\sigma'_y)^2] \right\}, \text{ booms/day} \quad (3-2)$$

where N = Number of ACM sorties per month

X, Y = the distances from the center of the ellipse along the minor and major axes respectively.

σ_x = standard deviation of DNCL pattern along the minor axis of the ellipse = 11.1 miles

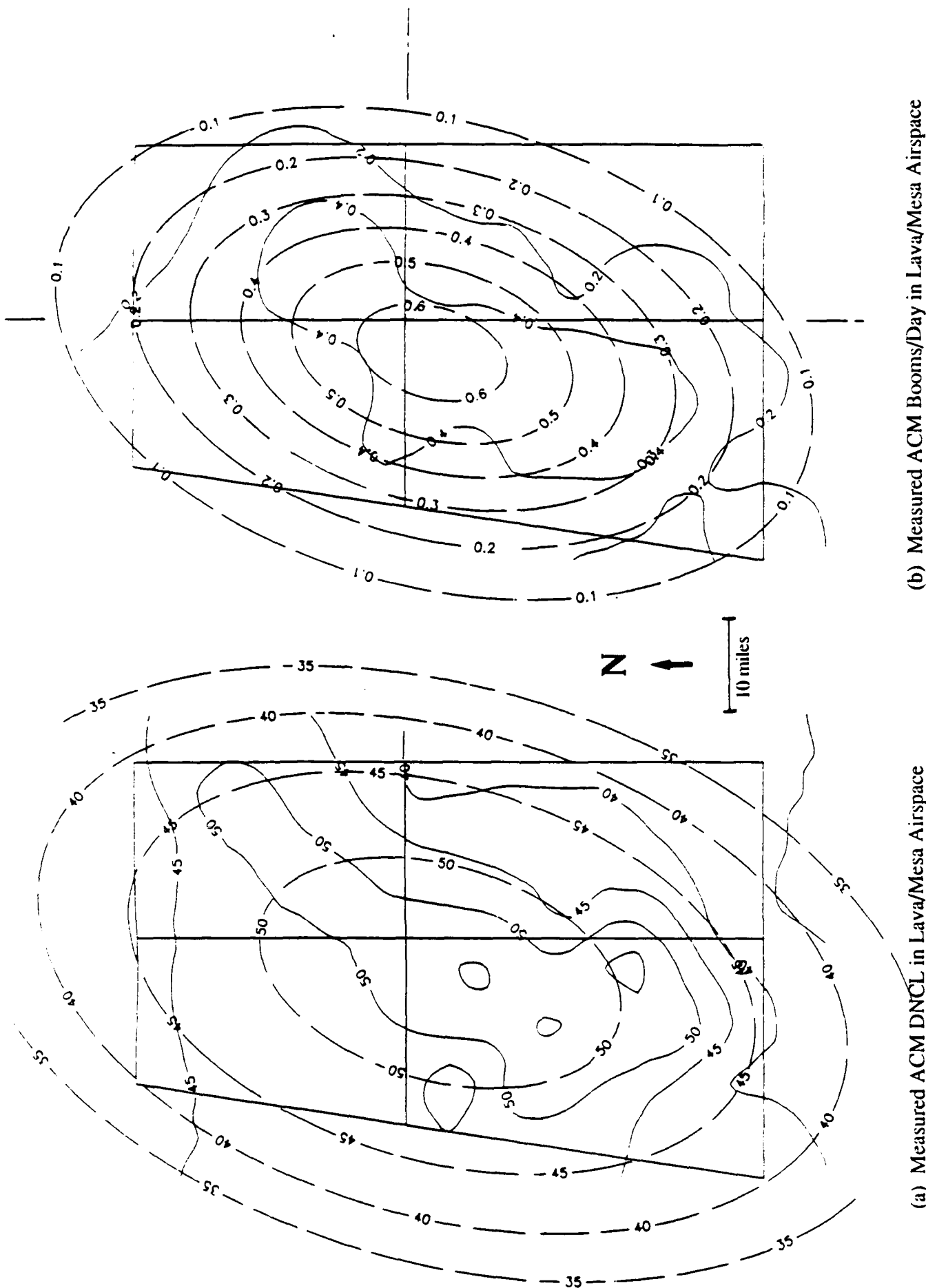


Figure 3-2. Contours of Measured Values and Gaussian Distribution Models Fitted for DNCL and Number of Sonic Booms per Day from WSMR Tests (Based on 550 ACM Sorties per Month) (from Plotkin, et al., 1989).

σ_y = standard deviation of DNCL pattern along the major axis of the ellipse = 18.9 miles

σ'_x = standard deviation of pattern for n along the minor axis of the ellipse = 13 miles

σ'_y = standard deviation of pattern for n along the major axis of the ellipse = 21.4 miles.

This refined model, based on actual noise measurements, retains the concept of noise contours in the form of elliptical patterns, but differs from the earlier model in three aspects:

- (1) The ellipses are described by two-dimensional Gaussian (normal) distribution curves that have exactly the same shape (for a given type of contour) regardless of their size. This contrasts with the use of separate power law fits for each axis of the two-dimensional flight track data distribution in the earlier model. This caused the ellipse shape (i.e., eccentricity) to change with its size (Galloway, 1983). There is no obvious justification for one approach over the other. However, a careful mathematical analysis of the large data base of measured noise levels from the WSMR tests considered several analytical forms to fit the data, including power laws. The two-dimensional Gaussian distribution produced the best fit (Plotkin, et al., 1989).
- (2) The predicted maximum number of sonic booms which reach the ground per sortie was 0.1, according to the measurements which is less by a factor of about 8 than the estimate of 0.8 in the earlier model (Galloway, 1983). However, it must be acknowledged that this measured number is strictly valid for the operations at the WSMR range but is believed to be a more valid estimate of the real situation.
- (3) As explained below, the measured WSMR data indicate a lower figure for the long time average peak sonic boom pressure at the center of the ellipse.

It is important to recognize that the patterns shown in Figure 3-2 are for a specific number (N) of 550 ACM sorties per month corresponding to the approximate average experienced during the WSMR measurement program. These expressions also provide one basis for predicting the spatial variation in the long time average value of the peak pressure for each of the sonic booms

occurring under the SOA. To develop this pattern, it is only necessary to combine Eqs. (3-1) and (3-2) to eliminate the variable N . The result can be given in the form of the usual expression for the total Average Day-Night C-Weighted Sound Level from a series of n single events (all in the daytime) which have a constant C-Weighted Sound Exposure Level (abbreviated CSEL and symbolized by L_{CE} in equations). To combine Eqs. (3-1) and (3-2) it was necessary to assume that the values of the standard deviations (σ'_x and σ'_y) for the "n ellipse" are simply scaled up by a constant factor from the corresponding values for the "DNCL ellipse." In fact, the ratios (σ'_x/σ_x) and (σ'_y/σ_y) are equal to 1.13 and 1.17 respectively, so that a constant value of 1.15 was assumed for this scaling ratio between the two ellipses.

Based on this assumption, the result of combining Eqs. (3-1) and (3-2) to eliminate N is:

$$L_{CDN} = 25 + 10 \text{ Log } (n/[0.0012 \exp (-\frac{1}{2}Z^2 c^2)]) + 10 \text{ Log } [\exp(-\frac{1}{2}Z^2)], \text{ or}$$

$$L_{CDN} = [25 + 29.2 + 49.4] + (1-c^2) 10 \text{ Log } [\exp (-\frac{1}{2}Z^2)] + 10 \text{ Log } (n) - 49.4, \text{ or}$$

$$L_{CDN} = 103.6 + 2.44 \text{ Log } \exp [(-\frac{1}{2}Z^2)] + 10 \text{ Log } (n) - 49.4, \text{ dB}$$

from which one obtains the expression for the C-Weighted Sound Exposure Level, CSEL as

$$L_{CE} = 103.6 + 2.44 \text{ Log } [\exp (-\frac{1}{2}Z^2)], \text{ dB} \quad (3-3)$$

where $Z = [(X/\sigma_x)^2 + (Y/\sigma_y)^2]^{1/2}$, a dimensionless distance

and $c = 1/1.15$, the inverse of the average ratio between the standard deviations of the "n" and "DNCL" ellipses (e.g., $\sigma'_y/\sigma_y = 1.13$, $\sigma'_x/\sigma_x = 1.17$).

The resulting constant 103.6 dB is the apparent long time average C-Weighted Sound Exposure Level in dB at the center of the ellipse (where $X, Y = 0$). This number may be compared with the estimated long time space average value at the center of the ellipse for the C-Weighted Sound Exposure Level of 100.3 (for F-15 fighters operating in the Luke SOA) developed from the earlier study (Galloway, 1983). (The constant 49.4 is a basic correction factor which is an inherent part of the definition for DNCL and which is equal to 10 times the logarithm to the base 10 of the number of seconds in a day.)

The C-Weighted Sound Exposure Level of a sonic boom is a logarithmic measure of the time-integrated square of the acoustic pressure which has been frequency-weighted to

attenuate frequency components below about 20 Hz. Such a frequency-weighted measure of a sonic boom pressure signal drastically changes the true time history (see Figure 3-3) but faithfully registers the peak pressure of the sonic boom overpressure pulse and its duration and thus retains basic information pertinent to the acoustic loading of sonic booms on most structures (Sutherland, 1968a, 1985).

3.1.2 Spatial Variation of Peak Pressure from WSMR Data

As indicated in Figure 3-3, the value of the peak flat (unweighted) sound pressure L_{pk} (94 dB for the example 1 Pa peak N-wave illustrated) is 24 dB above the C-Weighted Sound Exposure Level, CSEL of 70.0 dB. This is a computed value based on a mathematical model for the response of a sound level meter, with and without C-weighting, to an ideal N-wave (Sutherland, 1985). A digital analysis of 42 graphic records of measured sonic boom waveforms more representative of the type generated by ACM activity, carried out in Galloway, 1983, showed that the difference between L_{pk} and L_{CE} had an average value of 24.6 dB with a standard deviation of 2.59 dB. Spectrum analysis of seven of the sonic booms measured for the WSMR tests produced an average value of 25.0 ± 1.0 dB for the difference between L_{pk} and L_{CE} (Plotkin, et al., 1989). The weighted average value for this difference for all of these data is 24.7 dB with an estimated standard deviation of 2.4 dB. This average measured value is utilized here to convert Eq. (3-3) into an expression for a first approximation for the long time average peak pressure due to ACM activity anywhere in the WSMR SOA. This first approximation can be derived from the first two terms in Eq. (3-3) which define the C-Weighted Sound Exposure Level L_{CE} as a function of position X,Y. Thus, since the sound pressure level for a 1 psf sound pressure is 127.6 dB:

$$20 \text{ Log } [P_{pk}(\text{psf})] = L_{pk} - 127.6 = L_{CE} + 24.7 - 127.6, \text{ dB or}$$

$$20 \text{ Log } [P_{pk}(\text{psf})] = 103.6 + 2.44 \text{ Log } [\exp (-\frac{1}{2}Z^2)] + 24.7 - 127.6, \text{ or}$$

$$20 \text{ Log } [P_{pk}(\text{psf})] = 0.7 + 2.44 \text{ Log } [\exp (-\frac{1}{2}Z^2)], \text{ dB re: 1 psf, or}$$

$$P_{pk} (\text{psf}) = 1.08 \exp (-\frac{1}{2}[(X/\sigma_x)^2 + (Y/\sigma_y)^2])^{0.122}, \text{ psf} \quad (3-4)$$

where $\sigma_x, \sigma_y = 11.1$ miles and 18.9 miles respectively.

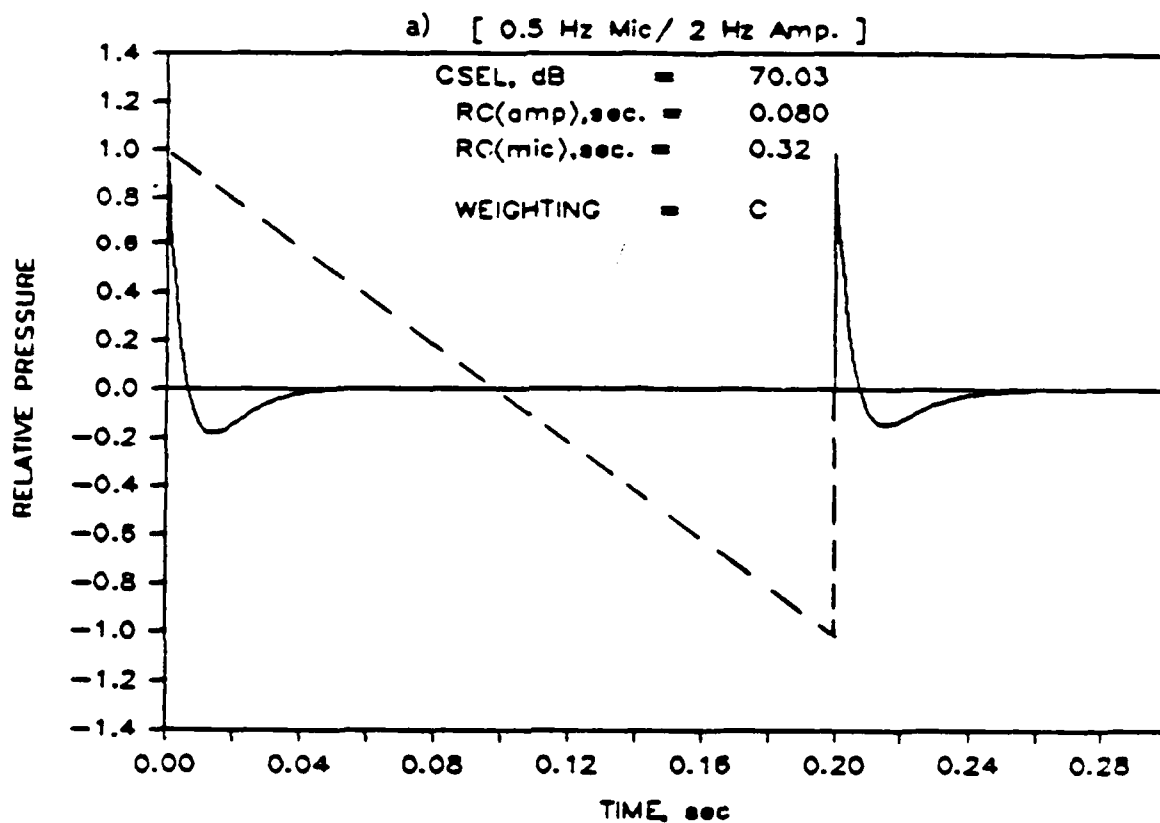
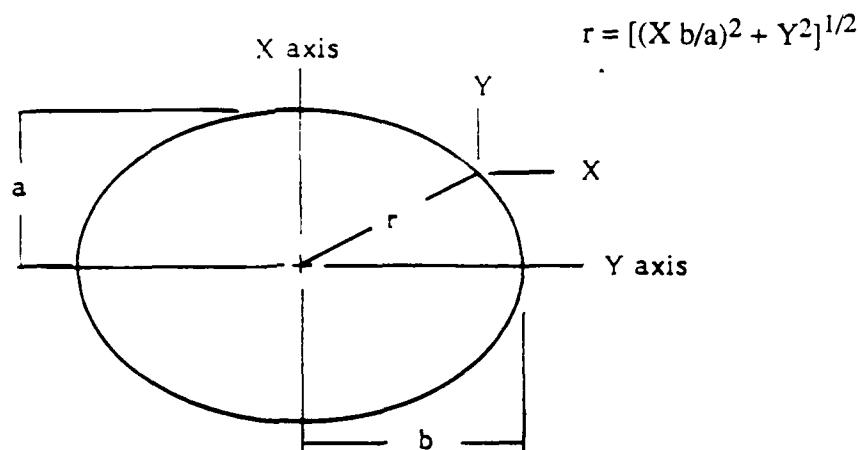


Figure 3-3. Computed C-Weighted Response of Sound Level Meter with Cut-Off Frequency of 0.5 Hz and 2 Hz for the Microphone and Pre-Amplifier Respectively to 0.2 Second N-Wave. Dashed line shows ideal N-wave (the SEL is a C-weighted value for an N-wave with a peak pressure of 1 μPa corresponding to a peak sound pressure level of 94.0 dB re 20 μPa). (From Sutherland, 1985.)

It is also desirable to compare this expression, derived from the mathematically smoothed fit to the measured spatial variation in long time energy average peak sound pressures, with the spatial variations in the raw, unsmoothed measured values from each measurement point for the WSMR test. The most convenient way to evaluate this spatial relationship in the measured data is to define the variation in the measured peak pressure as a function of a single distance variable identified here as an "elliptical radius" r illustrated in the following sketch.



Sketch of Concept of "Elliptical Radius"

This dimension r can be defined in terms of the basic equation for an ellipse which describes the shapes shown earlier in Figure 3-2. This equation can be expressed in two alternate forms as (Eshbach, 1952):

$$(X/a)^2 + (Y/b)^2 = 1 \quad (3-5a)$$

or
$$(X/b)^2 (b/a)^2 + (Y/b)^2 = 1 \quad (3-5b)$$

where $2a$ and $2b$ are the lengths of the minor and major "diameters" of the ellipse respectively.

Now, if the dimension X is transformed to $X' = X/(a/b)$, then Eq. (3-4b) can be expressed in the usual form for the equation of a circle as:

$$(X'/b)^2 + (Y/b)^2 = 1 \quad (3-6a)$$

or
$$X'^2 + Y^2 = b^2 = r^2 \quad (3-6b)$$

where r can be considered to be the constant radius of an ellipse that is transformed into a circle with the transformed coordinate X' and the unmodified coordinate Y . For a constant value of this radius $r = \sqrt{X'^2 + Y^2}$, the contour parameters in the elliptical pattern (i.e., the value of DNCL or n) are constant. This makes it possible, then, to examine the variation in the peak pressure of the sonic booms in terms of just one spatial variable - the elliptical radius r . Table 3-1 lists the summary data from the WSMR tests at each monitor station and defines the coordinates X, Y the transformed coordinate X' and the "elliptical" radius r for each measurement point as well as the long time arithmetic average and maximum peak pressure and DNCL.

Before the smoothed and raw measured values of the peak pressures can be compared, it is first necessary to convert both to the same statistical base. The smooth values (from Eq. (3-4) represent an energy average as required for computation of DNCL while the raw measured values represent an arithmetic average of the data. What is desired is the log mean value, which differs from the other two. The log mean is necessary to employ in this report for the statistical damage prediction model outlined in Section 2 for the case where the excitation (i.e., peak pressure) has a log-normal distribution. For a quantity Y' that has such a distribution, which is the case here, the ratio between the energy mean value, call it $\langle Y' \rangle$, and log mean value, call it Y'_L , and between the arithmetical mean value Y'_m and the log mean value Y'_L varies with the standard deviation, σ_L , of the log of Y' in the manner shown in Figure 3-4.

The values in Figure 3-4 were computed numerically for an arbitrary log-normal distribution of Y using the expressions:

$$\text{Energy Mean of } Y', \langle Y' \rangle = [(1/N) \sum Y_i'^2]^{1/2} \quad (3-7a)$$

$$\text{Arithmetic Mean of } Y', Y'_m = [(1/N) \sum Y_i'] \quad (3-7b)$$

$$\text{Log Mean of } Y', Y'_L = 1.0 \quad (3-7c)$$

$$\text{Probability density for } Y'_i = [1/\sigma_L \cdot \sqrt{2\pi}] \cdot \exp[-\frac{1}{2}(\text{Log}(Y')/\sigma_L)^2] \quad (3-7d)$$

where it is assumed for simplicity that the mean of $\text{Log } Y'$ is 0 (i.e., the log mean of Y' is 1).

As indicated by Figure 3-4, the ratios $\langle Y' \rangle/Y'_L$ and Y'_m/Y'_L increase at different rates, with increasing values of the standard deviation σ_L . As will be shown shortly, the peak pressures for the WSMR data did indeed have a log-normal distribution and the standard

Table 3-1

Summary of WSMR Measurements and Coordinates of Measurement Points in Terms of Actual (X, Y) and Transformed (X', Y and R) Coordinates Which Define the Ellipse Describing the Spatial Variation in Peak Pressure (Data from Plotkin, 1989)

Site No.	⁽¹⁾ ----- Coordinates -----			Radius R, of Equivalent Circle	CDNL (dB)	AVG Ppk (psf)	MAX Ppk (psf)
	X (Miles)	Y ⁽²⁾ (Miles)	X' ⁽³⁾ (Miles)				
2	-14.7	18.5	-24.6	30.8	45.6	0.49	2.61
3	-7.6	9.0	-12.7	15.6	47.0	0.59	4.42
4	-10.2	1.2	-17.1	17.1	48.6	0.64	2.62
5	-6.7	23.3	-11.1	25.8	46.3	0.65	3.69
7	6.2	32.3	10.3	33.9	40.4	0.64	1.59
8	11.9	26.1	19.9	32.8	53.2	0.60	4.42
9	7.6	12.3	12.7	17.7	51.4	0.72	4.22
10	5.7	6.7	9.5	11.6	50.4	0.74	3.94
11	-15.2	-1.0	-25.4	25.5	46.6	0.63	2.60
12	-10.7	-5.7	-17.9	18.8	40.5	0.56	1.40
13	-4.8	-3.3	-7.9	8.6	52.7	0.95	5.25
14	0.5	-1.4	0.8	1.6	55.2	1.19	6.67
15	-10.0	-10.5	-16.7	19.7	52.4	1.01	4.41
17	1.4	-6.7	2.4	7.1	55.8	0.70	5.25
18	-10.9	-19.5	-18.3	26.7	48.4	0.80	3.76
19	-7.6	-16.2	-12.7	20.6	51.3	0.89	6.61
20	-2.4	-12.8	-4.0	13.4	49.1	0.70	2.79
21	4.3	-12.8	7.2	14.7	52.2	0.96	3.05
22	-5.5	-21.6	-9.1	23.5	50.0	0.68	2.72
23	0.5	-18.1	0.8	18.1	52.4	0.92	4.26
24	6.7	-18.5	11.1	21.6	57.9	0.64	1.86
25	-7.4	-26.1	-12.3	28.9	42.9	0.65	3.13
26	-2.6	-28.5	-4.4	28.8	44.5	0.55	2.79
27	0.5	-25.9	0.8	25.9	54.6	0.59	5.89
28	-2.1	-33.3	-3.6	33.4	38.3	0.55	2.21
29	1.4	-30.9	2.4	31.0	45.9	0.65	3.41
30	-6.2	-35.6	-10.3	37.1	41.9	0.42	2.24
31	9.0	6.7	15.1	16.5	38.7	0.51	1.30
32	7.1	-5.7	11.9	13.2	50.4	0.72	5.12
33	8.8	-11.4	14.7	18.6	43.3	0.62	1.97
34	20.4	-11.9	34.2	36.2	41.7	0.51	1.76
35	11.4	-23.3	19.1	30.1	45.3	0.53	2.88
36	23.8	-19.5	39.7	44.3	37.6	0.52	0.99
37	12.3	-28.0	20.7	34.8	36.6	0.45	0.99
38	28.0	-27.1	46.9	54.2	35.8	0.39	1.09

(1) Origin located 3.6 miles south and 3.0 miles west of center of range.

(2) Y axis rotated 15.4 degrees clockwise from true north.

(3) $X' = X \cdot (\text{major cord/minor cord})$.

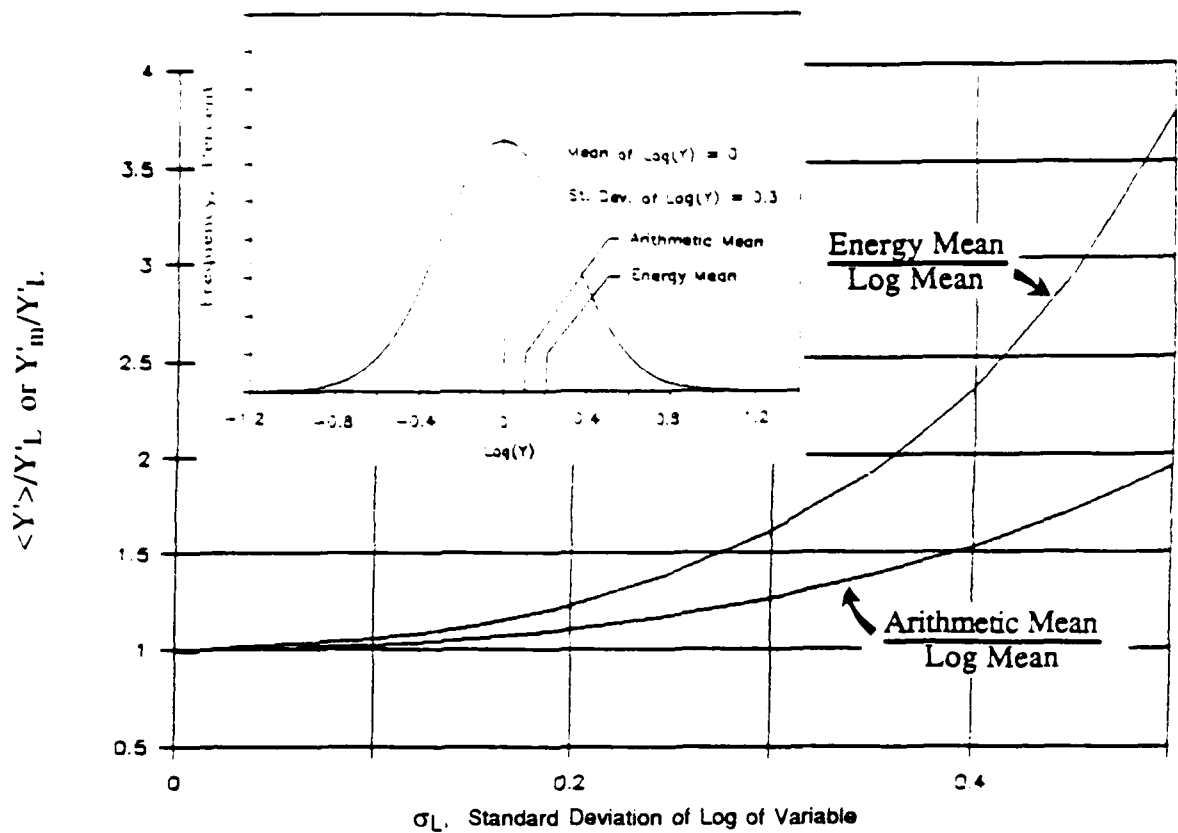


Figure 3-4. Relationship Between Energy, Arithmetic and Log Mean Values for Any Variable with a Log-Normal Distribution as a Function of the Standard Deviation of the Log of the Variable.

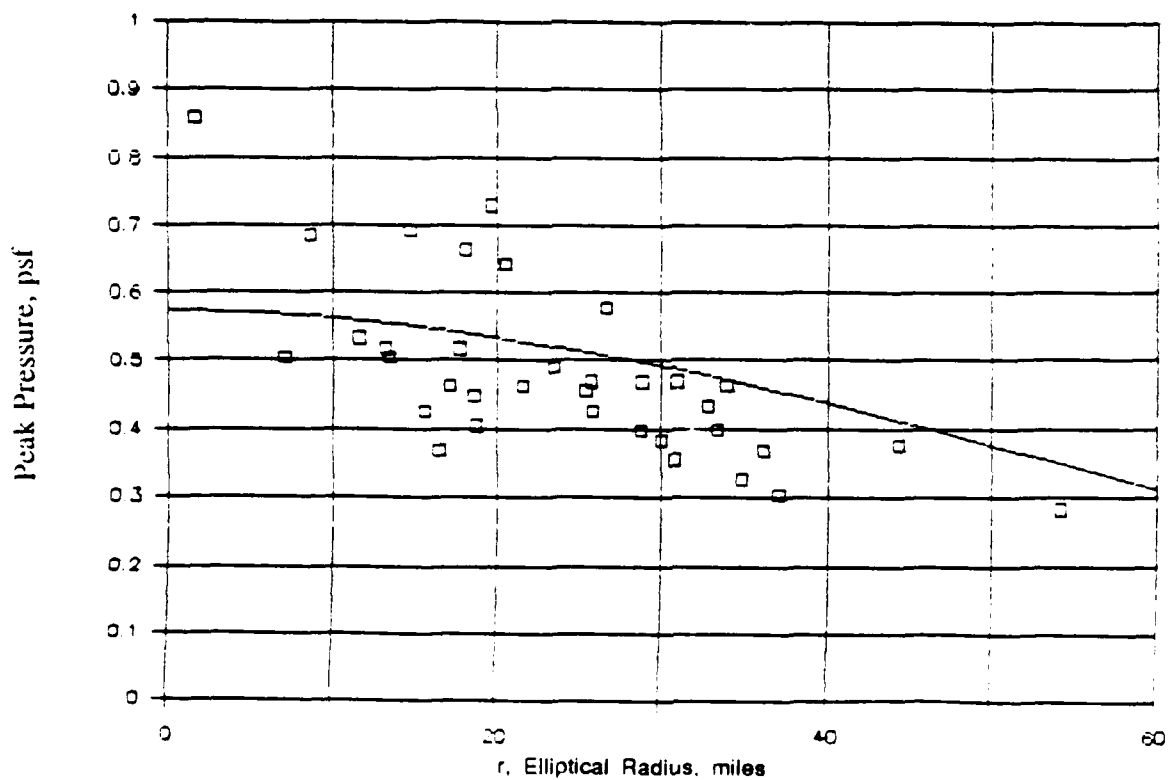


Figure 3-5. Comparison of Measured (□) and Predicted (—) Long Time Average Peak Pressures (Adjusted to Log Mean Values) as a Function of the Elliptical Radius (from WSMR data, Plotkin, et al., 1989).

deviation of this distribution corresponded to a value for σ_L of about 0.35 (equivalent to 7 dB).

For a value of σ_L of 0.35, the ratios $\langle Y' \rangle / Y'_L$, and Y'_m / Y'_L are 1.915 and 1.384 respectively. Thus, the long time energy average peak pressure predicted by Eq. (3-4) was converted to a predicted log mean by multiplying Eq. (3-4) by (1/1.915) to give the desired expression for the predicted spatial variation in the long time log mean value of peak pressure under an ACM area, identified here as the nominal value P_0 :

$$P_0 = 0.56 \exp (-1/2[(X/\sigma_x)^2 + (Y/\sigma_y)^2])^{0.122}, \text{ psf} \quad (3-8)$$

where σ_x and σ_y equal 11.1 and 18.9 miles respectively.

Correspondingly, the measured (arithmetic mean) long time arithmetic average peak pressures from Table 3-1 were multiplied by (1/1.384) to convert these data to the same log mean basis.

Figure 3-5 shows the relationship between the long time log mean peak pressure and the "elliptical radius r " based on the new Eq. (3-8) and the raw measured WSMR data listed in Table 3-1 after incorporating the above correction. The radius r is equal to $\sqrt{(X/0.6)^2 + Y^2}$ and X, Y are the true coordinates of the measurement points along the minor and major axes respectively of the SOA ellipse and the constant 0.6 is the approximate average ratio of σ_x to σ_y and σ_x' to σ_y' for the "DNCL" and "n" ellipses in Figure 3-2 (see Eq. (3-5)). While there is considerable scatter in the measured data about the prediction line of Eq. (3-8), the agreement is quite sufficient to demonstrate the basic validity of Eq. (3-8).

The standard deviation $\sigma_L(P_0)$ of the log of the long time average or nominal peak pressure data about the prediction line of Eq. (3-8) corresponds to a standard deviation in sound level of 1.67 dB. While other simpler forms of the relationship expressed by Eq. (3-8) between the nominal peak pressure and the elliptical radius r were possible, Eq. (3-8) was the preferred form due to the implicit interrelationship between the "DNCL" and "n" ellipses derived from Eqs. (3-1) and (3-2).

3.1.3 Model for Statistical Variation of Sonic Boom Peak Pressures in WSMR SOA

Eq. (3-8) establishes, for computational purposes, a model for a small but systematic spatial pattern for the otherwise random variation in the long time average or nominal peak pressure P_0 of sonic booms within an SOA. The remaining variation in peak pressure for any

one single sonic boom anywhere within the SOA needs to be defined. To establish a reliable estimate of the standard deviation of the log of P_f/P_o for any one sonic boom, it is assumed that the distribution of these peak pressures is made up of the combined effect of:

- the spatial pattern in long time average peak pressures at any position that is predicted by Eq. (3-8)
- the random deviation in individual long time average peak pressures at any position from the spatial variation of Eq. (3-8), and
- the residual random variance due to weather and aircraft speed and altitude deviations about long time averages.

This final source of variation could be expected to have a statistical variation, due primarily to weather, no less than the variation that has been observed in the past from controlled sonic boom tests (Maglieri, et al., 1969). However, for ACM operations, variations in aircraft speed and altitude should be much greater than for these controlled flight tests so that the overall variation in sonic boom pressures would also be greater. This is borne out by the cumulative probability distribution data in Figures 3-6 and 3-7. Figure 3-6 shows the distribution of the actual free field peak pressure P_f relative to the long term mean value at each measurement site (taken here to be the same as the nominal peak pressure P_o) for the controlled supersonic flight tests over Oklahoma City (Hilton, et al., 1964) and similar distribution data from the earlier ACM sonic boom monitoring test in the Reserve SOA (Brown, et al., 1985). For the Oklahoma City tests, the distribution is shown for three measurement points at 0, 5 and 10 miles to the side of the nominal flight track for one aircraft type. (The results were essentially the same for the other aircraft.) The Reserve SOA data represent the distribution of the CSEL, again relative to the long time average value at each monitor position, for all of the 54 boom-site records at 17 monitor positions. As explained earlier, CSEL correlates well with peak pressures for sonic booms. Similar distribution data measured for more precisely controlled tests at Edward AFB on weather effects on sonic boom signatures had slightly smaller standard deviations as shown in Figure 3-6 (Maglieri, et al., 1969).

In all cases, the distributions of the values of P_f/P_o (or the equivalent) are approximately log-normal over most of the range of variation, especially over the upper part where P_f/P_o is greater than 1. The approximate log-normal distributions for these data correspond to standard deviations $\sigma_L(P_f/P_o)$ of the log of the relative peak pressure as listed in Table 3-2. (20 times this standard deviation is the equivalent value in decibels.)

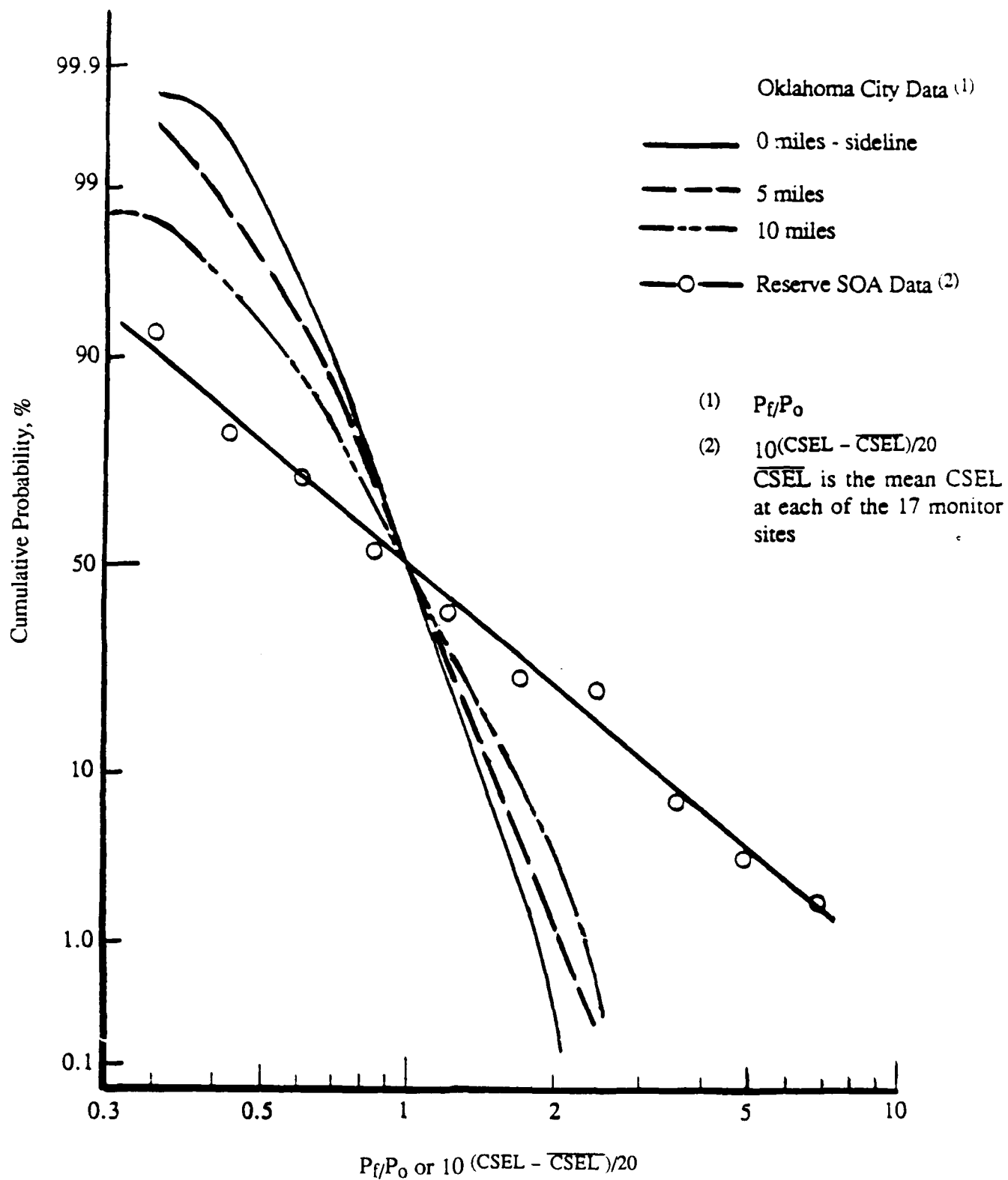


Figure 3-5. Cumulative Probability Distribution of Relative Peak Sonic Boom Pressures from Oklahoma City Test for Airplane A (Hilton, et al., 1964) and Relative C-Weighted Sound Exposure from Reserve SOA Test (Brown, et al., 1985).

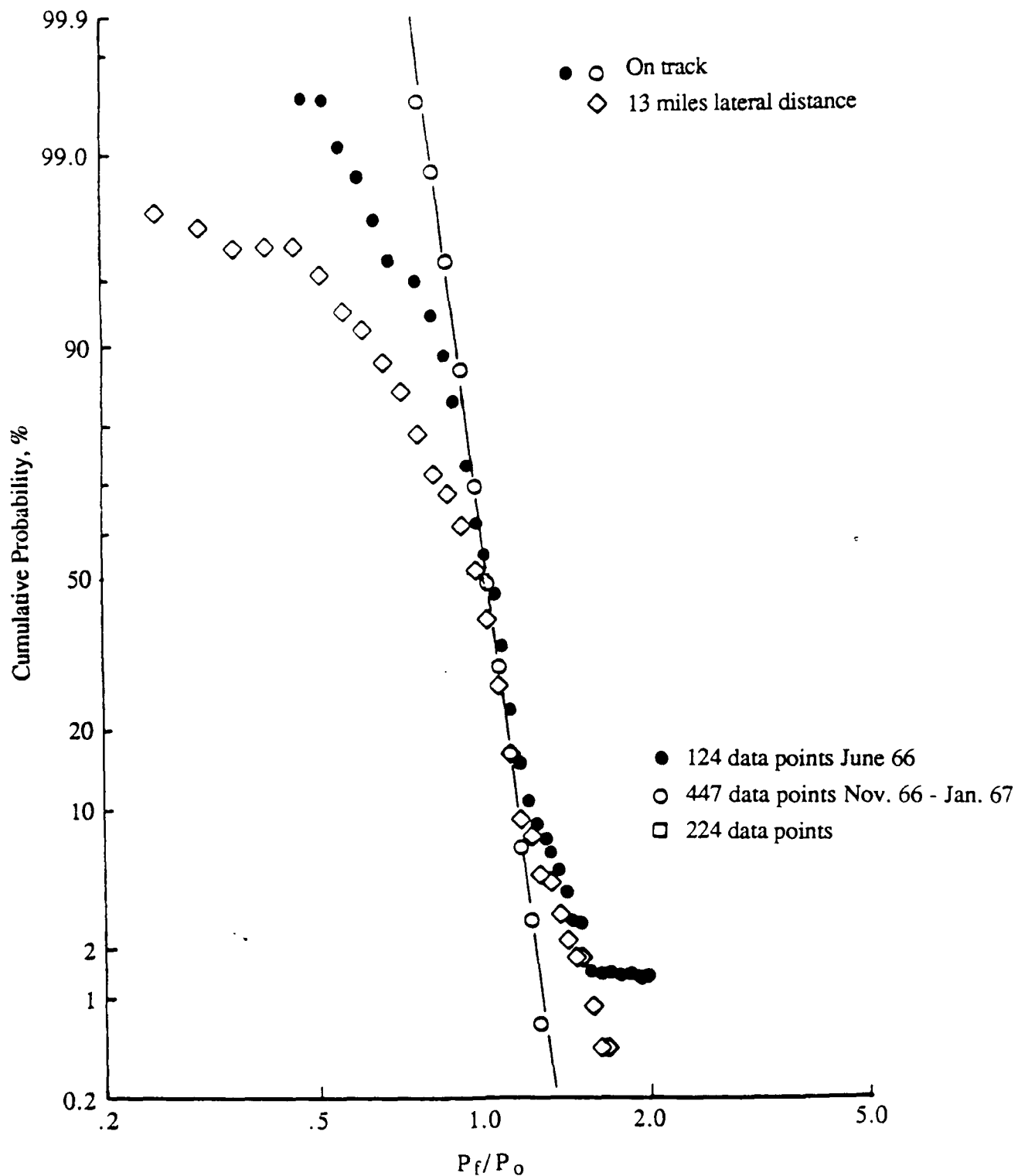


Figure 3-7. Cumulative Probability Distribution of Ratios of Measured to Long Time Average Overpressures for the XB-70 Aircraft for Measuring Stations on the Track and at a Lateral Distance of 13 Miles (Based on Maglieri, et al., 1969).

Table 3-2

Standard Deviations of Log-Normal Distribution of Sonic Boom Peak Pressures
from Controlled and ACM Supersonic Flights

<u>Type of Test</u>	<u>Location</u>	<u>Sideline Position</u>	<u>$\sigma_L(P_f/P_0)$</u>	<u>$20 \cdot \sigma_L(P_f/P_0)$</u>
Controlled	Oklahoma City	0 miles	0.114	2.28 dB
		5 miles	0.139	2.78 dB
		10 miles	0.172	3.44 dB
Controlled	Edwards AFB			
		(winter) 0	0.053	1.06 dB (winter)
		(summer) 0	0.068	1.36 dB (summer)
	(winter)	13	0.087	1.74 dB
ACM	Reserve SOA	All 17 monitors	0.40	8.0 dB

The comparable distribution for individual values of P_f relative to their long term average P_0 at each site was not available for the WSMR data. However, the distribution of the actual peak pressure P_f for all 506 sonic booms measured on all the 35 monitors, taken as a whole, is shown in Figure 3-8. Again, the distribution is clearly log-normal. The standard deviation of the log of P_f is 0.369 corresponding to a standard deviation in sound level of $20 \times 0.369 = 7.38$ dB, slightly less than the value of 8 dB found for the Reserve data. However, the latter involved only 13 sonic booms, so the reliability of the 8 dB value is poor.

The variance of the log of the average peak sound pressure computed according to Eq. (3-8) over all 35 measurement points is $(.0437)^2 = .0019$. This represents the variance (i.e., the square of the standard deviation) for the first component of variation cited above and corresponds to a standard deviation (in decibels) of $20 \times 0.044 = 0.9$ dB. If this variance is subtracted from the total variance for all 506 of the WSMR peak pressure data points (7.38 dB), the remainder should be approximately equal to the second and third components of variance combined which establishes that part of the total variance in peak sound pressures which is random and which can be applied to the statistical damage prediction model.

Carrying out this analysis, the standard deviation $\sigma_L(P_f)$ of the log of the peak sound pressures at each position about the log mean value predicted by Eq. (3-8) is estimated to be:

$$\sigma_L(P_f) = \sqrt{[(7.38)^2 - (0.9)^2] / 20} = 0.366 \quad (3-9)$$

To summarize for SOAs, the spatial variation in the nominal (long time log mean) sonic boom peak pressure P_0 due to ACM activity is defined by Eq. (3-8). The standard deviation of the

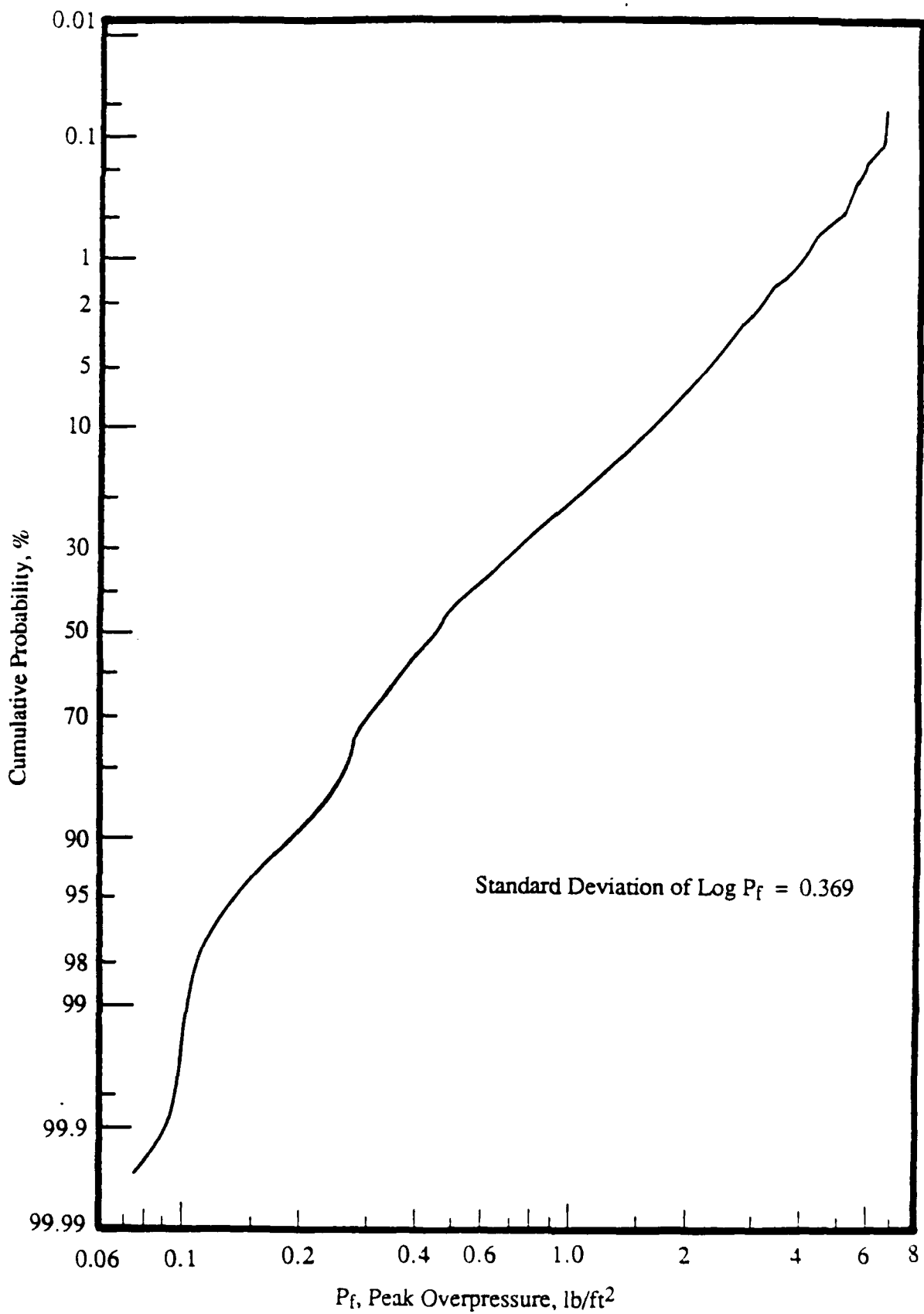


Figure 3-8. Cumulative Probability Distribution of Pooled Data of Individual Values of Peak Overpressures from WSMR Test (Based on Plotkin, et al., 1989b).

log of this nominal peak pressure is estimated to be 0.366, corresponding to 7.32 dB. Finally, Eq. (3-2) defines the estimated number of sonic booms per day which reach the ground at any position within an SOA. Now, before considering other types of supersonic flight activity, briefly consider possible variations in the above ACM model for other SOAs.

3.1.4 Possible Variations in ACM Model for Other SOAs

Centered inside the elliptically-shaped maneuvering area of an SOA, typically about 35 by 60 miles, the end or set points for aerial combat are typically separated by about 30 to 50 miles along the major axis of the SOA ellipse (Plotkin, et al., 1989). Thus, for any other SOA, once this engagement line and the set points are known, the orientation and position of the elliptical noise patterns can be established. However, the supersonic operating area or maneuvering area within the SOA is itself an ellipse identified for convenience here as the SOA ellipse whose size and shape is approximately constant (for current aircraft flight technology) and independent of the number of sorties per day carried out in it. The engagement line becomes the major axis of the SOA ellipse, the middle of the ellipse is the middle of the engagement line, and the eccentricity parameter, e , can be assumed to be the value derived from the noise analysis. From Eq. (3-1) and Eq. (3-2), the average value of e is taken to be equal to approximately 0.8.

The length (b) of the major axis of this SOA ellipse can be conservatively assumed to be 60 miles, the larger dimension of the 35 to 60 mile supersonic operating area. Thus, a basic equation for this SOA ellipse of constant size is, from Eq. (3-6b):

$$X^2 / (0.6)^2 + Y^2 = (60)^2 \quad \text{mi}^2 \quad (3-10)$$

where X and Y are the true distances in miles relative to the center of the ellipse, normal to, and along the major axis, respectively.

It is reasonable to expect that this SOA ellipse would change size slightly from one SOA to another due to variations in natural geography (i.e., location of visual check points or terrain) under the SOA and variations in the dominant type of aircraft and/or their flight procedures. Any such scaling of the size of the SOA ellipse would be expected to be relatively small but would be accompanied by a corresponding change in the size of the DNCL or n (booms per day) ellipses.

For example, based on the data and analysis procedures in Galloway, 1983, the long time average CSEL at the center of the ellipse is predicted to be as indicated in Table 3-3 for several different aircraft operating out of Luke AFB or Nellis AFB.

While based on application of a carpet boom (i.e., straight and level flight) prediction model for sonic booms in ACM areas, these data could be used as one basis for a rough approximation of the relative change in the parameters indicated by the WSMR model had these same data been obtained at the other bases. In other words, the changes in number of booms per day and long time average CSEL₀ at the center of the ellipse relative to the values measured for the F-15 dominated operations at WSMR could provide a first estimate for these adjusted values. For example, the average CSEL₀ in Table 3-3 is 99.6 dB, which is about 1 dB lower than the value derived for the 41 F-15 tracks evaluated for Luke. Thus, a first estimate for an average CSEL₀ applicable to ACM operations at SOAs near the above bases (and possibly all other similar SOAs) would be the value from the WSMR study (103.6 dB) minus 1 dB, or 102.6 dB, a very small change in a baseline number for maximum long time average single event levels in SOAs. This 1 dB reduction in CSEL₀ would correspond to a small decrease in the maximum log mean peak pressure at the center of the ellipse from 0.57 psf, as indicated by Eq. (3-8), to 0.48 psf – a relatively insignificant change. The standard deviation of this estimated change in peak pressures could be taken to be the same as the standard deviation in Table 3-3, i.e., 2.5 dB. (Note that according to the last column of the above table, the estimated maximum long time average DNCL at the center of the noise ellipse would be about 63 dB for F-15 aircraft. This is about 11 dB higher than the experimentally-based average value from Eqs. (3-1).)

In the absence of more detailed measured sonic boom data on other SOAs, these concepts must remain as conjecture, so that for this report, Eqs. (3-2) and (3-8) are taken as givens for any SOA. However, the standard deviation of 2.5 dB indicated by the data in Table 3-3 could be used as a basis for the minimum uncertainty in CSEL₀, or the corresponding nominal peak overpressure P_0 at the center of SOAs to account to a first approximation for different aircraft and different types of operations that were not included in the WSMR data.

3.2 Sonic Boom Pressures for Other Types of Supersonic Flight Activity

For the other two types of supersonic flight activity identified at the beginning of this section (supersonic corridor flights and low altitude flights), general models for the spatial pattern of the flight tracks are not practical at this point. Therefore, data are presented in this

Table 3-3

Predicted Long Time Average CSEL_o and DNCL_o at the Center
of the ACM Noise Ellipse According to the Flight Track Data
and Noise Estimation Procedures in Galloway, 1983

Aircraft	Base	No. Tracks Evaluated	n, No. Booms per Sortie	CSEL _o ⁽¹⁾ dB(C)	DNCL _o ⁽²⁾ dB(C)
F-4	Nellis	6	1.1	102.0	65.2
"	Luke	8	3.1	99.5	62.7
F-5	Luke	20	0.7	98.0	61.2
F-14	Luke	3	0.4	103.2	66.4
F-15	Nellis	6	0.8	100.0	63.2
"	Luke	41	0.8	100.3	63.5
F-16	Nellis	6	1.1	98.9	62.1
"	Luke	6	0.6	95.0	58.2
		Avg.:	1.08	99.6	62.8
		Std. Deviation:	0.85	2.5	2.5

(1) CSEL_o = Space average rms carpet boom CSEL
+ 10 Log [rms carpet area, mi²/maneuvering area, 1866 mi²]
+ 2.2, dB(C) (per Galloway, 1983)

(2) DNCL_o = CSEL_o + 10 Log (n) - 49.4, dB where n is number of booms/day for 18
sorties per day (average for WSMR)

section which only attempt to define for such flights representative sonic boom peak pressures, the range of durations of the pressure waveform, and estimates of the approximate statistical variation in the peak pressures.

3.2.1 Sonic Boom Environments Under Level Flight Supersonic Corridors at Varying Altitudes

Current supersonic flight training and flight testing can involve operations consisting primarily of straight and level flight at moderate to high altitudes, usually above 5000 ft. (Plotkin, 1985b). As indicated by the bibliography in Appendix A, the literature applicable to sonic boom environments for this type of operation is very extensive. Particularly useful summaries are contained in Hubbard, et al., 1986 and Runyan and Kane, 1970. The following brief discussion is only intended to help provide some understanding of the key variables which affect the peak overpressure and duration of a sonic boom (Plotkin, 1989a). Detailed computations of carpet boom overpressures and spatial distribution can be carried out manually (Carlson, 1978) or by a simple computer model called PCBOOM (Bishop, 1988).

At altitudes above about 5000 ft, a highly simplified version of a well known model (Carlson, 1978) for the nominal peak overpressure P_o for straight and level flight can be expressed in the form:

$$P_o = K_a (M^2 - 1)^{1/8} (L/H)^{3/4} \cdot k_s \quad (3-11)$$

where K_a is an atmosphere-dependent variable which varies with the altitude of the aircraft, the pressure/temperature profile of the atmosphere, and to a minor degree with Mach number

M is the aircraft Mach number

L is the aircraft length

H is the effective altitude (equivalent to the actual altitude for an observer directly under the flight track)

and k_s is a shape factor dependent on the geometry of the aircraft.

Thus, for a given aircraft (constant length L and shape factor K_s) and atmospheric model (fixed relationship between K_a and altitude), the dominant variable which controls the magnitude of the sonic boom peak pressure observed directly under the flight track is the aircraft altitude.

This is borne out by the trend with altitude in the measured and predicted sonic boom peak pressures shown in Figure 3-9 for the case of a large supersonic aircraft flying at high altitudes (Carlson, 1964). The peak overpressures vary from about 1 to 3 psf for flights in the altitude range of 30,000 to 75,000 ft. The influence of changes in aircraft speed on this peak pressure is small as indicated by the second term in Eq. (3-11).

For straight and level flight at high altitudes, the sonic boom created on the ground usually has the classic time history approximating that of an N-wave with a duration typically in the range of 0.2 to 0.5 seconds depending on the aircraft length, speed and altitude (Carlson, 1978). In any event, this duration is much greater than the duration observed for low altitude supersonic flights which is simply:

$$T_o = (\text{aircraft length})/(\text{aircraft speed})$$

For such low altitude flights at a uniform speed on a level flight track, the time history of the sonic boom has a much more complex shape as illustrated by the actual measurements in Figure 3-10a (Nixon, et al., 1968; Maglieri, et al., 1966). Each of the multiple jumps in the pressure time history is associated with shock waves radiated by different parts of the aircraft.

For supersonic flight at such low altitudes, Eq. (3-11) overpredicts the peak sonic boom pressure by as much as a factor of about 1.7 at an altitude of 100 ft. However, as shown in Figure 3-10b, a simple analytical model makes it possible to accurately predict the effective peak pressure of an equivalent N-wave with the same peak pressure as the complex waveform actually present (Plotkin, 1989b). This figure shows a comparison between theoretical prediction models for sonic boom peak pressures for altitudes in the range of 100 to 20,000 ft for a representative case of an F-4 aircraft at Mach 1.22. A single data point shown on the figure corresponds to the actual measurements of Figure 3-10a. For these lower altitudes, the peak overpressures vary from about 3 psf for flight at 20,000 feet to over 100 psf for flight directly overhead at 100 ft.

The variation of the sonic boom peak pressure to each side of a supersonic flight track has the general pattern illustrated in Figure 3-11 for different altitude ranges (Maglieri, et al., 1966; 1967b). On each side of the ground track under a supersonic flight, the sonic boom propagation through the atmosphere reaches a so-called lateral cut-off point where refraction prevents the boom from reaching the ground. Near this position, a sonic boom tends to have a more rounded, sinusoidal time history and will be less likely to be of concern from the standpoint of potential structural damage.

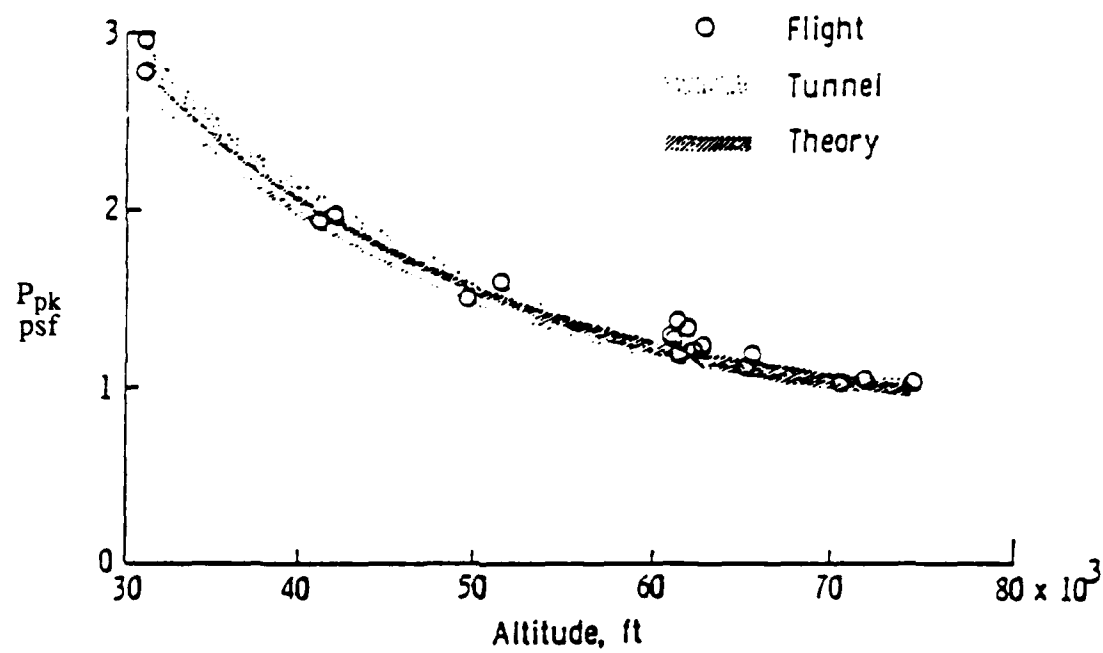
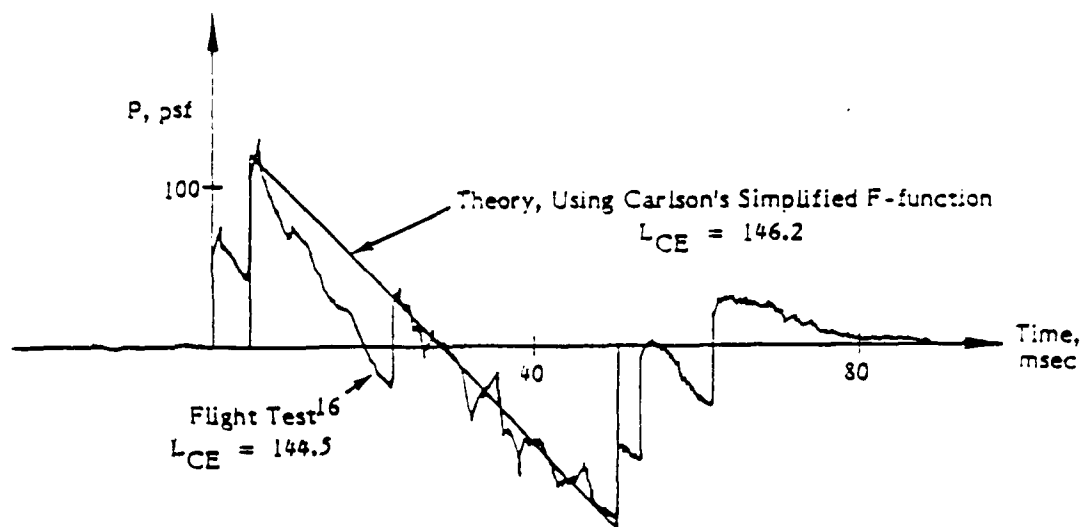


Figure 3-9. Comparison Between Theory, Flight Test, and Wind Tunnel Measurements for a Supersonic Bomber (from Carlson, 1964).



(a) Near-Field Sonic Boom Time History for F-4 at 100 ft, $M = 1.22$ (Nixon, et al., 1968)

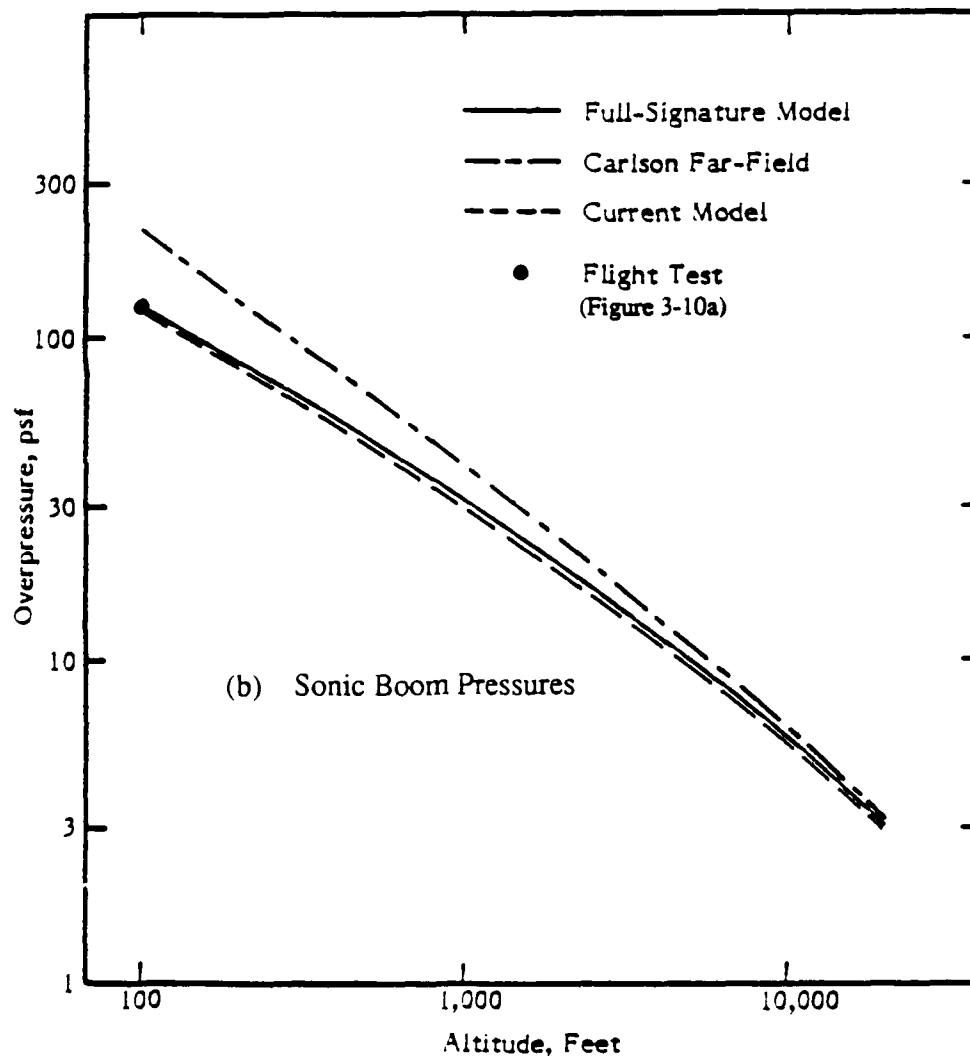
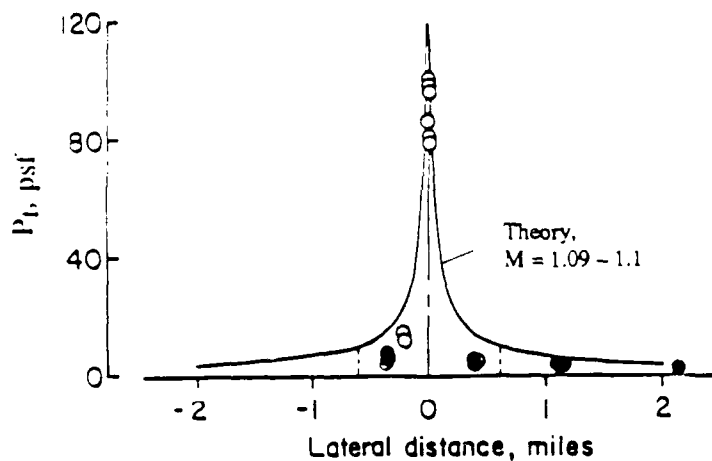
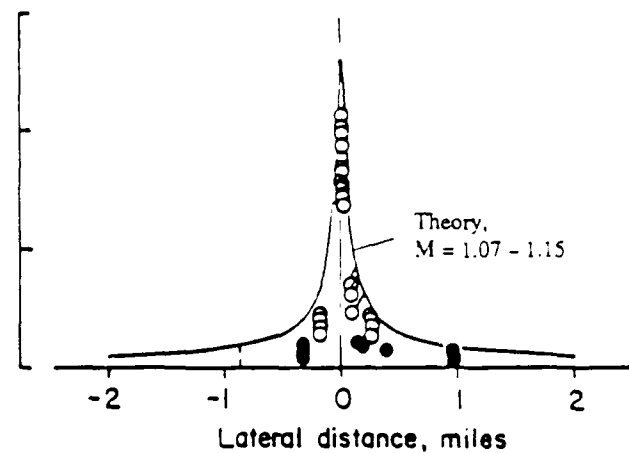


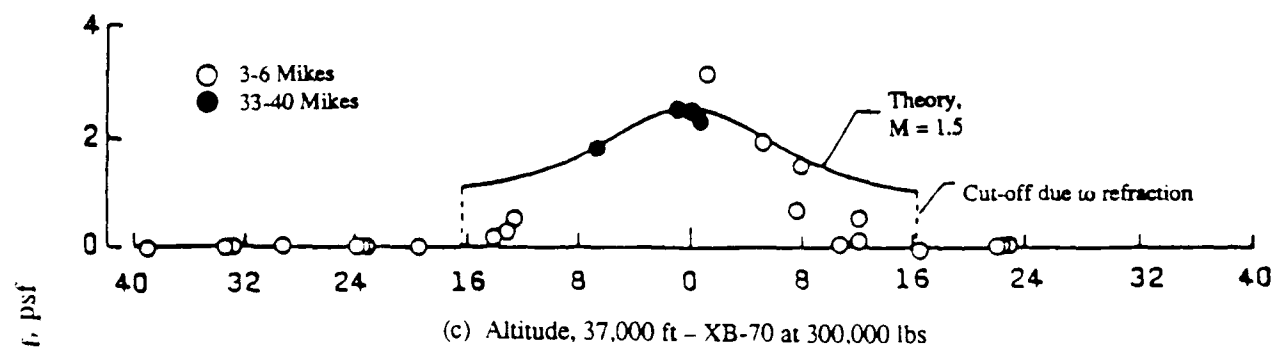
Figure 3-10. Comparison Between Full-Signature Boom Model, Carlson Far-Field Model, and Current Model (from Plotkin, 1989b).



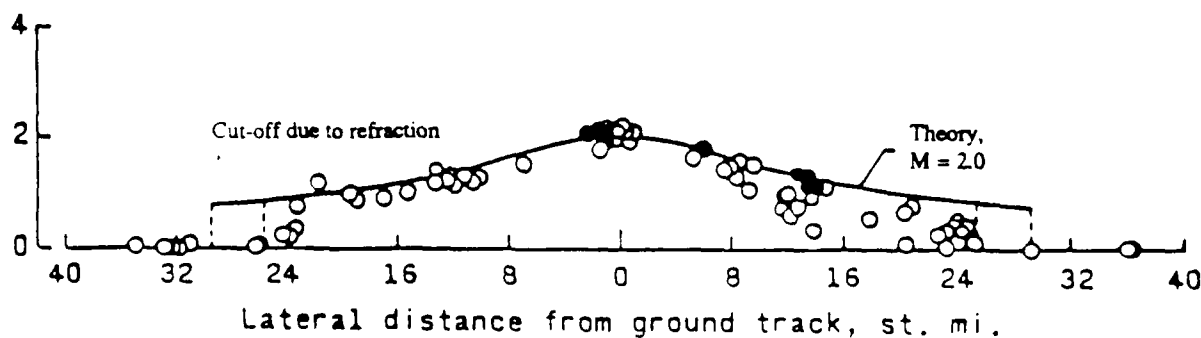
(a) Altitude range, 60 to 95 ft, Fighter Aircraft A



(b) Altitude range, 110 to 200 ft, Fighter Aircraft A



(c) Altitude, 37,000 ft - XB-70 at 300,000 lbs



(d) Altitude, 60,000 ft - XB-70 at 400,000 lbs

Figure 3-11. Lateral Spread of Sonic Boom Carpet Pattern for Very Low (a) and (b) and High (c) and (d) Altitudes. (Data for (a) and (b) from Maglieri, et al., 1966; data for (c) and (d) from Maglieri, et al., 1967b).

Given some definition of the expected nominal peak overpressure for level flight at a given altitude such as may be estimated from Figure 3-9 or 3-10b, the statistical variation about this nominal pressure may be estimated, at least for high altitude flights, by the information shown earlier in Figures 3-6 and 3-7 and summarized in Table 3-2 in Section 3.1.3. Values for the standard deviation σ_L in peak overpressure from the Oklahoma City tests of 0.114, 0.139 and 0.172 at sideline distances of 0, 5 and 10 miles respectively, are considered reasonable for purposes of this report as representative for positions directly under the flight track half way to the lateral cut-off point and about 0.8 of the way to the lateral cutoff point for any level flights in supersonic corridors at any altitude. This assumption is based on the observation that the variation in sonic boom signatures due to weather is influenced primarily by atmospheric conditions below about 2000 ft. (Maglieri, 1967b).

3.2.2 Sonic Booms for Flight at Low Altitude Not Restricted to Steady Flight

Other possible scenarios of supersonic flight training might involve non-uniform flight at low altitudes which could consist of a mixture of short level flight sections initiated and terminated by short periods of acceleration and deceleration respectively, and/or abbreviated maneuver sections (e.g., turns) all at altitudes from about 100 to 1,000 ft (Plotkin, 1989b).

Table 3-4 lists representative predicted peak overpressures for F-111 and F-15 aircraft for level flight portions (i.e., carpet booms) of such flights showing peak overpressures ranging from just under 2 psf to about 130 psf. These are estimated peak pressures in the absence of amplification by focusing due to maneuvers. Such focus or superboms would occur for the flights of the F-15 at the flight altitudes listed but would not occur for the F-111 flights due to the constraints placed on turn or acceleration rates at such low altitudes. When such superboms occur, they can increase the peak pressures by a factor of 2 to 5 times within a very small area (Plotkin, 1985a). Time histories of the sonic boom waveforms for such operations can be expected to be similar to those observed for ACM operations to be discussed in Section 3.4.

For purposes of assessing potential damage to unconventional structures under such flights, the same procedures employed for ACM and level flight corridors could be employed, giving due consideration to the possibility of superboms. However, the latter are already included in the statistical spread of peak pressure for ACM operations as shown earlier in Figure 3-8. In any event, it is not considered feasible at this point to attempt a detailed statistical analysis of the potential for damage for such operations in the absence of a more definitive scenario of flight tracks and altitude ranges.

Table 3-4

Carpet Boom Characteristics Estimated for a Variety
of Low Level Supersonic Flight Operations (from Plotkin, 1989b)

Aircraft	Altitude, kfeet AGL	Mach Number	Ppk, psf		Carpet Width, kfeet	Forward Projection, kfeet
			Center	Edge		
F-111	0.1	1.05	130	33.3	1.4	0.3
	0.5	1.05	44.0	10.5	7.2	1.6
	1.0	1.05	30.0	6.8	12.9	3.1
F-15	5	1.05	7.2	6.1	7.4	17.5
	5	1.4	9.2	4.	29.2	5.2
	10	1.1	4.3	3.3	21.7	24.7
	10	1.5	5.4	2.5	52.1	9.3
	15	1.1	3.1	2.6	22.1	40.6
	15	1.7	4.0	1.8	75.4	11.4
	20	1.15	2.4	1.9	37.2	43.1
	20	1.35	3.1	1.5	97.2	13.6
	25	1.15	1.9	1.8	31.5	58.8
	25	2.0	2.5	1.2	117.0	15.5
	30	1.2	1.6	1.4	46.7	59.5
	30	2.0	2.0	1.0	129.2	19.0

3.3 Correction from Free Field to Effective Pressure on Structure

The sonic boom peak pressures defined in the preceding sections were pressures in the absence of any reflecting surfaces. Two adjustments are necessary to this free field pressure to establish the effective sonic boom loading on an actual structure:

- change in effective pressure due to arrival of the sonic boom at angles other than normal to the surface, and
- increase in sonic boom pressure at the surface of a structure facing the direction of arrival of the sonic boom wave.

3.3.1 Correction Due to Angle of Incidence of Sonic Boom Wave

The evaluation of orientation effects on sonic boom sound levels near a structure (Hershey and Higgins, 1976) provided useful information that is assumed to be applicable here. Hershey and Higgins found that the log of the ratio for the peak sonic boom sound pressure P_e measured at the outside surface of a structure and the free field sound pressure P_f could be approximated by:

$$\text{Log } [P_e/P_f] = 0.1427 \cos(\theta) - 0.1258 \quad (3-12)$$

where θ is the angle, on the ground, of the aircraft flight track relative to a line perpendicular to the structural surface.

The average value of the right side of this equation for θ varying from 0° to 360° is about -0.126 , equivalent to $P_e/P_f = 0.75$. Since there is no way to predict the orientation angle for the general case, this correction is included in the ratio of effective to nominal pressure for all cases except those relating to seismic excitation of the ground. The variation of this correction about its mean value was estimated from the range of the value of $\text{Log } (P_e/P_f)$ according to Eq. (3-12) where it was assumed that this range (-0.268 to $+0.017$) corresponded to ± 3 standard deviations so that the standard deviation of $\text{Log } (P_e/P_f)$ was assumed to be $(0.268 + 0.017)/6$, or 0.0475 .

3.3.2 Effective Acoustic Pressure on Various Types of Structure

The following additional adjustments to the free field sonic boom pressures are required to define an effective pressure, P_e , to account for the pressure doubling effect that has already been included in the measurement and specification of the "free field" sonic boom pressures,

the same pressure doubling at the surface of an infinite rigid wall and the smaller increase in effective acoustic pressure on a wall with a large open window or a free-standing wall with no roof. Both of these latter situations are likely to be encountered in evaluating potential damage from sonic booms on historic or prehistoric ruins. Thus, the following correction to the free field pressures will be applied in all cases.

$$\text{Effective Sound Pressure, } P_e = P_f \cdot D \quad (3-13)$$

where P_f = free field sound pressure from Eq. (3-8)

D = 1 for wall and/or roof with no open windows (the pressure doubling has already been included in P_f)

D = 0.63 for wall with large open window(s) or large opening in roof

For free-standing wall with no roof,

$D = D_1 \cdot \sin(f \cdot H / 600)$ for $f \cdot H < 930$ ft/s

$D = D_1$ for $f \cdot H \geq 930$ ft/s

and D_1 = 1 for wall with no windows or 0.63 for wall with wide open windows

f = Fundamental resonance frequency of wall. 23 Hz can be used as a default value for a typical free-standing wall of a prehistoric ruin in the absence of any alternative data (Battis, 1988).

H = Height of wall in feet.

The above adjustments are based on approximations for the reduced net sonic boom pressure on a wall with a large aperture (Wilson and Soraka, 1965) or on an unbaffled obstacle (Sutherland, 1968b). Note that the factor D can approach 0 for low walls with low resonance frequencies since the sonic boom pressure wave will diffract around the back side of such a wall and thus reduce the effective acoustic loading significantly.

A precise evaluation of the effective sonic boom pressure acting on a surface would include the consideration of other factors including the presence of nearby reflecting surfaces, the height of the structure above the ground, and relative rigidity of the structural surface. However, extensive experimental evaluations of these factors during extended sonic boom test programs (Wiggins, 1965; Andrews, et al., 1965) indicate that they usually introduce relatively

minor variations in effective loading beyond that accounted for in Figure 3-11. They will not be considered in this report since the major source of variation in sonic boom pressure is due to the inherent variability of ACM operations. These are the primary type of supersonic operations of concern here.

In summary, a general method has been defined for estimating sonic boom loads from a wide range of supersonic flight operations. For ACM operations, the method involves the use of Eq. (3-8) to define long term or log mean sonic boom pressures, and to define sonic boom peak pressures as a function of position of a structure relative to the center (on the ground) of the supersonic operating area. For other types of supersonic activity, graphical or tabular data provide references on typical sonic boom levels that may be encountered. Eq. (3-13) defines a correction for the effective incident sonic boom pressure for these free field models.

Values have also been established for the standard deviation of the log of this pressure due to random deviations in the long time average pressure from an ideal spatial model for ACM operations, random deviations of the pressure due to weather and flight procedures, and random deviations due to angle of incidence of the sonic boom. All of these elements will be employed in the process utilized for estimating the probability of structural damage from ACM operations.

3.4 Time Histories and Frequency Spectra for Sonic Booms

Up to now, the evaluation of acoustic loads on structure has focused almost entirely on the peak sonic boom pressures. This will, in fact, be the primary variable to be used in this report for defining the probability of damage to unconventional structures. The effects on structural response of variations in the temporal patterns and corresponding frequency spectrum content of sonic boom waves forms are briefly considered here. However, it is important to point out that for estimating damage to structures under ACM areas, the probability of damage is influenced far more by the large variability in the peak pressure, as indicated earlier by Figure 3-8, than by variations in structural response for the same peak pressure due to variations in sonic boom waveforms or frequency content of their spectrum.

3.4.1 Time Histories of Sonic Booms

For straight and level supersonic flight at high altitudes, generally above about 5000 ft, the sonic booms generated by USAF airplanes are dominated by a relatively simple N-wave time history as shown in Figure 3-12. For ACM flight operations, the sonic booms have a much wider range of time history shapes. This complexity, reflecting the interaction of

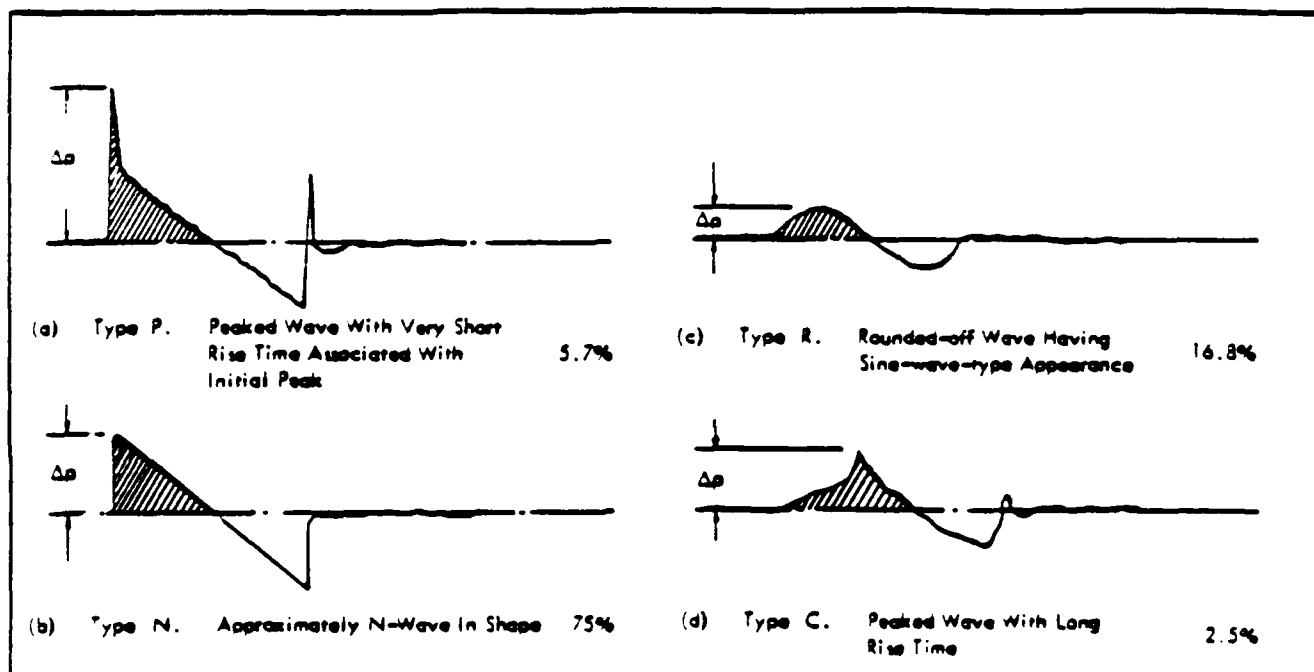


Figure 3-12. Schematic Diagrams Showing Relative Frequency of Occurrence of Categories of 1152 Waveforms Measured at Ground Level During Sonic Boom Tests on Four Airplanes (Adapted from Hilton, et al., 1964).

acceleration-generated sonic boom focus conditions and aircraft altitude, is illustrated conceptually in Figure 3-13 by the ray paths of the sonic boom from one aircraft at two different times along its flight path. The time histories of the sonic booms for the various combinations of amount of acceleration and aircraft altitude vary from the classic N-wave to U-waves and combinations of the two waveforms – the so-called superbooms (Plotkin, 1989a). Not shown are the rounded sinusoidal-shaped patterns for the weaker sonic booms occurring beyond the lateral cutoff point that are illustrated in Figure 3-12.

3.4.2 Frequency Spectra of Sonic Booms

It will be shown in Section 4 that the frequency spectra of time histories of sonic boom pressures play a significant role in defining their effective dynamic load characteristics. This spectral content is conveniently portrayed in terms of the Energy Spectral Density $E(f)$ (Kryter, et al., 1966) or the related measure, the Sound Exposure Spectral Density $SE(f)$ (Young, 1986). These two measures of spectral content at any frequency f of a transient signal are interrelated by the absolute value of the Fourier Spectra $|P(f)|$ of the pressure time history $P(t)$ as follows. (For simplicity, the usual designation of a complex argument (jf) for the Fourier Spectrum $P(f)$ is omitted here. See Appendix C.1.)

$$\text{Energy Spectral Density, } E(f) = |P(f)|^2 \quad (3-14a)$$

$$\text{Sound Exposure Spectral Density } SE(f) = 2|P(f)|^2 = 2E(f) \quad (3-14b)$$

$$\text{where } P(f) = \int_0^T P(t) \exp(-j2\pi ft) dt, \quad \text{the Fourier Spectrum.}$$

The two "density" quantities have the units of (pressure)²·(sec)².

For evaluation here, it is convenient to plot Sound Exposure Spectral Density in logarithmic form as the Sound Exposure Spectrum Level, $L_E(f)$ given by:

$$L_E(f) = 10 \text{ Log } [SE(f) / p_0^2 \cdot t_0 \cdot \Delta f], \text{ dB re: } (20\mu\text{Pa})^2 \text{ sec/Hz} \quad (3-15)$$

where p_0 is the reference pressure of $20\mu\text{Pa}$,

t_0 is the reference time of 1 second, and

Δf is the reference bandwidth of 1 Hz.

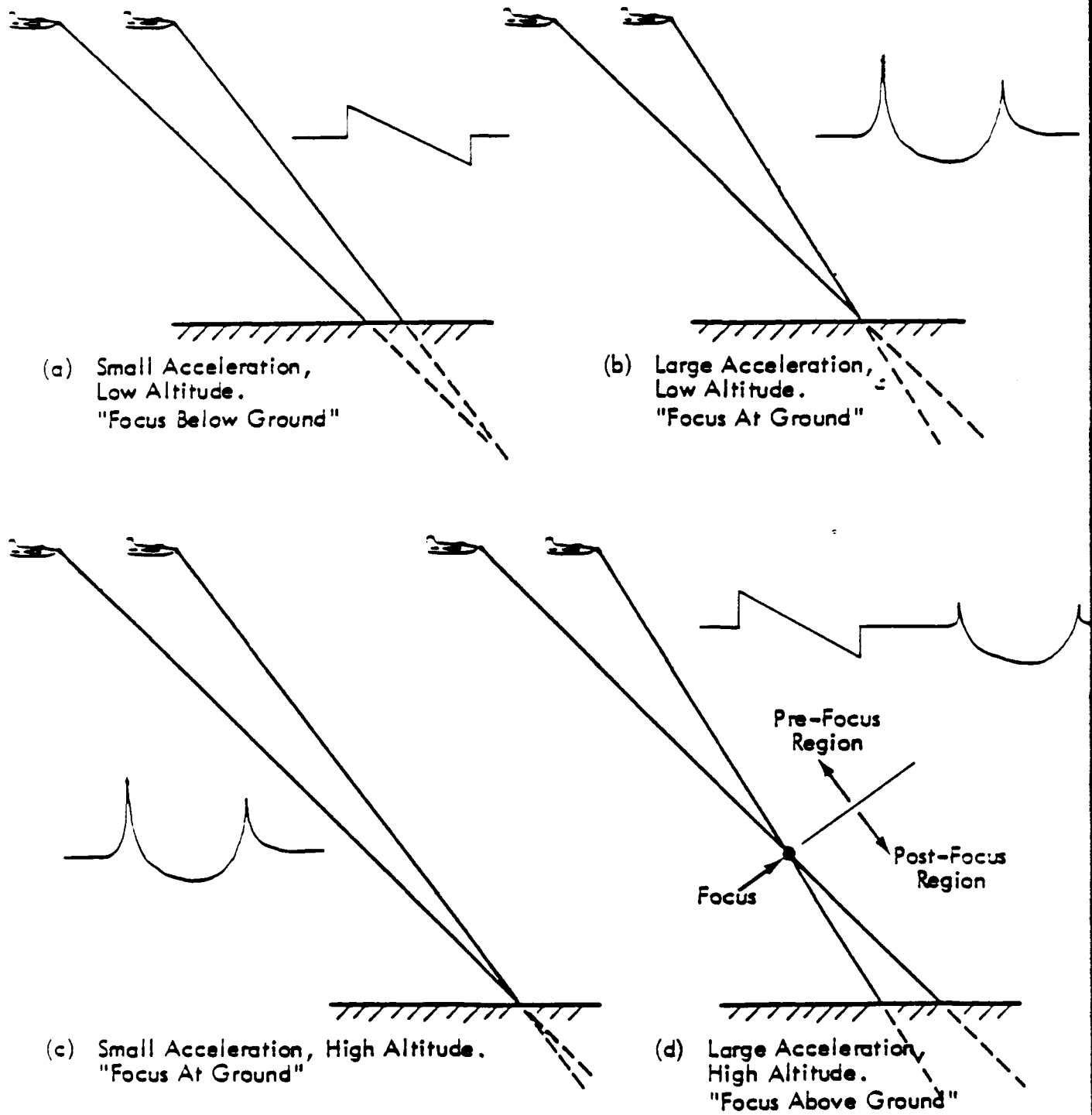


Figure 3-13. Converging Rays for Small and Large Acceleration, Low and High Altitude and Associated Nominal Sonic Boom Wave Forms (Adapted from Plotkin, 1984).

Figure 3-14a shows the Sound Exposure Spectrum Level for an ideal 1 psf sonic boom N-wave and the expected trend in the envelope of the Sound Exposure Spectrum Level for such this case (see Appendix C.1 for details).

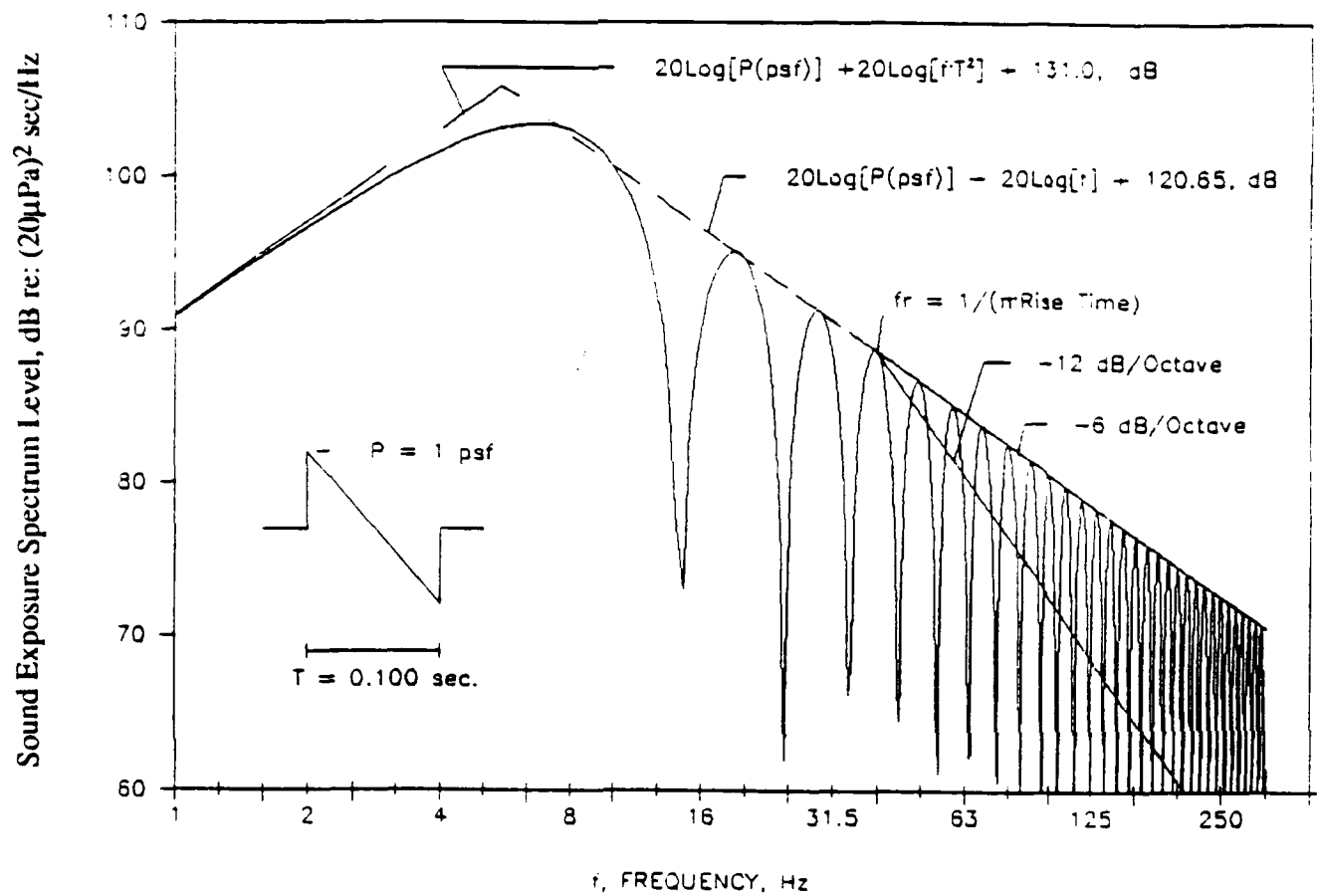
The equations for these lower and upper frequency envelope lines for the sound exposure spectrum level for the ideal N-wave which reach a peak at a frequency $f_{\max} = \sqrt{3}/\pi T$ (Appendix C) are:

$$L_E(f)|_{f < f_{\max}} \rightarrow 20 \text{ Log } [P_f(\text{psf})] + 20 \text{ Log } [fT^2] + 131.0, \text{ dB} \quad (3-16a)$$

$$L_E(f)|_{f > f_{\max}} \rightarrow 20 \text{ Log } [P_f(\text{psf})] - 20 \text{ Log } [f] + 120.6, \text{ dB} \quad (3-16b)$$

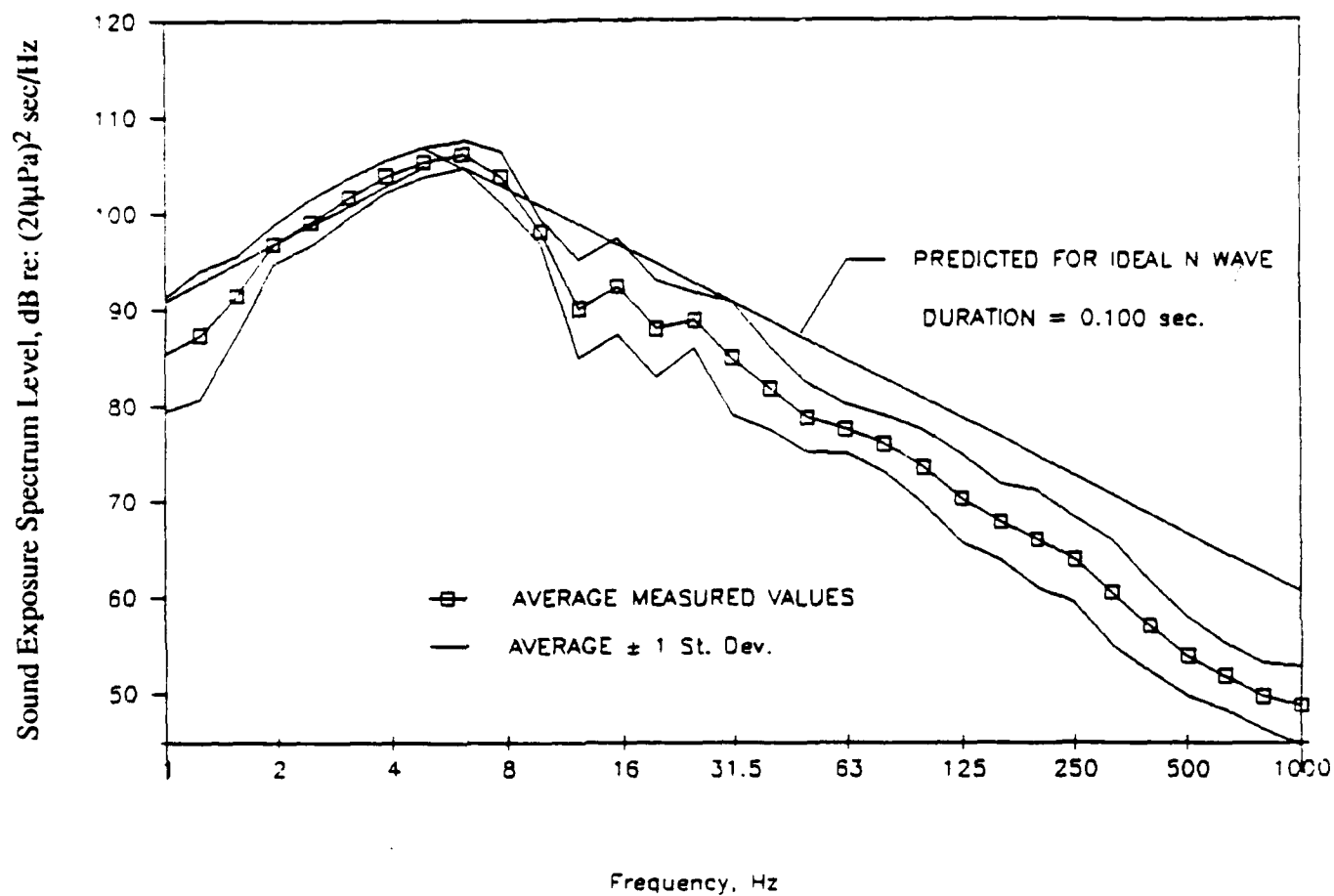
Also shown in the figure is the expected trend for additional roll-off (at -12 dB per octave) for the high frequency part of the spectrum for an N-wave with a finite rise time of 8 ms (Niedzwiecki, 1978). Figure 3-14b compares the spectrum level for the ideal N-wave to the arithmetic average and range of values for eight of the sonic booms measured in this program as discussed in more detail in Section 5. For this figure, all of the measured spectra have been normalized to a peak amplitude of 1 psf, and, for plotting purposes, averaged over one-third octave band intervals. Even with all the complexity of time histories anticipated for these sonic booms, according to the concepts shown earlier in Figure 3-13, these measured spectra show fairly close agreement to the expected trend for an ideal N-wave. Note, especially, that while the spectra do seem to show some roll-off at high frequencies greater than predicted for an ideal N-wave, they do not show the predicted full roll-off in high frequencies anticipated for an N-wave with a finite rise time. This can be attributed, in part, to the presence of many small fluctuations in the actual sonic boom pressure time history and to the more complex spectra expected for the other types of waveform, i.e., the U-wave, etc. (The deviation of the average measured data at low frequencies below about 5 Hz is due to low frequency limitations on the microphone response.) Thus, for evaluation of dynamic response of structure to sonic booms in ACM areas, it will be reasonable to assume that the actual sonic boom pressure time history, and corresponding shock spectra can be roughly approximated by that for an ideal N-wave.

For supersonic flight at very low altitudes, as indicated earlier in Figure 3-10, the sonic boom no longer has the nominal N-wave shape expected for straight and level flight at the higher altitudes. However, as indicated earlier in Figure 3-10a, an equivalent N-wave can be defined to predict the peak pressure. Similarly, for prediction of probability of structural damage, it will be sufficient to assume an ideal N-wave and the corresponding shock spectrum for this case.



(a) Predicted Values for N-Wave
 $(f_r = 39.8 \text{ Hz for } 8 \text{ ms rise time})$

Figure 3-14. Sound Exposure Spectrum Levels for Sonic Booms.



(b) Average Measured Values from Eight Sonic Booms in WSMR SOA for this Study vs. Values Predicted for N-Wave.

Figure 3-14. (Continued)

In summary, while real sonic boom signatures often contain far more complexity (and corresponding higher energy at high frequencies) than ideal N-waves, this complexity is not expected to be significant for purposes of estimating probabilities of structural damage to unconventional (or conventional) structures. This assumption is consistent with that made by many others in the assessment of structural damage from sonic booms (e.g., Hershey and Higgins, 1976; Haber and Nakaki, 1989).

4.0 MODELS FOR STRUCTURAL RESPONSE AND DAMAGE FROM SONIC BOOM

The prediction of potential damage to structures from the type of sonic boom excitation described in Section 3 can be defined in terms of analytical and empirical (experimentally derived) models for the vibration response of a structure to sonic boom excitation, and related models for the resulting stress response.

4.1 Vibration Response of Single Degree of Freedom Systems to Sonic Boom

In this section, models for this vibration response to sonic boom are defined for elements of a built-up structure as well as for ground surfaces.

When a panel is driven by a transient pressure load such as that generated by a sonic boom, the panel surface responds in a damped vibration mode, as illustrated by a typical example in Figure 4-1. (This example, obtained from data acquired for this program, is for the case of excitation by an N-wave followed by a U-wave sonic boom.) The response is transitory and usually has an amplitude 1.5 to 3 times greater than the deflection due to a static load with the same peak pressure. Note that in this case, the peak acceleration response occurs just after the end of the first N-wave and thus has the form of a free, damped, sinusoidal-like vibration.

The specific magnitude of this transient response can be predicted by the so-called shock spectrum $D(f)$ of the pressure time history. This is the effective value of a transient pressure load on a damped, linear single degree of freedom (SDOF) system (a linear damped mass-spring) as a function of the natural frequency of this simple oscillator. (In this case, the simple damped mass spring represents the fundamental mode of the panel.) The "effective" pressure load is the magnitude of a uniform static pressure which would produce the same maximum static deflection of the simple mass-spring system (i.e., the center of the plate) as that actually produced by the transient pressure pulse. When this shock spectrum is normalized by the magnitude of the peak pressure of the applied transient load, the resulting quantity is called the Dynamic Amplification Factor (DAF). Since the dynamic system is assumed to be linear, so that deflection or stress response is directly proportional to applied pressure, the DAF

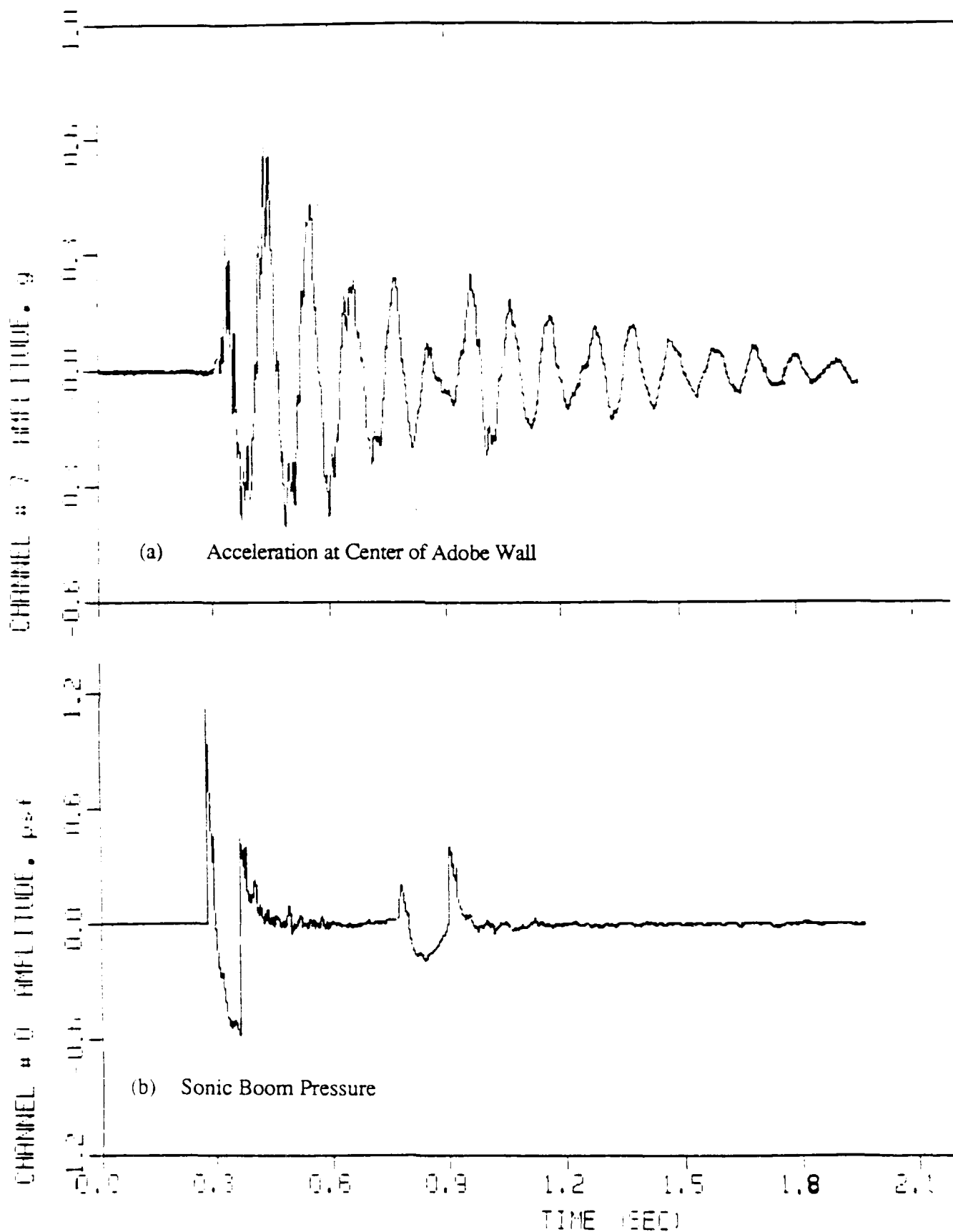


Figure 4-1. Typical Transient Acceleration Response of Structure to Sonic Boom: Response Measured on 18" Adobe Wall for Event MR081 for This Program (see Section 5.0).

can also be defined by the ratio of the peak dynamic stress response σ_{pk} for the actual transient pulse to the static stress response σ_s for a steady load with the same magnitude P_s as the peak applied pressure P_{pk} :

The same concept holds when DAF is defined by the ratio of peak dynamic deflection response X_{pk} to the static deflection response X_s for transient and static pressures with the same magnitude.

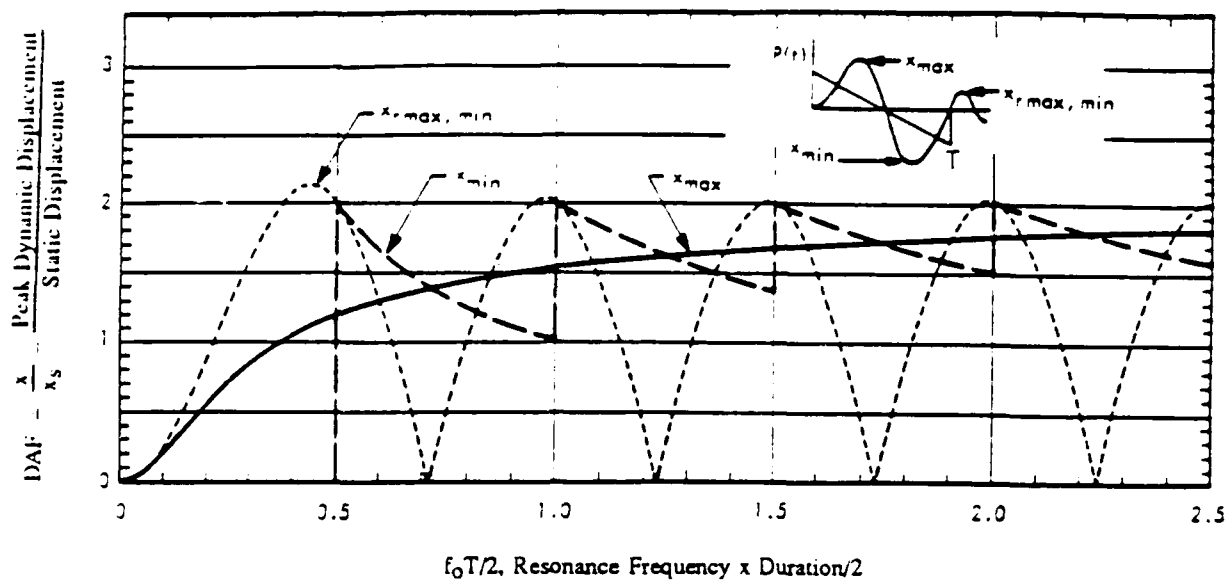
That is:

$$DAF = \frac{\text{Equiv. Static Which Produces Same Peak Response as Actual Applied Pressure}}{\text{Actual Applied Peak Pressure}} \frac{\sigma_{pk}}{\sigma_s} = \frac{X_{pk}}{X_s}$$

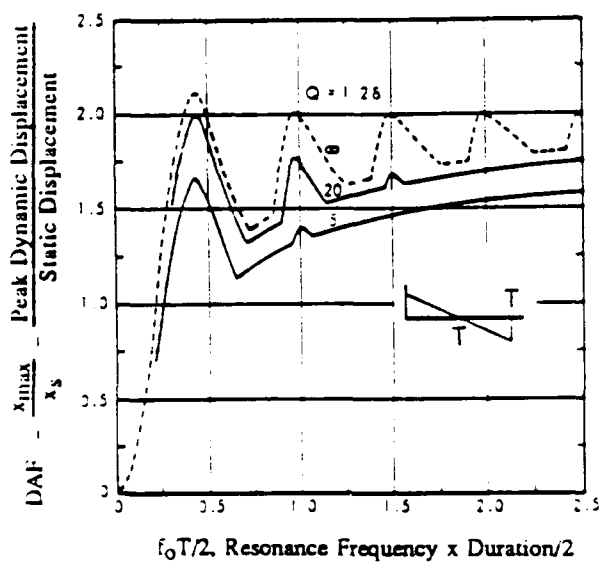
The predicted value for DAF is shown in Figure 4-2a for the case of excitation by an ideal sonic boom N-wave. As indicated by the figure, for the undamped system, DAF is a function of the natural resonance frequency f_0 . For analysis purposes, it is convenient to generalize this factor in terms of the product $f_0 T$ where T is the duration of the positive phase of the N-wave.

Figures 4-2b and 4-2c show the predicted values for DAF, with damping included, for displacement and acceleration response to an ideal N-wave. The displacement DAF shows decreasing sensitivity to damping as $f_0 T$ increases while the opposite is true for the acceleration DAF. The latter is expressed in terms of a non-dimensional quantity equal to the peak acceleration \ddot{X}_{max} divided by $[(2\pi f_0)^2 X_s]$ where f_0 is the fundamental resonance frequency of the system and X_s is its static deflection to a steady pressure within the same magnitude as the peak sonic boom pressure.

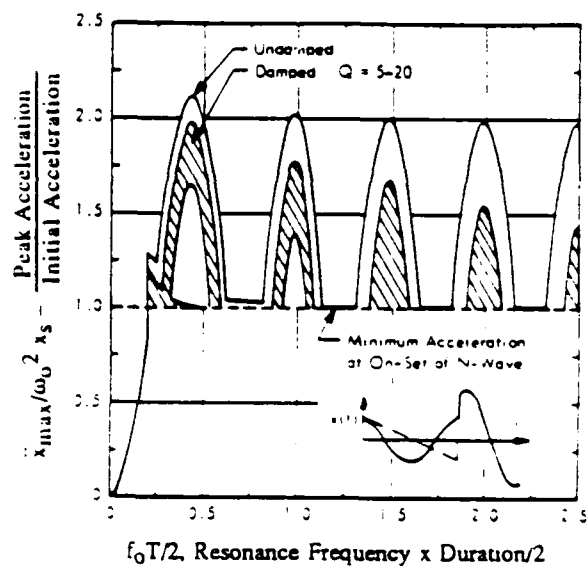
There are three different cases for occurrence of the peak response to the N-wave. *During* the N-wave, the peak response (e.g., deflection or stress) can be either: (1) positive, X_{max} , or (2) negative, X_{min} , depending on the product $f_0 T$. *After* the N-wave, the system responds systematically in free vibration and has equal (3) *positive* or *negative* dynamic responses, $X_{rmax,min}$. Note that the envelope of these peak responses following the cessation of the N-wave is equal to or greater than the peak responses during the N-wave. The unnormalized value of the DAF for the latter case, that is, the actual effective value of the dynamic pressure as a function of the resonance frequency, f_0 , is identified here as the Residual (Pressure) Shock Spectrum, $DR(f)$, where:



(a) Normalized Displacement Shock Spectrum for Ideal Sonic Boom N-Wave



(b) N-Wave Displacement Shock Spectrum for Damped System



(c) N-Wave Acceleration Shock Spectrum for Damped System

Figure 4-2. Normalized Shock Spectra for Excitation of (a) Undamped and (b) and (c) Damped System by Ideal N-Wave (from Sutherland, 1968a).

$$D_R(f) = P_e \cdot DAF(f) \quad (4-1)$$

and P_e is the effective peak pressure load, in psf, applied to the structure.

It is worth noting in Figure 4-2b and 4-2c that the DAF values for the residual (i.e., free vibration) displacement and acceleration of an undamped system are identical.

For damage assessment purposes, it will be desirable to define structural response to sonic boom excitation in terms of peak structural velocity instead of peak displacement or from theoretical expressions relating stress and applied pressure as employed in previous damage estimation studies (Hershey and Higgins, 1967; Haber and Nakaki, 1989). The reasons for this choice will become clear later in this section. This velocity response of a simple SDOF system to a sonic boom can be derived as follows with the aid of basic expressions for free sinusoidal vibration of such a system driven by a sonic boom N-wave and with the aid of relationships derived in Appendix C between the residual pressure shock spectrum and sound exposure spectral density.

For the residual (i.e., free vibration) response of the SDOF following the N-wave, the peak velocity V_{pk} in in/sec at the system resonance frequency f_0 can be defined, to a close approximation, in terms of the peak displacement X_{pk} at this same resonance frequency by:

$$V_{pk} = (2\pi f_0) \cdot X_{pk}, \text{ in/sec}$$

The peak displacement of the mass (representing a panel) can be defined in terms of the effective applied sonic boom pressure P_e , the displacement Dynamic Amplification Factor, $DAF(f)$, and the stiffness k of the SDOF system spring by:

$$X_{pk} = X_S \cdot DAF(f) = \frac{P_e A}{k} DAF(f) \quad (4-2a)$$

where A is the area of the panel represented by the mass.

The spring stiffness k can be expressed in terms of the mass $M = W/g$ and resonance frequency, f_0 , by:

$$k = 4\pi^2 \cdot f_0^2 \cdot W/g, \text{ lb/in} \quad (4-2b)$$

where g = acceleration of gravity, 386 in/sec²

Combining the above relationship, the peak velocity V_{pk} of the mass of this simple SDOF model at its fundamental resonance frequency, f_0 , is given by:

$$V_{pk} = \frac{P_e g DAF(f)}{(2\pi f_0) w}, \text{ in/sec} \quad (4-2c)$$

where w = surface weight in psf of the panel represented in this simple model by a lumped mass = W/A .

Consider, next, a simple way to define the Dynamic Amplification Factor for this SDOF model of the structure in terms of the sonic boom spectral content.

As outlined in Appendix C.1, a useful measure of the spectral content of a transient pressure signal is the Sound Exposure Spectrum $SE(f)$. This is essentially the frequency spectrum of the time-integrated value of the squared pressure of the transient pressure.

From Eq. (4-1) and the relationship for an undamped SDOF system between the Residual Shock Spectrum $D_R(f)$ and the Sound Exposure Spectrum $SE(f)$ developed in Appendix C.1, $DAF(f)$ can be given by:

$$DAF(f) = \frac{2\pi f_0}{P_e} \sqrt{1/2 SE(f)} \quad (4-3)$$

From here on it is assumed that the frequency f in the arguments for $DAF(f)$ and $SE(f)$ is the resonance frequency f_0 of the SDOF system and the free field pressure, P_f , used in Appendix C.1, is converted to the effective value, P_e .

Figure 3-14b has demonstrated that the sound exposure spectrum, for an ideal N-wave agrees reasonably well with the average values measured for this program.

As another check on this assumption, values for $DAF(f)$ reported in the extensive "carpet" sonic boom measurements (Wiggins, 1965) for the White Sands tests were examined and the results are summarized in Figure 4-3. These data covering 105 sonic boom records show a good agreement with theory and the central trend is close to the expected value for an ideal N-wave.

Now, combining Eqs.(4-1) to (4-3), the peak velocity response following the N-wave – call it the Residual Velocity Response Spectrum $V_R(f)$ – can be given by:

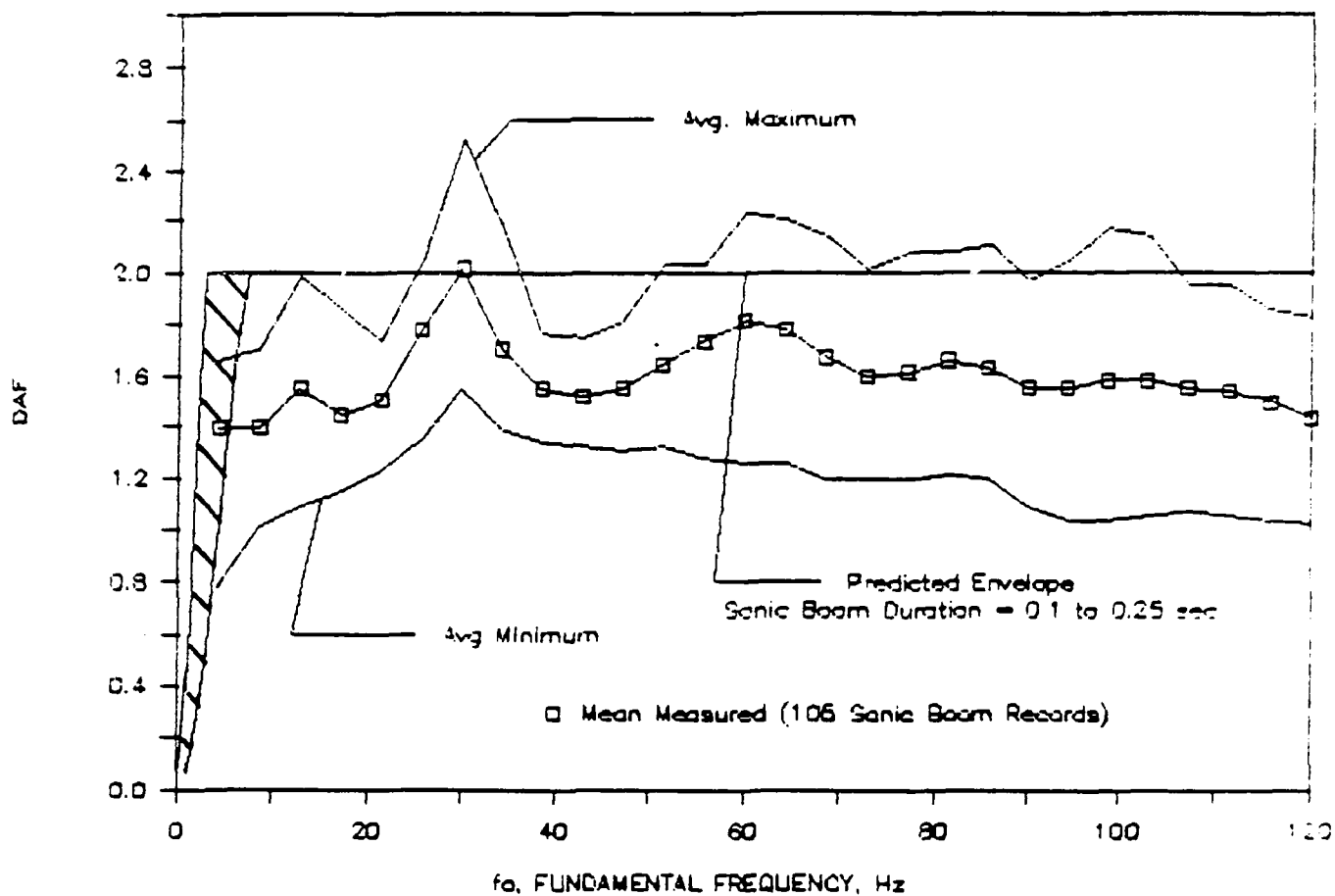


Figure 4-3. Summary of DAF Values Measured on Ground Microphones from Ninety F-104 and Fifteen B-58 Sonic Boom Records from White Sands FAA Test Program in 1965 (Data from Wiggins, 1965).

$$V_R(f) = \frac{g}{2\pi f_0 w} P_e \text{ DAF}(f) \quad (4-4a)$$

or

$$V_R(f) = \frac{g}{w} \sqrt{1/2 \text{ SE}(f)} \text{ in/sec} \quad (4-4b)$$

This velocity is often called a pseudo-velocity since it is strictly valid only for the case of steady-state sinusoidal vibration. However, for engineering purposes, Eq.(4-4) can be utilized to estimate, to a good approximation, the peak velocity response of a SDOF model for structure to a sonic boom.

The Residual Velocity Shock Spectra defined by these expressions are plotted in Figure 4-4, in log form for an ideal N-wave with a duration of 0.075 sec. Also shown are the low and high frequency envelopes for this spectra and the envelopes for the case where $T = 0.15$ sec. These envelope lines will become the basis for predicting structural velocity for built-up structures subject to vibration response like a panel. It can be shown (see Appendix C) that the equations for these envelope lines for the Residual Velocity Shock Spectra $V_R(f)$ are:

For $f_0 < \sqrt{3}/\pi T$

$$V_R(f) = \frac{\pi}{3} \frac{g P_e}{w} f_0 T^2 \text{ in/sec} \quad (4-5a)$$

and for $f_0 > \sqrt{3}/\pi T$

$$V_R(f) = \frac{2g P_e}{(2\pi f_0) w} \text{ in/sec} \quad (4-5b)$$

where $g = 386 \text{ in/sec}^2$

$P_e =$ Peak effective sonic boom pressure, psf

$f_0 =$ Fundamental resonance frequency of panel, Hz

$w =$ Surface weight of structure, in psf

$T =$ Duration of sonic boom, sec.

The mixture of ft-lb-sec and in-lb-sec units is employed here for consistency with the convention of expressing the peak pressure and surface weight in psf and structural velocity in in/sec. It will also be convenient from here on to refer to the peak velocity response, as defined by the Residual Velocity Response Spectra $V_R(f)$, by the symbol V_{pk} .

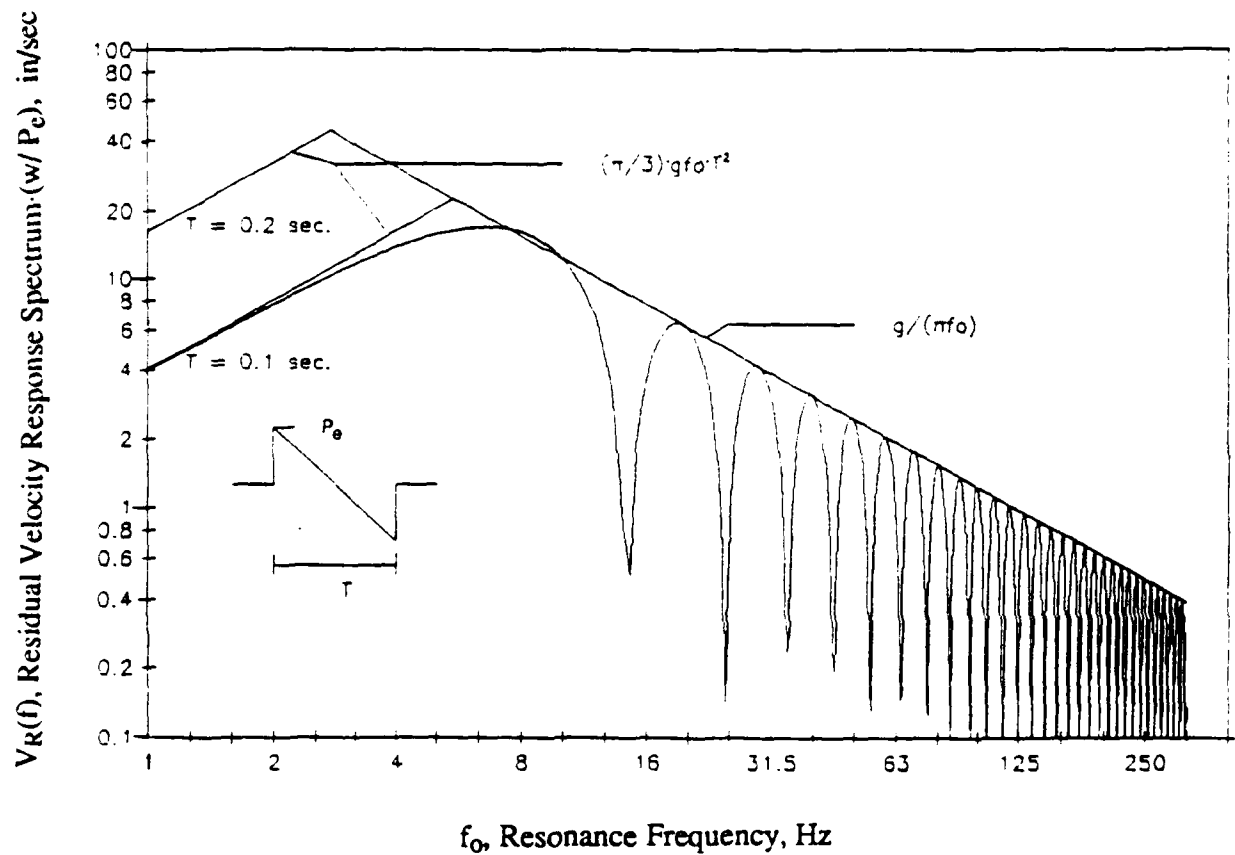


Figure 4-4. Normalized Residual Velocity Shock Spectrum for Predicting Peak Velocity Response of Structures with a Surface Weight w (psf) to a Sonic Boom with an Effective Peak Pressure P_e (psf).

4.1.1 Correction for Multimodal Response

The analytical models presented so far have only considered response at the fundamental resonance frequency of a simple lumped mass-spring model for a real structure. The total response of a structure in all modes requires a more detailed analysis of the time history of the response and summation of the combined time history of these modal responses. Such an analysis is summarized in Appendix C.2 based, in part, on previous studies (Blume and Associates, 1965; Crocker, 1967). As shown in Appendix C.2, a reasonable approximation to the total multimodal velocity response can be made by increasing the response envelope expressions of Eq.(4-5) by a factor of 2.0.

This simple approximate correction is based on the analysis in Appendix C.2 of the theoretical multimodal response of a simply supported panel for sonic boom durations of 0.1 and 0.2 seconds and for aspect ratios of the panel (side a/side b) of 1.0 and 0.2.

4.1.2 Vibration Response of Non-Structural (Terrain) Elements

Some of the structures of concern for this study are archaeological structures of various types which rest on, or are a part of, the local terrain and hence may be subject to damage from acoustically-excited seismic vibration. Complex analytical models have been developed to predict such seismic vibration from sonic boom or blast transient overpressure (Cook, et al., 1972) and from acoustic signals such as aircraft noise (Sabatier, et al., 1986). The theories predict two forms of seismic waves (Cook, et al., 1972): (a) a dilatational deformation of the ground due to the direct pressure loading, and (b) coupled Rayleigh (surface) waves which may precede or follow, in time, the direct dilatational response. In general, it is found that the direct response to the pressure loading is greater than the coupled, Rayleigh wave, response and consists primarily of a vertical ground motion whose velocity is directly proportional to the acoustic pressure. Although the transfer function between the ground velocity and pressure is both predicted and measured to be dependent on frequency for the usual type of stratified ground geology, it is not practical, for purposes of this document, to attempt to account for this refinement or to employ the theoretical models for purposes of predicting damage. Instead, reliance will be placed on measured seismic-acoustic transfer functions that seem to fall within a reasonably small range as discussed in Section 4.3.2. These transfer functions define the ratio of peak seismic velocity response to the peak free field pressure.

4.1.3 Vibration Response of Radio Telescopes to Sonic Boom

In a previous environmental study of sonic booms, concern had been expressed about the potential damage to, or excessive vibration response of, radio telescopes (U.S. Air Force). More recently, one incident has been reported of claimed potential sonic boom damage to an optical telescope located on the campus of a university situated near a USAF base (Hall, 1990). Such radio and optical telescopes, which certainly qualify as unconventional structures, will normally be quite complex in nature with a wide range of structural detail (Hey, 1973; Alter, et al., 1983). While excessive vibration of such structures detrimental to their sensitive operations may occur during exposure to a sonic boom, this problem is not addressed in this report since criteria were not available to define acceptable vibration limits of the structure and, more to the point, such vibration is not likely to result in structural damage. It would be possible, however, to make rough estimates of the peak ground vibration at the base of such systems induced by sonic booms with the use of the seismic transfer function data included in Section 4.3.2.1 in this report. Such estimates, coupled with a suitable analysis of the vibration response characteristics of the entire structure, could be used for a more detailed evaluation of environmental vibration concerns.

Many large radio telescope reflectors employ an open "wire mesh" for their parabolic reflector "surface." Mesh openings can be of the order of 2 inches or less (Hey, 1973) and can be assumed to present essentially an acoustically transparent surface to a sonic boom pressure wave so that structure loads on the mesh surface from the sonic boom overpressure would be minimal. The one potential sonic boom damage problem that is addressed here relates to the potential damage to the metal parabolic reflectors of that type of radio telescope which employs a solid surface for such reflectors. A similar potential structural damage problem relates to the hemispherical protective housing that some radio telescopes employ to protect the system from the weather (Hey, 1973). These housings can be similar to the familiar type employed for optical telescopes. In any event, the critical parameter here would be the surface weight, w , of the protective enclosure.

Radio telescopes that employ a solid reflector exposed to the weather can have diameters in the range of 25 to 140 ft (Hey, 1973). It has been shown that the effective acoustic load on a free obstacle, such as a disk, is greatest at a characteristic frequency, f_c , for which the front to back distance (equal, approximately, to the diameter, d , of the obstacle), is approximately $1/2$ wavelength (Morris, 1948; Sutherland, 1968b). Assuming a radio antenna diameter of 50 ft, this critical acoustic loading frequency would occur at $c/(2d)$ where c is the

speed of sound (about 1,117 ft/sec) so that, in this case, f_c would be $1,117/(2 \times 50) = 11$ Hz. As shown earlier in Figure 4-3, this is close to the peak frequency of the Sound Exposure Spectrum Level of a typical sonic boom with a duration of 0.1 sec. In this case, it turns out that the effective pressure load on an obstacle at this characteristic frequency is approximately two times the incident pressure. That is, for a radio telescope of about 50 ft diameter or more, the effective pressure load will be similar to that on a solid wall which does not have a direct acoustic path for the sonic boom pressure wave to diffract around such as a radio telescope antenna has. Thus, to a first approximation, the potential for structural damage to the solid radio reflector surface can be estimated in the same way as will be done for a solid wall – the key unknowns being the fundamental structural resonance frequency, f_0 , and the surface weight, w . For the purpose of estimating damage and providing very approximate values for the probability of damage, it will be assumed that the basic reflector surface is 14 gauge sheet metal with a thickness of 0.0766 inch. However, a total surface weight, including allowance for support structure, of 9.9 psf was assumed. This reflector skin was assumed to be supported on 2 ft x 2 ft centers on a back-up structure, the fundamental resonance frequency is estimated to be that of a simply supported 24 inch x 24 inch x 0.0766 inch plate (see Section 4.3.1.2 later for methods for estimating resonance frequencies of plates). The resulting fundamental resonance frequency is approximately 25 Hz. These frequency and surface weight parameters will be used for this report but must not be taken as authoritative values from any one specific antenna and are simply employed here as reasonable values to provide a rational basis for illustrating the method for, and obtaining rough estimates of, potential structural damage for such structures.

It must be emphasized that such large structures exposed to the elements must be designed to withstand severe wind loads which vary in magnitude depending on the geographic location from about 20 to 50 psf (Brekke, 1959). Thus, damage from typical sonic booms for supersonic flight above 5,000 ft can be expected to have a low probability. The analysis carried out here deals only with the potential damage to the thin metal reflector surface. No attempt is made to assess dynamic response and potential damage to the primary load-carrying structure of such a large radio telescope that might be possible for very high sonic boom pressures from the unlikely event of a low altitude supersonic flight close to such a structure.

4.2 Stress Response to Vibration Induced by Sonic Booms

Stress response of structure driven by acoustic loads could be derived on the basis of the peak dynamic displacement and known relationships between deflection and stress for

simple structural models. However, for this study it is more convenient to estimate stress in terms of structural velocity for two reasons: (1) this vibration measure is also widely used for damage assessment of structures near blasting and mining operations (Siskind, et al., 1980a,b), and (2) velocity is related in a simple way to stress in a vibrating structure, as outlined below.

A basic theoretical relationship exists between the magnitude of the peak velocity response in a structure undergoing sinusoidal vibration in a resonant mode and the peak stress in the structure in this same vibration mode (Hunt, 1960). According to this general relationship, the peak strain ϵ_{pk} in a structure vibrating in a resonant mode is simply equal to:

$$\epsilon_{pk} = K_S \cdot V_{pk}/C_L \quad (4-6)$$

where

V_{pk} = the maximum velocity in this mode, in/s

C_L = $\sqrt{E/\rho}$ the longitudinal speed of sound in the structural material (Note that the ratio V_{pk}/C_L can be considered equivalent to a structural vibration "Mach Number"), in/s

E = the Modulus of Elasticity of the material, psi

ρ = the mass density of the material, lb-s²/in⁴

K_S = a shape/vibration mode factor to be defined below.

The peak stress σ_{pk} corresponding to this strain is then

$$\sigma_{pk} = E \cdot \epsilon_{pk} = K_S \cdot E \cdot V_{pk}/C_L \quad (4-7)$$

This relationship can now be applied to estimate the vibration-induced stress in a variety of structures. (Values for the quantity E/C_L for typical materials are given below in Table 4-1.)

4.2.1 Stress Response of Building Elements

In Eq. (4-7), the shape/mode factor K_S has the following values (Hunt, 1960).

- For longitudinal vibration of bars, $K_S = 1$. (This value of K_S will also be assumed to apply for acoustically excited compressional or shear seismic waves in the ground.)

Table 4-1

Stress Factors K_S , E , C_L , and E/C_L Used in Eq. (4-7) to Relate Peak Velocity to Stress for Various Aspect Ratios of Simply Supported Plates Made from Different Materials Vibrating in the Fundamental Mode.

$\longleftrightarrow K_S \longleftrightarrow$				
Length of Shortest Side Length of Longest Side	Adobe Masonry/ Concrete ($\mu = 0.1$)	Glass ($\mu = 0.22$)	Douglas Fir ⁽⁴⁾⁽⁵⁾ ($\mu = 0.229$ to 0.45)	Steel ⁽⁵⁾ ($\mu = 0.3$)
0.2	1.68	1.72	1.73 - 1.90	1.77
0.4	1.52	1.58	1.59 - 1.79	1.64
0.6	1.33	1.41	1.42 - 1.66	1.48
0.8	1.13	1.24	1.24 - 1.52	1.32
1.0	0.96	1.08	1.09 - 1.41	1.18

Material	Ref.	E 10^6 psi	C_L 10^5 in/sec	E/C_L (lb/in ²)/in/s
Concrete Block	(1)	2.1 \pm 0.1	0.957 \pm 0.046	13.1 \pm 6.5
Masonry/Stone	(1)	9.3 \pm 4.6	1.93 \pm 0.510	48.2 \pm 28.6
Adobe	(2)	0.0228	0.114 \pm 0.011	2.0 \pm 0.2
Cement Mortar	(1)	5.2 \pm 0.3	1.56 \pm 0.03	33.3 \pm 1.0
Gypsum Plaster	(1)	2.15 \pm 0.25	1.18 \pm 0.05	18.2 \pm 3.6
Brick Wall	(1)	1.72 \pm 0.87	1.00 \pm 0.28	17.2 \pm 10.6
Gypsum Wallboard	(1/4 - 3/8") (1,3)	0.537 \pm 0.047	0.826 \pm 0.108	6.50 \pm 0.87
"	(1/2 - 5/8") (1,3)	"	0.680 \pm 0.061	7.90 \pm 0.71
Glass	(1)	10.7 \pm 1.7	2.16 \pm 0.20	49.5 \pm 9.3
Douglas Fir	(1,4)	1.6 \pm 0.4	1.95 \pm 0.31	8.2 \pm 2.5
Steel	(1)	29.8 \pm 0.4	2.01 \pm 0.015	148.0 \pm 3.0

(1) Sutherland, 1968a (see Appendix B).

(2) Smith, 1986

(3) Stagg, et al. 1984

(4) Approximate for Douglas fir for longitudinal/radial directions re: grain.

(5) See text on next page for adjustments to K_S for wood or steel frame structures.

- For lateral vibration of beams, $K_S = c/\sqrt{I/A}$ where c is the distance from the neutral (unstressed) plane of the beam to the outermost fiber, and I/A is the ratio of the area moment of inertia to the cross-sectional area for the beam. For uniform rectangular beams, it can be shown that $K_S = \sqrt{3} = 1.73$ and for circular bars, $K_S = 2$. (The general form for beams, $c/\sqrt{I/A}$, is used later to estimate K_S for stress response of non-homogeneous built-up panels.
- For lateral vibration of plates, $K = 1$ to 2 depending on the plate geometry, mode shape and Poisson's ratio for the plate material. For a plate which can be considered to be simply supported (a reasonable assumption for windows according to Crandall and Kurzweil, 1968) and building walls and floors (Clarkson and Mayes, 1972), K_S has the following values for the fundamental mode (Hunt, 1960).

$$K_S = \sqrt{3/(1-\mu^2)} \cdot [1+\mu \cdot ((a/m)/(b/n))^2] / [1 + ((a/m)/(b/n))^2] \quad (4-8)$$

where a, b are the dimensions of the short and long sides of the plate and m, n are the mode numbers along sides a and b respectively (e.g., $m, n = 1$ for the fundamental mode of the plate), and μ is the Poisson's ratio for the material. This expression has been used to compute the values for K_S in Table 4-1.

For analysis purposes, practical design values for the factor K_S are developed as follows.

- For homogeneous "plates" such as windows or masonry (stone, adobe, brick, etc.) walls, a logarithmic mean value of K_S is computed from Table 4-1 for "plate" aspect ratios (a/b) from 0.2 to 1. (A narrower range of a/b (i.e., $a/b = 0.5$ to 1) might be appropriate for typical walls but the method used was conservative.) The resulting values were:

Masonry, Stone, Adobe	$K_S = 1.34$
Glass	$K_S = 1.39$

- For non-homogeneous (built-up) walls such as standard wood or metal stud walls, K_S was computed by multiplying a baseline value of K_S derived from Table 4-1 by an adjustment factor equal to the ratio of the radius of gyration $\sqrt{I/A}$ of a uniform beam where I and A are the area moment of inertia and cross-sectional area of the beam, respectively. The resulting values of K_S used for analysis are as follows.

Wood Frame Walls

- Single skin (e.g., barns) $K_S = 1.19$
- Skin on both sides $K_S = 1.13$

Metal Walls $K_S = 0.89$

- It is apparent from Table 4-1 that the above baseline values of K_S for wood and metal frame walls are average values which do not seem to reflect the variation in the values of K_S in Table 4-1 for wood, to the range of Poisson's ratio. For example, even though the aspect ratio for wood frame walls was assumed to be essentially constant at 0.2, corresponding to a typical 16" x 8' section, the actual value of K_S could vary due simply to the variation in Poisson's ratio (see Eq.(4-8)). For metal walls, K_S may vary significantly for various aspect ratios of metal walls. However, this statistical variation in K_S , which depends so strongly on the geometry of the structural element, will also be reflected in the statistical variation in resonance frequency. Therefore, to avoid compounding the consideration of these variations, it was assumed that the above values of K_S would be constant with no variation about their mean. (Subsequent evaluation demonstrated that this assumption had very little effect on the predicted probability of damage of structures from sonic boom.)

In summary, the above parameters combined with Eqs. (4-5) and (4-7) and the correction of 2.0 for multimodal velocity response provides the basis for making estimates of the nominal peak stress in a structural element due to sonic boom loading. The structural response prediction models employed are necessarily simplified for purposes of this report and are not intended to serve as the basis for detailed design of structures exposed to severe sonic boom loads from low altitude supersonic flights.

4.2.2 Response of Non-Structural Elements

Acoustically-induced stresses in archaeological ruins, water tanks and wells and potential avalanche or earth-slide areas are considered in the following.

4.2.2.1 Acoustically-Induced Stresses in Archaeological Structures

Stresses in archaeological structures induced indirectly by seismic response of the adjacent ground to sonic booms will be estimated from experimental data on such ground vibration (see Section 4.3.2.1). Stresses induced directly by the effective acoustic loading can

be estimated using the theory and supporting experimental data outlined in Sections 4.2.1 and 4.3 respectively.

4.2.2.2 Acoustically-Induced Stresses in Water Tanks and Wells

Water tanks consist of elevated metal or wood tanks resting on heavy columns large enough to support the mass of the tank filled with water, or surface-mounted concrete or stone tanks resting on the ground. The acoustic pressures on the support structure of elevated tanks or walls of ground-mounted tanks generated by sonic booms from ACM operations would not exceed about 6 lb/ft² (see Figure 3-8). This pressure is much less than the inherent hydrostatic pressures (62.4 lb/ft² per foot of water depth) associated with the weight of the water inside the tanks so that acoustic loading from ACM operations is not a significant problem for such partially filled tanks. For empty elevated metal tanks, only the walls would be of concern for this study and their vibration response and resulting stresses can be estimated in the same way as for other building structures using theory and supporting experimental data as indicated in the preceding paragraphs. For supersonic flights at lower altitudes than employed for ACM operations (normally above 5000 ft), sonic booms can approach this inherent hydrostatic pressure (~60 psf) and could thus present a potentially serious problem. As pointed out in the public response published in some Final EISs for SOAs, cattle ranchers worry about the prospect of sonic boom-induced leaks in such water tanks located in remote areas of a cattle range where loss of water could lead to serious loss of cattle (U.S. Air Force). However, the potential for damage in such cases is expected to be clearly indicated by estimates of potential damage to the metal walls of empty tanks.

For water wells, which are below ground except for the opening, vibration or seismic stresses on the well walls induced by noise will be insignificant, as will be shown later in discussions of experimental data relating to seismic vibration from sonic boom.

4.2.2.3 Acoustically-Induced Stresses in Avalanche and Slide Areas

Estimates of the potential for avalanches or earth slides will be made on the basis of estimated shear stresses, computed by Eq. (4-7). The "shape factor" K_S in Eq. (4-7) will be taken as unity as expected for vibration involving a shearing motion, the Modulus of Elasticity, E , will be replaced by the Modulus of Rigidity (i.e., Shear Modulus G), and the longitudinal speed of sound, C_L will be replaced by the speed of shear waves, C_S (Hunt, 1960). The velocity, V_{pk} will be based on the same experimental data on seismic-acoustic coupling just mentioned. Thus, following the same approach employed in a previous evaluation of seismic

response to sonic boom pressures (Cook, et al., 1972), acoustically-induced seismic shear stresses σ_s will be estimated from this modified form of Eq. (4-7) using available values for the shear wave speed C_s , and Shear Modulus G for snow and landslide materials. Comparison of these estimated shear stresses with estimated shear strengths of the materials will provide a rough estimate of the potential for triggering landslides or avalanches by sonic booms.

4.3 Experiment-Based (Empirical) Models for Response to Sonic Boom

Experimental data on response of structures to sonic boom excitation provide critical support to the preceding analytical models in two key areas:

- Data on vibration and stress response of structures to blast or sonic boom help to validate the preceding concepts and define typical resonance frequencies of real structures.
- Velocity response of the ground to acoustic loading help to define values for the seismic-to-acoustic coupling transfer function for a variety of ground conditions.

4.3.1 Experimental Data on Structural Response to Noise

In this section, published experimental data as stress response of building structures and seismic response of ground surfaces to sonic boom or other types of acoustic excitation are reviewed.

4.3.1.1 Structural Stress Response to Sonic Booms

Experimental data are available on measurements of the peak strain ϵ_{pk} in various types of residential building components to sonic boom from several programs (Mayes and Edge, 1964; and Power, 1964). Using representative values for the Modulus of Elasticity, E , for such components, such as in Table 4-1, the apparent peak stress σ_{pk} associated with the measured strain can be computed from $\sigma_{pk} = E \cdot \epsilon_{pk}$. Results of such computed stresses, bases on measured strains, are shown in Figure 4-5a for various building components exposed to sonic boom loads. Also shown is the predicted stress based on the use of Eq. 4-7, the sonic boom shock response spectrum shown in Figure 4-2, and available information on the dynamic response characteristics of the measured structures (Sutherland, 1968a). While the structures involved, in this case, are not necessarily representative of unconventional structures of

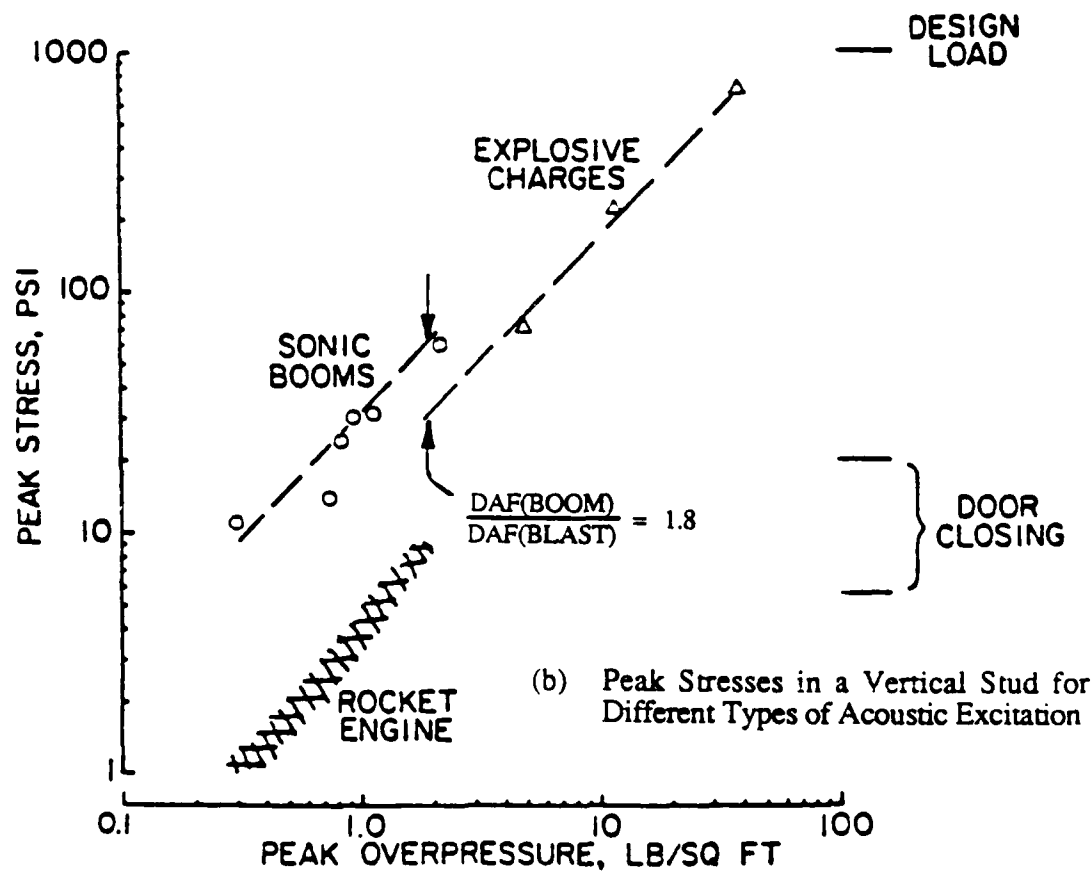
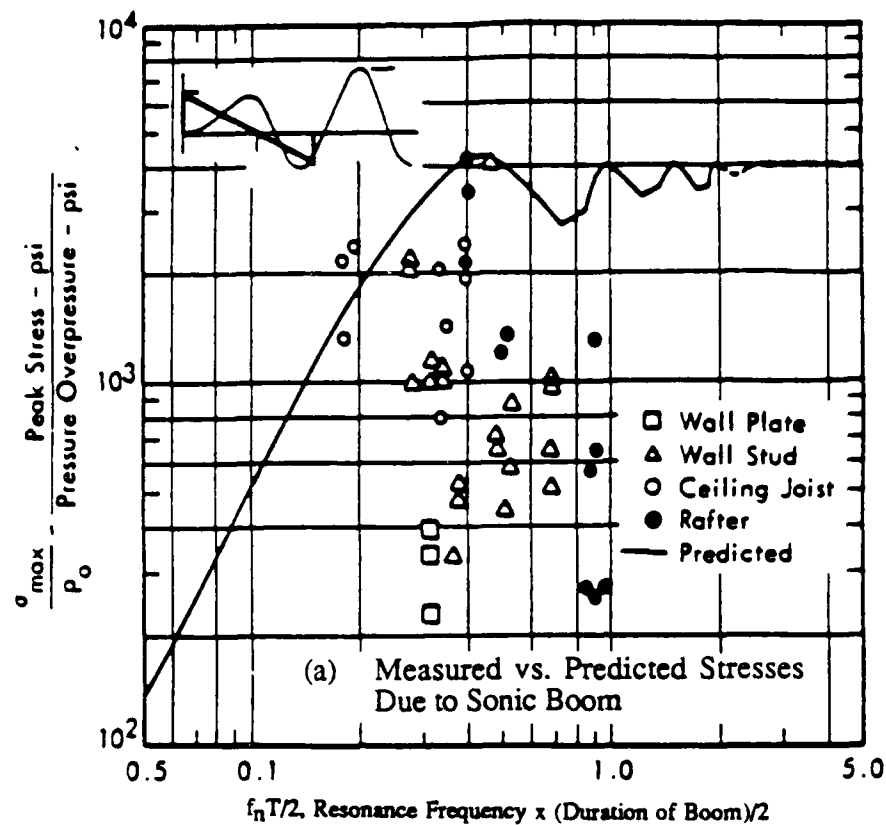


Figure 4-5. Measured and Predicted Peak Sonic Boom-Induced Stresses in Various Building Elements (Data from Mayes and Edge, 1964; Power, 1964).

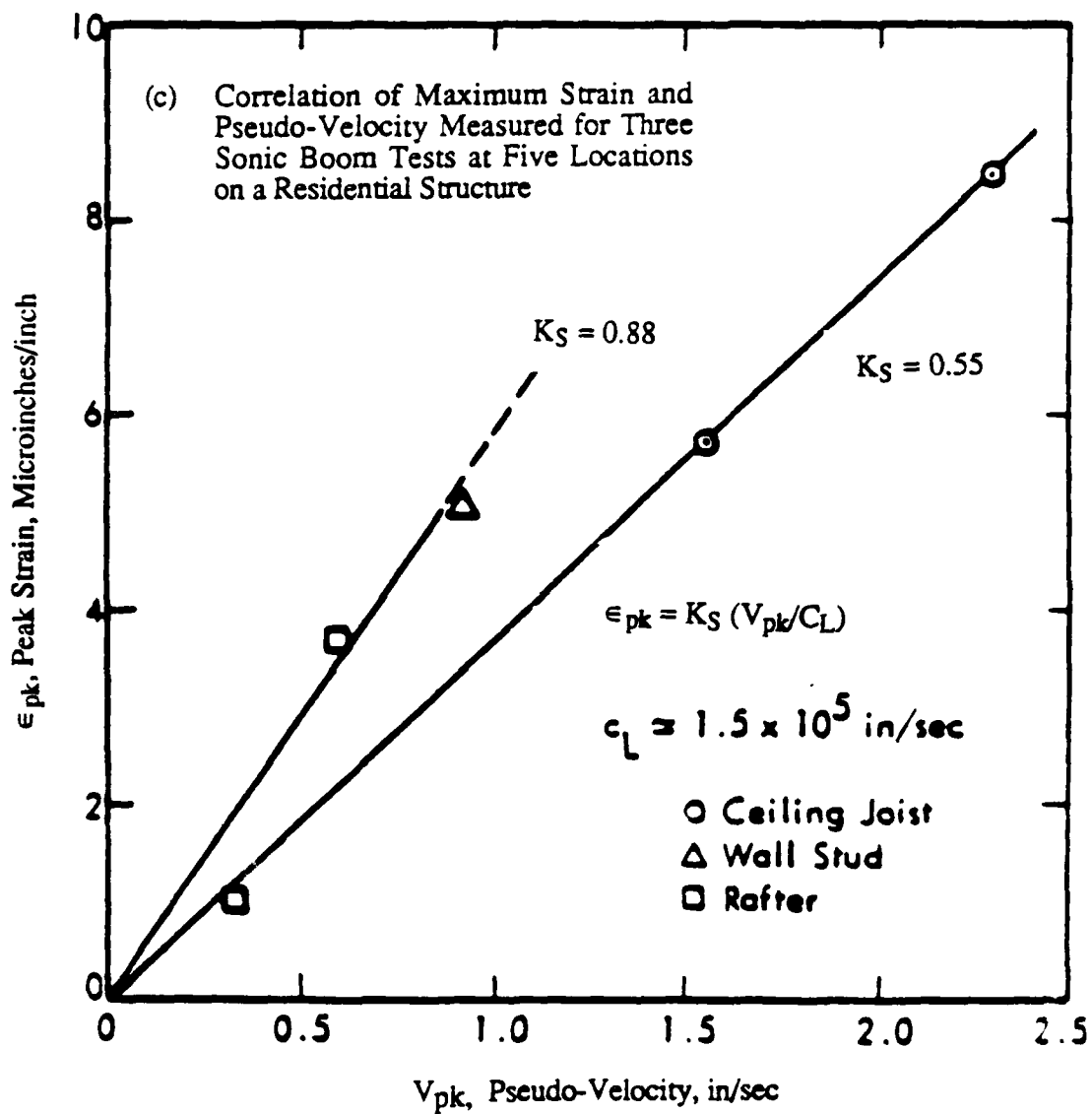


Figure 4-5 (Continued)

concern here, the figure serves to illustrate that for the structural locations measured, the predicted stresses closely represent the upper bound of the measured values.

Figure 4-5b shows more data from one of these earlier programs which evaluated building responses to sonic loads (Mayes and Edge, 1964). In this case the data show the linear relationship between measured peak pressures and measured stress (computed from measured strain) for one specific building component – a wall stud in a particular test structure – for several different types of sonic loading. The relationship between peak stress and peak pressure for sonic boom loading indicates a stress to pressure relationship of about 32 psi stress per psf of pressure load. A predicted value for this quantity, using a process outlined in Sutherland, 1968a, indicated a value of 28 psi stress per psf of sonic boom peak pressure. Note, as indicated in the figure, that the stress/peak overpressure relationship is about 1.8 times greater, as expected, for sonic boom excitation than for blast excitation (Sutherland, 1968a).

Finally, Figure 4-5c shows additional information available from one of these earlier sonic boom tests (Power, 1964) in the form of a correlation between the peak pseudo-velocity V_{pk} computed from the measured peak acceleration a_{pk} and the measured peak strain ϵ_{pk} in several residential building components. In this case, the experimentally derived value for the factor K_S in Eq. 4-6 varies from 0.55 to 0.88, roughly half the value expected according to Table 4-1. These values for K_S were computed from the following equation:

$$K_S = \epsilon_{pk} / (V_{pk} / C_L) = \epsilon_{pk} / (a_{pk} \cdot g / 2\pi f C_L) \quad (4-9)$$

based on a value for the longitudinal speed of sound C_L in the wood material of 1.5×10^5 in/sec which is nearly the same as the value (1.6×10^5) in Table 4-1.

To summarize, the experimental data shown earlier in Figures 3-14b and 4-3 indicate that experimentally measured values for the velocity response spectra $V_R(f)$ or the related Dynamic Amplification Factor, DAF, based only on measured pressure spectra of sonic booms, are very close to expected results for an ideal sonic boom. The very limited data on stress response to actual sonic booms in Figure 4-5 indicate that the predicted stress response to sonic booms generally agrees with measurements but may in some cases be on the conservative side, as desired, by no more than a factor of about 2. (Note that this possible overestimate by a factor of 2 in stress response is in the opposite direction from the predicted two-fold increase in actual peak velocity (and hence stress) response of a multimodal system over that of a SDOF system, as discussed earlier.) The possible overestimate in stress

response could be due in part to the neglect of any damping effects in peak response of the structure. In any event, no change in the damage prediction model will be made at this point on the basis of these limited, previously published experimental stress response data since they are not considered sufficient to warrant adoption of an empirically-derived correction, up or down, in predicted stress response. Furthermore, they were not obtained on representative unconventional structures and seem to indicate that the stress prediction models may be conservative as desired.

4.3.1.2 Resonance Frequencies

The resonance frequency of many structural elements, such as windows, can be estimated by treating the structure as a simply supported uniform plate. In this case, the fundamental resonance frequency f_0 , can be estimated by:

$$f_0 = (\pi/2) [1/a^2 + 1/b^2] \sqrt{EI' / (\rho A' (1 - \mu^2))} \quad (4-10a)$$

where a, b = side dimensions of the plate, inches ($a < b$)

E = Modulus of Elasticity of the plate material, psi

I' = area moment of inertia of a unit width strip of the plate (equal to $h^3/12$ for a uniform plate), in^4

A' = cross-sectional area of the same unit strip (equal to h for a uniform plate), in^2

ρ = mass density of the plate material, $\text{lb sec}^2/\text{in}^4$

μ = Poisson's ratio for the plate material (see Table 4-1)

h = thickness of a uniform plate, in.

For glass window panes and reasonably homogeneous adobe or masonry walls which can be approximated as uniform, simply supported plates, this expression can be simplified to:

$$f_0 = C_m [1 + (a/b)^2] (h/a^2) 10^4, \text{ Hz} \quad (4-10b)$$

where $C_m \approx 10.0 \pm 1.0 \text{ Hz}\cdot\text{in}$ for glass (see Sutherland, 1968a)

$\approx 9.5 \pm 1.0$ for steel (see Sutherland, 1968a)

$\approx 5.2 \pm 1.0$ for masonry and concrete (see Sutherland, 1968a)

≈ 0.047 for adobe (Smith, 1986)

Most building walls of current technology other than solid masonry, concrete or adobe are effectively orthotropic plates with a different stiffness in each direction and cannot be treated as uniform plates. While expressions are available to define resonance frequencies for such structures (Timoshenko and Woinowsky-Kreiger, 1959, and Sutherland, 1968a), for purposes of this report, experimental data provide a more convenient and potentially more reliable basis for estimating typical values. Table 4-2 lists representative values for the fundamental resonance frequency, dynamic magnification factors at midwall locations and approximate surface weights of typical non-uniform walls measured in residential buildings, as well as values derived from field measurements on several types of unconventional structures. In one case (King and Algermissen, 1987), sufficient data were available to provide an empirical expression, indicated in Footnote 8 of Table 4-2, for estimating resonance frequencies of 7 to 19 ft free-standing masonry walls, circa 1200 A.D. as a function of height. Note that the expression was selected to have the theoretically expected relationship between resonance frequency and the inverse of the square of wall height. However, the accuracy of this prediction equation is limited as indicated by the large standard deviation in the regression constant (i.e., $466 \pm 127 \text{ Hz}\cdot\text{ft}^2$).

4.3.2 Experimental Data on Seismic/Structural Response to Noise

Two types of experimental data on seismic responses to acoustic excitation are available: (1) seismic motion of the ground itself, and (2) structural response to acoustically-induced seismic motion at its base.

4.3.2.1 Experimental Data on Seismic Response of Terrain to Noise

Data on the vertical ground velocity relative to the local acoustic pressure obtained from a number of studies and representative results are summarized in Table 4-3. The data include studies of nominally steady-state seismic response to both acoustic noise from a loudspeaker source and rocket noise, as well as response to blast and sonic boom. The measurements of seismic response to a loudspeaker source exhibited a very strong dependence on frequency which is expected for the complex acoustic-seismic transfer function for a layered ground (Bass and Bolen, 1980). The peak response frequency varied by about 40 percent with changes in incidence angle of the sound impinging on the ground so that no one single frequency response pattern can be easily defined for seismic excitation by a moving aircraft. Furthermore, no such frequency dependence was found from analysis of data on seismic excitation by rocket noise at launch (Mickey, et al., 1962) nor was any frequency dependence required to predict with reasonable accuracy the seismic responses observed from sonic booms

Table 4-2

Typical Fundamental Resonance Frequencies, f_0 , Dynamic Magnification Factors, Q
and Surface Weights, w (lb/ft²) for Some Building Walls

Type of Wall	Sample Size	<----- f_0 , Hz ----->		<----- Q ----->		w , Surface Wt	
		Mean	Std.Dev.	Mean	Std.Dev.	lb/ft ²	psi
<u>Conventional Structures</u>							
Wood Frame Wall (Wallboard)	40 (1)	16.7	5.6	23.0	6.1	5.0 (3)	0.0347
Wood Frame Wall (Plaster)	10 (1)	15.7	4.6	10.4	1.0	9.75	0.0677
Wood Frame Wall	4 (2)	15.2	3.5	NA		5.4 (3)	0.0375
Brick Wall	1 (2)	12.3	5.7	NA		66.7 (3)	0.463
Concrete Block Wall		25.0		NA		38.0	0.264
Building Stone	5 (3)	NA	NA	NA	NA	110	0.764
Plaster Ceiling 3/4 in thick	2 (1,5)	14	±1.1	18.0	±5.5	9.74 (7)	0.0677
Metal Wall (Industrial Bldg)	4 (3)	14	±3.4	25		1.6-4.0	0.0194 (avg)
<u>Unconventional Structures</u>							
2.5 ft Limestone Block Wall (6 in thick)	1 (4)	26				63.5 (9)	0.441
3.5 ft Limestone Block Wall (9.6 in thick)	1 (4)	23				102 (9)	0.708
10 ft Adobe Wall (17 in thick)	4 (5)	11	2.8	21	±5.1	148-228 (6)	0.97-1.50
6.9-19 ft Masonry Walls	12 (8)	(See Note 8)		14.5	±3.2	180 (9)	1.25
10.5-12 ft Adobe Walls	12 (10)	16.6	1.4	16.7	±4.2	NA	NA
17-19 ft Adobe	5 (10)	11.4	2.9				

(1) Data from Siskind, et al., 1980a,b

(2) Data from Siskind, et al., 1976

(3) Estimated from Sutherland, 1968a

(4) Data from Brumbaugh (estimated resonance frequencies consistent with measurements of vibration response). (Data obtained at prehistoric Anasazi site, Grand Canyon.)

(5) Data from Section 5 of this report

(6) Surface weight based on range of densities for adobe of 98.5 lb/ft³ (Smith, 1986) to 152.3 lb/ft³ (Brumbaugh)

(7) Surface weight of roof structure (~6 psf) and plaster ceiling (3.85 psf) combined

(8) Data from King and Algermissen, 1987. Masonry walls (~1200 A.D.). Wall resonance frequency data described by: $f_0(\text{Hz}) = [466 \pm 127] / [h(\text{ft})]^2$

(9) Surface weight based on density of Chaco Canyon masonry wall (approximately 1200 A.D.) of 127 lb/ft³ (Lekson, 1984)

(10) Data from King, et al., 1988

Table 4-3

Summary of Average Measured Values for the Vertical Peak Ground Velocity, V_{pk}
Relative to the Local Peak Acoustic Pressure, P_{pk}

Type of Ground (Type of Source)	Ref	Density lb/ft ³	C_D (1) ft/s	V_{pk}/P_{pk} , (in./s.)/(psi) Mean \pm St. Dev.
(a) (Continuous Noise or Sine Sweep)				
Silt Loam	(2)	(106)	345	2.71 ± 1.0
Loess	(2)	96.8	740	2.17
Dredged Sand	(2)	106.1	890	3.61
Cape Kennedy (sand)	(3)	(115)*	(800)	$1.0 \pm 200\%$
Huntsville (clay)	(4)	(115)	(800)	1.2 ± 1.0
(b) (Sonic Boom, Blast or Gunshot)				
Clay Lake Bed	(5)	(125)	1970	0.567 ± 0.034
Rock Outcrop	(5)	(180)	6560	0.421 ± 0.028
Decomposed Granite	(5)	(170)	810	0.313 ± 0.150
Friable Sandstone	(5)	158	2165	0.230
Rock Shelter	(6)	155	(6560)	0.20 ± 0.06
Boulder Field	(6)	110	1480	0.35
Clay Lake Bed	(7)			0.77
Nevada Test Site	(8)	115	1000	0.80 ± 0.5
China Lake	(9)	125	1510	0.92 ± 0.3
Gravel-Sand-Silt mix	(10)	(106)	1725	1.87 ± 0.1
Snow (10 in. deep)	(10)	(14)		1.60 ± 0.2
Snow (4.6 ft deep)	(11)	15.6	2820	1.84 ± 0.8

* Parentheses signify estimated values.

- (1) C_D is measured or estimated dilatational (compressional) wave speed in ground
- (2) Bass and Bolen (1980) – Loudspeaker source
- (3) Mickey, et al. (1962) – Rocket noise, launch
- (4) Eldred and Sutherland (1965) – Rocket noise, static test
- (5) Goforth and McDonald (1968) – Sonic boom
- (6) Battis (1983) – Sonic boom
- (7) Cook, et al. (1972) – Sonic boom
- (8) Merritt and Newmark (1964) – Blast
- (9) Mickey and Shugart (1964) – Blast
- (10) Albert and Orcutt (1989) – Gunshot
- (11) Gubler (1977) – Explosive charge

(Goforth and McDonald, 1968). Therefore, it will be assumed for this study that the ratios of peak velocity response to peak acoustic pressure in the following table are independent of frequency in the low frequency range of interest.

The data in Table 4-3 were separated into values for acoustic excitation of the ground by (a) quasi-continuous noise, and (b) an impulsive sound. This was done in anticipation of a possible difference between the acoustic admittances for the two cases, since the first type of excitation would allow a possible resonant build-up in ground vibration as compared to the transient response of the ground to an impulsive sound. While the two sets of data appear at first to show evidence of such a trend, a more detailed evaluation shows that the values of V_{pk}/P_{pk} for roughly comparable types of soil, i.e., the logarithmic average value 1.9 (in/sec)/psi for the loose types of soil in part (a), and the value of 1.87 (in/sec)/psi for comparable soil type (gravel-sand-silt mix) in part (b), are approximately the same.

Thus, a design value for V_{pk}/P_{pk} of 1.9 (in/s)/psi will be employed to estimate the seismic response of loose soil areas (i.e., landslide areas) to sonic booms. Based on the variance in the data in Part (a) of Table 4-3, the estimated value for σ_L (the standard deviation of the log of this admittance value) is 0.236 (4.7 dB).

For harder ground surfaces, such as would be encountered at archaeological sites, one baseline value for the ground admittance would be 0.33 (in/s)/psi, which is the average for the rock-type materials in Table 4-3. However, for conservatism in evaluating these sensitive locations, the geometric mean between loose soil and hard rock was used to obtain a design value of $\sqrt{(1.9)(0.33)} = 0.79$ (in/sec)/psi. The value of σ_L was assumed to be the same as for loose soils, or 0.236.

For avalanche-prone areas, the limited but consistent data in Table 4-3 for snow were used to define an admittance equal to an average of 1.72 (in/sec)/psi. σ_L is estimated to be 0.16.

4.3.2.2 Amplification of Building Vibration Due to Seismic Excitation

For some types of structures (e.g., historic structures with no roof), vibration response due to excitation by acoustically-induced seismic vibration of the ground nearby may exceed the direct acoustically-driven structural vibration.

At the estimated resonance frequency of any historic or prehistoric structure which has no roof, the estimated amplitude of vertical seismic ground velocity at the base of a wall is

expected to increase by a factor of about 6.5 (corresponding to an increase of about 16 dB) to account for the amplification of vertical vibration at the base of a structure to horizontal vibration (normal to a wall) at a point well above the ground. Amplifications in the range of 1.4 to 30 have been observed in vibration studies of archaeological ruins (King and Algermissen, 1987). The amplification factor of 6.5 is a geometric mean of these observed amplifications derated by 75 percent to account for the lower horizontal ground vibration relative the vertical ground vibration for the same acoustic loading that has been observed in sonic boom tests (Goforth and McDonald, 1968). However, subsequent analysis shows that the direct acoustic response of the walls, even in the absence of roof structure, is expected to exceed even this amplified wall motion attributable to acoustically-induced seismic response of the ground at the base of the wall. Hence, seismic excitation of buildings or prehistoric walls to sonic booms can be discounted as not significant when compared to the direct acoustic excitation.

4.3.2.3 Response of Wells and Water Tanks to Seismic Excitation by Sonic Booms

The seismic response of the ground surface around a well or water tank located on the ground can be determined from the data in Table 4-3. Below the ground, the seismic vibration amplitude response has been observed to attenuate rapidly with depth, decreasing by a factor of 75 (-37.5 dB) between the surface and a depth of 44 ft (Goforth and McDonald, 1968). Thus, the seismic ground vibration responses specified in Table 4-3 could decrease by about $(37.5/44)$ or 0.8 dB per ft below the surface of the ground. Since this figure is based on only one data point, it will be assumed, conservatively, that a design value for vertical attenuation of seismic vibration is 0.5 dB per ft. It should be pointed out that attenuation of seismic vibration along the surface of the ground from purely mechanical sources would be much less. In this case, a large body of data is available indicating that the attenuation rate for horizontal propagation of compressional waves varies directly with frequency and, at a typical structural resonance frequency of 20 Hz, has a value of 5.4×10^{-5} to 8.4×10^{-3} dB per foot, depending on the type of terrain (White, 1965). Although very small indeed, this attenuation rate for horizontally-traveling seismic waves is still much greater than the attenuation of acoustic waves in air in the same frequency range. Thus, directly-coupled acoustic excitation of seismic waves by sonic boom is generally more significant than ground-transmitted seismic waves generated by a distant sonic boom impingement on the ground.

In summary, seismic stresses on buried structures such as wells can be predicted from Table 4-3 for positions near the ground surface. The seismic stresses will attenuate rapidly below the surface and will be dominated by the direct excitation from an incident sonic boom.

4.4 Damage Threshold Stress Criteria for Unconventional Structures

To review, evaluation of potential damage to unconventional structures as a result of the structural response estimated according to the models outlined in the preceding sections is accomplished by the following steps.

- (1) Select candidate types of unconventional structures.
- (2) Define the overall statistical model for assessing damage potential
- (3) Define a statistical model for the actual exposure of structures to sonic booms from ACM and other supersonic training operations
- (4) Define peak stress response prediction models for structures exposed to this sonic boom environment
- (5) Define strength or damage threshold stress values for unconventional structural materials
- (6) Systematically apply the above four steps to estimate damage potential for each type of supersonic operation and structure based on the overall damage assessment model in Step 2.

Steps (1) through (4) have already been carried out in Sections 2 and 3, and the preceding parts of this section. The following focuses on Step (5). First, however, it is desirable to address one issue not considered so far; that of the potential for cumulative damage by fatigue effects from prolonged exposure to sonic booms.

4.4.1 Fatigue Considerations in Damage Assessments

The ultimate strength of many materials can be reduced by 50 percent or more after repeated cyclic loading involving a complete reversal of stress (i.e., from tension to compression and back again) (Trapp and Forney, 1965). While a rigorous analysis of fatigue effects was not feasible within the scope of this program, it is felt that the effect of fatigue on damage predictions will be negligible based on the following:

- (1) Every effort has been made to use conservative estimates of damage threshold stress levels for materials in order to at least partially compensate for possible effects of fatigue on material strength.

- (2) Some brittle materials, such as glass, seem to show relatively little reduction in strength due to fatigue (Kao, 1970), at least when exposed to repeated sonic booms, so no specific reduction in strength of glass due to fatigue was considered. However, basic strength values selected for glass are conservative.
- (3) Limited information on fatigue of unreinforced and reinforced concrete beams under random loading (Chan, 1966), indicates a complex pattern of behavior under such loading, including a reduction in strength, due to fatigue, to 35 to 50 percent of the ultimate strength for a one time static load after about 1 million cycles of cyclic random loading.
- (4) Finally and perhaps most important for fatigue, consider a structure located directly under the center of an ACM area, probably the worst location in terms of frequency of sonic boom exposure. As shown in Section 3, the maximum number of booms per day for the WSMR SOA was 0.6. Assuming three to four cycles of stress reversal per boom, the estimated total number of stress reversals would be of the order of 800 cycles per year, indicating a very low rate of fatigue damage accumulation. Only in the case of unconventional structures that area already close to a failure condition would such a low rate of intermittent cyclic loading be expected to be significant.

In summary, even with the small number of cycles of sonic boom-induced stress it is assumed that over a 30- to 50-year period, fatigue is not likely to be a significant factor in the assessment of damage. Exacerbation of damage by fatigue may become significant for an already very fragile structure subject to damage or failure from application of almost any additional stress, including normally occurring dynamic stresses from weather effects or vibration from activity of nearby highway or rail traffic or heavy machinery. Thus, beyond including conservative values for the damage threshold stresses as often as possible, no additional specific quantitative assessment of fatigue effects is attempted in this report.

4.4.2 Material Strength Data Applicable to Damage Prediction

4.4.2.1 Material Strength Data for Glass

Only limited consideration is given to glass damage in this report, since it has been covered thoroughly before (Hershey and Higgins, 1976; Haber and Nakaki, 1989). However, statistical data on glass strength or failure stress are perhaps more complete than for any other material, and thus provide a useful starting point for this section.

Unlike any of the other structural elements considered in this report, "damage" to glass is assumed to correspond to actual failure of the glass pane. Glass panels fail under dynamic or static pressure loads due to the combination of bending and membrane tensile stresses and their interaction with stress-raising surface flaws and edge constraints (Beason and Morgan, 1984).

The stress-strain relationship for glass becomes very non-linear for window deflections greater than the glass thickness. Overprediction of glass failure that can result from neglecting this non-linear behavior will be at least partially compensated for by the fact that used or older glass panels considered in this study have a lower failure stress, as indicated by the following data.

A collection of failure load data on new and 20 to 25 year old glass panes (Beason and Morgan, 1984) and corresponding stress levels estimated according to a conventional linear model (Roark, 1965) and nonlinear model (Seaman, 1967) for stress response of panels is provided in Table 4-4. With and without the sample of 132 panes, 25 years old, from Anton, Texas, the logarithmic mean of the failure stress for the old panes is about 1970 and 2940 psi respectively. Although the 132-pane Anton sample was larger than the others, the difference between the mean failure stress for this sample and the mean failure stress for the other three sample sets was too large to have occurred by chance alone. Therefore the Anton data set was considered atypical for older glass and was thus discarded for analysis in this report. Thus, a log mean failure stress for old glass is assumed to be 2940 psi. For analysis purposes, this failure stress is rounded to two significant figures. This procedure will be followed for all final damage analysis criteria to reflect practical limits on accuracy of damage stress criteria. This failure stress is about 25 percent of the log mean failure stress (11,600 psi) for new glass (Hershey and Higgins, 1976) observed for an extensive data set. These strength data for new glass exhibited a log-normal distribution with a standard deviation of σ_L of the log of failure stress of 0.216. Glass in historic buildings will be assumed to be a mixture of old (uncracked) glass and already cracked glass. A more detailed discussion of glass strength for old and new glass is also provided in Sutherland, 1989.

To summarize, window glass in maintained structures will be assumed to be "used" with a mean strength of 2900 psi. The strength of glass in historic buildings will be assumed to correspond to that of already cracked glass with a strength of $0.1 \times 11,600$, or 1200 psi. The standard deviation, σ_L of the log of the strength for both categories of glass panes will be assumed to be the same as that for new glass or ± 0.216 (± 4.32 dB).

Table 4-4
Comparison of Failure Load and Estimated Failure Stress of
Old vs. New Glass Window Panes of Thickness h and Side Dimensions a, b
(Data from Beason and Morgan, 1984)

Sample	Age Years	Sample Size	h in.	a in.	b in.	P, Failure Load (Mean \pm S.D.) psf	Estimated Failure Stress Linear ⁽⁴⁾ psi	Nonlinear ⁽⁵⁾ psi
GPL (1)	20	20	.2128	28.5	60.5	79 \pm 23.3%	6,100	1,790
GPL (1)	20	20	.2128	28.5	28.5	168 \pm 22.3%	6,105	3,370
Dallas (2)	20	22	.125	16.25	19.75	229 \pm 27%	10,480	4,210
Anton (3)	25	132	.25	14	36.25	134.3 \pm 25.1%	<u>1,975</u>	<u>595</u>
Log Mean (all samples)							5,245	1,970
Log Mean (without Anton samples)							7,270	2,940
New	0	NA	.125	16.25	19.75	427.7 \pm 18.1%	19,575	6,205

Average ratio of failure stress $\left\{ \frac{(\text{linear model})}{(\text{nonlinear model})} \right\} = \left\{ \begin{array}{l} 3.15, \text{ new glass} \\ 2.66, \text{ old glass} \end{array} \right.$

Notes:

- (1) Samples from GPL Building, Lubbock Texas (from Building Renovation)
- (2) Samples from Johnson Chevrolet Building, Dallas Texas (from Building Renovation)
- (3) Samples from Public School Building, Anton Texas (from Building Salvage)
- (4) Stress, σ (failure) = $K \cdot P \cdot (a/h)^2$, where K = function (a/b), linear model (Roark, 1965)

Note that this relationship between the factor K and the panel aspect ratio for this linear stress prediction equation is more complex than has been assumed by others (Hershey and Higgins, 1976; Haber and Nakaki, 1989) and correctly predicts stresses which are 15% to 50% higher for a simply supported plate with aspect ratios of 1:1 and less than 0.2 respectively than the incorrect equation utilized in these prior studies.

- (5) Stress, σ (failure) computed from non-linear theory (from Seaman, 1967)

$$q = 4.93 S_b + 0.0329 S_b^3$$

where $q = P(a/h)^4/E$, nondimensional load

$S_b = \sigma(a/h)^2/E$, nondimensional bending stress

P = Static Pressure Load

E = Young's Modulus

To estimate the probability of failure of glass panes of different sizes and thicknesses, only one of five different categories of window used in Haber and Nakaki, 1989 are employed for this report. The basic dynamic characteristics of these five categories, including their estimated fundamental resonance frequencies are given in Table 4-5. Note that estimates of the resonance frequency according to Haber and Nakaki, 1989 and Eq. (4-10) are in close agreement. The category selected for this study as realistic for historic buildings was Category B, a 2 to 10 sq. ft window. The latter value for Category B was used for this report.

4.4.2.2 Material Strength Data for Plaster, Masonry and Adobe Walls

Damage criteria for maximum partial velocity of the ground near masonry structures (e.g., stone, concrete and brick) subject to damage from blasting operations and data from static load tests on such walls provides the following estimates of failure (or damage) stress values. These data are summarized in Table 4-6.

The Level of Damage classification indicated in Table 4-6 is taken from the following universal classification scheme used for assessing damage from blasting operations (Siskind, 1980):

- Threshold = Loosening of paint; small plaster cracks at joints between construction elements (i.e., bricks, wall panels, etc.); lengthening of old cracks.
- Minor = Loosening and falling of plaster; cracks in masonry around openings near partitions; hairline to 3-mm cracks (0 to 1/8 inch); fall of loose mortar.
- Major = Cracks of several millimeters in walls; rupture of opening vaults; structural weakening; fall of masonry, e.g. chimneys; load support ability affected.

The data in Table 4-6 provide the basis for the following design values for the average damage stress levels for building stone, concrete block and brick walls.

The damage stress threshold for relatively new building-stone walls is estimated from Table 4-6 to be 280 psi and the corresponding standard deviation σ_L of the log of the average damage stress is estimated to be ± 0.214 . This is the rms sum of the corresponding values (0.092, 0.15 and 0.12) for the standard deviations of the logs of the three terms, K_S , (E/C_L) and V_{pk} that define the calculated damage stress for building stone based on a threshold value for blast damage peak velocity, V_{pk} . In the absence of any known sources of actual damage or

Table 4-5

Size Categories and Associated Parameters
Used in Evaluation of Potential Window Damage

Category ⁽¹⁾	Area ft ²	^h Thickness inches	Surface Wt. psi	^{a(2)} inches	$f_o^{(1)}$ Hz	$f_o^{(3)}$ Hz	S.D. ⁽⁴⁾ -	a/h
A	0-2	3/32	.00814	14	95	96	0.138	149
B (6)	2-10	3/16	.0163	25	60	60	↓	133
C	10-50	1/4	.0217	57	18	15.4	↓	228
D	50-100	5/16	.0271	100	6	6.2	↓	320
E	>100	3/8 ⁽⁵⁾	.0326	120	4	5.2	↓	320

(1) From Haber and Nakaki, 1989.

(2) Assumed length or width of square plate.

(3) Computed from Eq. (4-10). (For evaluation purposes, the resonance frequencies for Categories A and B windows were assumed to be 100 and 63 Hz respectively.)

(4) Estimated Standard Deviation of Log (f_o) based on range specified in Haber and Nakaki, 1989.

(5) Thickness for this category increased from 5/16 inch in Haber and Nakaki, 1989 to 3/8 inch to be consistent with maximum allowable ratio of a/h of about 330 from Uniform Building Code for windows of this size (Seaman, 1967).

(6) Category selected for this report for historic buildings.

Table 4-6

Summary of Estimated Failure or Damage Stress Values for Various Types of Masonry Walls
Based on (a) Blast Damage Criteria and (b) Static Test Data

Type of Masonry Wall	Thickness in.	Level of Damage ⁽⁵⁾	Peak Velocity in/sec	E/C _L psi/in/s	Estimated Stress ⁽⁴⁾ psi
(a) Blast Damage Criteria					
Stone and Mortar Basement Walls ⁽¹⁾	18-24	None	3.4 ± 1.3	48.2 ± 12.5	220 ± 110
	18-24	Minor	10.3		665 ± 175
Stone and Mortar ⁽¹⁾	NA	None	3.4		220 ± 58
	NA	Threshold	4.5		284 ± 75
	NA	Minor	7.0		452 ± 118
	NA	Major	10.0		646 ± 168
Concrete Block ⁽¹⁾	8-10	None	3.0	13.1 ± 6.5	53 ± 27
	8-10	Threshold	3.0+		53 ± 27
	7-9	Threshold	10.0		176 ± 87
Brick Wall ⁽¹⁾	4	Threshold	>12 ⁽⁶⁾	17.2 ± 4.8	>280 ± 77 ⁽⁶⁾
Type of Masonry Wall	Thickness in.	Level of Damage ⁽⁴⁾	Peak Velocity in/sec	P Static Load psi	Estimated Stress psi
(b) Static Test Data					
Brick Wall ⁽²⁾	4	First Cracks	NA	0.418 ± 153%	
Brick Wall ⁽³⁾	6-8	NA	NA	0.528 ± 410%	
	4-8		Average	0.473	55 ⁽⁷⁾
Brick Wall 1:3 mortar ⁽⁸⁾	4-8	Failure	NA	NA	18.5 ± 10.3 ⁽⁸⁾
Brick Wall, high bond mortar ⁽⁸⁾	4-8	Failure	NA	NA	190 ± 84 ⁽⁸⁾

(1) Stagg, et al., 1984

(2) Hershey and Higgins, 1976, average for two samples of four different walls with low strength (1:1:4 mix) and high bond mortar.

(3) Average for four mortar mixes, low to high strength (Appendix B).

(4) Estimated damage stress, in psi, $\sigma = K_S \cdot (E/C_L) = 48.2 \text{ psi}/(\text{in}/\text{sec})$ for typical masonry walls (see Table 4-1 and text in Section 4.2.1).

(5) Level of damage as defined in Uniform Classification Scheme (Siskind, et al., 1980b)

(6) Estimated based on Peak Strain > 160 μ in/in (Stagg, et al., 1984), $E = 1.72 \times 10^6 \text{ psi}$ and $K_S = 1.34$.

(7) Estimated based on $\sigma = K \cdot (a/h)^2 \cdot P$ and $K(a/h)^2 = 116$ for 4 ft x 8 ft brick wall test specimen (see Eq. 4-11).

(8) Yokel, et al., 1971, estimated stress is actually computed modulus of rupture assuming partial end fixity.

failure stress data for historic (unoccupied but maintained) and prehistoric stone masonry buildings or partial building segments, such as free-standing walls, it was assumed that the damage threshold stress would be respectively one and two standard deviations (in terms of logarithms of the stress) below that for current building-stone walls. The resulting values were 170 and 100 psi respectively for historic and prehistoric stone masonry walls. These are considered reasonably conservative values since, in fact, some stone masonry structures constructed by early Americans (the Anasazi) in the 11th century are still standing, often in remarkably good condition (Lekson, 1984).

For concrete block walls, the average of the two values for damage threshold stress in Table 4-6 is approximately 120 psi. In the absence of more complete data, it was assumed that the standard deviation, σ_L of this damage threshold stress for concrete blocks is the same as for building stone, ± 0.214 (± 4.28 dB).

For brick walls, the log mean damage threshold stress was estimated to be 55 psi for the first two data sources identified in Table 4-6. This estimate is based on the computed stress (Roark, 1965) for the average damage threshold (i.e., first appearance of cracks in the joints) for a static load of 0.473 psi. The average static damage loads for the two sets of data differ by only 26 percent. However, it should be noted that within each data set, there was a very large range in the values of static load for failure or damage of bricks walls – a variation as much as ± 400 percent. This wide range is due to: (1) real differences in the strength of brick walls as a function of their geometry and type or mix of mortar, and (2) the complex, potentially inelastic behavior of brick walls under severe lateral loads (Yokel, et al., 1971). As cracks develop in a masonry wall from large lateral loads, the wall may no longer behave elastically (Stagg, et al, 1984), so that estimated stress values based on linear stress response theory can be suspect. For historic brick buildings, a reduced damage threshold stress of 17 psi was assumed that corresponds to the estimated strengths for older, low-strength mortar brick walls. The last two entries for estimated damage stress levels for brick walls are actually computed values for the Modulus of Rupture for four different types of low strength (1:3 mortar mix) and high strength mortar (Yokel, et al., 1971). Unfortunately, this parameter is not a reliable measure of the actual fiber stress in a structure at failure (Eshbach, 1952). A large statistical data base was not available for these estimates of damage threshold stress values for brick so it was assumed that the more extensive data base on strength of adobe bricks, considered below, should be used to define σ_L for conventional (fired clay) brick walls. The resulting value is ± 0.239 .

4.4.2.3 Adobe Walls

For adobe walls, data from static loading tests conducted on approximately five adobe bricks of various types from each of 58 manufacturers (Smith, 1982), provide a substantial statistical data base for the static load strength of adobe bricks typically about 10 x 4 x 14 inches in size. The log mean compressive strength and Modulus of Rupture from these data were 400 psi and 49 psi respectively. See Figure 4-6 for an illustration of the apparent log-normal distribution for the reported Modulus of Rupture values for this important data set. The corresponding values for the standard deviation of the log of the Modulus of Rupture ± 0.239 . However, only this measure of statistical variation, σ_L of ± 0.239 was considered useful to apply to adobe structures since, as noted above, the Modulus of Rupture is not a reliable measure of actual failure or damage stress. It was assumed, in the absence of other data, that the ratio between the compressive strengths of adobe (400 psi as stated above) and conventional (fired clay) bricks (an average of 2565 psi for three grades of conventional brick according to Eshbach, 1964) could be used as a correction factor to adjust the damage threshold stress of brick walls of 55 psi to provide an estimate for the damage threshold stress for adobe walls. The resulting value was equal to $(400/2565) \cdot 55 = 8.5$ psi (rounded to the nearest 0.5 psi). Thus, 8.5 psi is taken as a baseline estimate for the damage threshold stress for an adobe wall with a corresponding value for the standard deviation of the log of this stress of ± 0.239 . This baseline value for the strength of adobe walls was considered applicable for current construction.

One pair of data points was also available (Smith, 1982) for the Modulus of Rupture of about 10 year old and 145 year old Terrón adobe, a particular type of adobe. For this particular set of data, the Modulus of Rupture for the "new" adobe was 53 psi and 20 psi for the 145 year old adobe. Based on these two data points, and in the absence of any other information on strength of old adobe, the log mean strength of old adobe walls found in historic buildings was assumed to be equal to $(20/53) \times 8.5 = 3.2$ psi; the standard deviation of the log of the strength was assumed to be the same as for new adobe, ± 0.239 . For prehistoric adobe buildings, some of which are centuries old and at least partially intact, the damage threshold stress was assumed to be equal to one standard deviation, (in terms of logarithms) below the value for "old" adobe or $3.2 \cdot 10(-0.239) = 1.8$ psi. Again, the same value for σ_L of ± 0.239 (± 4.78 dB) was assumed for the variation in log of damage threshold stress for these very old structures.

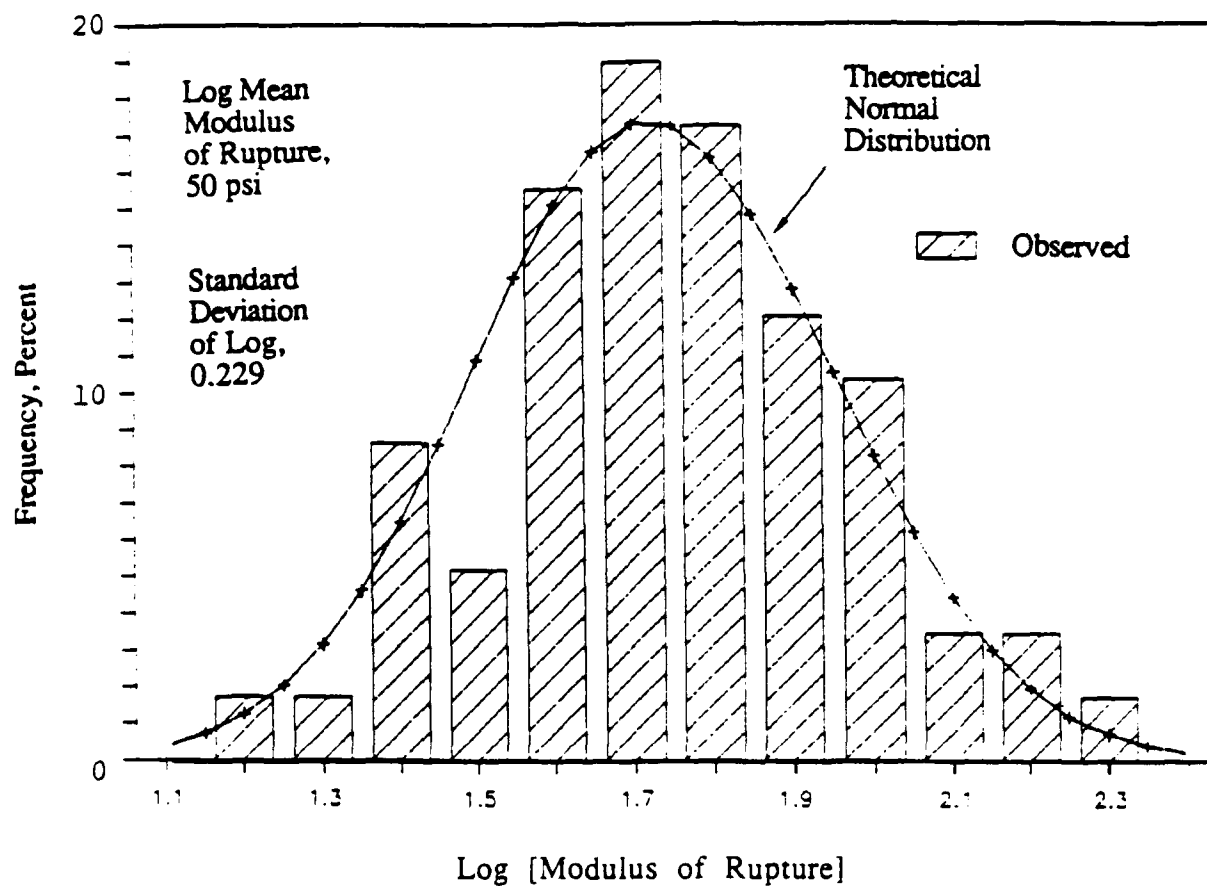


Figure 4-6. Distribution of Logarithm of Modulus of Rupture for 58 Tests of Adobe Bricks from Various Manufacturers Compared to Theoretical Log-Normal Distribution (Data from Smith, 1982).

4.4.3 Material Strength Estimates for Wood Frame Buildings

Interior walls of wood frame historic buildings are expected to be either plaster or wood. Damage threshold values are considered for such walls in this section.

4.4.3.1 Plaster Interiors

While wood frame buildings of current construction will normally have an interior wall finish of wallboard (also called plasterboard or drywall), it is assumed that interior walls of unconventional historic wood frame buildings used plaster instead. This assumption is consistent with actual field investigation of two such typical structures (Hershey et al., 1975). This structural element will tend to be the most susceptible to damage when such buildings are exposed to sonic booms. The basic dynamic stress prediction model developed in Section 4.2 is strictly applicable only for homogeneous walls and must be modified to predict stress and estimate damage probability of non-homogeneous built-up walls such as used for standard wood frame construction. For the same reasons, stress in such panels under static loads must be evaluated differently from stress in homogeneous plates under the same type of load. The bending stress σ in a wall or equivalent beam under a static load is equal to Mc'/I where M is the bending moment associated with a lateral load on the wall, c' is the distance from the neutral bending axis to the outermost fiber (approximately equal to one-half the wall thickness), and I is the area moment of inertia for a unit width strip of the wall. This relationship can be used to derive the following basic expression for stress σ in a homogeneous wall (or equivalent plate) with a short side a and thickness h , under a static pressure, P :

$$\sigma = K \cdot (a/h)^2 \cdot P \quad (4-11)$$

where K is a function of the plate aspect ratio (Roark, 1965) with a value of about 0.75 for a 16 inch by 96 inch "plate" corresponding to one section between studs of a standard 8 ft wood stud wall. (Note that the comparable expression in Hershey and Higgins [i.e., their Eq.(1)] would predict $K = 0.486$, low by 35 percent.) For a non-homogeneous (built-up) wood frame wall, the same basic expression, $\sigma = Mc'/I$, can be used to show that the maximum stress under static loading, which occurs at the inner or outer surface of the wall, can be defined from a modified version of Eq.(4-11) equal to:

$$\sigma = K_b K (a/h)^2 P \quad (4-12)$$

where K , a , h and P are the same as before (h being the total thickness of the wall) and the added term K_b is approximated for a typical wood frame wall by:

$$K_b = \left[\left(\frac{b}{a} \right)^2 \frac{1}{(3nt/d + w'/a)} \right] \quad (4-13)$$

where a, b = short and long sides, respectively, of the 16" x 96" section of a standard wood frame wall.

n = 1 or 2 for a wood frame wall with one or two covering surfaces (i.e., exterior only for a typical barn, or both exterior and interior covering for a typical dwelling).

t = the thickness of the inner and outer surfaces of the wall (assumed equal to 3/4")

d = thickness or depth (3 5/8") of a 2" x 4" framing stud

w' = width (1 5/8") of the stud.

For these assumed dimensions of a typical wood frame wall, the value of K_b is approximately 27 for a wood frame wall with covering (exterior and interior) on both sides of the wood studs, and 50 for $n=1$ (bare studs inside). Thus, Eq. (4-12) provides one way to estimate damage stresses in building walls based on published static load data where failure load is only given in terms of the static pressure on the wall.

For dynamic loads, the same basic expression relating peak stress, σ_{pk} and peak velocity, V_{pk} , given by:

$$\sigma_{pk} = K_S (E/C_L) \cdot V_{pk} \quad (4-14)$$

is still valid. However, the constant K_S must be defined by the general expression, $c'/\sqrt{I/A}$, treating the wall as an equivalent beam, where c' can be taken as approximately equal to half of the built-up wall thickness, I is the area moment of inertia of a unit width of the "beam" and A is its cross-section.

Assuming a typical 2" x 4" x 8' wood stud wall with studs 16" on centers,* it was shown in Section 4.2.1 that for external and internal skin coverings 3/4" thick, K_S has a value of approximately 1.13, and for no internal covering, a value of 1.19. As discussed earlier, σ_L

* A change in the spacing to 24 inches, more representative for older wooden buildings, does not change the value of K_S significantly.

of the log of K_S will be assumed to be zero since this variance will tend to be already included in the variation of resonance frequencies of walls.

With this modified relationship, it is now possible to relate two sets of data on damage thresholds for such walls for historic dwellings – one set defining limiting values of structural velocity from blast damage criteria from which damage threshold stresses can be calculated, and the other defining static load failure stresses in the interior skin materials (e.g., plaster). This same process has also been applied for estimating potential damage to gypsum board walls of conventional structures exposed to noise from low-flying military aircraft (Sutherland, 1989).

Table 4-7 summarizes the recommended criteria for peak velocity (or displacement) of structure (or of the adjacent ground surface) to prevent damage from blasting operations (Siskind, et al., 1980b). More specific criteria suggested by the same Bureau of Mines studies are shown in Figure 4-7 for typical wood frame buildings in terms of damage threshold values of peak velocity or displacement, measured at the base or foundation of the building, as a function of frequency (Siskind, et al., 1980a). The Bureau of Mines test data also showed that at a typical fundamental resonance frequency of interior walls (e.g., 10-20 Hz), the peak vibration at the center of a wall due to blasting operations was about 2.5 times the vibration measured at the base of the structure (Siskind, et al., 1980b). Thus, to a first approximation, threshold levels for damaging stresses in the wall materials can be estimated from Eq. (4-14) and the data in Table 4-7 or Figure 4-6 but accounting, where applicable, for the higher vibration at the wall relative to the particle vibration on the ground. As indicated in Table 4-7, many separate individuals or organizations have proposed varying criterion levels for these vibration parameters for different types of structure. The criteria listed in Table 4-7 that are applicable to unconventional structures vary by a factor of about 6 from a minimum of about 0.08 inches per second (2 mm per second) to 0.5 inches per second. Different limits on structural velocity are recommended by some organizations according to the type or historical importance of the structure.

However, in one case (King and Algermissen, 1987) a much lower velocity of 0.004 in/sec (0.1 mm/sec) is recommended for sensitive prehistoric structures exposed to seismic vibration to allow for an amplification of vibration by a factor of 20 (as estimated by the authors) between the ground at the base of a wall and a point on the wall. While such an amplification is feasible, it is only expected to occur for essentially steady-state vibration, a condition not applicable for structural response to sonic booms. All of the other displacement

Table 4-7

Criteria for Maximum Structural Displacement and Velocities to Avoid Damage to
Prehistoric, Historic, Sensitive and Conventional Structures

Reference	Type of Structure	Frequency Range Hz	Displacement inches	Criteria Velocity in/sec
King and Algemissen, 1987	Prehistoric (Chaco Canyon)	1-20		0.08 (1)
King, et al., 1985	Prehistoric (Hovenweep)	1-10		0.004 (2)
Saurenman, et al., 1982	Historic/Sensitive			0.04 (1)
Konon and Schuring, 1985	Historic/Sensitive	< 10 Hz > 40 Hz		0.25 (1) 0.5 (1)
German DIN 4150 (3)	Ancient ruins and historic buildings Buildings with visible damage/cracks in masonry Buildings in good condition with possible cracks in plaster Industrial and concrete structures without plaster			0.08 (2) 0.16 (2) 0.32 (2) 0.4-1.56 (2)
Australian Standard (3)		<15 >15	0.008	0.75 (2) 0.2 (2)
U.K. (3)	(Blasting only) (Steady state vibration)			0.4-1 (2) 0.2 (2)
Ashley (3)	Ancient and historic monuments Housing in poor repair Good residential, commercial and industrial structures Welded gas mains, sewers, engineered structures			0.3 (2) 0.47 (2) 1.0 (2) 2.0 (2)
Esteves (3)	Historical monuments, hospitals, very tall buildings Current construction Reinforced construction (e.g., earthquake resistant)			0.1-0.4 (4) 0.2-0.8 (4) 0.6-2.4 (4)
Siskind, et al., 1980a (See Figure 4-5)	Wood frame (plaster interior)	<2.7 2.7-10 10-40 >40	0.03 0.008	0.50 2.0

(1) Peak velocity of structure

(2) Peak velocity of ground at base of structure

(3) As cited in Siskind, et al., 1980b, Appendix A

(4) Range of velocities for ground varying from incoherent loose soil (lowest velocity) to coherent hard soil or rock

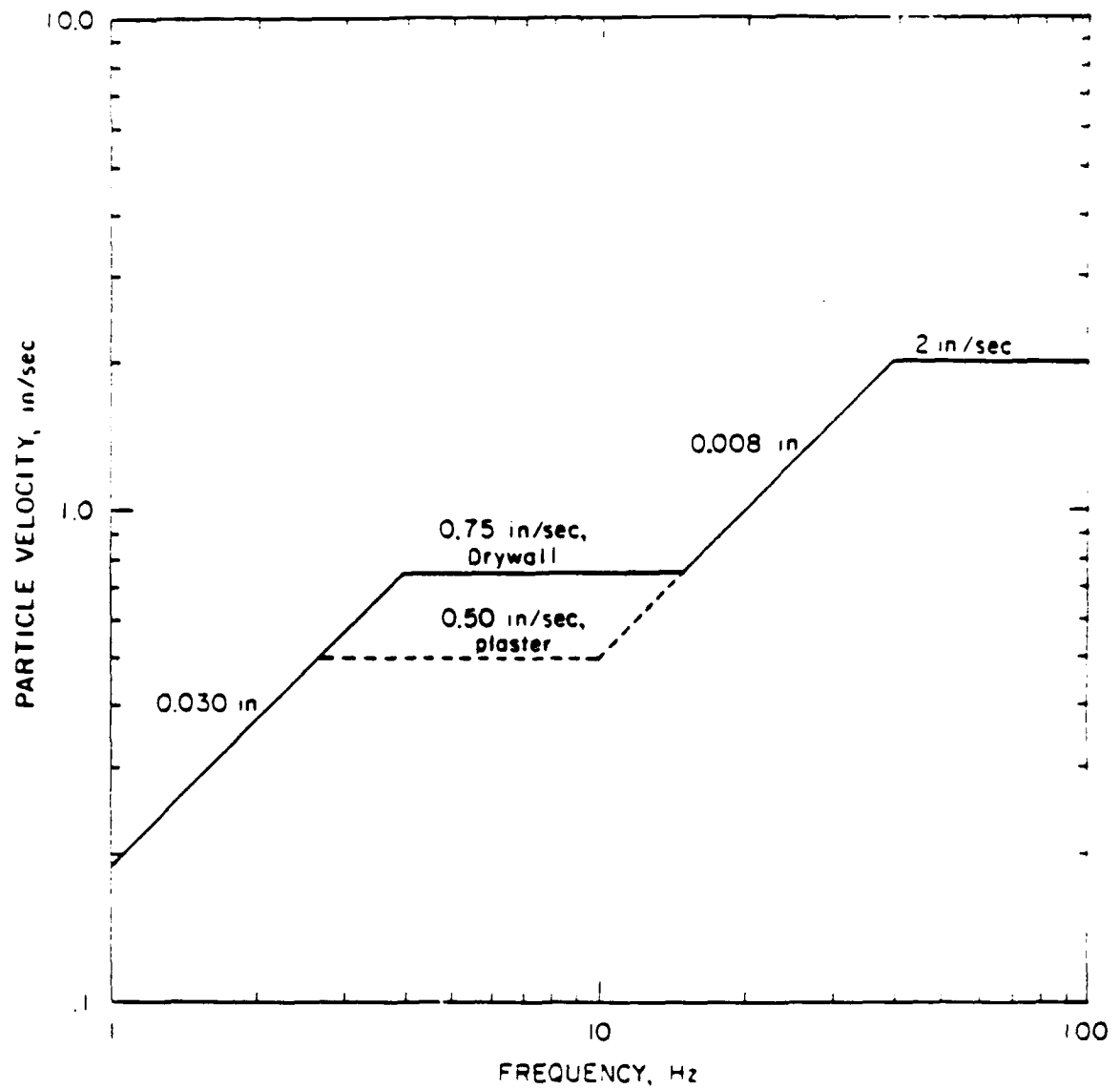


Figure 4-7. Safe Levels of Blasting Vibration for Houses Using a Combination of Velocity and Displacement (from Siskind, et al., 1980a).

or velocity limits listed in Table 4-7 are believed applicable only for structural response to blasting (and sonic boom) and correspond to limits of vibration measured on (or in) the ground or at the base of a structure (Siskind, 1980b). This is a vital point relative to the application of the data in Table 4-7 or Figure 4-6 to this program. It should also be pointed out that for such transient excitation, as shown earlier in Figure 4-5c, dynamic magnification of the structural response (i.e., DAF) for blasting is expected to be lower than the DAF for sonic booms by a factor of about 1.8 (Clarkson and Mayes, 1972) due to the differences in pressure time history between blast and sonic boom overpressures. Thus, the criteria in Table 4-7 and Figure 4-5 could be reduced by such a factor of 1.8 to be more realistic for application to sonic boom damage assessment.

In their Table 22, Hershey and Higgins summarize tensile strength data on a variety of plaster materials, from which a log mean strength of 140 psi and standard deviation of the log of strength of 0.185 is estimated. In their interpretation of these same data, Haber and Nakaki, 1989, estimate log mean failure loads in the range of 11 to 61 psf for various types of interior and exterior plaster walls. An average value for these failure loads for plaster walls is about 28 psf which corresponds, according to Eqs. (4-12) and (4-13), to an estimated failure stress for a 3/8" thick, 16" x 86" plaster panel of 150 psi. Data on tensile strength of 3/8" plaster beams under alternative loads indicate failure in one cycle at a stress of 300 psi and 200 psi after 10,000 cycles (Stagg, et al., 1984). Other test data on tensile strength of plaster mortar from a variety of sources (summarized in Appendix B) indicate a range of tensile strength of 165 to 350 psi. Thus, for analysis purposes, the average of the lower end of this range of failure stresses (e.g., 140 to 165 psi) or 150 psi, will be used, along with a value of ± 0.185 (± 3.7 dB) from the Hershey and Higgins statistical data on mortar strength for the standard deviation σ_L of the log of failure strength of plaster walls.

A limited correlation can be drawn between these static failure load data for plaster and the statistical data shown in Figure 4-8 on damage threshold values for ground velocity at the base of structures exposed to blasting operations (Siskind, et al., 1980b). Based on a median velocity of about 5.3 in/sec (measured at the ground) in Figure 4-7, a value for K_S of 1.19 (see Table 4-1) and an average value of 18.2 for E/C_L for plaster (Table 4-1), and allowing for an amplification between the ground and wall vibration of 2.5, the estimated peak stress is about $(1.19) \cdot (18.2) \cdot (5.3) \cdot (2.5) \approx 290$ psi.

This is within the range of the static failure stress of 140 to 350 psi indicated above for plaster. On this basis, the peak velocity criteria in Table 4-7 and Figure 4-7 are believed to be reasonably consistent with actual material strength data for plaster. (Note that Eq. (4-14)

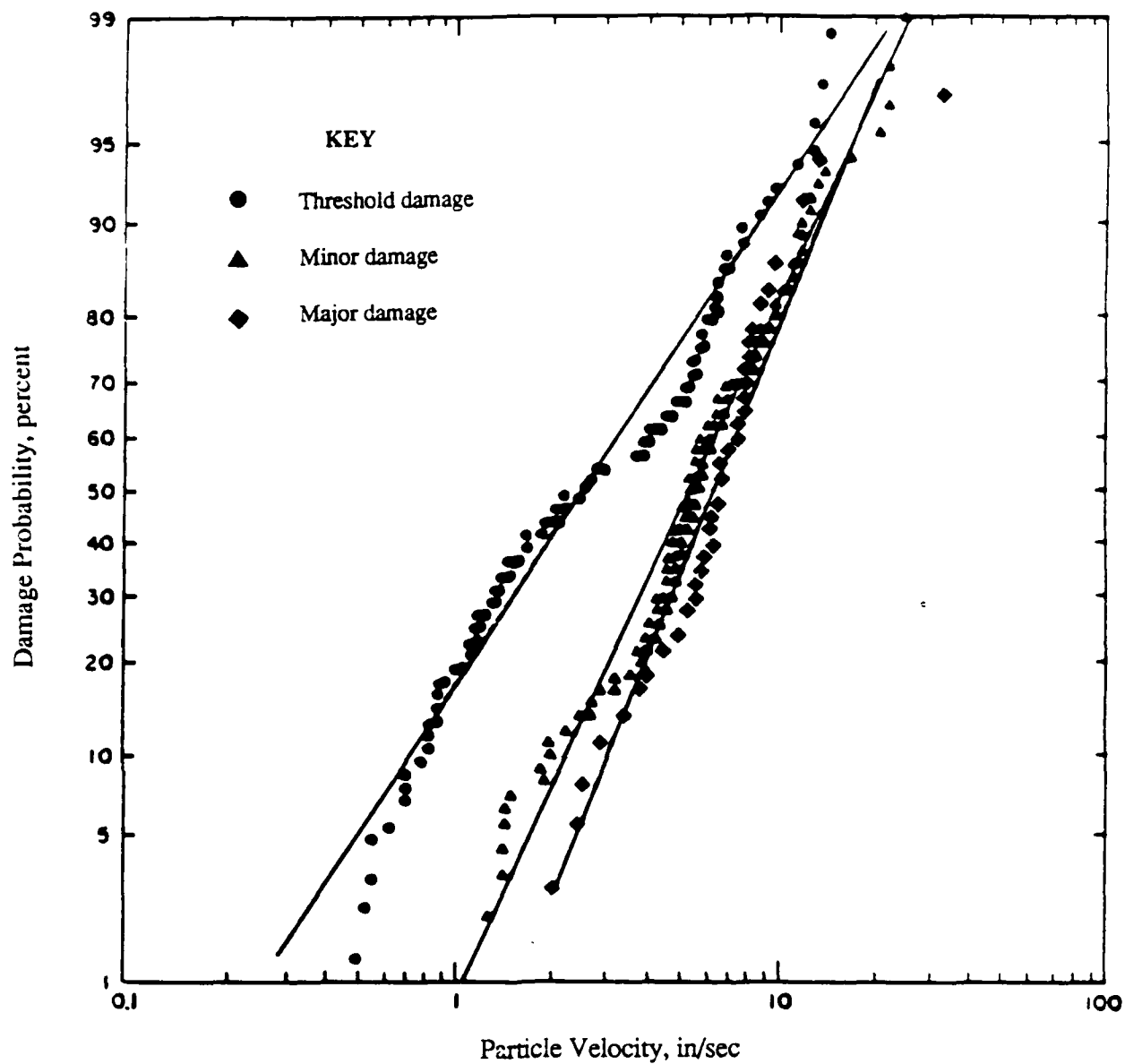


Figure 4-8. Probability Damage Analysis of Nine Sets of Data for Typical Residential Walls Exposed to Vibration from Surface Mine Blasting or Mechanical Shaker Tests (from Siskind, et al., 1980b).

could also be applied to estimate damage threshold stresses for homogeneous walls such as adobe or masonry, and can then be compared with the values defined earlier in Section 4.4.2.2.)

4.4.3.2 Wood Interiors

For old wood frame buildings with bare wood walls inside, Eqs. (4-12) and (4-13) are used along with data on typical failure loads (1.5 to 2 psi) on wooden walls (Appendix B). The constants K_b and K in Eq. (4-12) are estimated to be 27 and 0.75 respectively for a wood frame 7 x 4 stud wall with an interior and exterior wood skin of 3/4" panels or boards, the estimated log mean damage threshold stress is 410 to 540 psi for current construction. The failure stress for older historic buildings is arbitrarily set at 1 standard deviation below the current log mean value, so that for wooden structures the design value for damage threshold stress for wood walls will be the geometric mean of the above range (470 psi) times $10^{-\sigma_L}$ or 0.617 where $\sigma_L = 0.210$ is an estimated σ_L for wood based on the range in failure loads. This gives an estimate of $\sigma_s = 290$ psi.

4.4.4 Material Strength Estimates for Metal Frame Buildings

The same process just outlined for wood frame buildings can be applied to the type of lightweight metal frame utility buildings that can be found on farms or in industrial plants. These are included in the category of unconventional structures. Such buildings commonly have vertical metal channel "studs" or columns, and horizontal stiffeners, or girts, covered by a thin corrugated metal skin. For a minimum form of such construction consisting of an 18 gage (0.049 inch) steel skin supported by 1.5 x 3 inch channel 18 gage steel columns spaced 16 inches on centers, the factor K_b to be used in Eq. (4-12) to define the peak stress in a 16" x 96" panel section of such a wall under a static load respectively can be approximated by:

$$K_b = \left(\frac{b}{a}\right)^2 / [(3t/d)(1+w'/a) + t/a] \quad (4-15)$$

where a, b = the short (16 inch) and long (96 inch) sides of a panel section, respectively

t = thickness of the metal skin and channel (0.049 inch)

d, w' = depth and width of channel = 3 inches and 1.5 inches respectively.

In this case, K_b has the value of 635. The modified value for the constant K_s in Eq. (4-12) for such metal walls is 0.89 (see Table 4-1). Using Eq. (4-12), static failure loads are of the order

of 1.2 psi for such a wall (Appendix B) or, using Eq. (4-14), estimated peak vibration velocities for dynamic loads at damage thresholds are estimated to be about 35 in/sec. Applying the preceding expression, it is estimated that these static and dynamic loads would produce peak stresses of about 4,000 and 4,700 psi respectively. Allowing for stress concentration factors of 2 to 4 which would be typical for such steel structures (Eshbach, 1952), the resulting peak stresses would be in the range of 8,000 to 18,800, values which bracket the typical maximum allowable working stress of common structural steel of 15,000 psi, but which are well below the ultimate failure stresses of structural steel of about 49,000 psi for cold-rolled steel or 33,000 psi for annealed steel (Eshbach, 1952). Since this allowable working stress includes a factor of safety to insure that actual stresses are well below ultimate failure stresses, 15,000 psi is considered a suitably conservative design value for a damage threshold for typical structural steel for this study. This stress and a value for K_S of 0.89 will therefore be used herein for analysis of potential damage to lightweight steel buildings. In the absence of more definitive data on the variation of this damage threshold stress, from the above estimate of variation (e.g., stress concentration factors, etc.), the log of the standard deviation of the failure stress or strength for metal buildings is assumed to be ± 0.15 (equivalent to ± 3 dB). These same values are used for the rough estimates of potential damage to radio telescopes constructed with a solid metal parabolic reflector as discussed in Section 4.1.3.

4.4.5 Estimated Damage Stresses for Seismically Sensitive Structures

Structures in the category of seismically sensitive structures are wells and water tanks, early American archaeological caves or rocks with valuable pictographs or petroglyphs, and snow on soil slopes subject to avalanches or landslides.

4.4.5.1 Wells and Water Tanks

For wells and water tanks, only elevated empty metal water tanks are considered potentially susceptible to damage from all but very low altitude supersonic flights. In the most extreme case, the acoustic pressure loads from sonic boom will be much less than the average hydraulic pressure on the sides of wells or ground mounted stone, masonry or metal tanks containing as little as six inches of water. For such an amount of water in a well or tank, the hydraulic pressure on the sides, equal to the water weight density (62.4 lb/ft^3) times the water depth would vary linearly with depth from zero at the top surface of the water to $(1/2) \cdot 62.4 = 31.2 \text{ psf}$ at the bottom of the 6 inch water depth. Thus, the average hydraulic pressure of just 6 inches of water would be about 15 psf, over 30 times greater than the average sonic boom

pressure under ACM activity in the WSMR tests, and about 3.5 psf higher than the highest sonic boom pressure (6 psf) observed in these tests (see Figure 3-8).

For empty elevated water tanks, typically constructed of low strength sheet iron or galvanized steel, the damage stress threshold will be assumed equal to a value of 11,000 psi based on an estimated reduced strength for the weaker of these materials, cast iron, resulting in a reduction in strength comparable to that assumed above for structural steel to allow for stress concentration and fatigue effects. Actual ultimate strength of cast iron lies in the range of 20,000 to 40,000 psi (Eshbach, 1952). The standard deviation σ_L of the log of this damage stress will be assumed to be the same as for structural steel, or ± 0.15 (± 3 dB).

4.4.5.2 Archaeological Sites

For archaeological sites, one estimate of the damage threshold stress is provided by assuming that the stress is the same as that of old adobe, or 3.2 psi. A second basis for this important strength parameter is provided by the most conservative criteria for critical ground velocity given in Table 4-7 (1 mm/sec or 0.08 in/sec) to prevent damage from blasting to historic structures. This is used in Eq. (4-14) along with a value of 1 for K_S and 48.2 for E/C_L for stone (see Table 4-1). This gives a stress of 3.9 psi. An average value for the failure stress of prehistoric stone walls of 3.5 psi is therefore used for analysis. In the absence of any other data source, the standard deviation σ_L of the log of this damage stress is assumed to be 0.239 which is the same as the value obtained for the substantial set of measured failure data on adobe discussed earlier.

4.4.6 Avalanche Sites and Landslide Areas

While the likelihood of triggering a dangerous avalanche or landslide by sonic booms from most supersonic flight operations is apparently small, the potential consequences of such an event justify some care in making an evaluation of this possibility.

Anecdotal evidence exists to the effect that sonic booms have been used to intentionally trigger unstable snow avalanche-prone areas in Glacier National Park (The Seattle Times, 9 February 1960). It is also customary, in Switzerland, to cancel supersonic flights of military aircraft over avalanche-prone areas during recognized moderate to severe avalanche hazard conditions (Rathe, 1986).

However, definitive knowledge of the magnitude of sonic boom pressures required for, and probability of, triggering avalanches by sonic booms is extremely limited. A previous

attempt to trigger an avalanche by sonic boom was not successful (Lilliard, et al., 1965) due, apparently, to unsuitable weather conditions for avalanches at the time of the test. A more recent effort involving 20 flights over 7 days successfully triggered two avalanches, both on the same day (Perroud and LeComte, 1987). Based on the measured peak sonic boom overpressures of about 12.5 psf for this recent test and the estimated seismic coupling factors for snow listed in Table 4-3, the estimated shear stress for avalanche conditions was about 0.08 psi. Closely related information is available (Gubler, 1977) on the approximate required blast pressures from explosive charges used to trigger avalanches. Peak pressures on the order of 5 to 40 psf are indicated by the latter data straddling the 12.5 psf figure noted above. However, lower sonic boom pressures may apply for two reasons:

- (1) The sonic boom N-wave may generate a higher effective response for the same peak pressure as the blast wave (evidence to this effect was shown earlier in Figure 4-5c.
- (2) A sonic boom carpet pattern would expose a much wider area than is possible by maximum explosive charges (approximately 2 kg of TNT) allowable for safety reasons for avalanche triggering.

A somewhat similar situation exists for triggering of earth slides by sonic booms. One credible observation of a slide triggered by a sonic boom was reported by a National Park ranger (Holbrook, 1980). In this case, however, no information was located relative to explosively triggering an earth slide with relatively small surface charges such as for avalanches.

The magnitude of acoustic pressures required to trigger an avalanche or landslide is also estimated on the basis of limited experimental data on avalanche and landslide internal stresses, supported by extensive published background on their mechanics. It must be emphasized, however, that the physical mechanisms involved in triggering avalanches or landslides are complex and are not fully addressed here (Perla, 1980; Terzaghi, 1950). Rather the objective here is to provide a reasonable basis for evaluating the general magnitude of the potential hazard.

4.4.6.1 Snow Avalanches

Avalanches can be divided into two categories: (a) loose snow avalanches involving common and frequently harmless sloughing off of loose snow from a slope, and (b) a slab avalanche involving fracture and slipping of a large mass of snow that can, depending on the size of the avalanche, result in major damage to anything in its path (Forest Service, 1968).

An avalanche occurs when external forces (including simply gravity) cause internal stresses within the snow mass to exceed the restraining forces, resulting in an unstable condition. A basically unstable condition is reached when the shear stress (normally due to the component of gravity parallel to the slope) exceeds the shear strength (Forest Service, 1968). This may be achieved by an increased snow load or a decrease in strength (resulting from weather-induced changes in the geophysical structure of the snow (Perla, 1980). The shear stress due to gravity can be calculated rather simply if the thickness, mean density, and slope angle of the snow slab are known (Forest Service, 1968).

Avalanche potential depends on several variables: angle of slope (see Figure 4-9 for typical range of slope angles for slab avalanche), temperature, depth and density of snow (see Figure 4-10 for relationship between density within a slab avalanche and the stress at the interface between the slab and the remaining snow), ground cover under the snow, i.e., natural snow retention capability) and grain size and structure of snow crystals.

Avalanche triggering can be caused by a change in any of these variables in the direction which reduces stability of the snow slope. Stability is measured by the ratio of internal shear resistance to external stress. Triggering can also be caused by any addition to the external stress caused, for example, by the transient pressure of a skier passing over a section of a snow bank which is close to an unstable condition or by the pressure of an explosive charge intentionally set off in an attempt to trigger the avalanche (Forest Service, 1968). "It is conceivable that a much weaker sound (than that produced locally by an artillery blast or some other explosive charge) could trigger a slide when extreme instability exists" (Forest Service, 1968). This is the case of concern here since the acoustic pressures associated with sonic booms can be comparable to those from explosive charges.

Avalanches occur regularly in the winter time in certain areas in the U.S. For example, the rate is as high as about 90 per year along U.S. 550 in southwest Colorado (Armstrong and Ives, 1976). However, due in part to attention paid by Federal and State personnel to safety of winter sports activity in snow areas, these avalanches are seldom a hazard to skiers. Not only is avalanche forecasting improving (Armstrong and Ives, 1976), but, where necessary, steps are often taken to trigger an avalanche artificially with explosives (Gubler, 1977) on an unstable snow slope to minimize the risk of an unpredictable avalanche occurrence. However, the science is still young and avalanche hazards still remain for snow recreationists.

To support this very limited analysis of the potential for triggering an avalanche or landslide by noise from sonic booms, the additional data on soil and snow dynamic properties

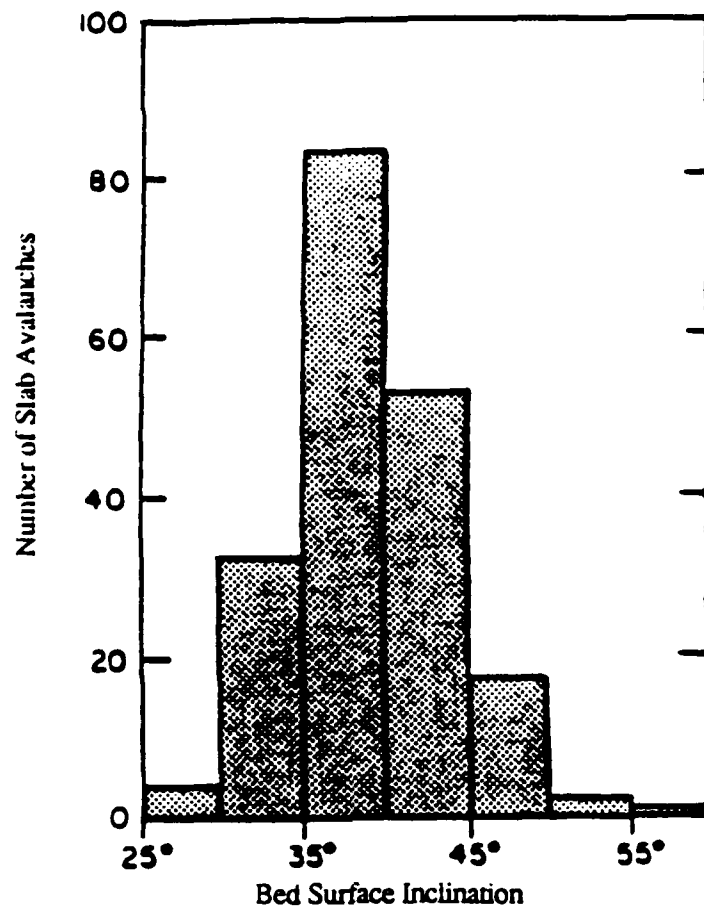


Figure 4-9. Number of Slab Avalanches Versus Bed-Surface Inclination θ (194 cases) (from Perla, 1980).

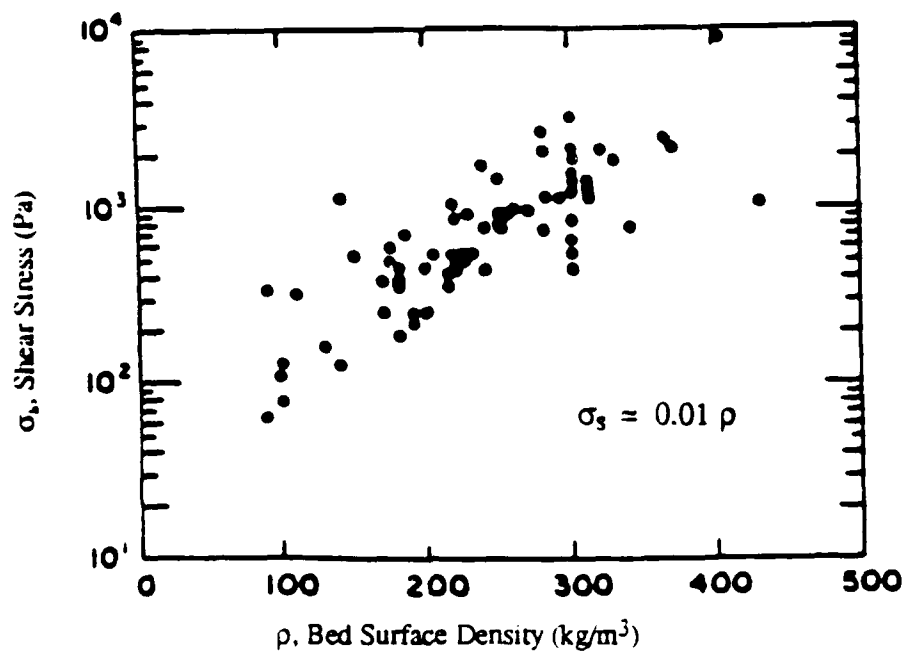


Figure 4-10. Shear Stress at Bed Surface Versus Bed-Surface Density (from Perla, 1980).

Table 4-8

Static and Dynamic Properties of Soils and Snow

		Allowable									
		Load	Density	E(10)	G(10)	Wave Speed (9)	Poisson's Ratio	G/C(S)			
No.	Note	N/m ² x10 ⁵	Kg/m ³	N/m ²	N/m ²	C(L)	C(S)		psi per		
		(7)		x 10 ⁷	x 10 ⁷	m/s	m/s	Comp'd Est	at'd	in/sec.	

SOIL MATERIALS											
1	(1)	Gray Plastic silty clay with sand & organic silt	0.98	(1,760)	3.04	1.79	131	(78)	0.42	0.35	
2	(1)	Brown saturated silty clay with sand	1.47	(1,760)	4.31	2.56	156	(93)	0.42	1.01	
3	(1)	Dense silty clay with some sand (above water table)	4.90	(1,760)	28.90	10.30	405	(240)	0.42	1.58	
4	(1)	Medium moist sand	1.96	1,620	5.30	3.22	181	(110)	0.35	1.08	
5	(1)	Dry sand with gravel	1.96	1,700	5.30	3.33	(177-432)	250	0.265	0.35	
6	(1)	Fine saturated sand	2.45	1,650	8.34	5.00	(211-225)	110	0.392	0.35	
7	(1)	Medium-grained sand	2.45	1,650	8.14	4.81	(222-318)	160	0.434	0.35	
9	(1)	Loess with natural moisture	2.94	1,670	11.30	6.70	(260-511)	260	0.416	0.40	
10	(1)	Moist loessial soil	2.94	(1,760)	11.80	7.03	(259)	(155)	0.40	1.67	
11	(1)	Moist clay		1,800			(316)	150	0.492	0.50	
12	(1)	Medium-sized gravel		1,800			(366)	180	0.456	0.40	
13	(4)	Gravel/Sand/Silt 0 - 0.2m top layer		1,700			(101)	60	0.429		
14	(4)	Gravel/Sand/Silt 1.5 to 4m depth					(617)	360	0.467		

SNOW											
		N/m ² x10 ²									
		(8)									
15	(2)	Snow Slab (Thickness = 0.08 to 4.2 m)	0.65-90.5	60-460					0 to 0.5		
16	(2)	Snow (From Perla's best fit line through data -	1.0	100							
17	(2)	Snow (Shear Stress, N/m ²) = 0.01 (Density, Kg/m ³)	4.0	200							
18	(2)	Snow	9.0	300							
19	(3)	Snow - Estimated properties in field experiment		100	2.5-10		500-1000		(0.3)		
20	(4)	Snow-properties within 0.12 m thick layer over soil		192-288							
22	(5)	Snow		210	3	1.1	(378)	229	0.36	0.18	
24	(5)	Snow		250	8.5	3.5	(583)	375	0.21	0.34	
25	(5)	Snow		300	20	7.5	(816)	500	0.33	0.55	
26	(6)	Snow		120-210	(.55-.97)		(215)		(0.3)		

Notes

- () Signifies estimated or range of computed values
 (1) Based on, or computed from, data in Barkan, 1962
 (2) Based on, or computed from, data in Perla, 1977
 (3) Gubler, 1977
 (4) Albert and Orcutt, 1989
 (5) Johnson, 1982
 (6) Albert, 1989
 (7) Allowable Load under Compression
 (8) Shear Stress at failure
 (9) C(L) = speed of longitudinal waves
 C(S) = speed of shear waves
 (10) E, G = Young's Modulus and Shear Modulus, respectively.

SUMMARY - G/C(S), (psi/in/s)

	Avg	St.Dev.
	----	-----
Soil Materials	1.16	± 0.38
Snow	0.36	± 0.15

listed in Table 4-8 were collected. The data provide specific details on soil and snow properties relative to prediction of the possibility of triggering an avalanche by sonic booms.

4.4.6.2 Acoustic Triggering of an Avalanche

The strength or critical shear stress σ_s at the failure point (i.e., initiation of an avalanche) is estimated from Figure 4-9 according to the empirical relationship developed by Perla, 1980, between this stress and the snow density ρ (in kg/m^3) at the surface of the snow bed. This relationship, illustrated in the figure, can be conveniently expressed in terms of the stress in psi as:

$$\sigma_s = 1.45 \cdot 10^{-6} [\rho (\text{kg/m}^3)]^2, \text{ psi} \quad (4-16)$$

According to the data in Table 4-8 and Figure 4-9, the density ρ for slab avalanche areas is estimated to have a mean value of about 210 kg/m^3 . For loose snow avalanches, the corresponding estimate for mean density ρ is 77 kg/m^3 .

Based on Eq. (4-16), these correspond to failure stresses (or strengths) of 0.062 psi and 0.0087 psi for slab avalanches and loose snow avalanches respectively. The estimated failure stress of 0.062 psi is close to the value (0.08 psi) derived from the tests by Perroud and LeComte (see Section 4.4.6). The standard deviation of the log of these stresses are computed from the rms value of the sum of the estimated variances for the regression constant ($1.45 \cdot 10^{-6}$) in Eq. (4-16) (based on Figure 4-10) and the density ρ for the two types of avalanches. The resulting values for σ_L are 0.33 for slab avalanches and 0.25 for loose snow avalanches.

4.4.6.3 Landslides

For landslides, the critical shear strength will vary widely for similar reasons as for snow avalanches except time and water content will tend to replace temperature and grain size and structure of snow crystals as dependent variables (Terzaghi, 1950). A design value for this critical stress was made from estimated shear stresses for a large number of fissured clay slide areas observed over many years in England (Skempton, 1948). From this trend over time in shear stress, illustrated in Figure 4-11, a minimum value for the shear stress was estimated to be in the range of 0.1 to 0.35 metric tons/ ft^2 . In the absence of more complete data, the lower end of this range of shear stress for landslides in fissured clay (0.1 metric tons/ ft^2 or 1.5 psi is used as an estimated shear resistance of landslide areas). The value for σ_L was estimated to be 0.18 based on the range.

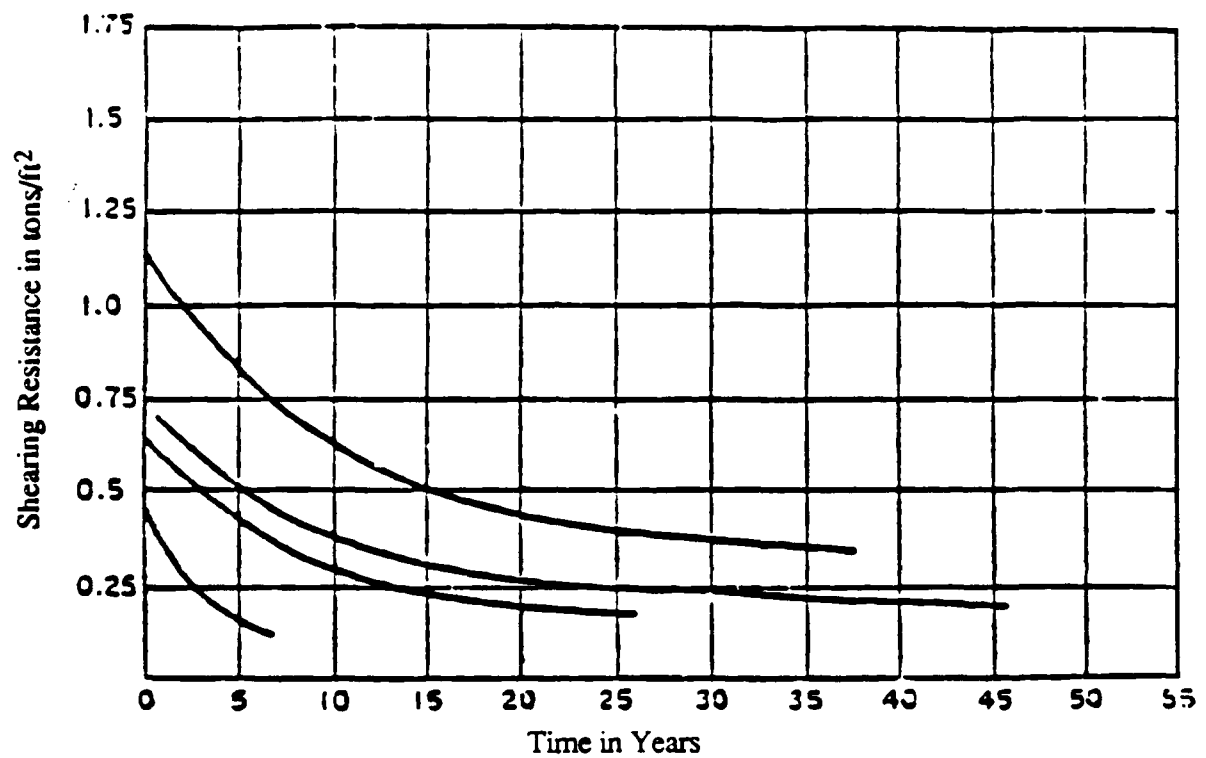


Figure 4-11. Diagram Showing Gradual Decrease of Shearing Resistance of Stiff, Fissured London Clay. The curves are based on the results of a statistical study of slope failures in the London area. Each curve represents a different locality. (From Skempton, 1948.)

These estimated values for the shear strength of snow banks and earth slopes are believed to be at least within an order of magnitude of correct values and should provide the basis for reasonable estimates of the potential for triggering avalanches or landslides by sonic booms. Such events will be assumed to occur when the acoustically induced peak shear stress σ_{pk} in these materials, computed according to the procedures specified in Section 4.3.2, exceed these shear strengths.

4.4.7 Summary, Damage Stress Criteria

This last section completes definition of the basic models needed to estimate stress response, and strength, and hence potential damage for unconventional structures. The models have sacrificed precision for generality to allow a more reasonable basis for application of the predictive models to cases for which experimental data are lacking. The next section presents results of an experimental program designed to help validate some aspects of the models and to explore techniques for detecting or documenting potential structural damage.

5.0 EXPERIMENTAL EVALUATION OF DYNAMIC RESPONSE OF UNCONVENTIONAL STRUCTURES

This section describes the experimental portion of this program which evaluated the response of two unconventional structures to excitation from sonic booms generated by ACM activity. The following procedures were employed and evaluated during these tests:

- Acoustic measurements of the sonic boom environment.
- Mechanical impedance measurements of adobe walls.
- Structural response measurements of various structural elements of these two structures.
- Photographic analysis of wall cracks.

Measurements of structural response to sonic boom were made over a 2¹/₂ month period from February to April, 1989 at two different historical adobe structures at White Sands Missile Range (WSMR) in New Mexico. At the first structure the system was installed and left in place for 4 weeks of data acquisition, while at the second structure, 2 weeks of data were obtained. During these two periods sonic boom pressure levels and the structural response of the buildings were recorded. The two structures, although both adobe houses, were distinctly different; the first is completely enclosed with intact doors and windows while the second structure is in poor condition missing doors, windows, and several walls.

The structures are located in an area close to the middle of the Lava/Mesa airspace within the WSMR which is designated as a supersonic training area. An extensive series of sonic boom measurements were also carried out in this area for another program from July 1988 to January 1989. The acoustic data from these earlier measurements are contained in Plotkin, et al., 1989. As discussed in Section 3.0, results of this earlier study produced estimates of the average level generated by sonic booms and also the number of booms produced per day. Figure 5-1 illustrates the distribution of sonic boom impacts over the area of the training range and the location of the two structures examined during the present study.

5.1 Structure Description

The two structures instrumented are called the George McDonald Ranch House (Structure A) and the McDonald Brothers Ranch House (Structure B).

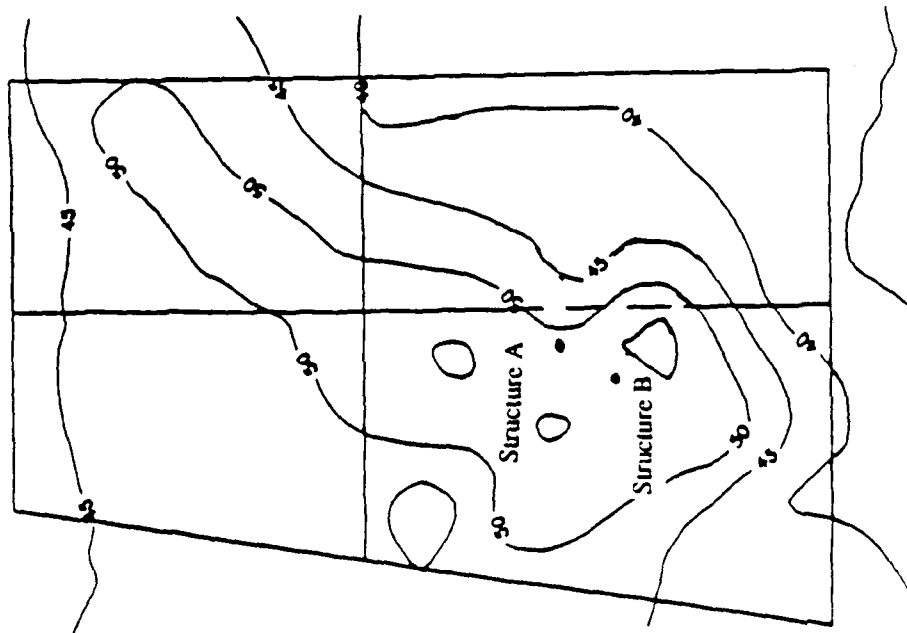


Figure 5-1a. Measured ACM Day-Night Average C-Weighted Sound Level in Lava/Mesa Airspace (from Plotkin, et al., 1989).

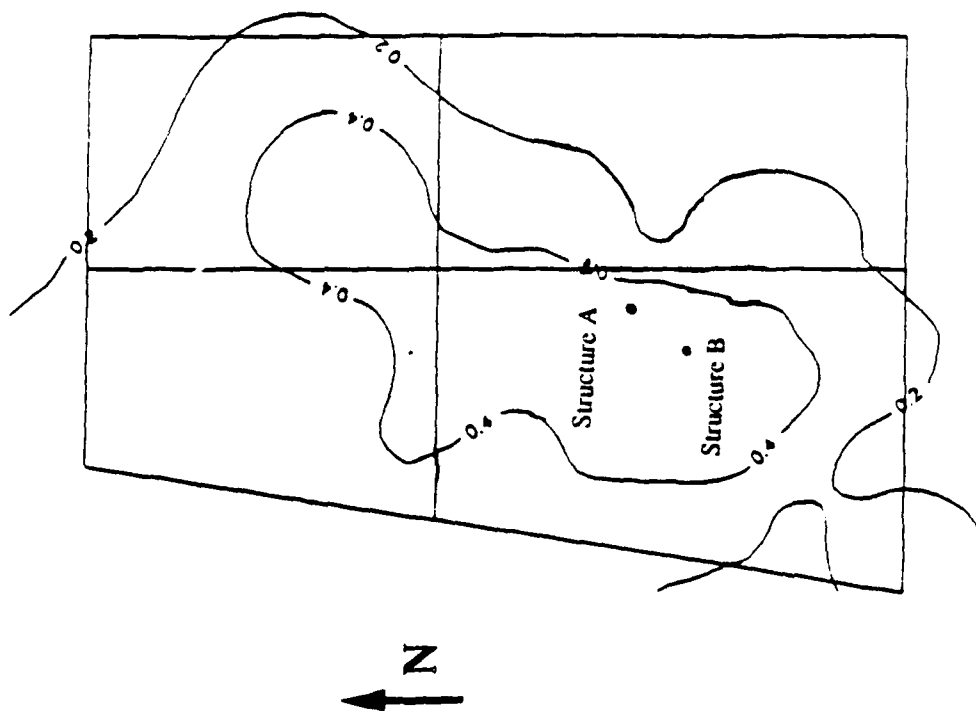


Figure 5-1b. Measured ACM Booms Per Day in Lava/Mesa Airspace (from Plotkin, et al., 1989).

5.1.1 Structure A Description

The George McDonald Ranch House is located west of the Oscura Mountains at WSMR as illustrated in Figure 5-2. Also shown on this figure is the location of the site where weather data was gathered during the tests. The ranch house is designated as a National Historic Site because of its use as the location for the assembly of the trigger for the first atomic bomb detonated on July 16, 1945 at the Trinity Site, which is approximately 2 miles north-northwest of the ranch house. The ranch house was first built in 1913 with the subsequent addition of two north rooms in 1918; in 1965 it was taken over by the National Park Service who have maintained it since that date (McMullan, 1987)

The ranch house is approximately 2 miles north of a test site currently used by the Defense Nuclear Agency (DNA) for non-nuclear, high explosive effects tests conducted since 1981 (Smith, 1985; McMullan, 1987). For some of their tests, the DNA have reinforced the structure to minimize damage from blast effects from overpressures in the range of 23 to 119 psf, which is well above the range expected from sonic booms overpressure (Gambill, et al., 1988). Although not quantified, it can be assumed that the structure has suffered some damage from these tests. The structure, shown in Figure 5-3, consists of 18" thick adobe brick walls with a painted plaster covering on both the inside and outside walls. This plaster surface is basically intact for most of the walls, but has many small cracks varying in size and length. The low pitched roof is supported on a wood frame resting on the adobe walls.

5.1.2 Structure B Description

Structure B, also a ranch house, is shown in Figure 5-4 and was built by the McDonald brothers in about the same period as Structure A. It is of a similar adobe block construction, but the house has not been maintained and, as indicated in Figure 5-4, is in poor condition. All doors and windows are missing and several walls are gone. The roof and most of the floors are intact, though some of the flooring is damaged. The house has been used as a haven by small animals and is not in a habitable condition.

5.2 **Structural Response and Acoustic Measurement Systems**

The measurement systems were designed to automatically record acoustic and structural response data from single events resulting from sonic booms generated by aircraft operating at WSMR. The following techniques were utilized:

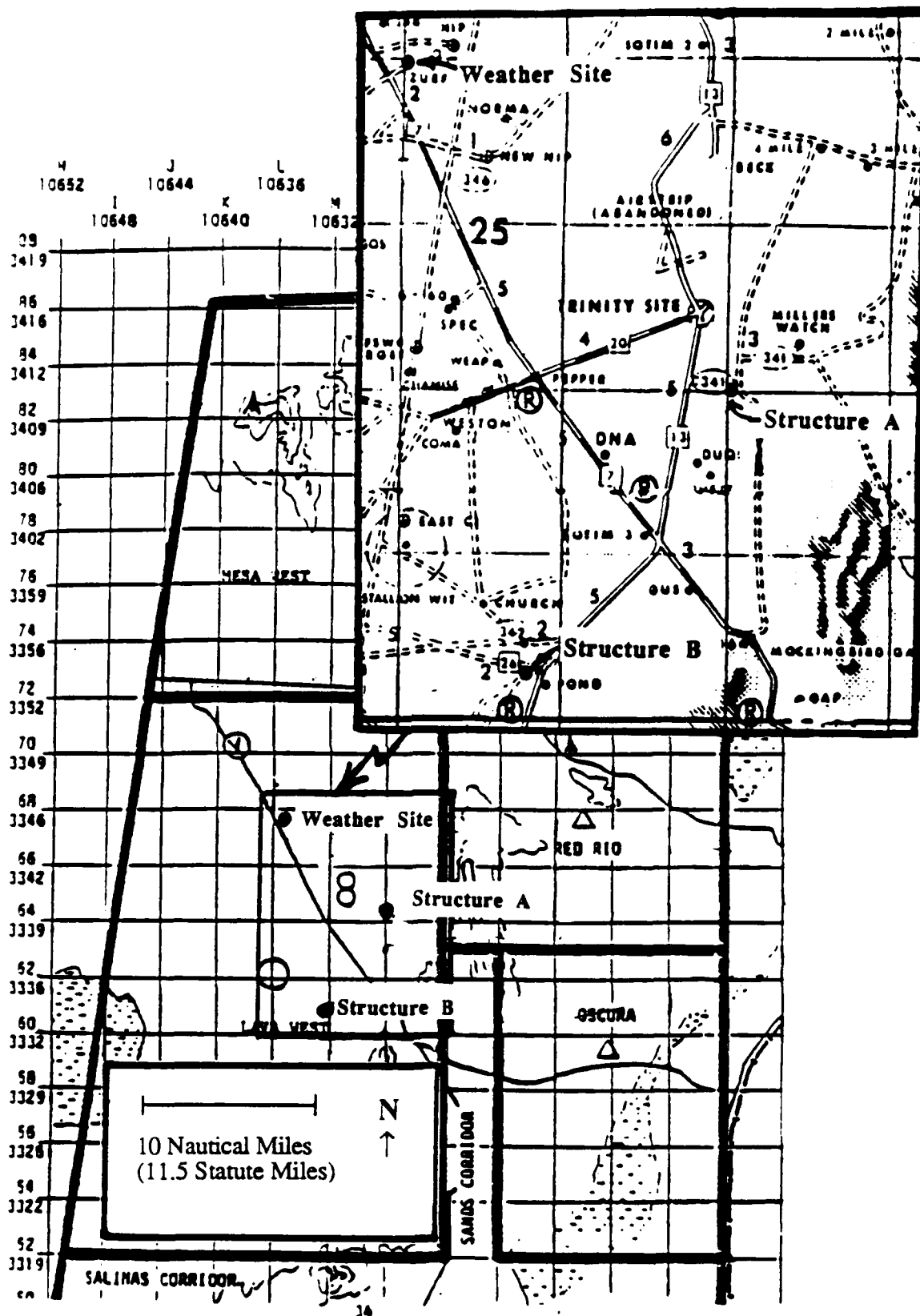


Figure 5-2. WSMR Lava/Mesa Airspace and Coordinates.

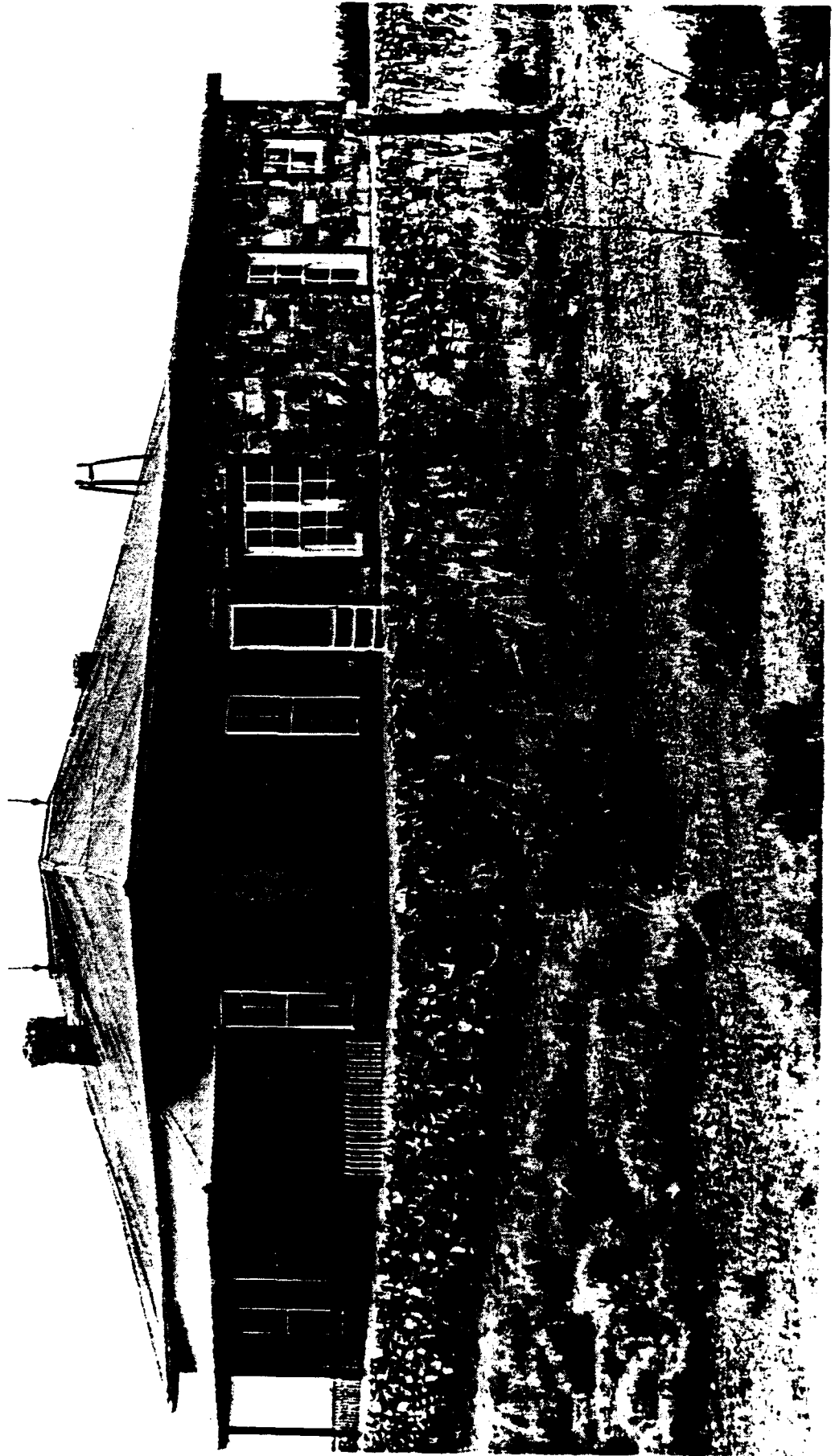


Figure 5-3. George McDonald Ranch House (Structure A)



Figure 5-4. McDonald Brothers Ranch House (Structure B)

- The acoustic signal and the resultant response of the two structures were recorded by a digital data acquisition system. The system was activated by the acoustic signal (sonic boom) detected with a microphone placed outside the structure.
- The arrival direction of the acoustic signal was determined by three SBM-1 digital acoustic monitors.
- A single Boom Event Analyzer Recorder (BEAR) system was utilized to define the acoustic signature of the sonic booms.

Detailed descriptions of these sonic boom measurement systems are provided in Plotkin, et al, 1989.

5.2.1 Acoustic and Structural Vibration Measurement Instrumentation

A block diagram of the structural response system is shown in Figure 5-5. The system consists of several transducers, mostly accelerometers, that are interfaced to a Compaq Portable III computer through a 16 channel A to D converter. A hard disk in the computer with a capacity of 20 megabytes could store up to 100 single events. Each event stored was 2 seconds long at a sampling rate of 50,000 samples per second. Each sample was a 12 bit word, therefore, 2 bytes (1 byte = 8 bits) of memory were required per sample, allowing 10 million samples to be stored on the hard disk. The computer system and the signal conditioning equipment (installed in Structure A) are shown in Figure 5-6.

Transducers in the system required signal conditioning of various types in order to provide the proper signal to the A to D converter. Each type of transducer was interfaced to the system as follows:

- The microphone, a GenRad type 1971, was connected directly to a PCB line driver amplifier which obtained its power from the coaxial line connected to the interface board. According to the manufacturer's specifications, the frequency response of the microphone itself was down 3 dB at 2 Hz. The cut-off frequencies (3 dB down points) for the PCB line driver amplifier and input coupling circuit to the interface board were 0.12 Hz and 0.32 Hz, respectively. This microphone was

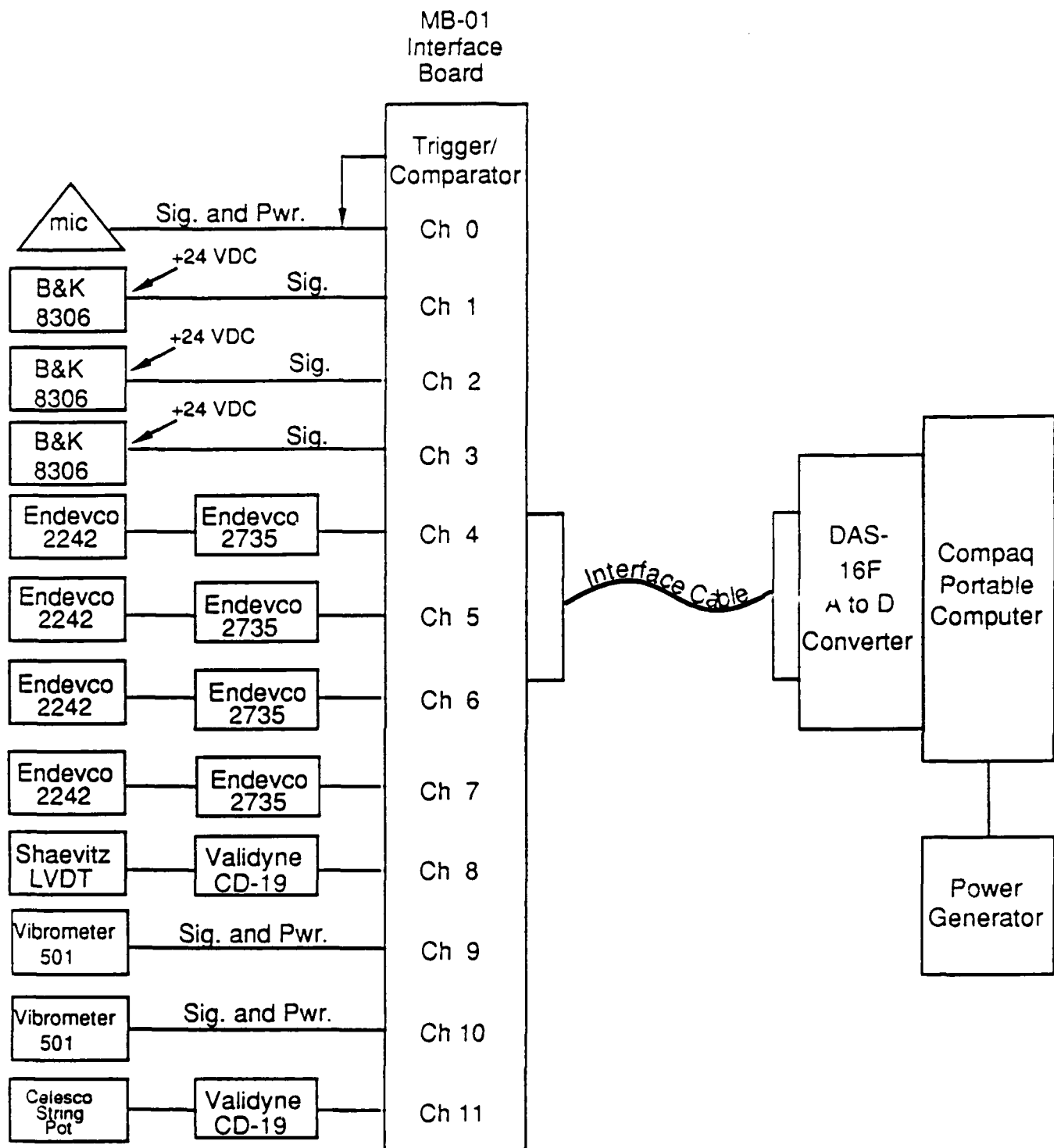


Figure 5-5. Structural Response Measurement System Block Diagram.

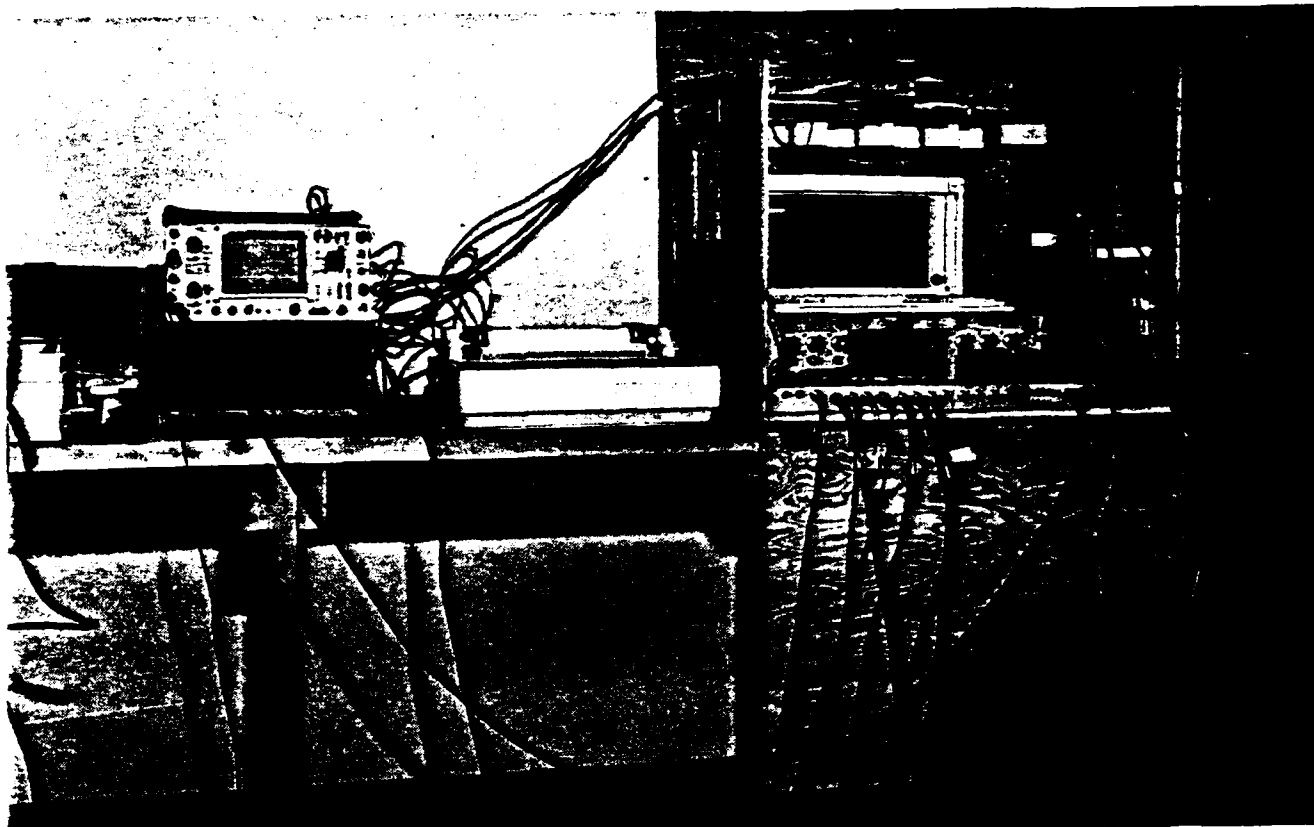


Figure 5-6. Data Acquisition Hardware and Computer



Figure 5-7. Acoustic Instruments – BEAR, SBM-1 and Microphones

placed in the conical windscreen with the BEAR and SBM-1 microphones as illustrated in Figure 5-7.

- Three B&K 8306 accelerometers with built-in amplifiers were attached to the interface board with separate coaxial cables for signals and a 24 VDC power supply.
- Four Endevco 2242 accelerometers were connected to model 2735 charge amplifiers which were in turn connected to the interface board.
- The LVDT was driven by a Validyne CD-19 Carrier Demodulator, which translates the displacement between a cylindrical transformer and a movable core into a DC voltage.
- The two miniature Vibrometer accelerometers have built-in amplifiers and are connected directly to the interface board which supplies power to them on the coaxial line.
- The Celesco string potentiometer is driven with the Validyne CD-19 Carrier Demodulator which generates a voltage proportional to displacement.

The interface board contains several custom-made circuits which decouple DC power, provide current sources for the microphone and some of the accelerometers amplifiers, provide additional amplification for some channels, and also contains the trigger circuit and comparator. The interface board was connected to the A to D converter. The computer, interface board, and the necessary power supplies were housed in a plywood enclosure to provide some protection from the environment and from casual visitors to the sites.

Table 5-1 illustrates the assignment of transducers to the computer system channels. These same transducers were utilized for the acquisition of data at Structure B. This table lists the primary characteristics of each instrumentation channel in the system. Note that the upper frequency limit of all channels was controlled by the sampling rate of the A to D converter, e.g., for 12 channels and a rate of 50,000 samples per second, the maximum frequency is $50,000/12 = 4167$ divided by the Nyquist criterion (2.56), therefore the highest observable frequency would be $4167/2.56$ or approximately 1600 Hz.

Table 5-1
Instrumentation Characteristics
(Set-Up in Structure A)

A-D Chan	Transducer Type	Location	Sensitivity at IV Output	Frequency Range(l)
0	GR 1971 Mic	50 ft south of house	131 dB	2 Hz to 5 kHz
1	B&K 8306 Accel.	Ground near front porch	0.1 g	0.1 Hz to 1 kHz
2	B&K 8306 Accel.	Base of wall 101	0.1 g	0.1 Hz to 1 kHz
3	B&K 8306 Accel.	Center of wall 101	0.1 g	0.1 Hz to 1 kHz
4	Endevco 2242C Accel.	Water tank	1 g	2 Hz to 7 kHz
5	Endevco 2242C Accel.	Center of 101 floor	1 g	2 Hz to 7 kHz
6	Endevco 2242C Accel.	Center of 101 ceiling	1 g	2 Hz to 7 kHz
7	Endevco 2242C Accel.	Center of wall 101S	1 g	2 Hz to 7 kHz
8	Schaevitz 200HR LVDT	Crack on wall 101S	0.01 in	DC to 10 Hz
9	Vibrometer 501 Accel.	On wall 102S, window & wall center	1 g	2 Hz to 5 kHz
10	Vibrometer 501 Accel.	On wall 104W	1 g	2 Hz to 5 kHz
11	Celeco String Pot	Floor to ceiling, room 101	~1 in	DC to 10 Hz
	BEAR (2)	50 ft south of house		DC to 3 kHz
	SBM-1 (2)	50 ft south of house		0.5 Hz to 5 kHz
	SBM-1 (2)	1 mile north of house		0.5 Hz to 5 kHz
	SBM-1 (2)	1 mile west of house		0.5 Hz to 5 kHz

1) 3 dB Down Point

2) Special unmanned sonic boom recording systems.

5.2.2 System Operation

The system was set up to record data for a selectable time period when the acoustic level exceeded a preset threshold level. The computer program ran continuously waiting for a trigger created when the acoustic level exceeded a threshold level of 110 dB SPL. When the trigger occurred, the computer would store a 2 second block of data, which included a selected number of samples before the trigger (usually 1000 samples). When the program was running, data were written to two 16K RAM files until the trigger was received, at which time data from the RAM files and incoming data were written directly to the hard disk. Recording the pre-trigger block of data guaranteed the complete signal, i.e., single event signature, was stored. In most cases, data from the channels recording structural response data occurred after the acoustic signal. Thus, this data was always recorded. Although several non-sonic boom acoustic events were recorded during the study, most of the "real" booms were accurately stored together with the mechanical response of the structure.

5.2.3 Transducer Mounting

Due to the fragile nature of the wall surfaces in the structure where measurements were to be made, transducers were usually braced against the wall instead of being firmly bonded, as is the common practice. Figure 5-8 illustrates the plastered adobe on the outside of Structure A at the front porch. This plaster on the outside of the house was quite coarse and approximately 3/4 inches thick. Inside the houses, the plaster was much thinner, less than 1/4 inch. Figure 5-9 illustrates a typical area inside Structure B. This photograph shows both the underlying plaster scratch coat and the finish coat. The transducer shown is a Vibrometer accelerometer.

Figures 5-10 and 5-11 depict the procedures used for mounting two types of transducers, accelerometers and LVDTs. In order to prevent damage to the surfaces, especially in Structure A where the adobe was covered with plaster, transducers were placed in direct contact with the wall and held in place by a soft mounting brace which ensured firm contact with the wall but did not add any significant stiffening to the wall. A similar type of procedure was used for mounting a vibration exciter to the wall for mechanical impedance measurements. The mounting procedures were evaluated in the laboratory as described in Section 5.2.4.1.



Figure 5-8. Front Porch Area of Structure A



Figure 5-9. Plaster and Adobe on Inside Wall of Structure B

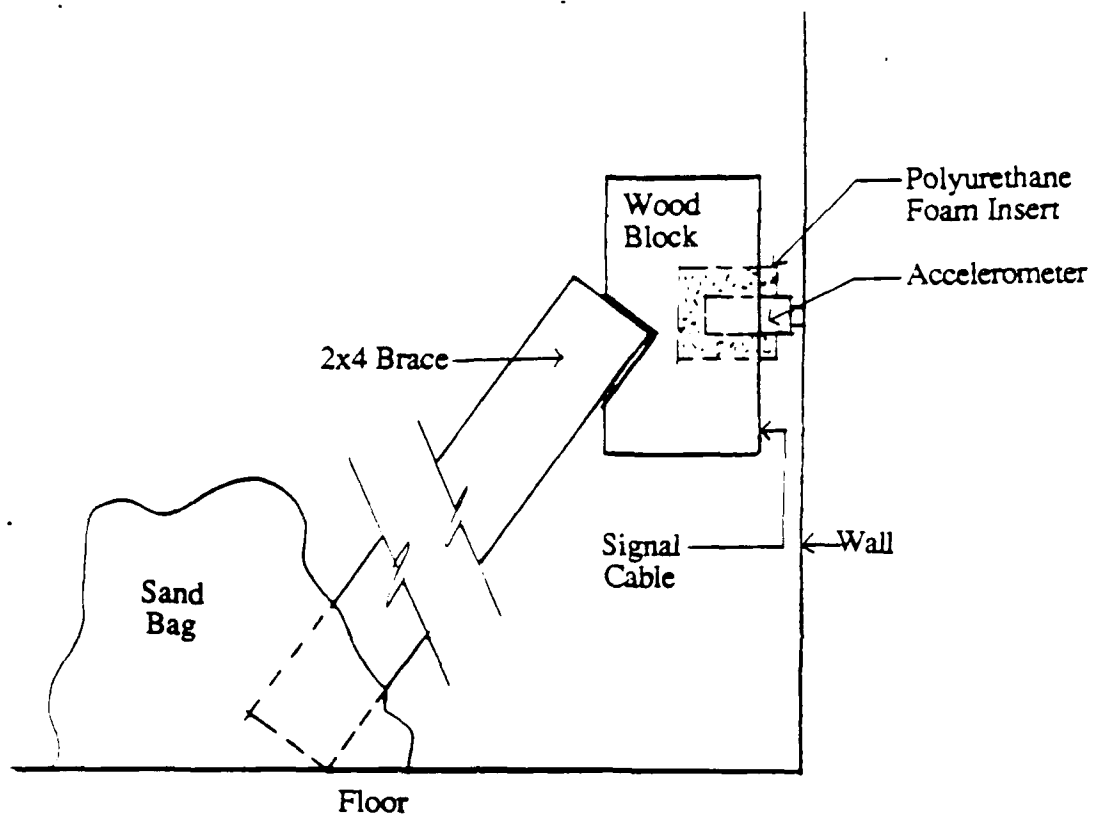


Figure 5-10. Side View of Mounted Accelerometer

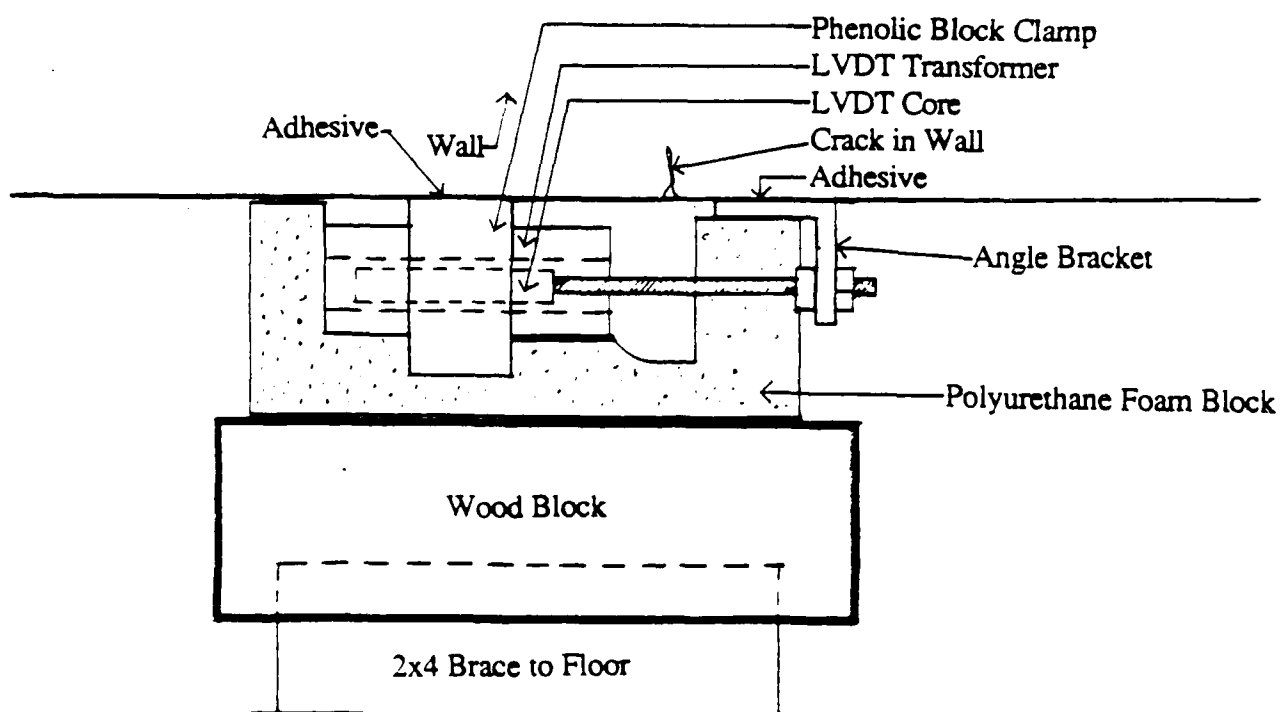


Figure 5-11. Top View of Mounted LVDT

5.2.4 Mechanical Impedance Measurements

In exploring possible methods used for evaluating pre- and post-exposure conditions of wall surfaces, mechanical impedance tests were conducted on at least two locations on each of two walls of the two test structures. The mechanical impedance of a surface is the ratio of the input force to the resultant velocity of the surface. The impedance was investigated through trial evaluations, with both a sinusoidal sweep or an impulse input. This task was complicated by the fragile nature of the wall surfaces. The plaster coating was variable in thickness and it did not uniformly adhere to the adobe, thus there were pockets covered with very thin layers of plaster which could easily be fractured. The intent was to see if gross, readily observable, changes in point input impedance would appear as a result of sonic boom damage. Such an impedance measurement does not attempt to simulate sonic boom loading but may serve to detect surface or buried flaws in a structure.

5.2.4.1 Sinusoidal Response

To determine the point input mechanical impedance of the adobe wall to a sinusoidal force input, a drive was provided by a mass-loaded electrodynamic transducer which was originally a hi-fi system driver. This unit was designed to "attach" to a wall and, when driven by a power amplifier, the wall would generate the sound. To measure the response of the wall, an accelerometer was mounted adjacent to the driver. Prior to the field test, experiments were conducted in the laboratory to determine the frequency response (measured by the accelerometer) using either resilient or hard mounting for both the driver and the accelerometer. Resilient mounting was based on bracing the transducers against the wall with a polyurethane foam block. The hard mount for the driver was a steel stud in the wall; the accelerometer was bonded to the wall for a hard mount.

The two mounting configurations (i.e., driver hard- and soft-mounted; accelerometer hard- and soft-mounted) were tested and the frequency response characteristics for each configuration were compared. For the first, with the driver hard- and soft-mounted, as shown in Figure 5-12, between the lowest observable frequency of 200 Hz and up to approximately 1200 Hz, the difference in response is less than ± 3 dB. With the driver hard mounted on the wall, a comparison between the accelerometer hard mounted (attached to an accelerometer pad bonded to the wall) and pressed against the wall with the resilient mount, the frequency response was compared. For frequencies below 1,000 Hz, of primary concern for this program, the difference was also less than ± 3 dB.

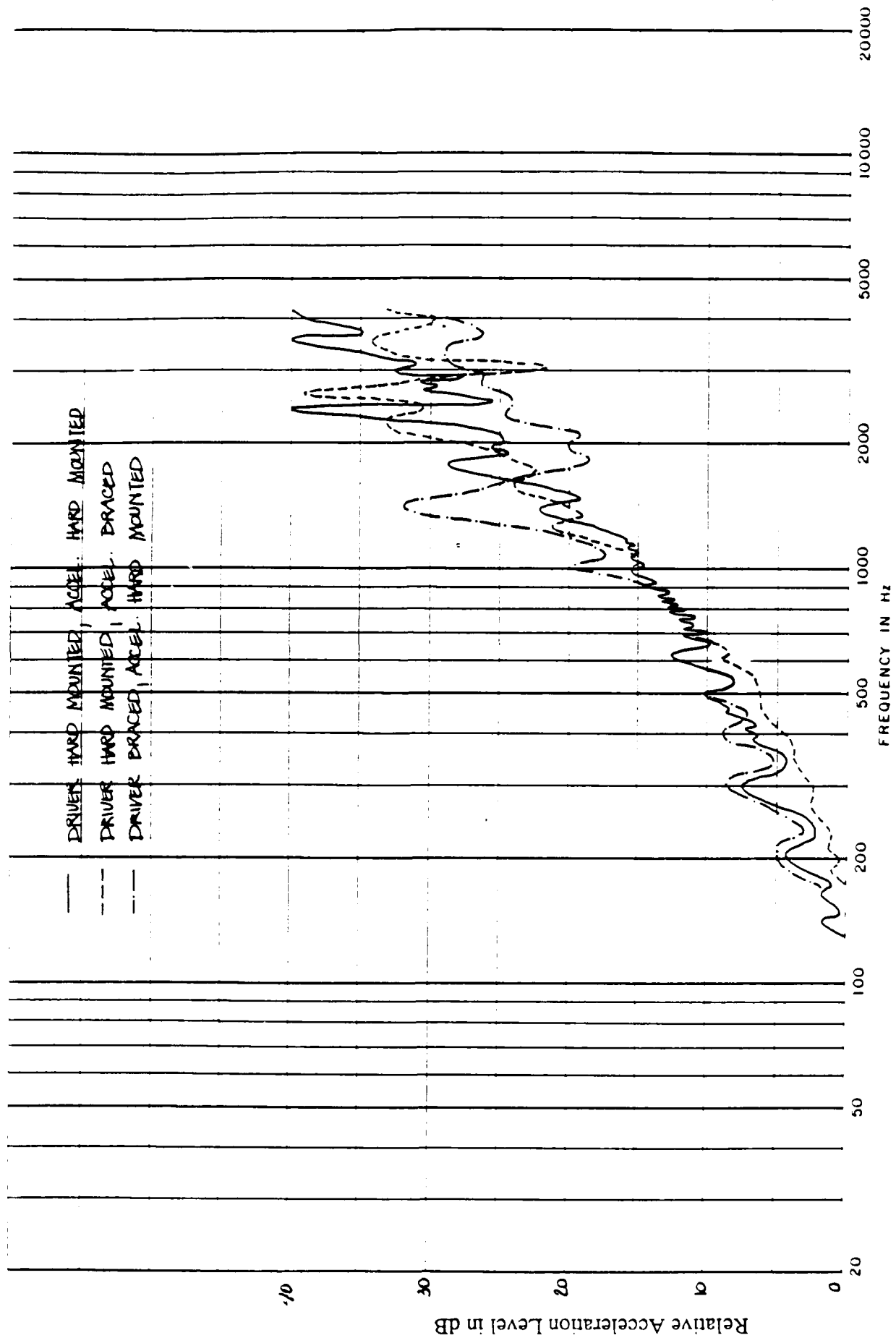


Figure 5-12. Frequency Response Variations Between Driver and Accelerometer Mounting Configurations

5.2.4.2 Impulse Response

An impedance hammer was constructed to provide an impulsive input to the wall. A common machinists hammer was modified by attaching a force gage and accelerometer to the head. The two-sided hammer head was approximately 1 inch in diameter with plastic sections on each face. A PCB 231A force link transducer was attached to one face and a Endevco 2242C accelerometer was attached to the other. Each transducer was interfaced to an Endevco charge amplifier to provide signal conditioning. The wall surface was tapped lightly with the force gage and the response from both transducers was recorded by the digital system. Measurements were made of the impedance and the response at nearby wall positions where accelerometers were located. Figure 5-13 illustrates the impedance hammer and Figure 5-14 shows two accelerometers braced against a wall in Structure A.

5.2.5 Structural Response Measurements

The structural response measurement system was set up at each house in a fashion that would allow sonic boom response data to be recorded automatically for over 2 days. For each of the structures, a BEAR sonic boom monitor was set up outside the house to record the waveform of each boom received. One SBM-1 monitor was located adjacent to the structure; one unit was located 1 mile north of the house; and the third unit was located 1 mile west. These three units were time-synchronized and were used to determine the direction of propagation of the booms.

Except for a few instances, the structural response measurement system was serviced daily. The primary limitation for system operating time was the operation of the power generator. The generator provided approximately 1800 watts at 120 VAC, although only about 500 watts was needed most of the time. An auxiliary 20 gallon fuel tank was added, that allowed over two days running time. Two days was also the limit for the oil in the motor which would cause the motor to shut down when too low. In total however, very few problems were met with the system.

Structure A

The computer and most of the signal conditioners were set up in the house, which remained closed and locked during all measurements. The motor generator was set up outside the stone wall, north of the house. The wall and house provided enough attenuation to prevent any interference with the acoustic systems which were deployed south of the house. At the location of the microphones, the generator was almost inaudible.

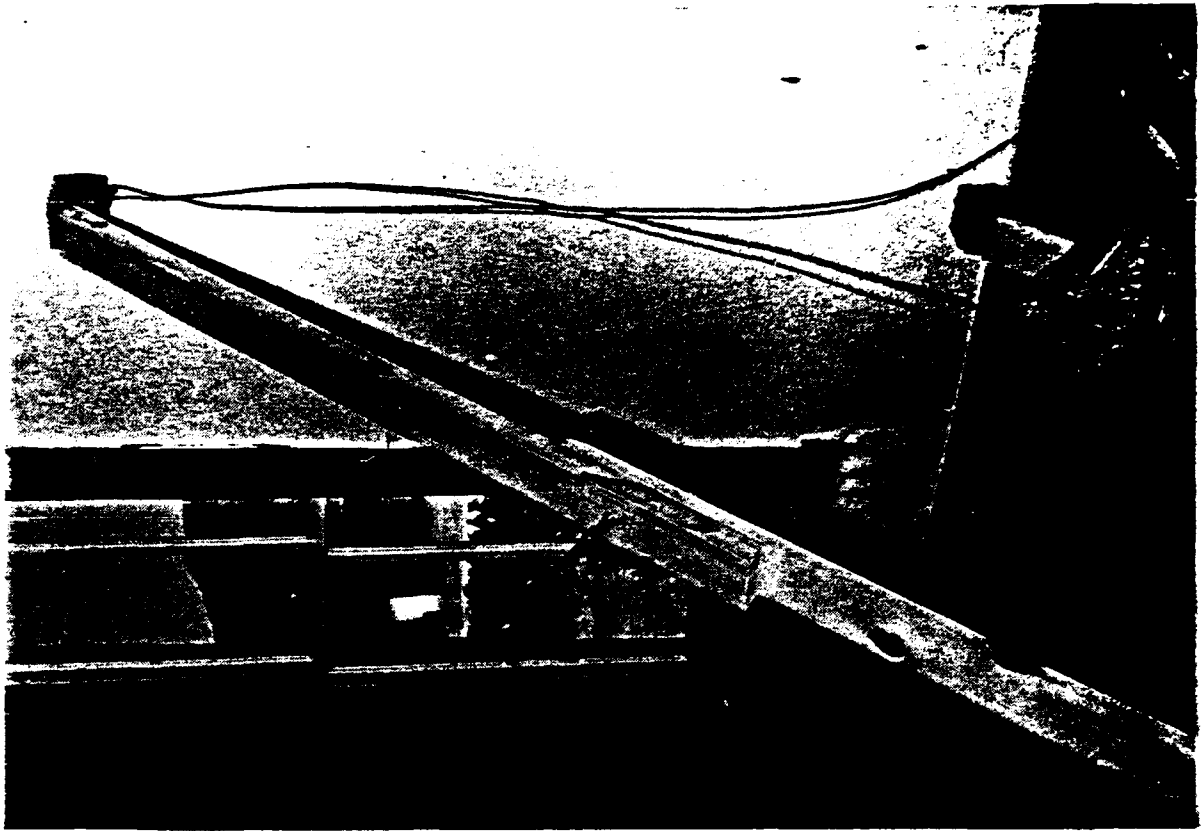


Figure 5-14. Accelerometer Mounted on Wall

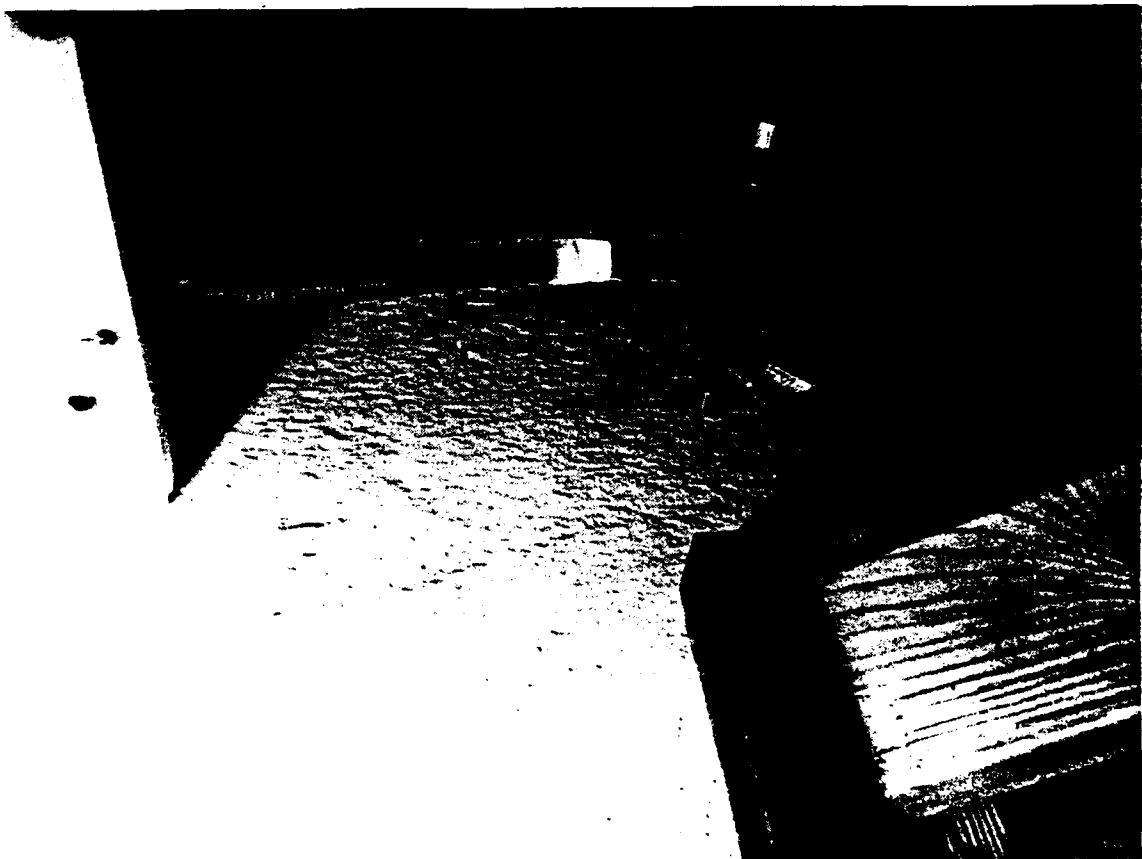


Figure 5-13. Impedance Hammer

Figure 5-15 illustrates the floor plan of Structure A, with the rooms numbered and the locations of the instrument transducers identified. The particular transducers were located as follows:

- The acoustic systems, a BEAR, a SBM-1, and the structural system trigger microphone were placed approximately 50 feet south of the house.
- An accelerometer was mounted in a vertical position on top of a steel spike in the ground very close to the wall outside the house.
- An accelerometer was braced against the wall in a horizontal position at the base of the east wall in room 101 (Wall 101E).
- A second accelerometer was braced against the wall near the center of wall 101E.
- An accelerometer was braced against the middle of one section of wall 104W.
- An accelerometer was braced against the middle of one section of wall 102S.
- An accelerometer was braced against the middle of one section of wall 101S.
- An accelerometer was placed on the floor in the center of room 101 with a 10-lb. sand bag on top to hold it in place. (This added mass loading will not have a significant influence on the dynamic response.).
- An accelerometer was placed in the attic on top of a ceiling joist in the center of room 101 with a sand bag on top to hold it in place.
- A string potentiometer was placed on the floor in the center of room 101 with a sand bag on top and the string (actually a wire in this case) was attached to the ceiling directly above.
- An LVDT was braced against wall 101S near a crack and the core was attached to a bracket on the other side of the crack. The bracket was semi-permanently attached to the wall using a "Post-It" adhesive strip.
- An accelerometer was bonded in a horizontal position near the top of the west wall of the water tank. Data obtained from this transducer early in the program was

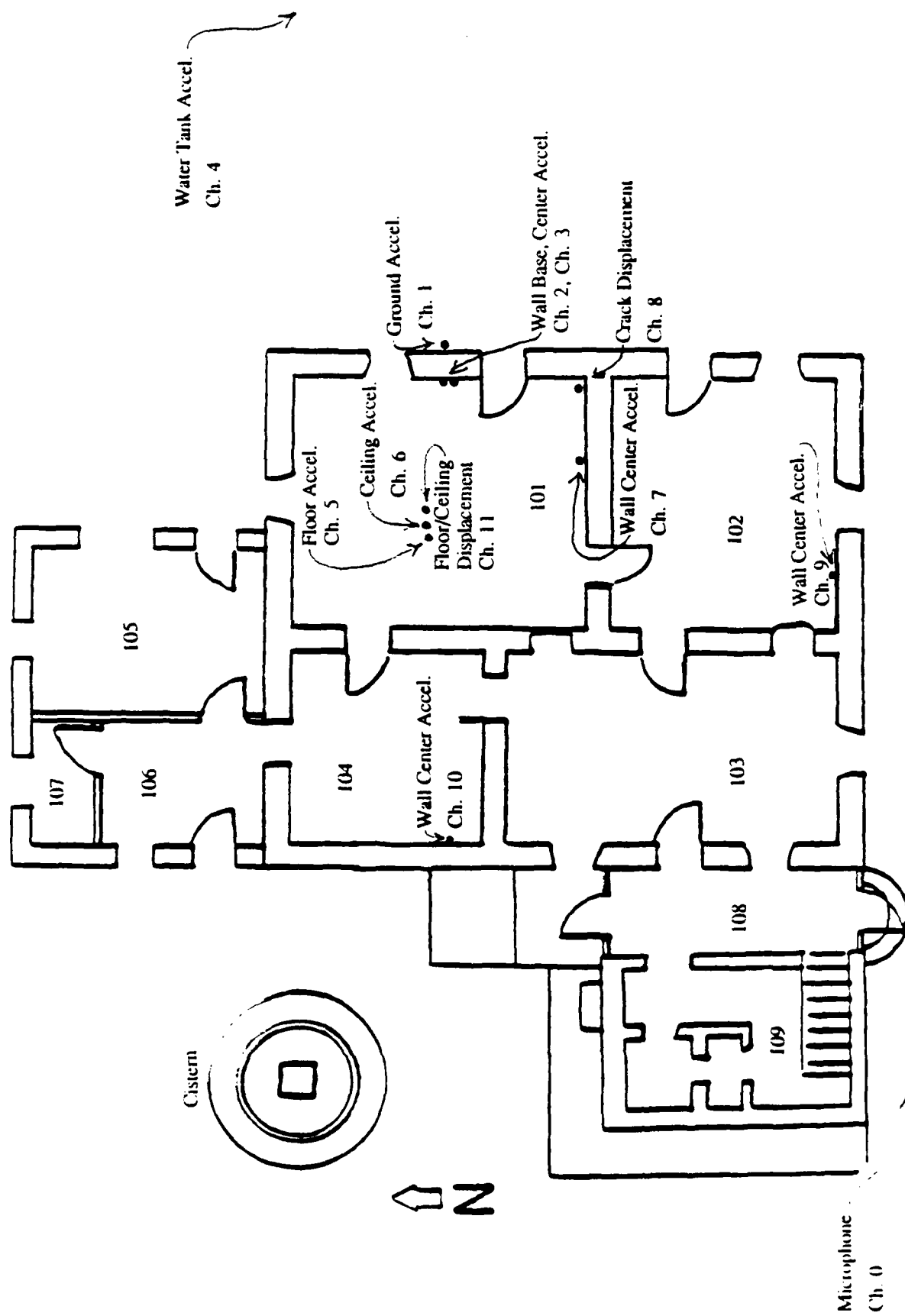


Figure 5-15. Floor Plan of Structure A

erroneous due to a long coaxial cable coupling it to the charge amplifier. This cable was excited directly by the boom, creating a high level signal.

Structure B

The computer and signal conditioners were set-up within this structure; however, the structure was completely open. The motor generator was placed on the west side of the house, while the acoustic systems were deployed on the east side at a distance of approximately 50 feet from the structure. Acoustic interference from the motor generator was non-existent.

Transducers to monitor the acoustic levels and the structural response for measurements at Structure B, as indicated in Figure 5-16, were deployed as follows:

- Acoustic systems, a BEAR, a SBM-1, and the structural system trigger microphone were placed approximately 50 feet east of the house.
- An accelerometer was mounted in a vertical position on top of a steel spike in the ground very close to the wall outside the house.
- An accelerometer was braced against the wall in a horizontal position at the center of one section of the west wall in room 103(Wall 103W).
- An accelerometer was placed on the floor in the center of room 103 with a sand bag on top to hold it in place.
- An accelerometer, attached to a aluminum block, was bonded to a ceiling joist in the center of room 103. Access was obtained through a hole in the ceiling.
- An accelerometer was bonded to the wall near the center of wall 107W.
- An accelerometer was bonded to the wall near the top of the porch wall at a height of approximately 10 feet.
- An accelerometer was bonded to the middle of one section of the porch wall.
- A string potentiometer was placed on the floor in the center of room 104 with a sand bag on top and the string (actually a wire) was attached to the ceiling directly above.

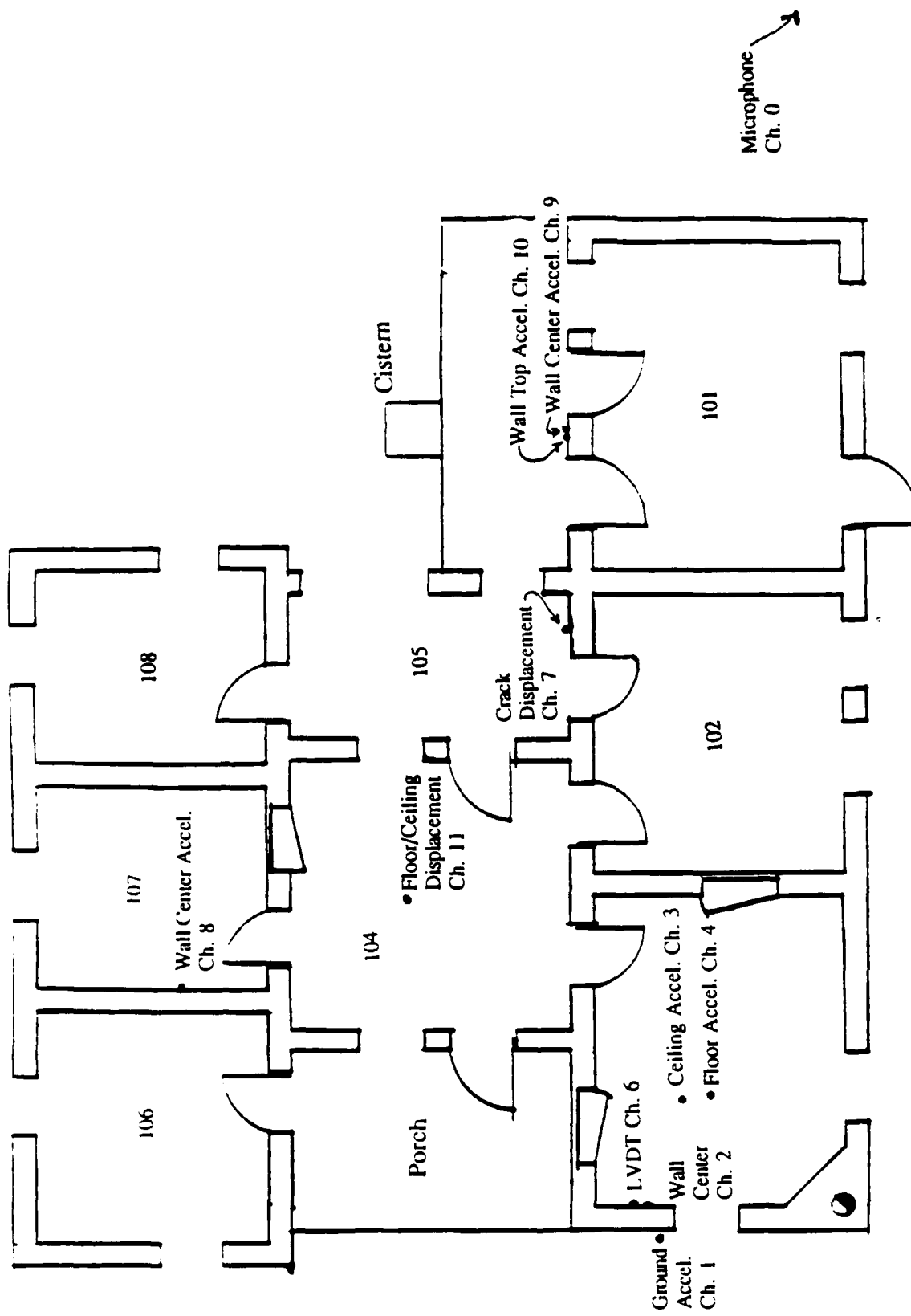


Figure 5-16. Floor Plan of Structure B

- An LVDT was braced against wall 105S near a crack and the core was attached to a bracket on the other side of the crack. The bracket was bonded to the wall.
- An LVDT was braced against wall 103W near a crack and the core was attached to a bracket on the other side of the crack. The bracket was bonded to the wall.

5.3 Test Results

The overall results of the evaluation of the two structure are presented in this section. An evaluation of these results is provided in Section 5.4. In summary:

- Photographs were taken to determine if cracks in the structure walls had been altered during the study; no visible changes were observed in five-fold enlargements of the photos.
- Mechanical impedance measurements were made on Structure A before and after the measurement period. The results were inconclusive since the test-retest repeatability was no better than impedance variations before and after sonic boom exposure.
- Extensive acoustic event and structural response data were acquired. A summary of time histories for these data is presented in Appendix E. A typical example time history for a sonic boom is shown in Figure 5-17. This figure illustrates the acoustic signal and the resultant acceleration at three locations within Structure A. Analysis of these data in Section 5.4 indicates that the structural response measurements on the walls were reasonably close to expectations.

5.3.1 Photographic Examination

A series of photographs were taken of Structure A before and after the monitoring period. Overall photos of the structure as well as close-up pictures of specific areas were taken. The small study areas were selected based on the presence of cracks in the wall that had the greatest potential to grow or elongate. Figure 5-18 illustrates a typical section of wall in Structure A.

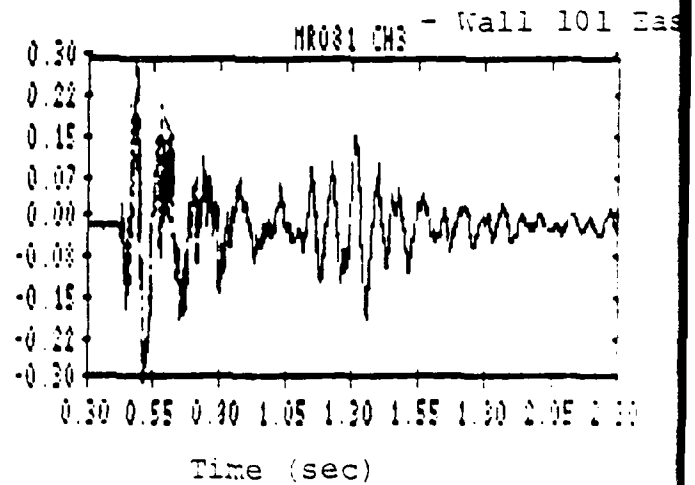
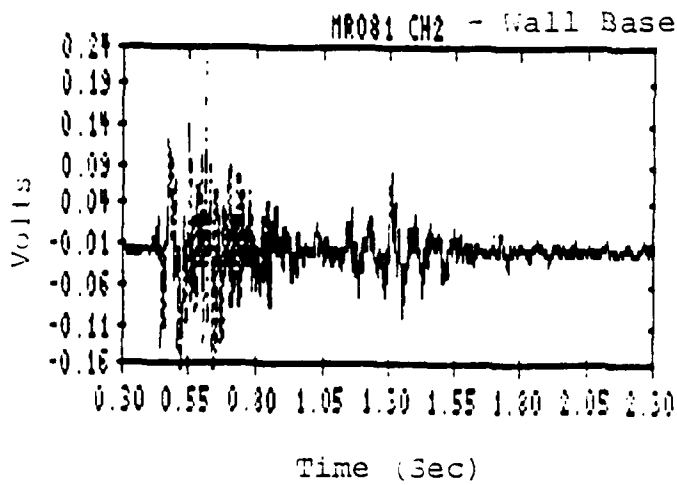
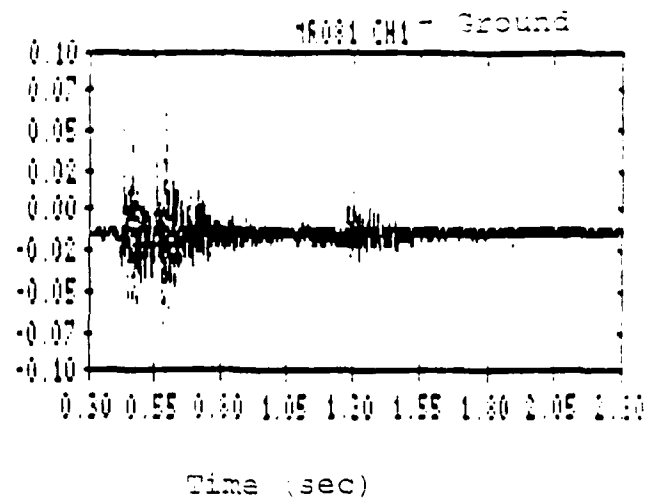
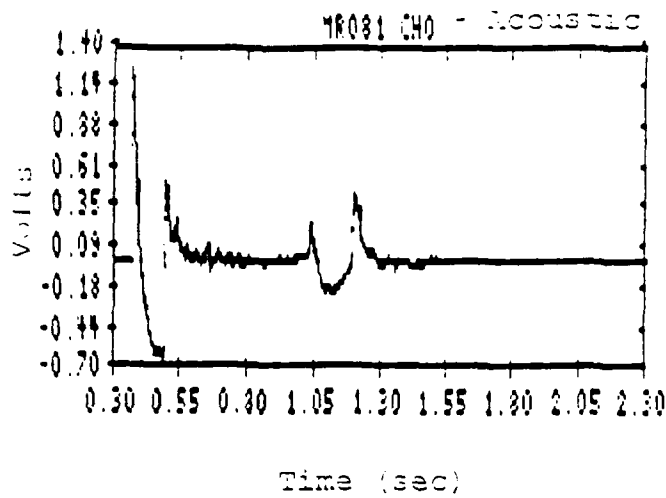


Figure 5-17. Typical Sonic Boom Event with Selected Response Channels
(Boom Event #081)

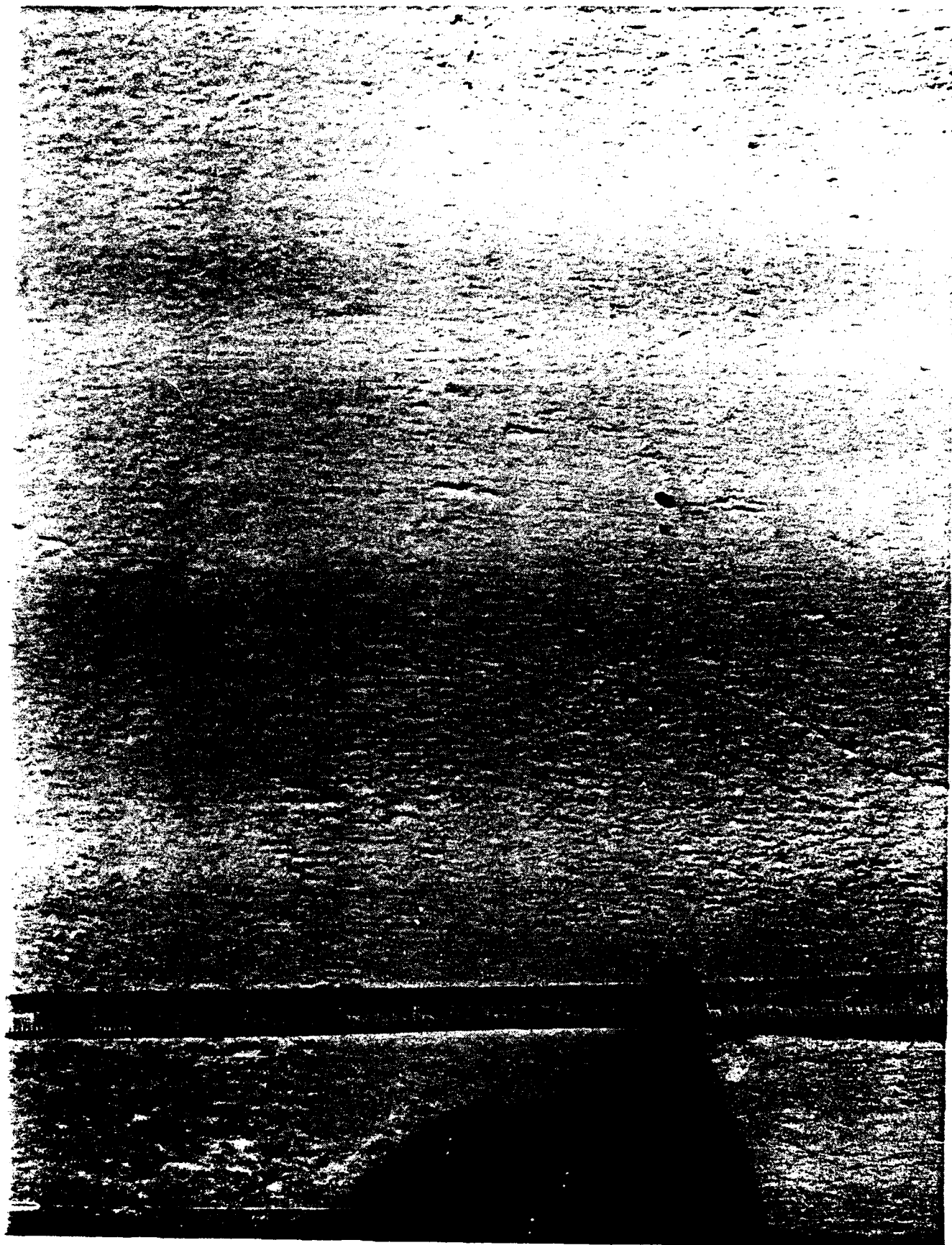


Figure 5-18. Typical Wall Surface of Structure A

5.3.1.1 Analysis Procedures

The contact prints of the negatives were assembled and arranged according to the pre- and post-testing photo log. After performing an overall general inspection of the photos, several were selected and 8x10 color prints were obtained. Comparison of before and after shots were made using two magnifiers. A 6X magnifier was used to select areas for examination and then a 50X microscope was used for the more detailed examinations.

5.3.1.2 Photographic Analysis Results

An analysis of the photographs led to several conclusions regarding structural changes caused by sonic booms during the test period.

- The primary objective was to determine if clear, photographically documented evidence of changes such as the appearance of new cracks or elongation and/or widening of existing cracks could be established. However, there was no noticeable visual difference between the pre- and post-experimental photographs. Appendix D contains samples of the photographs taken. No clear evidence of macroscopic difference exists between them.
- The photographs cover a span of 6 weeks. Since the ranch house is over 50 years old, this may be too short a timeframe to establish any evidence of structural damage from the sonic booms that occurred during the test period. The true degradation caused by the booms, such as the development of new cracks, may only appear after a much longer period of exposure. Furthermore, the lack of evidence of damage is consistent with the low probability of sonic boom damage predicted for this type of structure (see Section 6).
- It is possible that the explosive tests conducted at the White Sands Missile Range have had a cumulative "burn-in" effect on the ranch houses and the structures were fully stress-relieved before the photographic session began.

5.3.2 Mechanical Impedance Measurements

5.3.2.1 Test Procedures

Table 5-2 lists the series of impedance tests performed on the two structures. Tests were made on Structure A before and after the 1-month period of monitoring.

Table 5-2

Summary of Impedance Tests Performed on Structures A and B

Filename	Channels	Transducers	Location	Type
Structure A				
Pre-tests				
FS101E1	4	FT, 3 Wall Accels	Wall 101E	Freq. Sweep
FS101E2	4	FT, 3 Wall Accels	Wall 101E	Freq. Sweep
EH101E1 & 2	4	FT, 3 Wall Accels	Wall 101E	Hammer
EA101E1 & 2	4	FT, Hann. Accel, 2 Wall Accels	Wall 101E	Hammer
EA101S1 & 2	4	FT, Hann. Accel, 2 Wall Accels	Wall 101S	Hammer
EH101S1 to 4	4	FT, 3 Wall Accels	Wall 101S	Hammer
FS101S1 & 2	4	FT, 3 Wall Accels	Wall 101S	Freq. Sweep
PH101E1	2	FT, Hann. Accel	Wall 101E	Hammer
PH101E2	2	FT, Hann. Accel	Wall 101E	Hammer
PH101E3	2	FT, Hann. Accel	Wall 101E	Hammer
PH101S1	2	FT, Hann. Accel	Wall 101S	Hammer
PH101S2	2	FT, Hann. Accel	Wall 101S	Hammer
PH101S3	2	FT, Hann. Accel	Wall 101S	Hammer
Post-tests				
I01S1 & 2	4	FT, Hann. Accel, 2 Wall Accels	Wall 101S	Hammer
IH1S1 & 2	2	FT, Hann. Accel	Wall 101S	Hammer
IH1S3 & 4	2	FT, Hann. Accel	Wall 101S	Hammer
IH1S5 & 6	2	FT, Hann. Accel	Wall 101S	Hammer
IH1E1 & 2	2	FT, Hann. Accel	Wall 101E	Hammer
IH1E3 & 4	2	FT, Hann. Accel	Wall 101E	Hammer
IH1E5 & 6	2	FT, Hann. Accel	Wall 101E	Hammer
I01E1 & 2	4	FT, Hann. Accel, 2 Wall Accels	Wall 101E	Hammer
Structure B				
I03W1 & 2	3	FT, Hann. Accel, Wall Accel	Wall 103W	Hammer
I03W3 & 4	3	FT, Hann. Accel, Wall Accel	Wall 103W	Hammer
I03W5 & 6	3	FT, Hann. Accel, Wall Accel	Wall 103W	Hammer
I04S1 & 2	3	FT, Hann. Accel, Wall Accel	Wall 104S	Hammer
I04S3 & 4	3	FT, Hann. Accel, Wall Accel	Wall 104S	Hammer
I04S1 & 2	3	FT, Hann. Accel, Wall Accel	Wall 104S	Hammer
I04S3 & 4	3	FT, Hann. Accel, Wall Accel	Wall 104S	Hammer
I04S5 & 6	3	FT, Hann. Accel, Wall Accel	Wall 104S	Hammer

Note: FT = Force Transducer

Measurements were made using the impedance hammer as an input device, and thus each tap on the wall resulted in a slightly different force input. In order to check repeatability of these measurements, at least two strikes were made for each test. Figure 5-19 illustrates the results of two taps at the same location. The data represents the transfer function between the force input and the velocity response measured at three different locations. Accelerometers were braced against the wall (Wall 101E) using the previously-described system and one accelerometer was mounted on the hammer head. Conversion of acceleration to velocity was performed through division of the Fourier Spectrum by angular frequency. The plots shown here portray the relative mechanical impedance of the wall (i.e., ratio of applied force spectrum to velocity response spectrum) and illustrate the typical repeatability of the tests.

Spectrum plots in this report, unless otherwise noted, were obtained from an FFT narrow-band analysis program. Narrow-band values were calculated and the average value in each one-third octave band was determined. This value was then normalized to a 1 Hz bandwidth. Each value shown in the plots represents the average 1 Hz band level within each one-third octave. This spectral smoothing technique was employed to provide a more useful output format since the unsmoothed Fourier spectra contained so much fine structure with sharp peaks and valleys making it very difficult to read.

The regular impedance measurements were made at several positions. The impedance hammer was used to lightly tap the wall and a recording of the impulse was made using the computer. In Structure A these measurements were made before and after the boom measurement series. An example of the impulse impedance data measured before and after the test period is shown in Figure 5-20. Clearly, the difference between pre- and post-test impedance measurements are comparable to the pre-test repeatability tests in Figure 5-19. Thus, this technique, as applied to the study, is not reliable as a means of assessing potential damage.

At this same location on Wall 101E, the wall driver was utilized to determine the frequency response characteristics of the wall. This involved measurement of the force input to the wall and the resultant acceleration at different points on the wall. The same wall locations were used as those used for the impedance hammer tests. This wall is constructed of adobe blocks covered with a thin layer of plaster. The plaster on top of the adobe was approximately 1/4 inch thick.

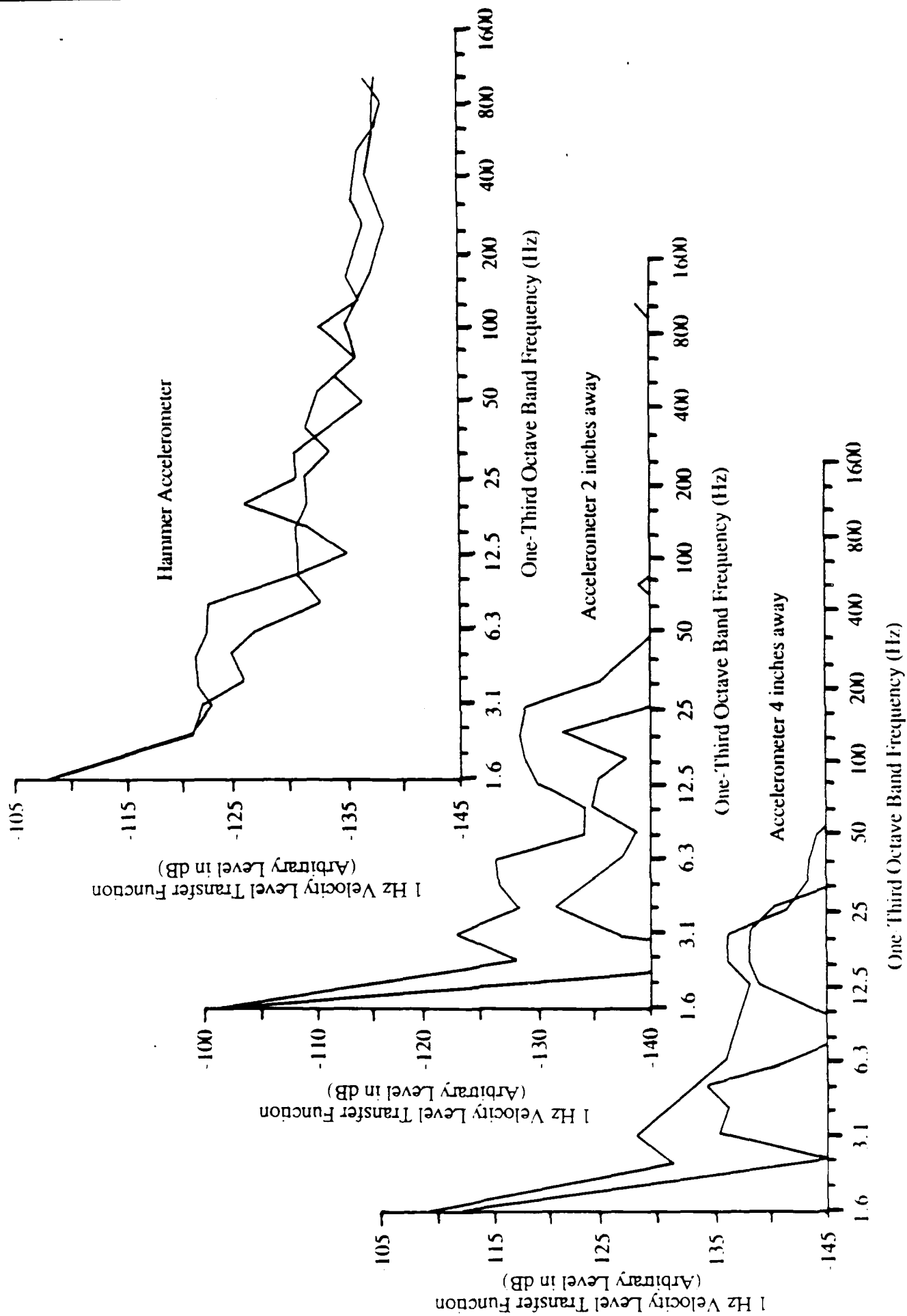


Figure 5-19. Impedance Test on Wall 101E - Repeat Tests

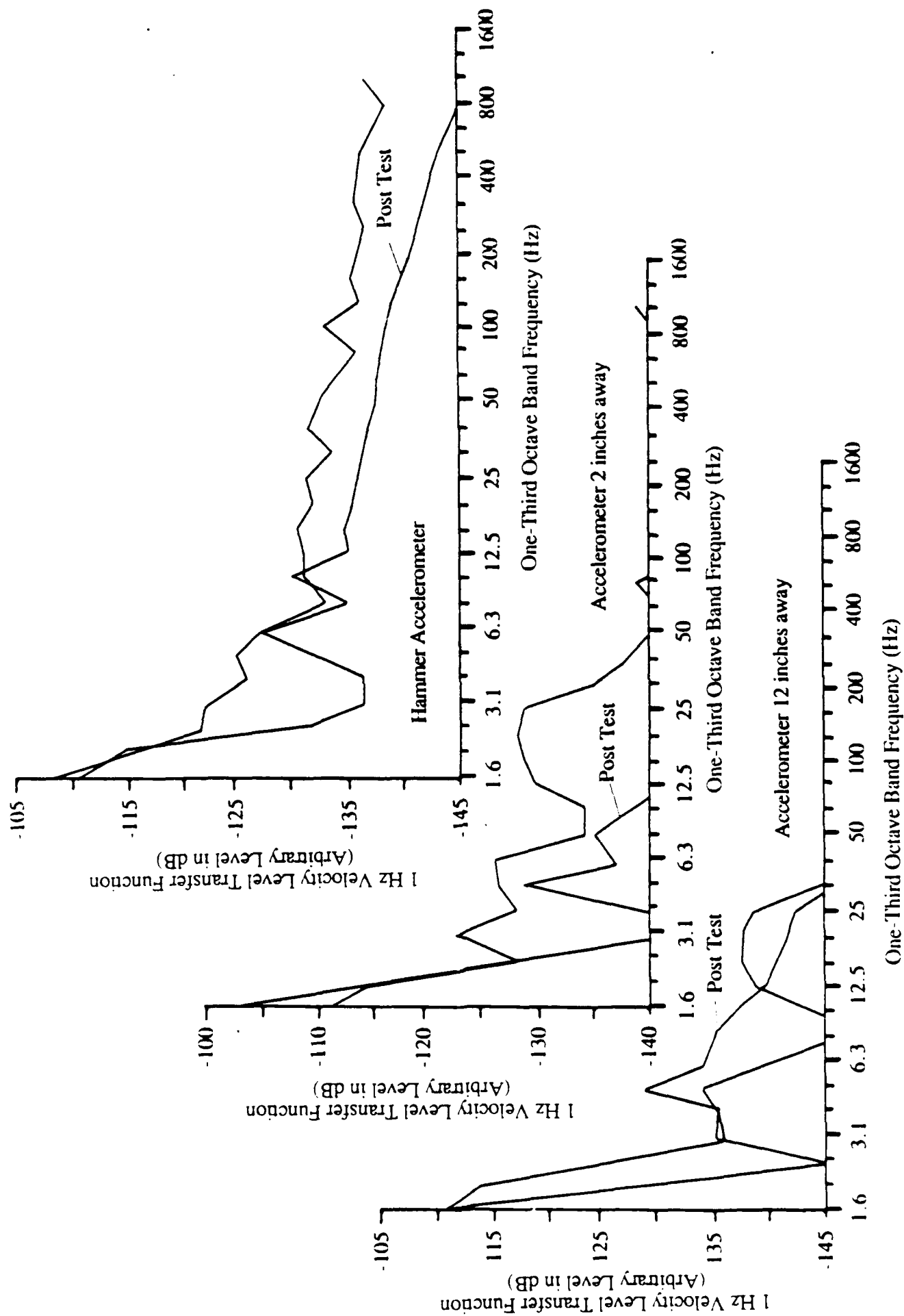


Figure 5.20. Impedance Test on Wall 101E - Before and After Boom Monitoring

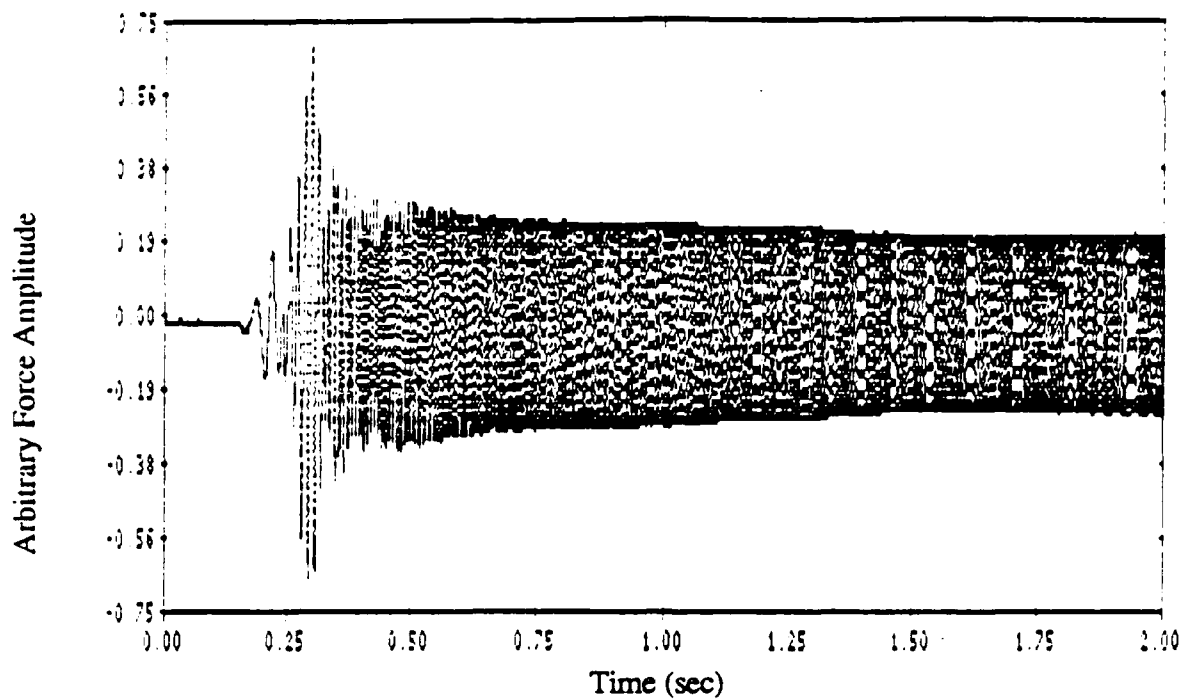
The wall driver was braced against the wall and supported by a soft foam layer between the driver and the floor brace. Coupling between the driver and the wall was made through the force transducer. A frequency sweep rate was set to cover the range from 0 to 1 kHz in about 4 seconds. The 4 seconds of data, which included the input force and three accelerometer channels, were then stored on the computer disk.

Figure 5-21 illustrates the data obtained from the force transducer during a frequency sweep. The top plot shows the time domain force levels coupled to the wall while the lower plot shows the frequency spectrum of these data. Figures 5-22 and 5-23 show the acceleration data obtained from two accelerometers braced against the wall beside the wall driver. Accelerometer locations were 2 inches and 12 inches from the driver, respectively.

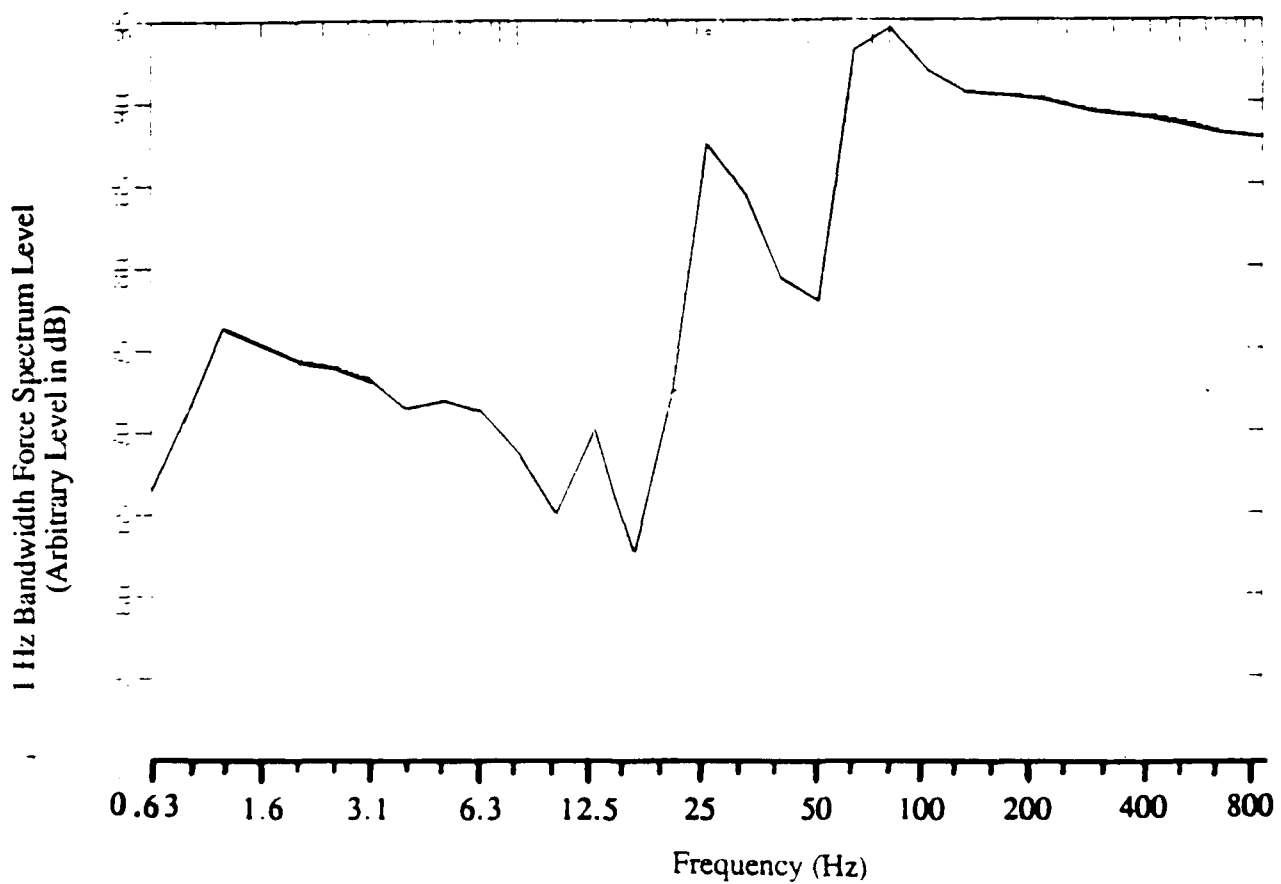
5.3.2.3 Impedance Measurement Results

The impedance measurements produced results which were reasonable for relative values of mechanical impedance. For both impulsive and sine sweep measurements, the following conclusions were drawn:

- Most of the wall surfaces were quite fragile and thus it was difficult to perform the measurements and avoid possible damage to the structure.
- The wall surfaces were quite rough making it difficult to find a suitably flat surface on which to place a transducer such as an accelerometer. Being unable to smooth the surface or apply any adhesive left few satisfactory positions for measurements.
- Repeatability of impulse measurements was not good. Repeated taps of the hammer produced similar results but not an identical response. This problem made pre- and post-exposure evaluation very difficult. If this technique is considered worthy of further evaluation, a larger number of baseline measurements would be needed to establish some statistically reliable baseline (i.e., before exposure) impedance data.
- Sinusoidal frequency response measurements produced results that were not easily interpreted. Small changes in position of either the driver or receiving accelerometer results in large changes in frequency response. This technique would similarly require additional study before it could become a viable evaluation tool for assessing structural damage.



a) Time History of Frequency Sweep - Force Input to Wall



b) Force Spectrum Level

Figure 5-21. Wall Driver Force Input (Test FS 101E1)

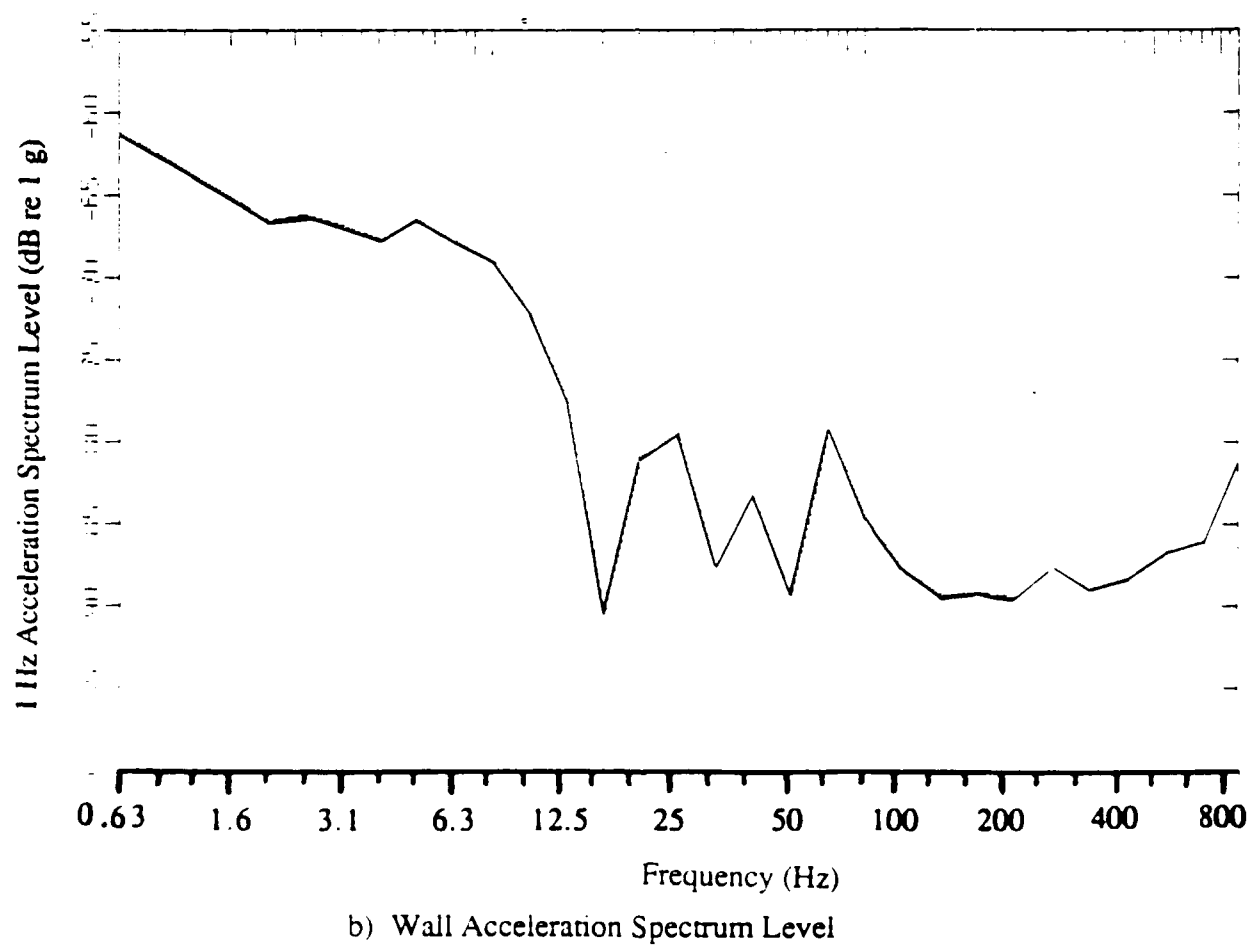
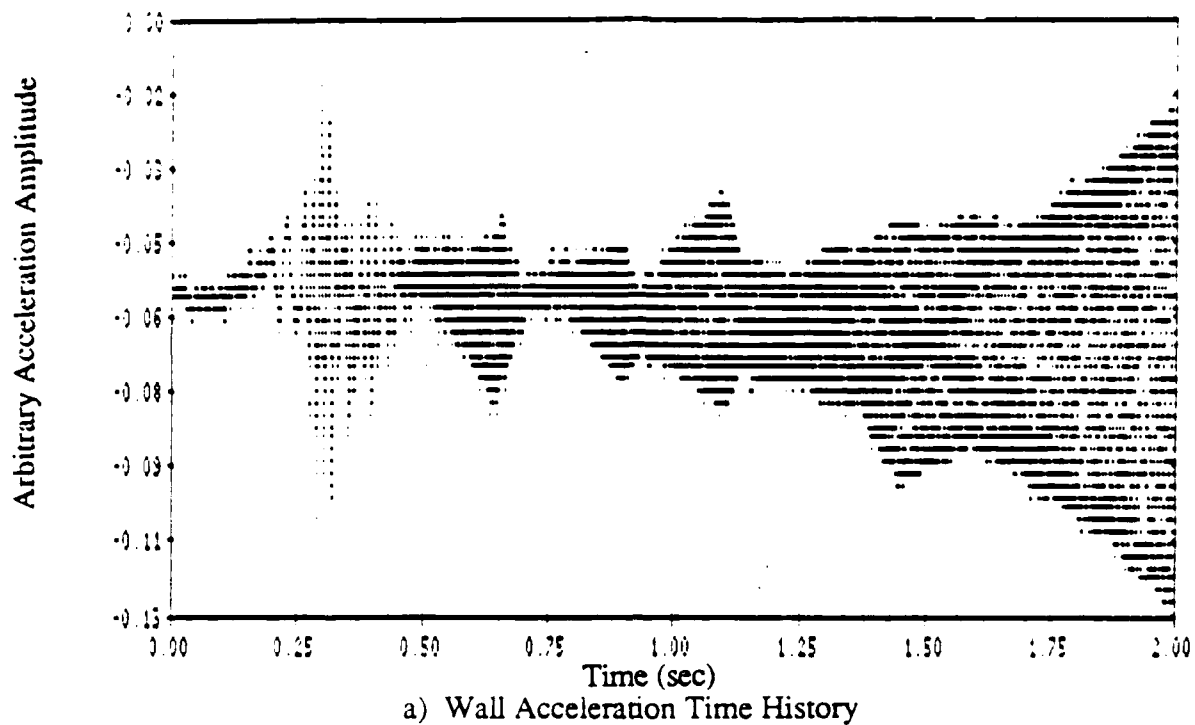
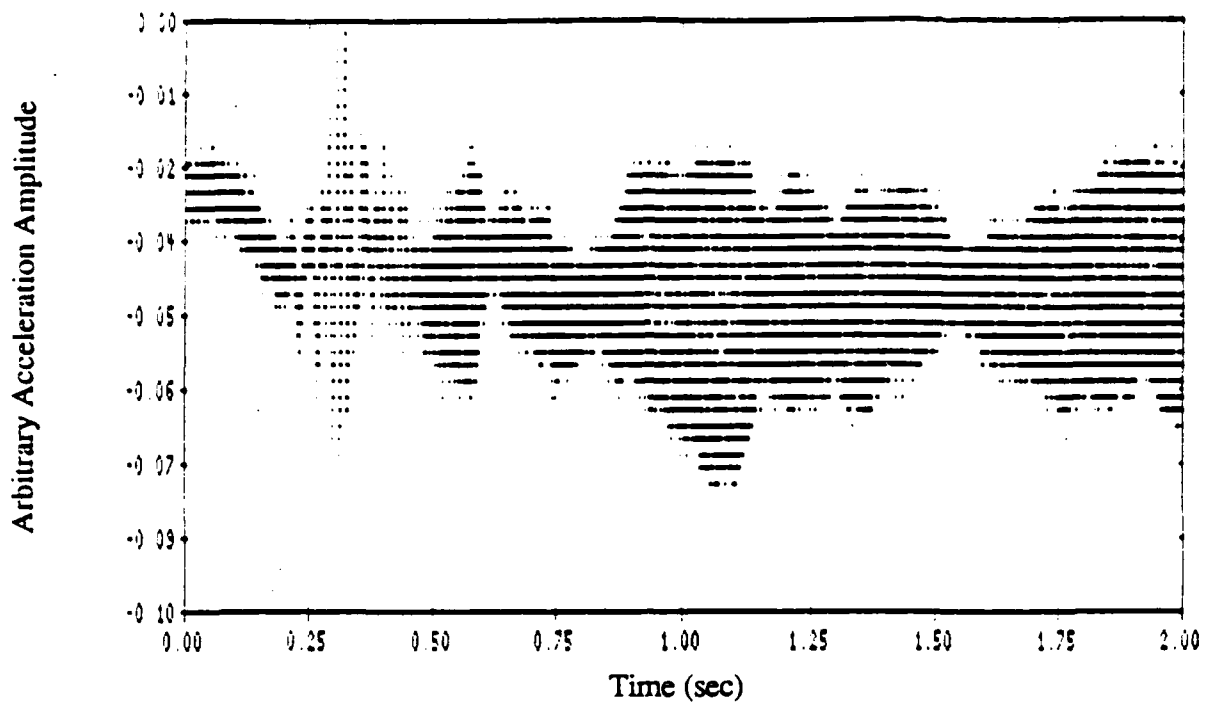
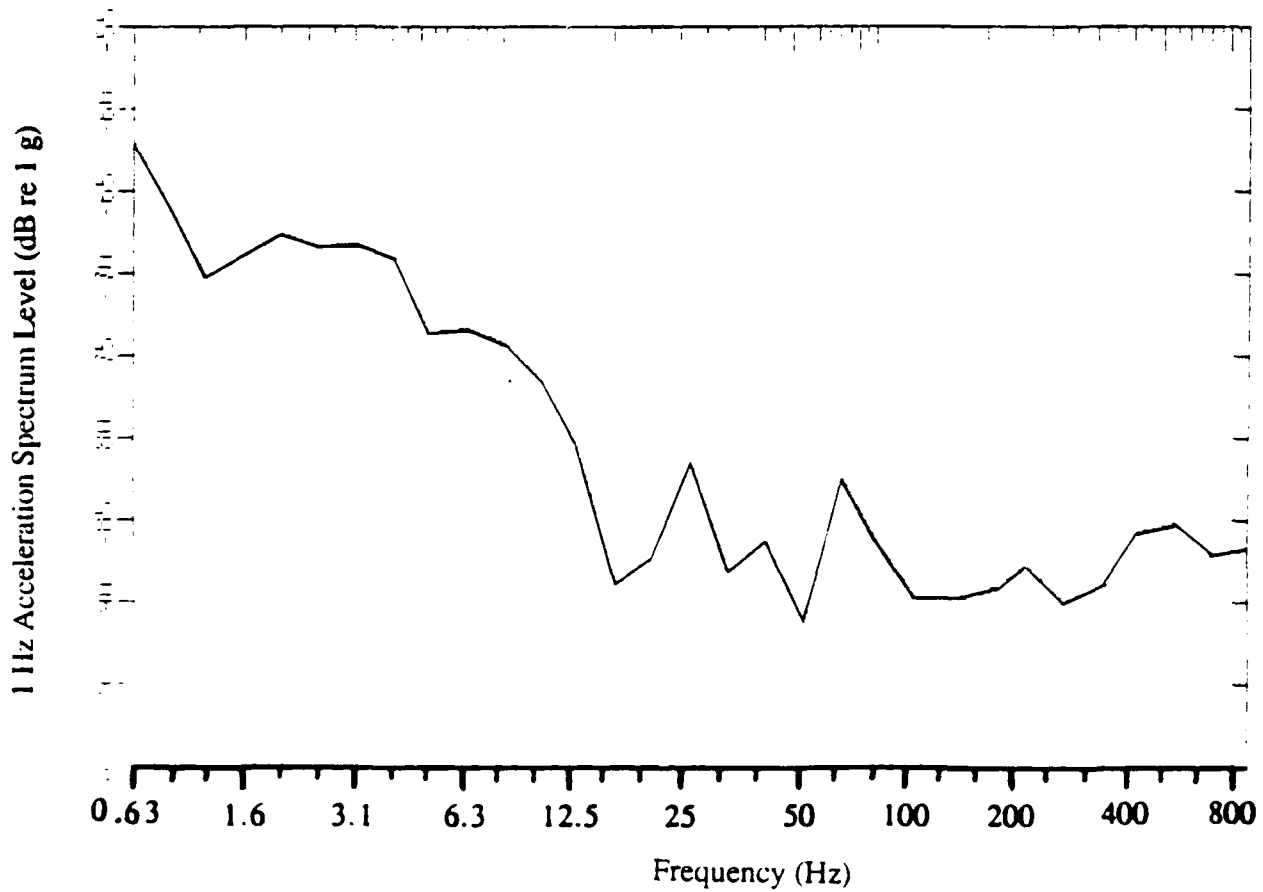


Figure 5-22. Wall Acceleration 2 inches from Driver (Test FS 101E1)



a) Wall Acceleration Time History



b) Wall Acceleration Spectrum Level

Figure 5-23. Wall Acceleration 12 inches from Driver (Test FS 101E1)

5.3.3 Structural Response Tests

5.3.3.1 Test Data

A listing of the structural response test data is provided in Table 5-3. Data in this table represent each event identified as a sonic boom and also a few events considered to be low altitude subsonic flyovers of Structure A. The data were obtained during the six week monitoring period of the two structures at WSMR.

Figure 5-24 illustrates the general frequency response characteristics of the structure at the respective location of each transducer by sample time histories of response for one sonic boom event. Thus, the relative response of the structural components can be compared to one another. Similar data are shown for all events in Appendix E. The highest acceleration amplitude observed (nearly 1g peak) for this boom was from Channel 6, which was the ceiling. Another large response was that of wall 101S, Channel 7, which had nearly a 1g response level. The base of wall 101E (Channel 2), as expected, had the lowest acceleration level, an amplitude of about 0.02 gs. Appendix E contains a complete set of the time history plots for all data. Appendix F contains a listing of the weather data (during the measurement period) obtained at White Sands Missile Range.

Structural Response Results

An analysis of the data obtained from the LVDT mounted on the crack in Structure A is shown in Figure 5-25 and illustrates the displacement observed during 12 sonic booms occurring during the tests. During the tests, the LVDT was not intentionally moved so all displacement shown in this figure occurred naturally. Of course, it is possible that the brace supporting the LVDT could have moved slightly producing some of the large shifts between booms. On the plot of Figure 5-25, a negative change in displacement corresponds to a widening of the crack.

All but one boom produced an apparent widening of the crack, noted as a shift in the DC level of the LVDT before and after the dynamic response from the boom. The average change in displacement observed during the tests was 0.00044 inches, not a large value but quite significant if real.

Table 5-3

Summary of Tyndall Test Data Listing Peak Sonic Boom Pressures on Channel 0 and Peak Structural Responses and Ratios of Peak Acceleration or Displacement to Peak Pressure

Date	Time	File Name	Angle (2)	Acoustic Level Ch 0	dBpk psf	Booms		Ground Ch 1	Wall Base 101e		Wall 101e		Wall 101s		Floor 101	
						pk g's	g/psf	pk g's	pk g's	g/psf	pk g's	g/psf	pk g's	g/psf	pk g's	g/psf
2-23	0807	fc223	162	125	0.72	0.011	0.015	0.013	0.017	0.031	0.022	0.034	1.100	1.534	0.040	0.056
	0830	fc224	175	115	0.24	0.004	0.015	0.006	0.023	0.008	0.034	0.034	0.325	1.374	0.015	0.063
	0940	fc225	148	118	0.34	0.003	0.007	0.008	0.022	0.013	0.038	0.028	0.455	1.338	0.020	0.059
	0940	fc226	145	121	0.44	0.003	0.007	0.007	0.016	0.013	0.028	0.028	0.965	2.176	0.040	0.090
	1126	fc228	165	125	0.70	0.020	0.028	0.018	0.026	0.034	0.048	0.039	1.215	1.730	0.085	0.121
2-24	0633	fb231	142	125	0.76	0.040	0.053	0.020	0.026	0.030	0.048	0.040	1.195	1.569	0.065	0.085
3-07	0922	mr071	180	127	0.98	0.026	0.026	0.022	0.022	0.040	0.040	0.040	1.000	1.017	0.070	0.071
3-08	0811	mr081	47	131	1.41	0.007	0.005	0.020	0.014	0.031	0.022	0.047	0.850	1.602	0.060	0.042
	0824	mr082	168	124	0.64	0.003	0.003	0.015	0.024	0.030	0.047	0.047	0.765	1.203	0.030	0.047
	1013	mr084	182	124	0.67	0.009	0.013	0.018	0.027	0.023	0.034	0.034	0.880	1.308	0.050	0.074
3-09	0802	mr091	113	122	0.55	0.013	0.023	0.011	0.020	0.024	0.043	0.043	0.425	0.766	0.025	0.045
	1110	mr092	196	126	0.82	0.007	0.008	0.020	0.024	0.037	0.045	0.045	0.495	1.213	0.050	0.061
3-13	1021	mr131	93	122	0.92	0.004	0.004	0.011	0.011	0.024	0.026	0.026	0.245	0.265	0.035	0.040
3-17	0816	mr171	155	112	0.17	0.001	0.003	0.004	0.021	0.003	0.018	0.018	0.060	0.353	0.075	0.041
3-21	1349	mr211	165	127	0.89	0.012	0.014	0.013	0.015	0.009	0.010	0.010	0.365	0.411	0.040	0.045
3-22	1332	mr222	163	121	0.46	0.004	0.007	0.009	0.018	0.029	0.060	0.060	0.260	0.541	0.025	0.052
	1438	mr223	189	117	0.46	0.002	0.007	0.005	0.018	0.008	0.027	0.027	0.110	0.342	0.025	0.089
Mean						122.7	0.65	0.014	0.020	0.035	0.035	0.012	1.047	1.047	0.087	0.091
StdDev.						4.71	0.31	0.012	0.004	0.012	0.012	0.012	0.543	0.543	0.091	0.091
Structure A																
Possible Flyers (1)																
3-02	1020	mr022	225	116	0.26	0.010	0.037	0.005	0.017	0.011	0.043	0.043	0.065	0.251	0.015	0.058
3-14	0852	mr142	315	113	0.18	0.002	0.011	0.004	0.020	0.006	0.031	0.031	0.065	0.366	0.020	0.113
3-21	1504	mr213	200	112	0.16	0.016	0.098	0.015	0.092	0.003	0.018	0.018	0.025	0.154	0.015	0.092
3-23	1523	mr235	315	111	0.16	0.005	0.032	0.006	0.039	0.005	0.029	0.029	0.020	0.129	0.015	0.097
Mean						112.9	0.19	0.045	0.042	0.030	0.030	0.009	0.225	0.225	0.030	0.020
StdDev.						1.75	0.04	0.032	0.030	0.009	0.009	0.009	0.094	0.094	0.020	0.020
Structure B																
Booms						Acoustic Level Ch 0		Ground Ch 1		Wall 103w		Ceiling 103		Floor 103		Wall 103w
File Name						pk g's	g/psf	pk g's	g/psf	pk g's	g/psf	pk g's	g/psf	pk g's	g/psf	pk g's
4-06	1714	mr102	180	127	0.31	0.005	0.005	0.170	0.719	0.910	1.001	1.001	0.005	0.021	0.040	0.024
	1517	ap051	243	115	0.24	0.010	0.042	0.170	0.719	0.170	0.719	0.719	0.005	0.021	0.0100	0.0423
	1518	ap052	200	116	0.27	0.025	0.091	0.220	0.804	0.360	1.369	1.369	0.005	0.018	0.0100	0.0366
	1638	ap053	93	118	0.32	0.005	0.016	0.290	0.912	0.550	1.730	1.730	0.005	0.016	0.0100	0.0315
Mean						118.9	0.43	0.039	0.812	1.210	1.210	0.363	0.018	0.018	0.033	0.007
StdDev.						4.60	0.26	0.033	0.079	0.363	0.363	0.002	0.002	0.002	0.002	0.002

(1) Structural Response from Possible Low Level Subsonic Flyovers

(2) Direction of boom or acoustic signal arrival

[illegible]

(d) Structural Response from Possible Low Level Subsonic Fluctuations

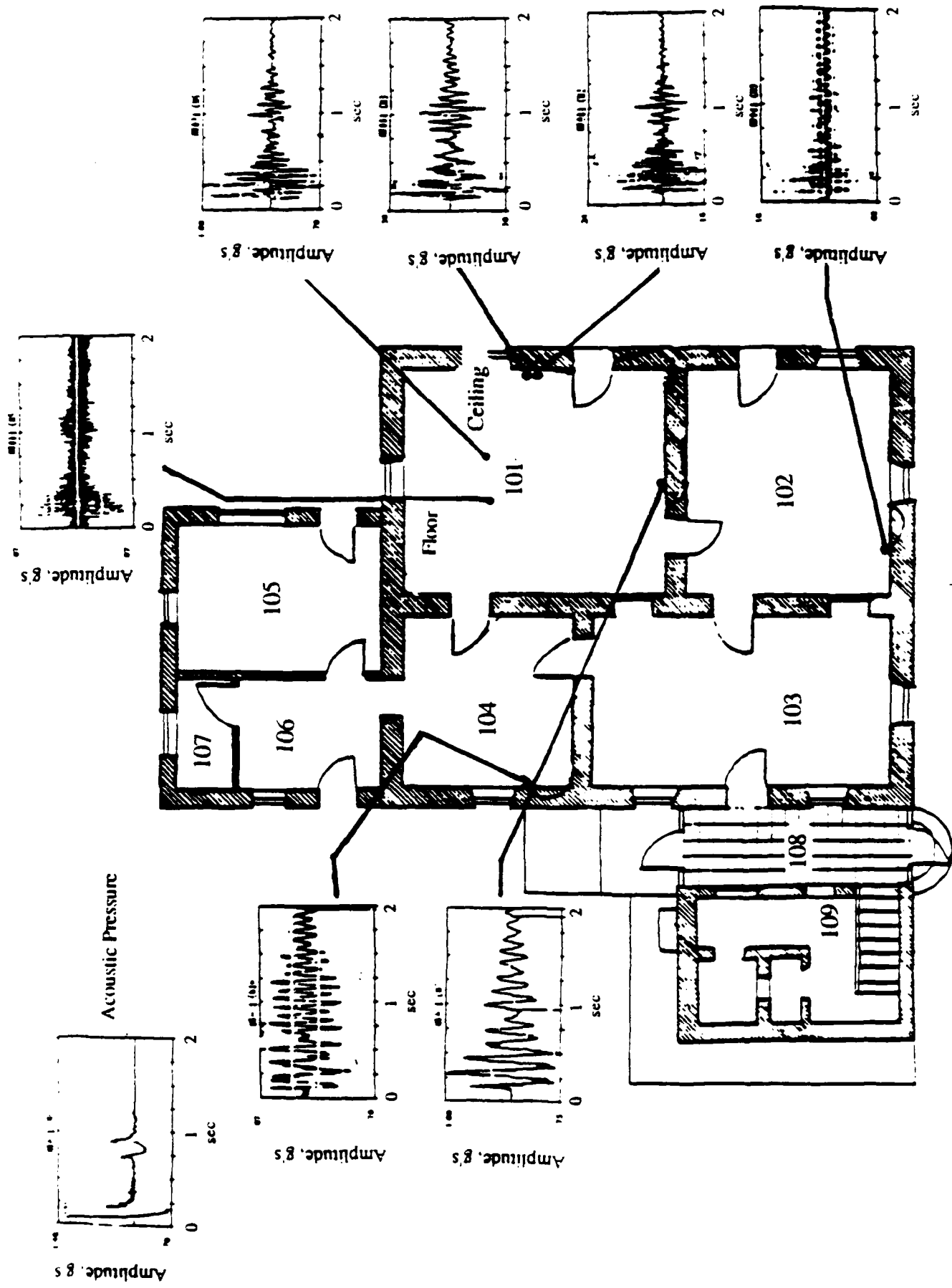


Figure 5-24. Typical Time History Curves of Acoustic Pressure and Response for Boom #MR 081 - Structure A
(Time history plots are shown in Appendix E)

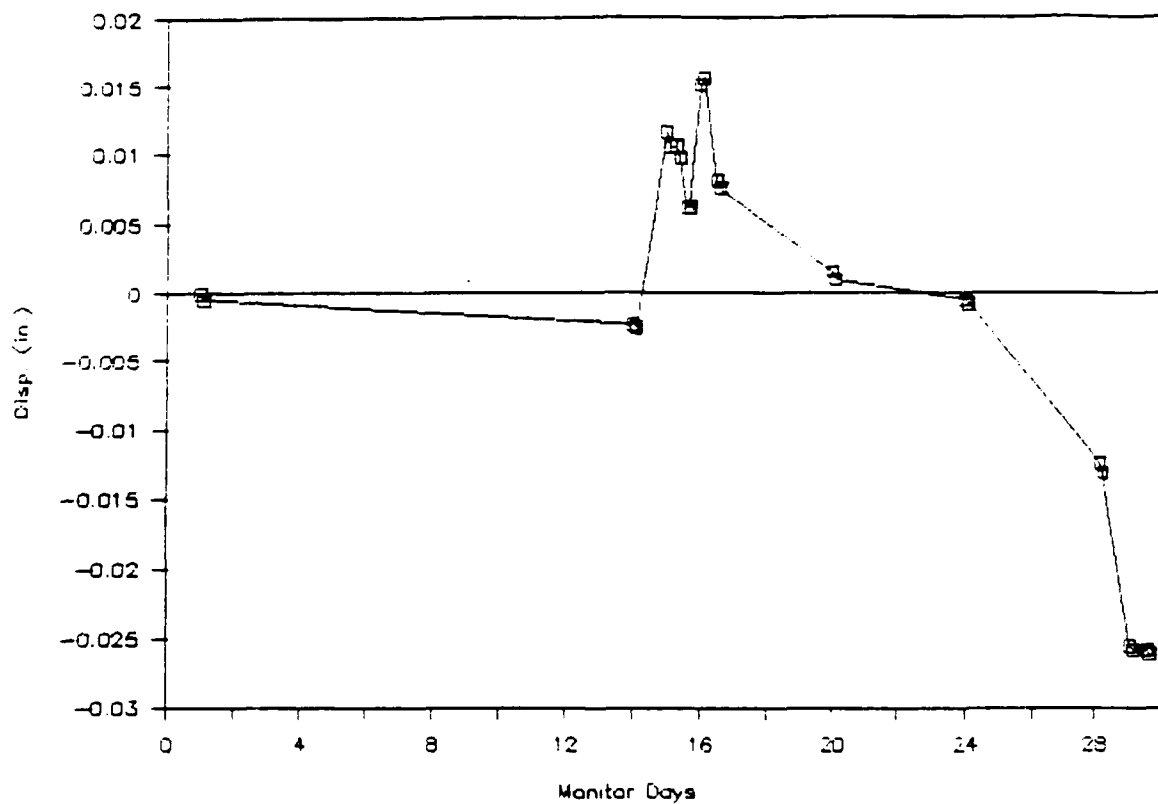


Figure 5-25. Displacement of Crack in Wall 101S of Structure A

Other comments based, in part, on an examination of detailed data plots (too numerous to include in this report) from Structure A are as follows:

- Comparison of the velocity response spectrum levels for Wall 101E show almost the same spectral shape at the base and at the wall center. However, the ratio of peak acceleration to peak sonic boom pressure at the wall center is about 75 percent greater than at the base of the wall. This is in the right direction but represents less amplification than expected on the basis of other similar data discussed in Section 4.3.2.2. However, the velocity response spectra at the wall center was higher by a factor of about 10 over the velocity response at the base. The dominant resonant frequency at both locations is between 6.3 and 16 Hz.
- Wall 101S has a very prominent resonance at 8 Hz with all other resonant frequencies at least 10 dB down. The low frequency content is also quite high.
- Wall 102S and 104W have similar resonance peaks at 8 and 12.5 Hz, although at lower levels than for the other walls. The ratios of peak acceleration to sonic boom pressures for Wall 102S are lower by a factor of about 2 than for Wall 104W. There is no obvious reason for this difference in behavior of the two walls which are believed to be very similar in construction.
- The vibration response of Wall 101S, an internal wall, was relatively high and could have been affected by the presence of a heating flue built into the wall, severely limiting the wall strength.
- Sonic booms occurring during periods when the system was being serviced were not recorded. At least two booms were noted by the field engineer while the system was off.

5.4 Evaluation of Test Results

The measured peak accelerations at the center of three outside walls and ceiling of Structure A have been evaluated and converted into peak pseudo-velocities by dividing the acceleration by 2π times the fundamental resonance frequency of the surface as determined from the time history records. These peak velocities, derived from the measurements, were

divided by the corresponding peak pressures to form a measured velocity to pressure transfer function. These experimental values are shown in Figure 5-26 compared to predicted values based on Eq.(4-5b) and estimated surface weights of 148 psf for the 18-inch adobe wall and 10 psf for the ceiling. A line is also shown representing a 50 percent overprediction case. The upper bound of the data seems to agree very well with the prediction model while the 50 percent overprediction line is generally on the low side of the data.

A more detailed evaluation of the measured data is provided by constructing the spectral content of the velocity response transfer function. This was simply the difference, on a decibel scale, between the velocity exposure spectrum level in dB re 1 inch/second and the sound exposure spectrum level in dB re 1 psf. The velocity exposure spectrum level, $L_{VE}(f)$, represents the spectral content of the time-integrated velocity signal formed from the Fourier Transform of the time-integrated acceleration signal and is given by

$$L_{VE}(f) = 10 \log [2g^2|A(f)|^2/(2\pi f)^2], \text{ dB re } (1 \text{ in/sec})^2 \cdot \text{sec/Hz}$$

where g = Acceleration of gravity, in/sec²
 $|A(f)|$ = Absolute value of Fourier Spectrum of Acceleration Signal, g's-sec
 f = Frequency, Hz

Note that both the velocity and pressure spectra are averaged over a one-third octave band interval for plotting purposes. This smoothing process also prevents computation of artificial peaks in the transfer function which can occur when the raw, narrowband spectra are used to compute a transfer function. The results of this analysis are shown in Figure 5-27a, b, and c from measurements at the center of three walls in Structure A. The data show the mean and mean ± 1 standard deviation for the transfer functions computed from the wall response and acoustic measurements for seven different sonic boom events.

Since these velocity to pressure transfer functions represent, in log form, the ratio of Fourier spectra of the velocity and pressure signals, respectively, they represent general velocity to pressure frequency response functions for each of the center wall positions. Thus, the peak in the transfer function of each curve in the region of 10 to 20 Hz corresponds to the fundamental resonance frequency of the wall and the magnitude of the peak transfer function represents the influence of damping.

An analysis similar to that developed in Appendix C.2 would show that the maximum value of this transfer function, expressed as the ratio of the velocity response spectrum $V(f)$ to

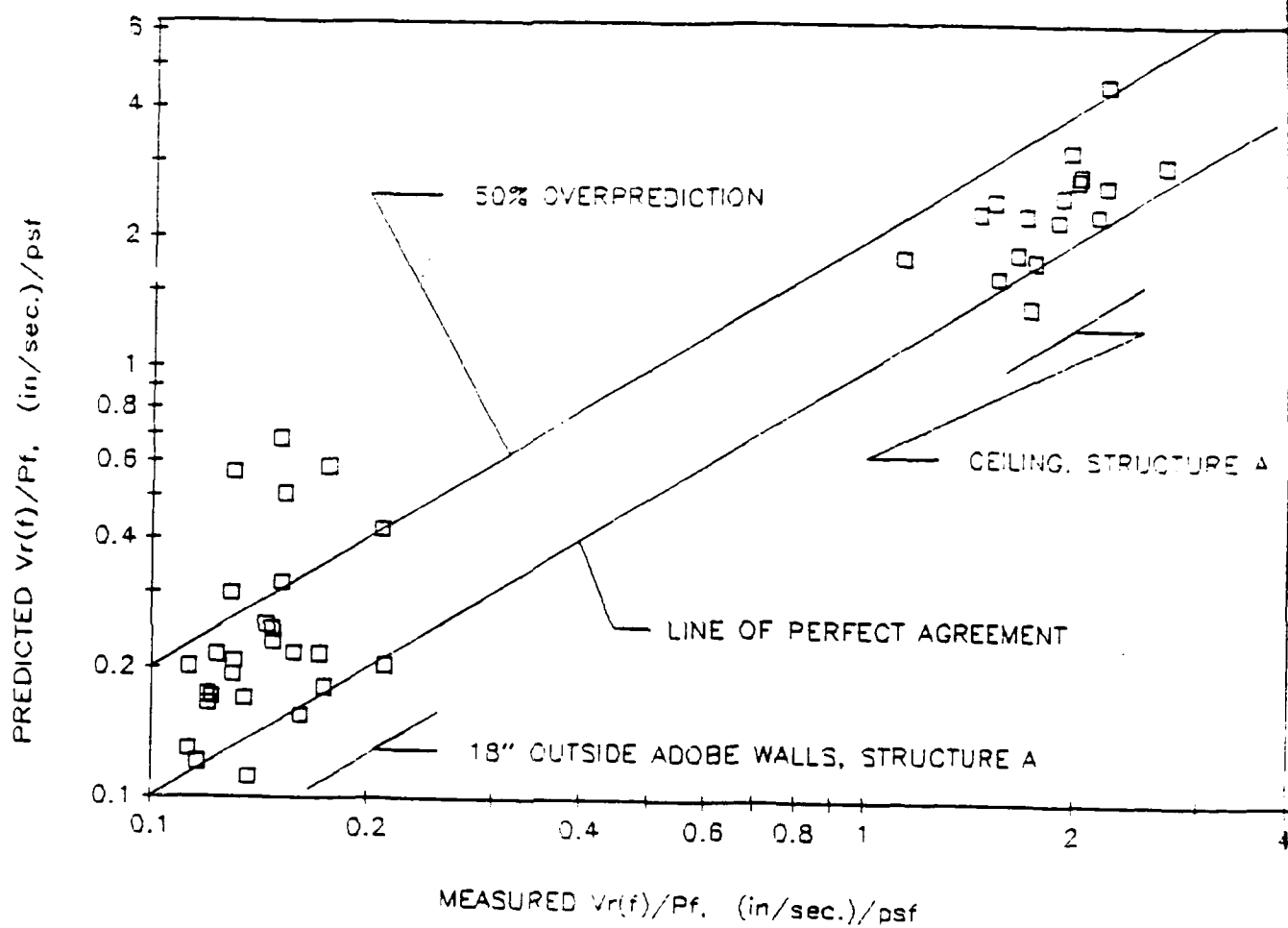


Figure 5-26. Comparison of Measured and Predicted Ratio of Peak Velocity Response, at Center of Three Outside Walls and in Ceiling, to Peak Sonic Boom Pressure on Nearby Ground Microphones for Structure A

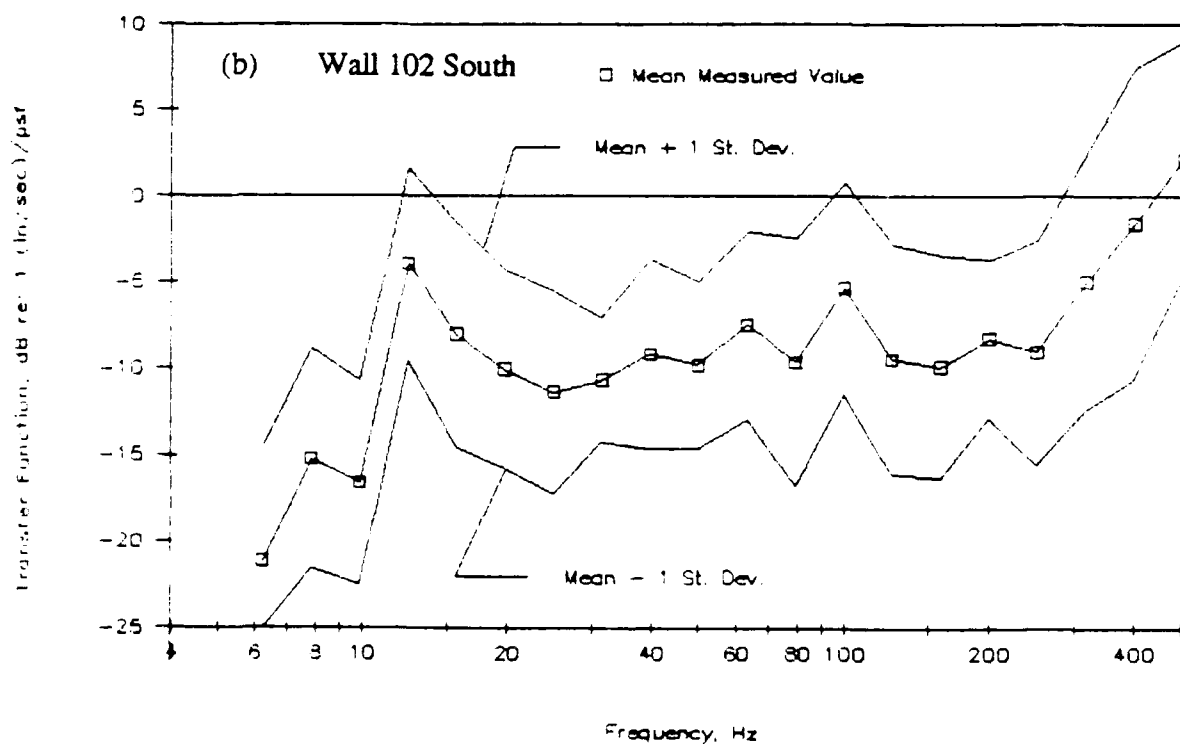
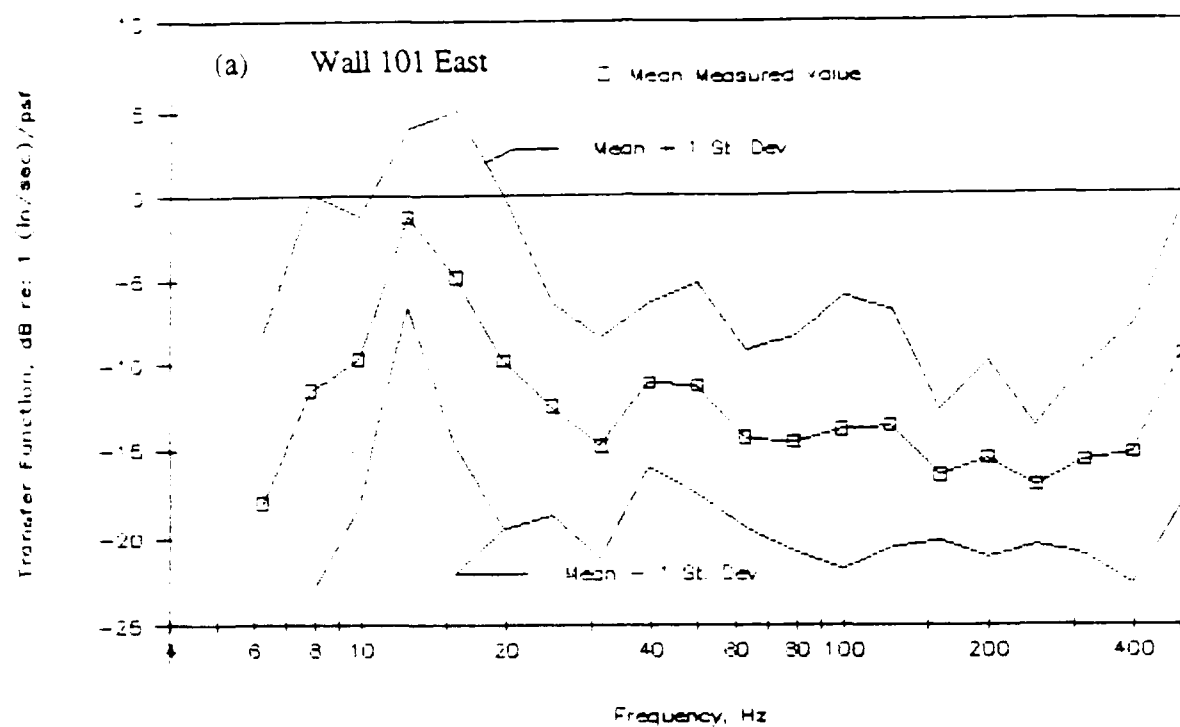


Figure 5-27. Velocity to Pressure Transfer Function Spectra Measured from Seven Different Sonic Boom Tests at the Center of Three Different Walls in Structure A

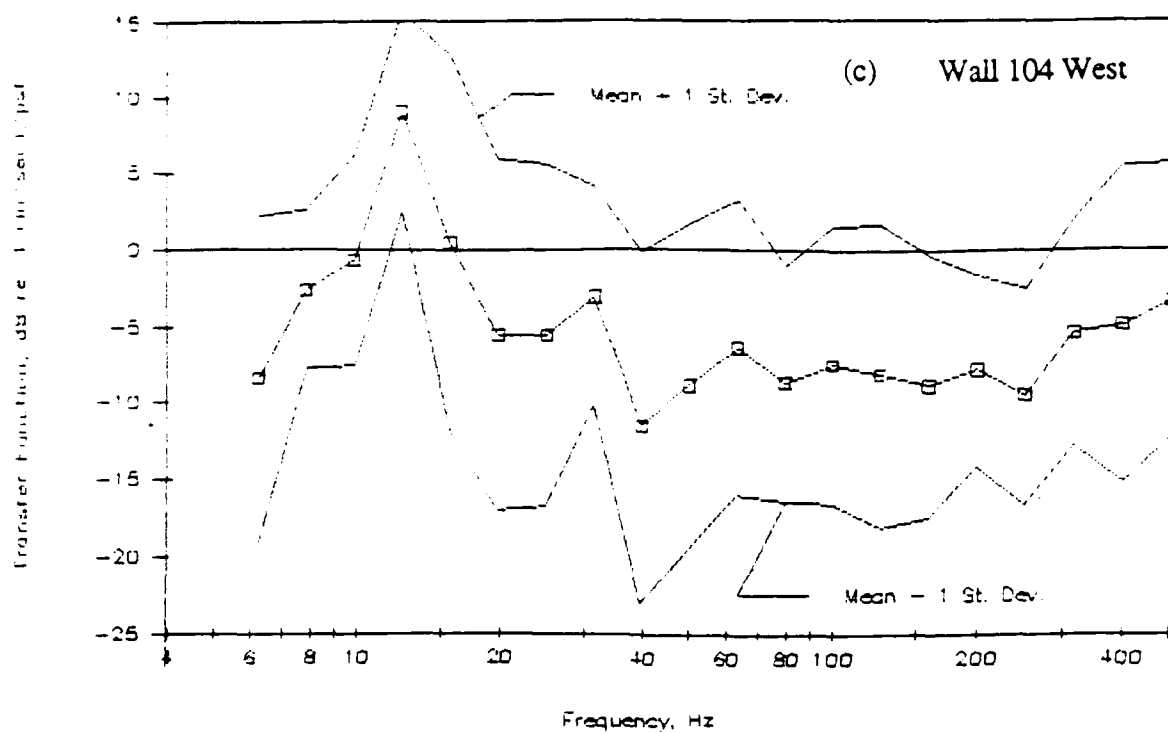


Figure 5-27 (Continued)

pressure spectrum $P(f)$, for a uniform, simply-supported panel in its fundamental mode should have the value:

$$V(f)/P(f)|_{\max} = \frac{16 gQ}{\pi^2 (2\pi f_0) \cdot w} \quad , \quad (\text{in/sec})/\text{psf}$$

where g = Acceleration of gravity (386 in/sec²)
 w = Surface weight, psf
 Q = Dynamic Magnification Factor
 f_0 = Fundamental Resonance Frequency

For these 18-inch adobe walls, the estimated surface weight is 148 psf and Q , derived from analysis of the damping decay in the sonic boom time histories, is estimated to be about 18 (Table 4-2), and the average resonance frequency is 12.5 Hz. Thus, the predicted maximum value of the transfer function at the fundamental resonance of the walls (assuming they behave as a simply supported panel), would be about $(16)(386)(18)/(\pi^2 (2\pi \cdot 12.5) \cdot 148) = 0.97$ or -0.3 dB re 1 in/sec per psf. The peak values for the transfer functions plotted in Figure 5-27 have an average value of about 1 ± 7 dB re 1 in/sec per psf, thus showing excellent agreement with the prediction.

In summary, measured dynamic responses of the two unconventional structures evaluated in this program have provided useful supporting data for the damage prediction model and have explored techniques for damage assessment in the field. Recommendations for improved procedures for the latter are presented in the final paragraph of this section.

5.5 Recommendations for Future Photographic Documentation

Examination of the detailed photographs of the study areas indicates the need for improvements in photographic techniques which should be incorporated in future studies:

- Slow speed color film should be used to obtain a finer grain photograph.
- The camera should be tripod-mounted at a well-defined and documented position. Distance from the film-plane to the wall should be documented and repeatable within ± 0.25 inches.
- The same lens focal length and aperture and shutter speed settings should be used for before and after photographs.

- Preferably, lighting should be provided by a battery-powered cine flood located to either side of the image area to accentuate the surface texture and presence of cracks. This allows lighting to be optimized before exposure.
- If a flash unit is used for lighting instead, it should be removed from the camera and located at about 45° to either side of, and aimed at, the image area.
- If possible, two photos should be taken with the flood or flash positioned on each side of the camera.
- A measurement scale should be held on the wall and be photographed with the detail area.

6.0 STRUCTURAL DAMAGE ASSESSMENT FOR UNCONVENTIONAL STRUCTURES

All of the necessary elements of a basic damage assessment model have been established in Sections 2 through 4 and related supporting data presented in Section 5. This section presents, in a summary step-by-step form, the algorithms, procedures, or data suitable for implementing a model for damage assessment of unconventional structures on the USAF NSBIT ASAN Program. The section will conclude with specific results of applying these procedures for a variety of unconventional structures and a range of sonic boom overpressures.

6.1 Step 1 – Selection of Structures

The first step is the definition of generic categories of structures covering the range of types which may be encountered under supersonic flight operations and for which a systematic assessment of potential damage can be made for each of the types of such flights.

Based on the analysis in Section 2, four broad categories of structure types were selected for analysis. The general categories of unconventional structure listed in Table 6-1 include (1) common types of construction for normally unoccupied historic buildings, (2) prehistoric structures, (3) seismically sensitive areas, and (4) miscellaneous utility buildings and metal structures. Only a Category B window (2 to 10 ft²) has been included in the first building category. Furthermore, the Category B window glass was assumed to be already cracked and to have a resonance frequency that was about 75% of that for an uncracked window. Types of prehistoric structures and archaeological sites included in this breakdown are intended to cover the range of structures built by early Americans that are found widely throughout many parts of the southwest (e.g., Lekson, 1984). Finally, avalanches and landslides are listed under the category identified as seismically sensitive areas implying sensitivity to acoustically induced ground vibration. Water tanks are also included in this category for convenience although the primary concern for water tanks is expected to be response from direct acoustic, rather than seismic, excitation induced by the aircraft noise (see Section 4.2.2.2).

6.2 Step 2 – Definition of Free Field Sonic Boom Pressures

Based on the details developed in Section 3, the sonic boom environments will be defined as follows for (1) ACM areas and (2) all other types of supersonic flight operations.

Table 6-1

Four Major Categories and Subcategories of Unconventional Structures
Evaluated for Potential Damage by Sonic Boom

Major Category	No.	Subcategory Type of Structure	Type of Construction
Historic Buildings	0	Windows	Category B, 2-10 ft ²
	1	Historic Buildings (1)	Masonry, Stone
	2	Historic Buildings (1)	Brick
	3	Historic Buildings (1)	Adobe
	4	Historic Buildings (1)	Wood Frame, Plaster Interior
	5	Historic Buildings (1)	Wood Frame, Wood Interior
	6	Historic Buildings	Covered Wood Bridge
Prehistoric Structures	7	Prehistoric Structures (2)	Masonry, Stone
	8	Prehistoric Structures (2)	Adobe
Seismically Sensitive Areas	9	Water Tanks/Wells	Metal/Stone (above ground)
	10	Geological/ Archaeological Sites (3)	Stone Caves/Rock Formations
	11	Loose Snow - Avalanche Areas	Loose Snow on Steep Slope
	12	Slab Avalanche Areas	Snow Slab on Steep Slope
	13	Slide Areas - Soil	Soil on Steep Slope
Misc. Structures	14	Utility Buildings	Concrete Block
	15	Utility Buildings	Wood Frame
	16	Utility Buildings	Metal Frame
	17	Radio Telescopes	Metal Frame

- (1) More than 50-100 years old (roof intact), unoccupied but maintained
 (2) Early American habitation/ceremonial sites (roof missing)
 (3) May contain petroglyphs or other Early American art

6.2.1 Air Combat Maneuver (ACM) Training

For ACM areas, the long time average of the log mean sonic boom pressure P_0 (i.e., the nominal value) anywhere within the SOA ellipse is given by:

$$P_0 = 0.56 \exp \left(-\frac{1}{2} [(X/\sigma_x)^2 + (Y/\sigma_y)^2] \right)^{0.122}, \text{ psf} \quad (6-1)$$

where X,Y are the coordinates along the minor and major axes of the supersonic main ellipse and σ_x , σ_y , are 11.1 and 18.9 miles, respectively. These last two parameters represent the standard deviations of the two-dimensional normal distribution of nominal sonic boom pressures within the SOA ellipse. The free field sonic boom pressure P_f any time or position is defined by the statistical variation in sonic boom pressure about the nominal value P_0 . For the analysis in Section 6.6, potential damage is estimated in terms of a probability for structures located along the major axis of the ellipse ($X=0$) at $Y=0, 20, 40$, and 60 miles from the center of the SOA ellipse and corresponding approximately to 0, 1, 2, and 3 times the standard deviation of the spatial normal distribution (in the Y direction) of the nominal peak pressures. As discussed in Section 3.0, these same nominal sonic boom pressures would apply at any point on an ellipse with the same "elliptical radius" $r = [(X\sigma_y/\sigma_x)^2 + Y^2]^{1/2}$.

The standard deviation σ_L of the log of this free field sonic boom pressure within SOAs is estimated to be 0.366 (corresponding to 7.32 dB). For this value of σ_L , the peak sonic boom pressure at the center of the ellipse is expected to exceed $0.56 \times 10^{(0.366 \times 1.282)} \approx 1.6$ psf and $0.56 \times 10^{(0.366 \times 2.326)} \approx 4.0$ psf for 10 percent and 1 percent of the time, respectively. These correspond to the probability of occurrence at 1.282 and 2.326 respectively times the standard deviation σ_L of the log of the sonic boom pressures.

6.2.2 Other Supersonic Flight Activity

In the absence of predefined specifications for the detailed nature of other types of supersonic operations, damage assessment will be carried out for the following specific nominal sonic boom pressures increasing in steps by a factor of 2 and corresponding, very approximately, to peak pressures under the flight track for the ranges of supersonic flight altitude indicated below.

Approximate Altitude Range, ft	Approximate Range of Sonic Boom Pressures, psf	Selected Nominal Sonic Boom Pressures, psf
70,000-30,000	1-3	1,2
30,000-10,000	3-10	4,8
10,000-100	10-130	16, 32, 64, 128

For structural damage analysis purposes, these nominal sonic boom pressures will be assumed to be the same as the corresponding long time average free field pressures at a structure located within the carpet boom pattern for such flights. The actual spatial variation of peak sonic boom

pressures within the carpet boom pattern is discussed briefly in Section 3.0. The standard deviation σ_L of the log of the free field sonic boom pressures for these conditions will be taken from the measured statistical distribution of sonic boom overpressures from the Oklahoma City tests (Hilton, et al., 1964) to give:

Location	σ_L	$20 \sigma_L$ dB
Directly Under Flight Path	0.114	2.3
To Side Near Lateral Cut-Off	0.172	3.4

The plotted data in Figures 3-9 to 3-11 in Section 3.0 can be used for initial rough estimates of carpet boom pressures; more exact estimates of carpet boom peak overpressure can be made using available manual (Carlson, 1976) or computerized (Bishop, 1988) sonic boom prediction models. For example, assuming that, on the basis of such models, it is estimated that the nominal peak overpressure is 8 psf for a structure located near the edge of a carpet boom pattern, then 10 percent and 1 percent of the time the peak pressures would be expected to exceed $8 \times 10 (0.172 \times 1.282) \approx 13$ psf and $8 \times 10 (0.172 \times 2.326) \approx 20$ psf, respectively. The damage probability prediction models employed here will, of course, inherently include this statistical variation in peak pressures when computing the probability of damage.

6.3 Step 3 – Definition of Effective Sonic Boom Pressures

The effective sonic boom pressure acting on a structure, P_e , is equal to:

$$P_e = P_o (P_f/P_o) (P_o/P_f) \quad (6-2)$$

where P_o = nominal sonic boom pressure as specified in Step 2.

P_f/P_o = free field sonic boom sound pressure at a given time and location for an arbitrary supersonic flight condition. (The log mean value of this ratio will be assumed to be unity. Thus, the standard deviation σ_L of the log of P_o and of P_f/P_o specified in Step 2 account for the overall statistical variation in P_f due to variations in weather and flight operations about long time mean values.

P_o/P_f = ratio between effective pressure representing the effective load on a structure and the incident free field pressure at the ground.

Table 6-2 defines the mean and standard deviation (in decibels) of the log of this ratio, P_o/P_f .

Table 6-2

Estimated Default Values for Ratio P_e/P_f of Effective to Free Field Sonic Boom Pressure and Corresponding Values of σ_L

Type of Structure	P_e/P_f	σ_L	$20 \sigma_L$ dB
<u>Windows</u>			
Orientation	0.75	0.048	0.95
<u>Surface Reflection</u>	<u>1.00</u>	<u>0.025</u>	<u>0.50</u>
Total	0.75 ⁽¹⁾	0.054 ⁽²⁾	1.07 ⁽²⁾
<u>Buildings with Roof Intact</u> ⁽⁵⁾			
Orientation Effects (see Section 3.3.1)	0.75	0.048	0.95
<u>Surface Reflection</u> (see Section 3.3.2)	<u>1.00</u>	<u>0.075</u>	<u>1.50</u>
Total	0.75	0.089	1.78
<u>Buildings with No Roof</u>			
Orientation	0.75	0.048	0.95
Surface Reflection	1.00	0.025	0.50
<u>Diffraction</u> (see Section 3.3.2) ⁽⁴⁾	<u>0.26</u>	<u>0.068</u>	<u>1.36</u>
Total	0.20	0.087	1.73
<u>Water Tanks</u>			
Orientation	1.0	0	0
<u>Surface Reflection</u>	<u>1.0</u>	<u>0.075</u>	<u>1.5</u>
Total	1.0	0.075	1.5
<u>Archaeological Areas</u>			
Orientation	0.5	0.048	0.95
<u>Surface Reflection</u> ⁽³⁾	<u>1.0</u>	<u>0.075</u>	<u>1.50</u>
Total	0.5	0.089	1.78
<u>Avalanches/Landslides</u>			
Surface Reflection	1.0	0.075	1.78

-
- (1) Product of individual values
 (2) rms sum of individual values
 (3) Worst case assuming normal incidence
 (4) Default value for typical prehistoric buildings based on typical values for height (9 ft) and resonance frequencies (23 Hz) for free-standing walls of such buildings. See Section 3.3.2 for equations for other heights or resonance frequencies.
 (5) Also applies to metal buildings and radio telescopes with diameter ≥ 50 ft and solid metal parabolic reflector antenna.

6.4 Step 4 – Define Peak Stress Response

Table 6-3 provides a summary of the structure-specific input parameters required to calculate the peak stress σ_L for sonic boom loading. The first two columns after the left-hand column of types of structures provides default values for the fundamental resonance frequency f_0 and the estimated value of σ_L for the log of resonance frequency for each type of built-up structure based primarily on data in Table 4-2. To estimate values for f_0 for other cases, refer to Eq. (4-10) in Section 4.3.1.2. The last category of miscellaneous metal structures, the values selected for f_0 and σ_L are simply estimates within a range of possible values (see Section 4.3.1.2).

The next two columns define the estimated surface weights w and corresponding values for σ_L based on the data in Table 4-2. For specific estimates of surface weight not covered by these default values, surface weight w can be computed by the product of weight density ρ_w and thickness t . Data on weight density covering a very large range of building materials is provided in Appendix B.

The next three columns define the default values of K_s (one of the velocity to stress constants used in Eq.4-7) and the default values for the other velocity to stress constant (i.e., E/C_L) used in this equation. Note that K_s and E/C_L were usually assumed to be deterministic variables with no statistical variation (i.e., $\sigma_L = 0$) since they depend on (1) material properties whose statistical variation is already accounted for in w and f_0 , and on (2) geometric shape and size parameters assumed to have exact (default) values which have no statistical variation by themselves since, here again, the defined statistical variations in surface weight w and resonance frequency f will account for any actual variation in shape and size parameters. One exception to this is that finite values of σ_L for E/C_L are applicable to seismic response areas since resonance frequencies and surface weights are not applicable in this case.

The next two columns define the predicted value of the ratio of peak stress σ_{pk} (signified in the table by S_{pk}) to effective peak pressure P_e and the associated estimate for the standard deviation of the log of this quantity. Since it is assumed or known that the parameters which define this transfer function have a log normal distribution, the value of σ_L is equal to the square root of the sum of the squares of σ_L for each component of the transfer function. For built-up structure, according to Eq. (4-7), this ratio σ_{pk}/P_e is given by:

$$\sigma_{pk}/P_e = K_s (E/C_L) (V_{pk}/P_e) \quad (6-3)$$

Table 6-3

Summary of Structural Response Prediction Model Parameters

----- STRUCTURAL PARAMETERS -----												
No.	TYPE OF STRUCTURE	Reson. Freq.		Surface Wt.		Velocity/Press.		Stress/Velocity Constants			Stress/Press.	
		fo		w		V(fo)/Pe		Ks	E/Cl		Spk/Pe	
		Mean Hz	20-SD* dB	Mean psi	20-SD dB	Mean in/s/psi	20-SD dB	Mean -	Mean psi/in/s	20-SD dB	Mean psi/psi	20-SD dB
----- HISTORIC BUILDINGS -----												
0	WINDOWS, TYPE B, 2-10 ft ²	46	2.76	0.016	0.91	334	5.40	1.39	50	0.00	23,200	6.13
1	MASONRY-STONE	25	2.34	0.760	2.10	13	3.00	1.34	48	0.00	832	4.35
2	BRICK	12	3.30	0.460	1.85	45	3.00	1.34	17	0.00	1,100	4.33
3	ADOBE WALLS	15	1.36	1.100	1.78	15	3.00	1.34	2.0	0.00	40	3.74
4	WOOD-FRAME, PLASTER	16	2.22	0.068	0.91	226	3.00	1.13	18	0.00	4,590	3.34
5	WOOD-FRAME, WOOD WALLS	15	2.50	0.042	0.91	390	4.50	1.13	8.2	0.00	3,610	5.23
6	WOOD-FRAME, OPEN (BRIDGE)	10	2.50	0.069	0.91	356	4.50	1.13	8.2	0.00	3,300	5.23
----- PRE-HISTORIC STRUCTURES -----												
7A	MASONRY/STONE-ROOF OK	5.1	3.78	0.73	4.53	56	3.00	1.34	48	0.00	3,630	6.52
7B	MASONRY/STONE-NO ROOF	5.1	3.78	0.73	4.53	56	3.00	1.34	48	0.00	3,630	6.52
8A	ADOBE - ROOF OK	11	3.78	1.20	1.78	19	3.00	1.34	2.0	0.00	50	5.14
8B	ADOBE - NO ROOF	7.3	3.78	1.20	1.78	28	3.00	1.34	2.0	0.00	75	5.14
----- SEISMICALLY-SENSITIVE AREAS -----												
9	WATER WELLS/TANKS	25	6.00	0.0380	0.91	259	4.50	1.46	100	0.00	37,300	7.56
10	EARLY AM. PETROG./CAVES	NA	Following values to			0.79	4.72	1	48	5.50	38	9.03
11	LOOSE SNOW AVALANCHE	NA	right are ratios of			1.72	3.20	1	0.36	3.00	0.62	4.39
12	SLAB AVALANCHE	NA	Peak Velocity to			1.72	3.20	1	0.36	3.00	0.62	4.39
13	LANDSLIDE AREAS	NA	Pressure, (in/s)/psi			1.90	4.72	1	1.2	2.40	2.3	5.30
----- MISC. UTIL./METAL STRUCTS -----												
14	UTILITY BLDGS-CONCRETE BLCK	25	2.34	0.260	2.50	38	3.00	1.34	13	0.00	659	4.55
15	UTILITY BLDGS-WOOD FRAME	15	2.50	0.042	0.91	390	4.50	1.19	8.2	0.00	3,310	5.23
16	UTILITY BLDGS-METAL FRAME	14	1.39	0.019	3.10	324	4.50	0.89	150	0.00	123,300	5.78
17	RADIO TELESCOPES	25	1.39	0.069	3.10	142	4.50	0.89	150	0.00	19,320	5.78

* 20-SD denotes 20 times
the Standard Deviation
of the Log of the Variable.

and the envelope for V_{pk}/P_e including the factor of 2 correction for multimodal response (see Section 4) is given by

$$V_{pk}/P_e = \begin{cases} \frac{2\pi}{3} (gf_0 T^2/w), & f_0 < \sqrt{3} / \pi T, \text{ (in/sec) / psf} \\ 2g/(\pi f_0 w), & f_0 \geq \sqrt{3} / \pi T, \text{ (in/sec) / psf} \end{cases} \quad (6-4a)$$

(6-4b)

where

- $K_S, E/C_L$ = parameters defined in Section 4 (default values listed in Table 6-3)
- g = acceleration of gravity, 386 in/sec²
- f_0 = resonance frequency of the built-up structures, Hz
- T = duration of sonic boom, sec
- w = surface weight, psf.

(Note that a mixed system of units is employed to continue the practice of expressing velocity in units of inches/sec and sonic boom overpressure and surface weight in psf.)

It should be pointed out that Eq. (6-4a) is very seldom applied since, even for a low nominal sonic boom duration of about 0.075 sec, the frequency for which this low frequency envelope applies in such a case (7.4 Hz) falls below the fundamental resonance frequency, f_0 of nearly all of the structures considered in this study.

The peak stress σ_{pk} is then computed from P_e and the ratio σ_{pk}/P_e just defined. Also required is the value of σ_L for this peak stress which is the square root of the sum of the squares of the corresponding values of σ_L for each term in Eq.(6-3).

6.5 Step 5 – Computation of Probability of Damage for One Sonic Boom

Next, the material strength or damage threshold stress σ_s is required from the data in Section 4.4 along with the corresponding value of $20 \sigma_L$. Default values for σ_s and the associated σ_L that were developed in Section 4.4 are summarized in Table 6-4.

Thus, given the strength σ_s and imposed stress σ_{pk} , and their corresponding values of σ_L , the factor of safety $F_S = \sigma_s/\sigma_{pk}$ is computed along with its value of σ_L (F_S) = $\sqrt{\sigma_L(\sigma_s)^2 + \sigma_L(\sigma_{pk})^2}$, and the generalized normal distribution variable:

Summary of Damage Probability Estimate for Unconventional Structure Located at Center of SOA Ellipse

[illegible]

derived from data in Tables 4.1, 4.3, 4.4, and 4.6. Beam strength estimated as 1.5 times beam area for occupied buildings; beam strength estimated as 2.5 times beam area for unoccupied buildings.

1. Nathan Land, 1946.
2. Hervey and Higgins, 1946.
3. Smith, 1949.
4. Hervey and Hervey, 1944.
5. Adapted from Higgins, 1946.

the $\mathcal{N}(\mathbf{X})$ denotes the null space of the matrix \mathbf{X} .

$$Z = \log (F_S)/\sigma_L (F_S) \sqrt{2} \quad (6-5)$$

Then, using the theory and computational algorithms outlined in Section 2.2 for evaluating the integral of the normal distribution, the probability of damage (POD) is computed for each type of structure for the basic value of the nominal pressure P_0 corresponding to a specified position for the structure within an SOA.

6.6 Step 6 – Calculation of Weighted Probability of Damage According to Estimated Frequency of Booms

6.6.1 Weighted Probability of Damage for SOA Used for ACM Training

The net result of applying the preceding calculation process is shown in Table 6-4 for a typical SOA for a structure located at its center. The columns to the right of the list of structure types defines the intermediate values necessary to compute the values of POD and a weighted value POD_n as explained below for a structure at one position for one sonic boom. Also shown at the far right of the table are computed values for the peak displacement, velocity and acceleration response for the one condition evaluated in the table. Information on expected ambient vibration response levels of structure from other sources of dynamic excitation of buildings, such as human activity, nearby road or rail traffic or weather (Sutherland, 1989) would show that the latter, in some cases, exceed the dynamic response of structures to sonic boom.

Table 6-5 presents a summary of the probability of damage occurring for an unconventional structure located at four different "elliptical" radii from the center of the SOA ellipse. The distance corresponds to positions along the major axis of the ellipse relative to the center. The same probabilities would apply to distances along the minor axis if these were reduced by the ratio σ_x/σ_y (≈ 0.6) of the standard deviations for the X and Y axes of the SOA ellipse. The damage probabilities listed in Table 6-5 have now been weighted by the variation in expected numbers of booms per day as a function of position within the SOA ellipse defined in Section 3 by Eq. (3-2). Thus, the probability of damage values listed in Table 6-5 represent the weighted probability of damage on any typical day according to a given number N of sorties per month. That is, the probability of damage POD_n occurring on a given day and location X,Y in an SOA ellipse is given by

$$POD_n = POD \cdot n \quad (6-6)$$

Table 6-5

Probability of Damage Per Day for Unconventional Structures Located at
One of Four Different Elliptical Radii ($X=0$) Under an SOA Ellipse
With an Average of 500 ACM Sorties per Month

		PROBABILITY OF DAMAGE PER DAY FOR AVERAGE OF 500 ACM SORTIES PER MONTH			
No.	TYPE OF STRUCTURE	ELLIPTICAL RADIUS, [X = 0], mi.			
		0	20	40	60
=====		=====			
HISTORIC BUILDINGS					
0	WINDOWS, TYPE B, 2-10 ft ²	5.4E-03	3.0E-03	5.1E-04	2.4E-05
1	MASONRY-STONE	4.5E-05	2.3E-05	2.9E-06	3.4E-08
2	BRICK	4.0E-02	2.3E-02	4.0E-03	2.1E-04
3	ADOBE WALLS	9.2E-04	4.9E-04	7.0E-05	2.6E-06
4	WOOD-FRAME, PLASTER	1.6E-02	8.6E-03	1.5E-03	8.7E-05
5	WOOD-FRAME, WOOD WALLS	1.4E-03	7.4E-04	1.1E-04	4.6E-06
6	WOOD-FRAME, OPEN (BRIDGE)	1.1E-03	5.8E-04	8.7E-05	3.5E-06
-----		-----			
PRE-HISTORIC STRUCTURES					
7A	MASONRY/STONE-ROOF OK	2.0E-02	1.1E-02	1.9E-03	1.4E-04
7B	MASONRY/STONE-NO ROOF	1.4E-03	7.5E-04	1.2E-04	5.3E-06
8A	ADOBE - ROOF OK	8.5E-03	5.8E-03	1.0E-03	5.0E-05
8B	ADOBE - NO ROOF	1.2E-03	6.4E-04	9.7E-05	4.0E-06
-----		-----			
SEISMICLY-SENSITIVE AREAS					
9	WATER WELLS/TANKS	2.1E-04	1.1E-04	1.7E-05	6.5E-07
10	EARLY AM. PETROG./CAVES	1.6E-03	8.9E-04	1.5E-04	7.3E-06
11	LOOSE SNOW AVALANCHE	8.4E-02	4.9E-02	9.7E-03	5.8E-04
12	SLAB AVALANCHE	3.1E-03	1.7E-03	2.8E-04	1.3E-05
13	LANDSLIDE AREAS	2.1E-06	1.0E-06	1.2E-07	2.9E-09
-----		-----			
MISC. UTIL./METAL STRCT'RS					
14	UTILITY BLDGS-CONCRETE BLCK	7.7E-05	3.9E-05	5.1E-06	1.6E-07
15	UTILITY BLDGS-WOOD FRAME	1.6E-03	8.5E-04	1.3E-04	5.4E-06
16	UTILITY BLDGS-METAL FRAME	3.6E-04	1.9E-04	2.6E-05	9.4E-07
17	RADIO TELESCOPES	3.4E-07	1.6E-07	1.8E-08	4.0E-10

where $POD =$ the probability of damage for one boom

and $n = \begin{cases} \text{the estimated number of booms per day at the specified location of} \\ \text{the structure} \\ 0.0012N \exp \left[-\frac{1}{2} \left(\frac{X}{\sigma'_x} \right)^2 + \left(\frac{Y}{\sigma'_y} \right)^2 \right] \end{cases} \quad (6-7)$

$N =$ Number of ACM sorties per month into SOA

$X, Y =$ Position coordinates of the structure in the SOA ellipse

$\sigma'_x, \sigma'_y =$ 13 and 21.4 miles respectively (based on the WSMR tests, Plotkin, et al., 1984, as outlined in Section 3.1.1).

The same information shown in Table 6-5 for structures located at the center of the SOA ellipses is also shown in Figure 6-1 in graphical form. The code numbers across the bottom of this chart correspond to the structure code numbers used in Table 6-1, 6-3 and 6-4. The estimated probability of damage at this "worst case" position in an SOA used for ACM training varies widely and it is helpful to list, as follows, the structure types in Figure 6-1 in descending order of the probability of damage events in any average day at the center of an SOA ellipse.

Code No.	Type of Structure	$POD_n @ X, Y = 0$	Range of POD_n
11	Loose Snow Avalanche	8.4×10^{-2}	1 - 10%*
2	Brick	4.0×10^{-2}	
7A	Masonry/Stone - Roof OK	2.0×10^{-2}	
4	Wood Frame, Plaster	1.6×10^{-2}	
8A	Adobe - Roof OK	8.5×10^{-3}	0.1-1%
0	Windows, Type B, 2-10 ft ²	5.4×10^{-3}	
12	Slab Avalanche	3.1×10^{-3}	
10	Early American Petroglyphs/Caves	1.6×10^{-3}	
15	Utility Buildings - Wood Frame	1.6×10^{-3}	
7B	Masonry/Stone - No Roof	1.4×10^{-3}	
5	Wood Frame, Wood Walls	1.4×10^{-3}	
8B	Adobe No Roof	1.2×10^{-3}	
6	Wood Frame, Open (Bridge)	1.1×10^{-3}	0.01 - 0.1%
3	Adobe Walls	9.2×10^{-4}	
16	Utility Buildings - Metal Frame	3.6×10^{-4}	
9	Water Wells/Tanks	2.1×10^{-4}	0.001 - 0.01%
14	Utility Buildings - Concrete Block	7.7×10^{-5}	
1	Masonry - Stone	4.5×10^{-5}	00001 - 0.0001
13	Landslide Areas	2.1×10^{-6}	
17	Radio Telescopes	3.4×10^{-7}	<.0001%

* This indicates that there is a 1 to 10% chance of a damage event occurring in any one given day for these structures.

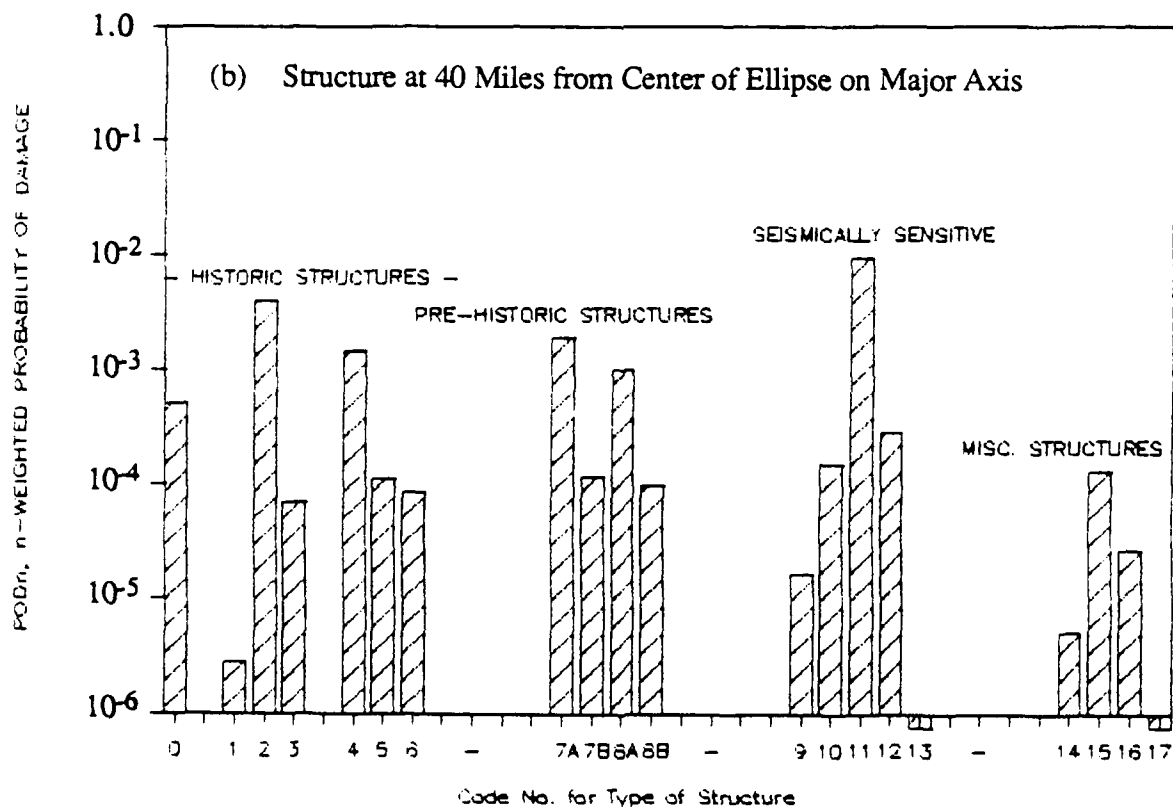
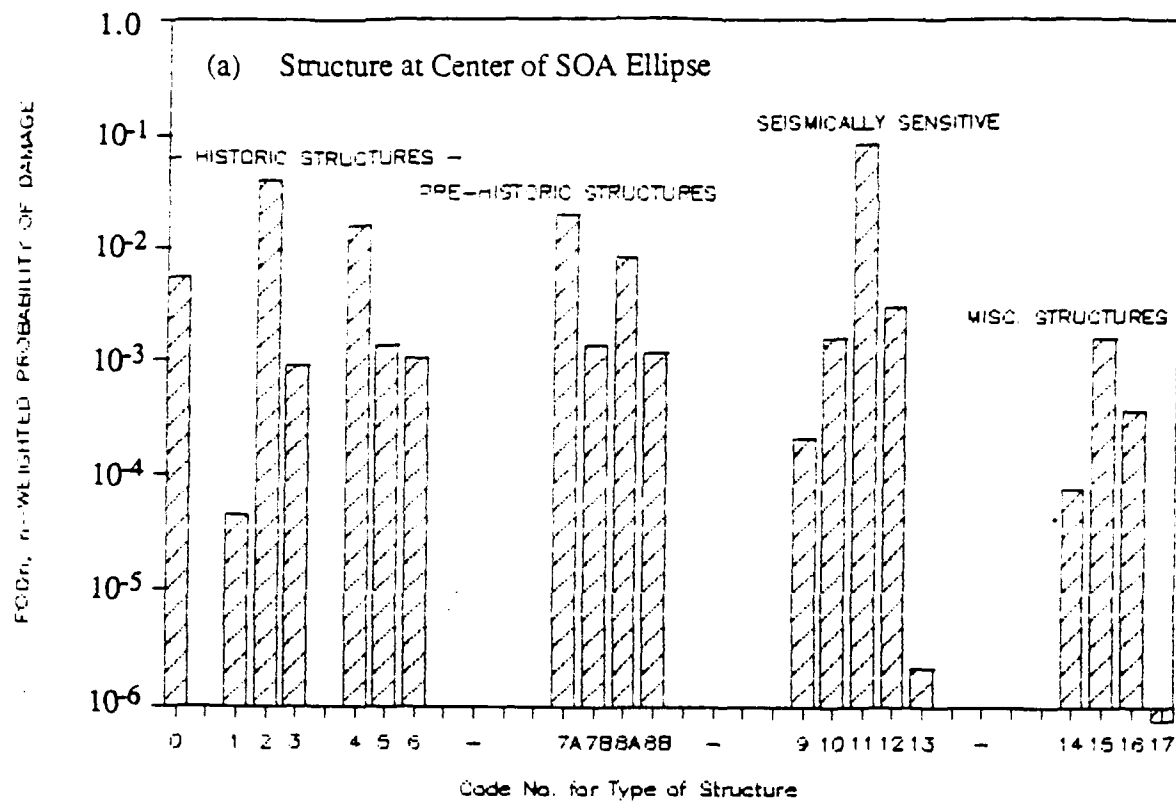


Figure 6-1. Graphic Summary of Predicted Probability of Damage Events Per Day for Unconventional Structures Located at the Center and 40 Miles (on Major Axis of Ellipse) from Center of an SOA with an Average of 500 ACM Sorties Per Month.

This listing has been broken down into ranges of probabilities differing by a factor of 10. The result indicates the most sensitive types of unconventional structures relative to potential sonic boom damage in an SOA area. It is not surprising to find a loose snow avalanche at the top of the list. However, recall from the discussion in Section 4.4.6 that:

- (1) such "avalanches" are not usually dangerous to people or structures, and
- (2) the probability of triggering such a moderate event is highly dependent on the simultaneous occurrence of the sonic boom with weather conditions for which such phenomena are most likely to occur.

Perhaps more surprising is the estimated high damage potential for brick (historical) buildings (code no. 2) and prehistoric masonry/stone structures with an intact roof (code no. 7A). However, it may be recalled from Section 4.4.2.2 that for historic brick structures, it was assumed that old, low strength mortar was involved and that for strength of prehistoric masonry or stone buildings, a conservative estimate was made for the damage threshold stress. The relatively high values for the estimated probability of damage to some unconventional structures located under ACM training areas are due, in part, to the larger variance in the sonic boom environments for such areas and the lower mean values and higher variance of the damage threshold stress for the more sensitive unconventional structures.

6.6.2 Sensitivity Analysis

To provide some indication of the sensitivity of these results to variations in the various parameters, a limited error analysis was made by examining changes in POD_n for three separate types of changes in the damage prediction model parameters.

- (1) Decrease the predicted stress response by 50% (this corresponded to a 6 dB decrease in 20 log of the peak stress and is equivalent to increasing the factor of safety by 2).
- (2) Increase the standard deviation σ_L in the log of the peak stress response by 0.15 (equivalent to a 3 dB increase in $20 \cdot \sigma_L$)
- (3) A similar increase in σ_L for the damage threshold stress

The effect of these different changes is summarized in Table 6-6 for all of the four elliptical radii positions in an SOA ellipse used for Table 6-5. For example, for brick historic buildings and radio telescopes located at the center of the ellipse ($X, Y = 0$), the values of POD_n change as follows:

<u>Change Condition</u>	<u>POD_n Brick Building</u>	<u>POD_n Radio Telescope</u>
Baseline – no change	4×10^{-2}	3.4×10^{-7}
Decrease σ_{pk} by 50%	9×10^{-3}	1.4×10^{-8}
Increase $20 \sigma_L$ of $\log \sigma_{pk}$ by 3 dB	7.4×10^{-2}	4.8×10^{-5}
Increase $20 \sigma_L$ of $\log \sigma_s$ by 3 dB	6.2×10^{-2}	4.8×10^{-5}

Thus, sensitivity of the damage estimate to changes in model parameters is low (changes are of the order of 2 to 4 times) for structures with high baseline values of POD_n and very high (changes of 1 to 2 orders of magnitude) for structures with low baseline values of POD_n .

6.6.3 Damage Estimates for Other Types of Supersonic Activity

Table 6-7 summarizes estimate of damage probabilities for the other types of supersonic activity identified earlier. These estimates cover overpressures ranging from 1 to 128 psf for structures located directly under the flight track (where the statistical variation in free field pressures is lowest) and from 1 to 8 psf for locations near lateral cut-off where statistical variation in free field pressures are highest.

As the overpressures increase, the probability of damage increases rapidly, eventually reaching a value greater than 1 according to the model. In other words, the model predicts 100% probability of damage for most unconventional structures when the peak overpressure reaches 128 psf – a very realistic overpressure for very low altitude supersonic flights.

It is important to recognize that the damage predictions in Table 6-7 are predicted probabilities per sonic boom. In the absence of any standard data on frequency of air traffic in supersonic corridors, it is not feasible, at this point, to define a value of POD_n for the probability of a damage event per day for such supersonic activity. It can be assumed, in this case, that every supersonic corridor flight will generate a sonic boom providing the flight conditions exceed the sonic boom speed and altitude threshold discussed in Section 3.1.

Table 6-6

(b) Decreasing Predicted Stress Response by 50%, (c) Increasing $20\sigma_L$ for Stress Response by 3 dB, or (d) Increasing $20\sigma_L$ for Damage Stress Threshold by 3 dB

(a) Accuracy Evaluation Factors		(b) Accuracy Evaluation Factors				(c) Accuracy Evaluation Factors				(d) Accuracy Evaluation Factors							
Change in 20 Lg(Sph) = 0.0 dB		Change in 20 Lg(Sph) = -6.0 dB				Change in 20 Lg(Sph) = 0.0 dB				Change in 20 Lg(Sph) = 0.0 dB							
Change in 20 SD of Lg(Sph) = 0.0 dB		Change in 20 SD of Lg(Sph) = 0.0 dB				Change in 20 SD of Lg(Sph) = 3.0 dB				Change in 20 SD of Lg(Sph) = 0.0 dB							
Change in 20 SD of Lg(Sa) = 0.0 dB		Change in 20 SD of Lg(Sa) = 0.0 dB				Change in 20 SD of Lg(Sa) = 0.0 dB				Change in 20 SD of Lg(Sa) = 3.0 dB							
± Equiv to ± Change in Sph		± Equiv to ± Change in Sph				± Equiv to ± Change in Sph				± Equiv to ± Change in Sph							
PROBABILITY OF DAMAGE PER DAY FOR AVERAGE OF 500 ACN SORTIES PER MONTH		PROBABILITY OF DAMAGE PER DAY FOR AVERAGE OF 500 ACN SORTIES PER MONTH				PROBABILITY OF DAMAGE PER DAY FOR AVERAGE OF 500 ACN SORTIES PER MONTH				PROBABILITY OF DAMAGE PER DAY FOR AVERAGE OF 500 ACN SORTIES PER MONTH							
ELLIPTICAL RADII, m		ELLIPTICAL RADII, m				ELLIPTICAL RADII, m				ELLIPTICAL RADII, m							
0	20	40	60	0	20	40	60	0	20	40	60	0	20	40	60		
HISTORIC BUILDINGS																	
0	WINDOWS, TYPE B, 2 1/2 (1)	5.4E-03	3.0E-03	5.1E-04	2.4E-05	1.0E-03	5.5E-04	0.4E-05	3.5E-06	1.6E-02	0.0E-03	1.7E-03	1.4E-04	0.4E-03	5.5E-03	1.2E-03	7.2E-05
1	MASONRY STONE	4.5E-05	2.3E-05	2.0E-05	0.4E-06	3.1E-06	1.5E-06	1.7E-07	4.2E-09	0.4E-04	5.2E-04	0.7E-05	4.3E-06	3.5E-04	1.0E-04	2.9E-05	1.2E-06
2	BRICK	0.0E-02	2.3E-02	4.0E-03	2.1E-04	9.0E-03	6.2E-03	1.1E-03	5.4E-05	7.4E-02	4.0E-02	9.2E-03	6.2E-04	6.2E-02	3.6E-02	7.3E-03	4.5E-04
3	DOOR WALLS	9.2E-04	4.9E-04	7.4E-05	2.6E-06	1.0E-04	5.3E-05	6.9E-06	2.1E-03	6.1E-03	5.5E-03	6.3E-04	3.5E-05	3.7E-03	2.1E-03	3.5E-04	1.0E-05
4	WOOD FRAME, PLASTER	1.6E-02	0.6E-03	1.5E-03	0.7E-05	3.6E-03	1.9E-03	3.0E-04	1.2E-05	4.6E-02	2.7E-02	5.2E-03	3.0E-04	3.2E-02	1.6E-02	3.2E-03	1.7E-04
5	WOOD FRAME, WOOD WALLS	1.4E-03	7.4E-04	1.1E-04	4.6E-06	1.9E-04	9.6E-05	1.3E-05	6.6E-07	9.9E-03	4.5E-03	0.4E-04	4.0E-05	4.3E-03	2.4E-03	4.2E-04	2.3E-05
6	WOOD FRAME, OPEN (BRIDGE)	1.1E-03	5.8E-04	0.7E-05	3.5E-06	1.4E-04	7.2E-05	9.0E-06	3.3E-07	6.7E-03	3.0E-03	7.1E-04	4.1E-05	3.5E-03	2.0E-03	3.4E-04	1.7E-05
PRE HISTORIC STRUCTURES																	
7A	MASONRY/STONE ROOF OR	2.9E-02	1.1E-02	1.9E-03	1.4E-04	5.9E-03	3.3E-03	5.7E-04	2.0E-05	4.7E-02	2.0E-02	5.0E-03	3.0E-04	3.4E-02	2.0E-02	3.7E-03	2.2E-04
7B	MASONRY/STONE NO ROOF	1.4E-03	7.5E-04	1.2E-04	5.9E-06	2.2E-04	1.1E-04	1.1E-05	6.4E-07	7.2E-03	4.2E-03	0.0E-04	4.0E-05	3.0E-03	2.1E-03	3.0E-04	2.0E-05
8A	DOOR	0.5E-03	5.8E-03	1.0E-03	5.0E-05	2.1E-03	1.2E-03	1.0E-04	7.0E-06	2.0E-02	1.5E-02	2.0E-03	1.0E-04	1.0E-02	1.0E-02	1.0E-03	1.0E-04
8B	DOOR NO ROOF	1.2E-03	6.4E-04	9.7E-05	4.0E-06	1.6E-04	0.4E-05	1.2E-05	4.1E-07	6.0E-03	3.0E-03	7.2E-04	4.2E-05	4.0E-03	2.2E-03	3.0E-04	2.1E-05
SEISMIC LT SENSITIVE AREAS																	
9	WATER WELLS/TANKS	2.1E-04	1.1E-04	1.2E-05	6.5E-07	2.6E-05	1.3E-05	1.0E-06	6.2E-09	2.2E-03	1.3E-03	2.3E-04	1.3E-05	6.0E-04	3.0E-04	5.0E-05	2.7E-06
10	EARLY AD PTDG / CAVES	1.6E-03	0.9E-04	1.5E-04	3.0E-06	3.1E-04	1.7E-04	2.0E-05	1.1E-06	7.1E-03	3.2E-03	0.1E-04	5.2E-05	3.0E-03	2.2E-03	4.1E-04	2.4E-05
11	LOOSE SOIL AVALANCHE	0.4E-02	4.9E-02	9.7E-03	5.0E-04	2.5E-02	1.4E-02	2.3E-03	1.6E-04	1.2E-01	7.1E-02	1.6E-02	1.2E-03	1.1E-01	6.4E-02	1.4E-02	9.0E-04
12	SLAB AVALANCHE	3.1E-03	1.7E-03	2.0E-04	1.3E-05	5.6E-04	3.0E-04	4.6E-05	1.0E-06	0.0E-03	6.3E-03	1.2E-03	7.6E-05	0.0E-03	5.2E-03	9.9E-04	5.0E-05
13	LANDSLIDE AREAS	2.1E-06	1.0E-06	1.2E-07	2.9E-09	1.1E-07	5.0E-08	5.1E-09	1.1E-10	1.4E-04	7.9E-05	1.2E-05	5.5E-07	2.6E-05	1.4E-05	1.0E-06	6.0E-06
MISC UTIL /METAL STRUCT BS																	
14	UTILITY BLDGS CONCRETE BLOCK	7.7E-05	3.9E-05	5.1E-06	1.6E-07	6.0E-06	3.0E-06	3.5E-07	9.0E-09	1.3E-03	7.3E-04	1.2E-04	0.7E-06	5.2E-04	2.0E-04	4.4E-05	1.0E-06
15	UTILITY BLDGS WOOD FRAME	1.6E-03	0.5E-04	1.0E-04	5.4E-06	2.2E-04	1.1E-04	1.6E-05	5.5E-07	0.5E-03	4.9E-03	9.2E-04	5.0E-05	4.7E-03	2.7E-03	4.7E-04	2.4E-05
16	UTILITY BLDGS METAL FRAME	3.6E-04	1.9E-04	2.6E-05	9.4E-07	3.7E-05	1.9E-05	2.4E-06	7.2E-09	3.6E-03	2.0E-03	3.7E-04	2.0E-05	1.2E-03	6.6E-04	1.1E-04	4.0E-06
17	RADIO TELESCOPES	3.4E-07	1.6E-07	3.0E-08	4.0E-10	1.4E-06	6.4E-08	6.2E-10	1.2E-11	4.0E-05	2.6E-05	4.0E-06	1.7E-07	4.4E-06	2.4E-06	3.1E-07	9.0E-09

Table 6-7

Estimates of the Probability of Damage Per Boom for a Range of Sonic Boom Pressures
from Supersonic Corridor (Level) Flights

Nominal Free Field Pressure 20(SD Dev) of Log(P/P ₀)	PROBABILITY OF DAMAGE PER BOOM FOR LEVEL SUPERSONIC CORRIDOR FLIGHTS				PROBABILITY OF DAMAGE PER BOOM FOR LEVEL SUPERSONIC CORRIDOR FLIGHTS				PROBABILITY OF DAMAGE PER BOOM FOR LEVEL SUPERSONIC CORRIDOR FLIGHTS			
	FREE FIELD PRESSURE, psf				FREE FIELD PRESSURE, psf				FREE FIELD PRESSURE, psf			
TYPE OF STRUCTURE	1	2	4	8	16	32	64	128	1	2	4	8
	[STRUCTURE UNDER FLIGHT TRACK]				[STRUCTURE UNDER FLIGHT TRACK]				[STRUCTURE NEAR LATERAL CUTOFF]			
HISTORIC BUILDINGS												
0 WINDOWS, TYPE B, 2-10 ft	5.9E-03	3.5E-02	1.6E-01	4.0E-01	7.6E-01	>1	>1	>1	8.3E-03	4.4E-02	1.7E-01	4.1E-01
1 MASONRY-STONE	1.2E-06	6.4E-05	1.7E-03	1.6E-02	1.3E-01	3.9E-01	8.1E-01	>1	5.1E-06	1.7E-04	3.0E-03	2.3E-02
2 BRICK	8.6E-02	2.9E-01	6.2E-01	>1	>1	>1	>1	>1	9.9E-02	3.0E-01	6.1E-01	>1
3 ADOBE WALLS	2.1E-04	4.2E-03	3.7E-02	2.0E-01	5.2E-01	>1	>1	>1	4.9E-04	6.9E-03	4.9E-02	2.2E-01
4 WOOD FRAME, PLASTER	1.7E-02	1.6E-01	4.9E-01	>1	>1	>1	>1	>1	2.7E-02	1.8E-01	4.9E-01	9.6E-01
5 WOOD FRAME, WOOD WALLS	6.1E-04	7.9E-03	5.3E-02	2.2E-01	5.2E-01	9.5E-01	>1	>1	1.1E-03	1.1E-02	6.5E-02	2.3E-01
6 WOOD FRAME, OPEN (BRIDGES)	4.2E-04	5.9E-03	4.1E-02	1.9E-01	4.7E-01	8.9E-01	>1	>1	8.1E-04	8.7E-03	5.2E-02	2.1E-01
PRE-HISTORIC STRUCTURES												
7A MASONRY/STONE-ROOF ON	3.9E-02	1.6E-01	3.8E-01	7.1E-01	>1	>1	>1	>1	4.7E-02	1.7E-01	3.9E-01	7.0E-01
7B MASONRY/STONE-NO ROOF	9.9E-04	8.7E-03	4.6E-02	1.9E-01	4.1E-01	7.4E-01	>1	>1	1.6E-03	1.2E-02	5.4E-02	1.9E-01
8A ADOBE-ROOF ON	1.3E-02	7.8E-02	2.7E-01	5.8E-01	>1	>1	>1	>1	1.5E-02	9.1E-02	2.8E-01	5.7E-01
8B ADOBE-NO ROOF	5.5E-04	6.8E-03	4.4E-02	1.9E-01	4.6E-01	8.6E-01	>1	>1	1.0E-03	9.7E-03	5.5E-02	2.1E-01
SEISMIC LY-SENSITIVE AREAS												
9 WATER WELLS/TANKS	7.7E-05	1.0E-03	8.6E-03	4.3E-02	1.7E-01	3.9E-01	7.1E-01	>1	1.4E-04	1.6E-03	1.1E-02	5.2E-02
10 EARLY AM.PETROG./CAVES	1.8E-03	1.1E-02	4.3E-02	1.5E-01	3.2E-01	5.8E-01	9.0E-01	>1	2.4E-03	1.3E-02	4.9E-02	1.6E-01
11 LOOSE SNOW-AVALANCHE	2.0E-01	5.0E-01	9.2E-01	>1	>1	>1	>1	>1	2.2E-01	5.0E-01	8.9E-01	>1
12 SLAB-AVALANCHE	3.1E-03	1.7E-02	9.6E-02	2.7E-01	5.5E-01	9.2E-01	>1	>1	4.4E-03	2.1E-02	1.1E-01	2.8E-01
13 LANDSLIDE AREAS	9.2E-09	9.2E-07	4.6E-05	1.1E-03	1.4E-02	9.1E-02	3.1E-01	6.8E-01	6.4E-08	3.8E-06	1.2E-04	2.1E-03
MISC. UTIL./METAL STRUCTS												
14 UTILITY BLDGS-CONCRETE BLOCK	3.7E-06	1.5E-04	3.1E-03	2.7E-02	1.7E-01	4.5E-01	8.9E-01	>1	1.3E-05	3.6E-04	5.2E-03	3.7E-02
15 UTILITY BLDGS-WOOD FRAME	7.6E-04	9.3E-03	6.1E-02	2.4E-01	5.5E-01	9.9E-01	>1	>1	1.4E-03	1.3E-02	7.4E-02	2.5E-01
16 UTILITY BLDGS-METAL FRAME	6.2E-05	1.4E-03	1.6E-02	9.8E-02	3.2E-01	6.0E-01	>1	>1	1.5E-04	2.4E-03	1.7E-02	1.1E-01
17 RADIO TELESCOPES	4.7E-10	6.7E-08	4.7E-06	1.7E-04	3.1E-03	2.4E-02	1.5E-01	4.2E-01	4.4E-09	3.5E-07	1.6E-05	3.7E-04

* 20 SD denotes 20 times the Standard Deviation
of the Low of the Variable.

6.7 Step 7 - Calculation of a Global Measure of Damage Potential

For a given study area, a global measure of the potential damage to any one type of unconventional structure can be computed by summing up the product of the probabilities of damage. P_n (weighted by the frequency of sonic booms) times the density of such structures over any given area to come up with a space average probability of damage. Such a process is discussed in more detail elsewhere for structural damage prediction under low altitude subsonic Military Training Routes (Sutherland, 1989). However, such a refinement may not be necessary in most cases since there will normally be a very limited number of unconventional structures of any one given type within any given sonic boom exposure area.

6.7 Summary

A step-by-step procedure has been defined along with the basic computational algorithms and supporting default structural response data for prediction of possible damage to unconventional structures from sonic booms. The procedure outlined lends itself to computer models, such as the USAF ASAN program, for a more detailed evaluation of damage potential for such structures than had been possible until now.

Further improvements in the prediction model are needed to refine and/or validate the many engineering estimates that had to be made concerning structural damage stress thresholds of many of the materials employed in unconventional structures. Fortunately, however, the damage prediction model is most accurate when the predicted damage probability is highest. Thus, while necessarily limited in accuracy, the methods presented in this report will provide a useful and rational basis for carrying out a preliminary analysis of potential damage to unconventional structures from sonic boom.

REFERENCES

- Abramowitz, M. and Stegun, I.A. (Eds.) (1972) Handbook of Mathematical Functions with Formulas, Graphs, and Mathematical Tables, National Bureau of Standards Applied Mathematics Series 55, December 1972.
- Albert, D.G. (1989) Personal Communication, U.S. Army Cold Regions Evaluation Laboratory, Hanover, N.H., August 30, 1989.
- Albert, D.G. and Orcutt, J.A. (1989) "Observations of Low-Frequency Acoustic-to-Seismic Coupling in the Summer and Winter," J. Acoust. Soc. Am. 86(1):352-359, 1989.
- Alter, D., et al. (1983) Pictorial Astronomy, Harper & Row, New York, 1983.
- Andrews Associates, Inc., et al. (1965) "Final Report, Structural Response to Sonic Booms," Prepared under Contract FA-64-AC-6-526 for the Federal Aviation Administration, February 1965.
- Andrews, D.K., et al. (1965) "Structural Response to Sonic Booms, Final Report, Vol. I and II," FAA Report SST-65-1, Andrews and Associates, Inc., and Hudgins, Thompson, Ball and Associates, Inc.
- Armstrong, R.L. and Ives, J.D. (1976) "Avalanche Release and Snow Characteristics, San Juan Mountains, Colorado," University of Colorado, Institute of Arctic and Alpine Research, Occasional Paper No. 19, May 1976.
- Bailey, W.H. and Kraska, I.R. (1970) "Penetrant Brightness Measurement Test," General American Transportation Corporation Technical Report AFML-TR-70-141, August 1970.
- Barkan, D.D. (1962) Dynamics of Bases and Foundations, translation from Russian, McGraw-Hill Book Co. Inc., New York, 1962.
- Bass, H.E. and Bolen, L.N. (1980) "Coupling of Airborne Sound Into the Earth: Frequency Dependence," J. Acoust. Soc. Am. 67(5):1502-1506, May 1980.
- Battis, J.C. (1983) "Seismo-Acoustic Effects of Sonic Booms on Archaeological Sites, Valentine Military Operations Area," Air Force Geophysical Laboratory, Report AFGL-TR-83-0304, November 1983.
- Battis, J.C. (1988) "The Effect of Low Flying Aircraft on Archaeological Sites, Kayenta, Arizona," Air Force Geophysical Laboratory Technical Memorandum No. 146, January 1988.
- Beason, W.L. and Morgan, J.R. (1984) "Glass Failure Prediction Model" J. Structural Engineering 110:197-212, February 1984.
- Bishop, D.E. (1988) "PCBOOM Computer Program for Sonic Boom Research: Technical Report Vol. 1," USAF HSD/YA-NSBIT Report No. HSD-TR-88-014 (Vol. I), October 1988.
- Blume, J.A and Associates (1965) "National Sonic Boom Study, Structural Reaction Program," FAA Report SST-65-15, Vol. 1 and 2, 1965.

- Brekke, B.N. (1959) "Wind Pressures in Various Areas of the United States," U.S. Dept. of Commerce Building Materials and Structures Report 152, April 1959.
- Brown, R, et al. (1985) "Sonic Boom Measurement Program – Reserve MOA," Wyle Laboratories Report WR 85-29, January 1986.
- Brumbaugh, D.S. (undated) "A Report on the Analysis of the Effect of Helicopter Vibrations on the Point Sublime Anasazi Site, Grand Canyon National Park," Northern Arizona University, Dept. of Geology, Contract Report for U.S. National Park Services, Division of Natural Resources.
- Carlson, H.W. (1964) "Correlation of Sonic Boom Theory with Wind Tunnel and Flight Measurements," NASA TR R-213, 1964.
- Carlson, H.W. (1978) "Simplified Sonic Boom Prediction," NASA Technical Paper 1122, 1978.
- Chan, G.C. (1966) "Fatigue of Reinforced Concrete Due to Sinusoidal and Random Loading" Wyle Laboratories Report WR 66-40, 1966.
- Clarkson, B.L. and Mayes, W.H. (1972) "Sonic-Boom Induced Building Structure Responses Including Damage," J. Acoust. Soc. Am. 51: 742-757.
- Cook, J.C., et al. (1972), "Seismic and Underwater Responses to Sonic Boom," J. Acoust. Soc. Am. 51: 729-741, 1972.
- Crandall, S.H and Kurzweil, L. (1968) "On the Rattling of Windows by Sonic Booms," J. Acoust. Soc. Am. 44: 464-472, 1968.
- Crocker, M.J. (1967) "Multimode Response of Panels to Normal and to Traveling Sonic Booms," J. Acoust. Soc. Am., 42(5):1070-1079, 1967.
- Eldred, K. McK. and Sutherland, L.C. (1965) "Estimating the Acoustic Loading on Building Structures Near Launch Sites," J. Acoust. Soc. Am. 37:1189 (A), 1965.
- Eshbach, O.W. (1952) Handbook of Engineering Fundamentals, John Wiley & Sons, New York, 1952.
- Forest Service (1968) Snow Avalanches – A Handbook of Forecasting and Control Measures, U.S. Department of Agriculture, Agriculture Handbook No. 194, October 1968.
- Galloway, W.J. (1980) "Development of C-Weighted Day-Night Average Sound Level Contours for F-15 Air Combat Maneuvering Areas," Bolt, Beranek and Newman Report 4430 August, 1980.
- Galloway, W.J. (1983) "Studies to Improve Environmental Assessments of Sonic Booms Produced During Air Combat Maneuvering," AFAMRL-TR- 83-078, October 1983.
- Gambill, J.B., et al., (1988) "Design and Evaluation of a Bracing System for McDonald's Ranch," U.S. Army Corps of Engineers, Construction Engineering Research Laboratory, Draft Technical Report, June 1988
- Goforth, T.T. and McDonald, J.A. (1968) "Seismic Effects of Sonic Booms," NASA CR-1137, September 1968.

- Gubler, H. (1977) "Artificial Release of Avalanches by Explosives," *Journal of Glaciology* 19(81):419-429, 1977.
- Haber, J. and Nakaki, D. (1989) "Sonic Boom Damage to Conventional Structures," BBN Laboratories Report No. 6829, NSBIT Task Order 0008(84), April 1989.
- Hall, S. (1990) Personal Communication, OL-AC HSD/YA-NSBIT, Wright-Patterson Air Force Base, Ohio, January 1990.
- Hershey, R.L. and Higgins, T.H. (1976) "Statistical Model of Sonic Boom Structural Damage," FAA-RD-76-87, July 1976.
- Hershey, R.L., et al. (1975) "Analysis of the Effect of Concorde Aircraft Noise on Historic Structures," FAA RD-75-118, July 1975.
- Hey, J.S. (1973) The Evolution of Radio Astronomy, Neal Watson Academic Publication, Inc., New York, 1973.
- Hilton, D., et al. (1964) "Sonic Boom Overpressures During FAA Community Response Studies Over a 6-Month Period in Oklahoma City Area," NASA TN D-2539, December 1964.
- Holbrook, J.R. (1980) "Historic and Current Disturbances to the Natural Resources of San Miguel Island," from Potential Effects of Space Shuttle Sonic Booms on the Biota and Geology of the California Channel Islands, J.R. Jehl and C.F. Cooper (Eds.), Center for Marine Studies, San Diego State University Technical Report 80-1, 1980.
- Hubbard, H.H., et al. (1986) "Sonic-Boom Research - Selected Bibliography with Annotation," NASA Technical Memorandum 87685, September 1986.
- Hunt, F.V. (1960) "Stress and Strain Limits on the Attainable Velocity in Mechanical Vibration," *J. Acoust. Soc. Am.* 32: 1123-1128, 1960.
- Johnson, J.B. (1982) "On the Application of Biot's Theory to Acoustic Wave Propagation in Snow," *U.S. Army Cold Regions Science and Technology* 6, 49-60, 1982.
- Kamm, H.W. and Kraska, I.R. (1971) "A Review of Nondestructive Methods for the Detection of Concealed Cracks," AFML-TR-71-120, July, 1971
- Kao, G. C. (1970) "An Experimental Study to Determine the Effects of Repetitive Sonic Booms on Glass Breakage," Wyle Laboratories Report for the Federal Aviation Authority FAA-NO-70-13, June 1970.
- King, K.W., et al. (1985) "Seismic and Vibration Hazard Investigations of Chaco National Historical Park," Open File Report 85-529, U.S. Dept. of the Interior, U.S. Geological Survey, 1985.
- King, K.W., et al. (1988) "Vibration Investigation of the Museum Building at White Sands National Monument, New Mexico," U.S. Department of the Interior Geological Survey, Open-File Report 88-554, 1988.
- King, K.W. and Algermissen, S.T. (1987) "A Vibration Study of the Archaeological Ruins, Hovenweep National Monument, Utah-Colorado," Dept. Of the Interior, U.S. Geological Survey Open File Report 87-181, June 1987.

Konon, W. and Schuring, J.R. (1985) "Vibration Criteria for Historic Buildings," *Journal of Construction Engineering and Management*, September 1985.

Kryter, K.D., et al. (1966) "Definition of the Effects of Booms from SST on Structures, People and Animals," SRI Report for National Sonic Boom Evaluation Office, June 1966.

Lekson, S.H. (1984) Great Pueblo Architecture of Chaco Canyon, New Mexico, University of New Mexico Press, Albuquerque, 1984.

Lilliard, D.C., et al. (1965) "Effect of Sonic Booms of Varying Overpressures on Snow Avalanches," FAA Report SST-65-9, 1965.

Maglieri, D., et al. (1966) "Ground Measurements of Shock-Wave Pressure for Fighter Airplanes Flying at Very Low Altitudes and Comments on Associated Response Phenomena," NASA TN D-2443, July 1966.

Maglieri, D., et al. (1967a) "Summary of Sonic Boom Signatures Resulting from Atmospheric Effects," Sonic Boom Experiments at Edwards Air Force Base, NSBEO-1-67, Annex C, Part 1, 1967.

Maglieri, D. (1967b) "Sonic Boom Flight Research - Some Effects of Airplane Operations and the Atmosphere on Sonic Boom Signatures," Sonic Boom Research, Seebass, A.R. (Ed.) NASA SP-147, 1967.

Maglieri, D., et al. (1969) "Variability in Sonic Boom Signatures Measured Along an 8000-ft Array," NASA TN D-5040, 1969.

Mayes, W.H. and Edge, P.M., Jr. (1964) "Effects of Sonic Boom and Other Shock Waves on Buildings," *Material Research and Standards*, 4:588-593, November 1964.

McClintock, F.A. and Argon, A. S. (1966), Chapter 15, "Brittle Fracture," Mechanical Behavior of Materials, Addison-Wesley Publishing Co. Inc., Massachusetts, 1966.

McMullan, Frank W. (1987), "McDonald Ranch Reaction to Misty Picture," Kaman Tempo, Albuquerque, NM., 1987

Merritt, J.L. and Newmark, N.M (1964) "Nuclear Geoplosics - Part V - Effects on Underground Structures," DASA Report 1285(V), May 1964.

Mickey, W.V. and Shugart, T.R. (1964) "Seismic Disturbances Generated by the Titan III 624A Solid Motor Sled Test," U.S. Dept. Of Commerce, Coast and Geodetic Survey, October 1964.

Mickey, W.V., et al. (1962) "Ground Motions Induced by Saturn SA-1 Launch at Cape Canaveral, Florida," U.S. Dept. Of Commerce, Coast and Geodetic Survey, June, 1962.

Morris, P.M. (1948) Vibration and Sound, McGraw-Hill Book Co. Inc., New York 1948.

Niedzwiecki, A. (1978) "On the Loudness of Sonic Booms and Other Impulsive Sounds," University of Toronto, Institute for Aerospace Studies, UTLAS RN-236, 1978.

Nixon, C.W., et al. (1968) "Sonic Booms Resulting from Extremely Low-Altitude Supersonic Flight - Measurements and Observations on Houses, Livestock and People," AMRL-TR-68-52, October 1968.

Perla, R.I. (1980) "Avalanche Release, Motion, and Impact," Chapter 7 of Dynamics of Ice and Snow Masses, S.C. Coldeck, (Ed.) Academic Press, Inc., New York, 1980.

Perroud, P. and LeComte, C. (1987) "Operation 'Bang Avalanches,' The Sonic Boom Effect on Avalanches, Avalanche Formation, Movement and Effects," Proceedings of the DAVOS Symposium, September 1986, IAHS Publication No. 162, pp. 215-222, 1987.

Plotkin, K.J. (1984) "Sonic Boom Focus Conditions Due to Tactical Air Operations," Wyle Laboratories Report WR 84-8, February 1984.

Plotkin, K.J. (1985a) "Focus Boom Footprints for Various Air Force Supersonic Operations," Wyle Laboratories Report WR 85-22, 1985

Plotkin, K.J. (1985b) "Sonic Boom Prediction Model for Supersonic Corridors," Wyle Laboratories Report WR 85-25, 1985.

Plotkin, K.J. (1989a) "Review of Sonic Boom Theory," AIAA Paper 89-1105, AIAA 12th Aeroacoustics Conference, April 1989.

Plotkin, K.J. (1989b) "Sonic Boom from Low Altitude Supersonic Flights" Wyle Laboratories TN 89-9, June 1989.

Plotkin, K.J., et al. (1989) "Measurement of Sonic Booms Due to ACM Training at White Sands Missile Range," Wyle Laboratories Report WR 89-18, September 1989.

Power, F.K. (1964) "Sonic Boom Effects on Light Aircraft, Helicopters, and Light Ground Structures," FAA paper before Am. Soc. Testing Materials, Chicago, June 1964.

Rathe, E.J. (1986) Personal Communication to H.E. von Gierke, U.S. Air Force, Wright-Patterson Air Force Base, 18 March, 1986.

Roark, R. J. (1965) Formulas for Stress and Strain, McGraw-Hill Book Co., New York, 1965.

Runyan, L.J. and Kane, E.J. (1970) "Sonic Boom Literature Survey, Vol 1, Summary of State of the Art, Vol 2, Capsule Summaries," FAA-RD-73-129, I and II, September 1973.

Sabatier, J.M., et al. (1986) "Acoustically Induced Seismic Waves," J. Acoust. Soc. Am. 80: 646-649, 1986.

Sabatier, J.M. (1988) Personal Communication, University of Mississippi Department of Physics, 1988.

Saurenman, H.J., et al. (1982) "Handbook of Urban Rail Noise and Vibration Control," DOT Report No. DOT-TSC-UMTA-81-72, Wilson, Ihrig & Associates, Oakland California, 1982.

Schroeer, et al. (1971) "Research on Exploratory Development of Nondestructive Methods for Crack Detection," AFML-TR-67- 167, Part IV, February 1971.

Seaman, L. (1967) "Response of Windows to Sonic Booms," Stanford Research Institute Interim Technical Report 7, SRI Project ETU-5297, June 1967.

Selner, R.H. and Tracy, N.A. (1972) "Summary of Nondestructive Testing Applications, Part I," AFML-TR-72-174, December 1972.

Siskind, D. E., et al. (1980a) "Structure Response and Damage Produced by Airblast from Surface Mining" U.S. Dept. of the Interior Bureau of Mines Report of Investigations RI-8485, 1980.

Siskind, D.E., et al. (1980b) "Structure Response and Damage Produced by Ground Vibration from Surface Mine Blasting," U.S. Dept. of the Interior Bureau of Mines Report of Investigations RI 8507, 1980.

Skempton, A. W. (1948) "The Rate of Softening of Stiff, Fissured Clay," Second Int'l Conference Soil Mech. Foundation Eng. Pr, Rotterdam, Volume II, p.50-53, 1948.

Smith, E.W. (1982) "Adobe Bricks in New Mexico," NM Bureau of Mines and Mineral Resources," 1982.

Smith, P.R. (1986) "Effects of 0.9 psi Overpressure on the McDonald Ranch House Walls," Letter Report Submitted to Kaman Tempo, Albuquerque, New Mexico, January 1986.

Stagg, M.S., et al. (1984), "Effects of Repeated Blasting on a Wood-Frame House," U.S. Department of the Interior, Bureau of Mines Report of Investigations RI-8896, 1984.

Sutherland, L.C. (1968a) (ed.) "Sonic and Vibration Environments for Ground Facilities - A Design Manual," Wyle Laboratories Report WR 68-2, 1968.

Sutherland, L.C. (1968b) "Forces Acting on Stationary and Moving Obstacles in Plane Wave Sound Fields," Wyle Laboratories Report WR 86-12, October 1968.

Sutherland, L.C. (1985) "Predicted Response of Sound Level Meters to Sonic Booms," Wyle Laboratories Report TN 85-5 for Systems Research Laboratories, April 1985.

Sutherland, L.C. (1989) "Assessment of Potential Structural Damage from Low Altitude Subsonic Aircraft," Wyle Laboratories Report WR 89-16 for Martin Marietta Energy Systems, Inc., October 1989.

Terzaghi, K. (1950) "Mechanism of Landslides," The Geological Society of America, Engineering Geology Volume, 83-123, November 1950.

Thoenen, J.R. and Windes, S.L. (1942) "Seismic Effects of Quarry Blasting," U.S. Bureau of Mines Bulletin 442, 1942.

Timoshenko S. and Woinowsky-Kreiger, S. (1959) Theory of Plates and Shells, 2nd Ed., McGraw-Hill Book Co. New York, 1959.

Trapp, W.J. and Forney, D.M. (1965), Acoustical Fatigue in Aerospace Structures, Syracuse University Press, 1965.

U.S. Air Force, Final Environmental Impact Statements for Valentine SOA, Gandy SOA, Nellis MOA, and Reserve SOA.

U.S. Navy (undated) "Final Comprehensive Environmental Impact Statement for the Proposed Supersonic Operating Area and Other Proposed Actions at Naval Air Station, Fallon Nevada."

White, J.E. (1965) Seismic Waves, McGraw-Hill Book Co., New York, 1965.

Whitman, R.V. and Clark, G.B. (1964) "Nuclear Geoplosics – Part II – Mechanical Properties of Earth Materials," DASA Report 1285(II), May 1964.

Wiggins, J.H., Jr. (1965) "The Effects of Sonic Boom on Structural Behavior – A Supplementary Analysis Report," John Blume and Associates, Final Report, Contract No. FA-SS-65-12, October 1965.

Wiggins, J.H., Jr. (1969) Effects of Sonic Boom, J.H. Wiggins Co., Palos Verdes Estates, California, 1969.

Wilhelmsen, A.M. and Larsson, B. (1973) "Sonic Boom and Structural Damage," D3: National Swedish Institute for Building Research, 1973.

Wilson, G.P. and Soroka, W.W. (1965) "Approximation to the Diffraction of Sound by a Circular Aperture in a Rigid Wall of Finite Thickness," J. Acoust. Soc. Am. 37(1):286-297, 1965.

Yokel, F.Y., et al. (1971) "Strength of Masonry Walls Under Compressive and Transverse Loads," National Bureau of Standards, COM-75-10286, March 1971.

Young, R.W. (1986) "Efficient Monitoring of Aircraft Noise Near a Military Operating Area," Paper before NATO Conference, Aircraft Noise in a Modern Society, Mittenwald, Germany, 1986.

APPENDIX A

Bibliography for Response of Unconventional Structures to Sonic Boom

Prepared by

J.J. Girard
Wyle Laboratories
128 Maryland St.
El Segundo, California

**WYLE RESEARCH
TECHNICAL NOTE
TN 89-3**

**BIBLIOGRAPHY
FOR RESPONSE OF
UNCONVENTIONAL STRUCTURES
TO SONIC BOOM**

Prepared for:
UNITED STATES AIR FORCE, HQ-ESC/RDCS
Tyndall AFB, Florida 32403

(Under Contract No. F08635-89-0044)

Prepared by:
J.J. Girard
L.C. Sutherland
WYLE RESEARCH
El Segundo, California 90245

(J/N 59585-01)

March 1989

INTRODUCTION

This bibliography has been assembled in response to item 4.1 of the contract statement of work. This literature is to aid in defining unconventional structures and their sensitivity, and response to sonic booms. Literature on objective analytical methods and means of non-destructive condition assessment has been included. To simplify utilization of this bibliography, the literature has been broken down into three broad categories: response, condition assessment, and damage.

The primary concern is response of unconventional structures to sonic boom. Literature reviews and papers on multiple or general topics have been grouped together under this heading. Several papers are also included on underwater and seismic response to sonic boom. Papers on the effect of sonic boom on structures have been placed into several sub-categories. The sub-categories include response of buildings, non-linear aspects, and response of specific structural elements such as windows, individual wall panels, or bearing members. Another sub-category concerns studies of the dynamics of liquid storage tanks.

Papers concerning other forms of acoustic excitation and response aspects have been included as well. For a broader understanding of response to transient sonic excitation, several papers on blast response have been listed. Papers regarding response of primitive structures, an important subject of this program, were concerned with a variety of excitation types. In order to group these together, a category was formed for aircraft and general noise excitation. Papers on the effect of structures on sonic boom signatures have been placed under the heading of Indirect Effects and may be of little concern to this study. The effect of ground motion on structures has also been placed under Indirect Effects, as a structure may be excited by a sonic boom through acoustic coupling to the ground. A category has also been included for response and damage prediction. This includes analytical and numerical codes for response prediction and statistical codes for damage probability.

The papers on condition assessment are grouped into two categories. Guidance on general assessment of aircraft noise effects may be found in the first list. The second is concerned with nondestructive evaluation. The techniques which were deemed most likely to be useful for unconventional structures are set

into sub-topics. These are photography, mechanical impedance, acoustic methods, and visual observation. These techniques may be helpful in documenting the damage an unconventional structure might sustain as a result of sonic boom exposure. This damage is likely to be slight for one given boom but may accumulate over time. For this reason accuracy in making an assessment of potential damage from a limited number of exposures to sonic boom is of prime importance.

Papers pertaining specifically to damage from sonic boom are listed together. Literature on sonic boom-induced avalanches and damage to structures and glass are set into subtopics. Papers on damage from blast and general noise are placed together. Analysis of damage claims from aircraft noise and environmental impact statements are included to aid in defining unconventional structures and their sensitivity.

The literature listed under the broad topics of response, condition assessment, and damage has been assembled and grouped for easy access. Under each subtopic, the literature is listed alphabetically by author.

TABLE OF CONTENTS

	<u>Page</u>
1.0 RESPONSE	A-6
1.1 Sonic Boom	A-6
1.1.1 Sonic Boom General Effects	A-6
1.1.2 Sonic Boom Response of Ground and Water	A-7
1.1.3 Structures	A-9
1.1.3.1 Sonic Boom Response of Buildings	A-9
1.1.3.2 Non-Linear Response to Sonic Boom	A-13
1.1.3.3 Sonic Boom Response of Structural Elements	A-13
1.1.3.4 Sonic Boom Response of Liquid Storage Tanks.	A-15
1.2 Blast	A-16
1.2.1 Blast Response of Ground	A-16
1.2.2 Blast Response of Structures	A-16
1.3 Aircraft and General Noise	A-17
1.3.1 Structural Response to Aircraft and General Noise	A-17
1.3.2 Response of Primitive Structures to Aircraft and General Noise.	A-18
1.4 Indirect Effects	A-19
1.4.1 Effect of Structures on Sonic Boom Signatures	A-19
1.4.2 Effect of Ground Motion on Structures	A-19
1.5 Modeling	A-19
1.5.1 Blast, Boom - Prediction, Simulation Codes for Response	A-19
2.0 CONDITION ASSESSMENT	A-20
2.1 Assessment of Aircraft Noise Effects	A-20
2.2 Methods Available	A-20
2.2.1 Photography	A-20
2.2.2 Mechanical Impedance.	A-20
2.2.3 Acoustic Methods	A-21
2.2.4 Visual Observation	A-21
2.2.5 Miscellaneous Methods of Condition Assessment.	A-21
2.2.6 Evaluation of Methods of Assessment	A-21
3.0 DAMAGE	A-22
3.1 Sonic Boom	A-22
3.1.1 Sonic Boom Damage to Structures.	A-22
3.1.2 Sonic Boom Damage to Glass	A-22
3.1.3 Sonic Boom and Avalanche	A-23
3.2 Blast and General Noise	A-23
3.2.1 Damage to Structures from Blast and General Noise	A-23
3.2.2 Avalanche from Blast and General Noise	A-24
3.3 Environmental Impact	A-24
3.3.1 Claims Analysis	A-25
3.3.2 Environmental Impact Analysis	A-25

1.0 RESPONSE

1.1 Sonic Boom

1.1.1 Sonic Boom General Effects

Boeing Co., "Sonic Boom - A Review of Current Knowledge and Developments," Boeing Company, Doc. D6A10598-1, 1967.

Cox, E. C., "Report on Physical Effects of the Sonic Boom," National Academy of Sciences, Washington, D.C., 1968.

Garwin, R.L., "Speculation on Long-Range Effects of Supersonic Flight", IBM Thomas J. Watson Research Center, 1978 (unpublished).

Gottlieb, J. J., "Sonic Boom Research at UTIAS," CASJ 20, pp. 199-222, 1974.

Hubbard, H. H., "Nature of the Sonic Boom Problem," J. Acous. Soc. Am. 39(5), pt.2, pp. S1-S9, 1966.

Hubbard, H. H., "Recent Results of Sonic Boom Research," presented at AFOSR-UTIAS Symposium on Aerodynamic Noise, Toronto Canada, May 20-21, 1968.

Hubbard, H. H., "Recent Results of Sonic Boom Research," NASA TM-X-61240, 1968.

Hubbard, H.H., et al., "A Selected Bibliography of Sonic Boom Research Documents with Annotation," NASA TM-87685, 1986.

Hubbard, H.H. and Mayes, W.H., "Sonic Boom Effects on People and Structures," NASA SP-147, pp. 65-76, 1967.

International Civil Aviation Organization, "Sonic Boom Panel Second Meeting, Montreal, 12-21 October 1970, Appendix A," Doc 8894, SBP/II, 1970.

Kryter, K. D., "Definition Study of the Effects of Booms from the SST on Structures, People, and Animals," Stanford Research Institute Report 1, SRI Project 5897, 1966.

Maglieri, D. J., et al., "Status of Knowledge of Sonic Booms," J. Noise Control Engineering 15(2), pp. 57-64, 1980.

National Research Council, "Report on Physical Effects of Sonic Boom," NRC Committee on SST-Sonic Boom, 1968.

National Research Council, "Report on Physical Effects of the Sonic Boom," National Academy of Sciences, February 1968.

Nixon, C.W., et al., "Sonic Booms Resulting from Extremely Low-Altitude Supersonic Flight: Measurements and Observations on Houses, Livestock and People," Aerospace Medical Research Laboratory, AMRL- TR-68-52, 1968.

Nowakiwsky, O.V., "Effects of Sonic Boom on Automobile Behavior," UTIAS TN-188, 1974.

Organisation for Economic Co-operation and Development, "Report on the Conference on Sonic Boom Research (Draft)," Committee for Research Co-operation, 1970.

Runyon, L.J. and Kane, E.J., "Sonic Boom Literature Review, Vol. I and II," FAA-RD-73-129, 1973.

Rylander, R. (Ed.), "Sonic Booms Exposure Effects: Report from a Workshop on Methods and Criteria," Stockholm, J. Sound Vib., Suppl. 20, pp. 477-544, 1972.

Shurcliff, W. A., SST and Sonic Boom Handbook, Ballantine Books, New York, 1970.

Slutsky, S., "Survey of Sonic Boom Phenomena for the Non-Specialist," FAA-RD-75-68, H. H. Aerospace Design Co., for U.S. Department of Transportation, 1975.

Sonic Boom Panel, "Report on the Sonic Boom Phenomenon, the Ranges of Sonic Boom Values Likely to be Produced by Planned SSTs, and the Effects of Sonic Booms on Humans, Property, Animals, and Terrain," Attachment A of ICAO Document 8894, SBP/II, Report of the Second Meeting of the Sonic Boom Panel, Montreal, October 1970.

Stanford Research Institute, "Sonic Boom Experiments at Edwards Air Force Base, Interim Report," National Sonic Boom Evaluation Office, NSBEO-1-67, 1967.

Teer, J. and Truett, J., "Studies of the Effects of Sonic Boom," Department of Transportation, Washington D.C, Report No. FAA-RD-148, 1973.

Wanner, J.C., "Certain Conclusions on the Supersonic Transport Aircraft Boom", NASA TT-F-17149, 1976.

Warren, C.H.E., "Noise From Aircraft at Supersonic Speeds", Nature 171, pp. 214-216, January 1953.

Warren, C. H., "Recent Sonic Bang Studies in the United Kingdom," J. Acous. Soc. Am. 51, pp. 783-789, 1972.

Wiggins, J. H., Effects of Sonic Boom, J. H. Wiggins Company, Palos Verdes Estates, California, 1969.

1.1.2 Sonic Boom Response of Ground and Water

Baron, M. L. et al., "An Investigation of Ground Shock Effects Due to Rayleigh Waves Generated by Sonic Boom," NASA CR-451, 1966.

- Bass, H. E., and Bolen, L. M., "Coupling of Airborne Sound Into the Earth," PARGLUM Report 84-01, University of Mississippi, 1984. See also: Bass, H. E., et al., "Coupling of Airborne Sound Into the Earth," J. Acoust. Soc. Am. 67, pp. 1502-1506, 1980.
- Blundell, C. R. K., "Response of Cliffs in Pembrokeshire to Concorde's Sonic Boom," Royal Aeronautical Establishment, England, 1971.
- Cook, J. C. and Goforth, T. T., "Ground Motion from Sonic Boom," J. Aircraft, 7(2), pp. 126-129, 1970.
- Cook, J. C. and Goforth, T., "Seismic Effect of Sonic Booms," NSBEO 1-67, 1967.
- Cook, R. K., "Penetration of a Sonic Boom Into Water," J. Acoust. Soc. Am. 47(2), pp. 1430-1436, 1970.
- Cooke, J. E., et al., "Seismic and Underwater Responses to Sonic Booms," J. Acoust. Soc. Am. 51, Part 3, pp. 729-741, 1972.
- Espinosa, A. F. and Mickey, W. V., "Observations of Coupled Seismic Waves from Sonic Booms, a Short Note," Acustica 20, pp. 88-91, 1968.
- Espinosa, A. F., et al., "Seismic Waves Generated by Sonic Booms: A Geo-acoustical Problem," J. Acoust. Soc. Am. 44, pp. 1074-1082, 1968.
- Frantti, G. E., "The Nature of High-Frequency Earth Noise Spectra," J. Geophysics, Vol. XXVII (4), pp. 547-562, 1963.
- Goforth, T. T. and McDonald, J. A. (1968), "Seismic Effects of Sonic Booms," NASA CR-1137, Teledyne Company.
- Goforth, T. T., and Rasmussen, R. K., "Study of the Characteristics of Seismic Signals Generated by Natural and Cultural Phenomena - Such as Earthquake, Sonic Booms, and Nuclear Explosions," NASA CR-132606, 1974.
- Grover, F. H., "Geophysical Effects of Concorde Sonic Boom," Royal Astronomical Society, Quarterly Journal 14, 1973.
- Henderson, H. R. and Huckel, V., "Sonic Boom Measurements Relating to Seismic Studies at the Payson, AZ and Vernal, UT Seismological Sites," NASA Langley Research Center, LWP No. 428, 1969.
- McDonald, J. A. and Goforth, T. T., "Seismic Effects of Sonic Booms: Empirical Results," J. Geophysical Res. 74(10), 1969.
- Oliver, J. and Isacks, B., "Seismic Waves Coupled to Sonic Booms," Lamont Geological Observatory no. 556, pp. 528-530, 1961.
- Schaffar, M., et al., "Effect of Sonic Boom on Avalanches," Institut Franco - Allemand de Recherches, St Louis, France, Report ISL-13/72, 1972.
- Urlick, R. J. and Tulko, T. J., "Sonic Booms in the Sea - A Recent Observation," J. Acous. Soc. Am. 52, Part 2, pp. 1566-1568.

Waters, J. F. and Glass, R. E., "Penetration of Sonic Boom Energy Into the Ocean: An Experimental Simulation," Hydrospace Research Corp. Report 288, 1970.

1.1.3 Structures

1.1.3.1 Sonic Boom Response of Buildings

Amrhein, J. E., et al., Masonry Design Manual, Masonry Industry Advancement Committee, 1979.

Andrews D. K., et al., "Structural Response to Sonic Booms Final Report," SST 65-1, Volumes 1 and 2, Andrews Associates, Inc. and Hudgins, Thompson, Ball and Associates, Inc, 1965.

Anonymous, "Sonic Boom is No Threat to Buildings," Engineering News Record, July 1964.

Arde Associates, "Response of Structures to Aircraft Generated Shock Waves," United States Air Force, WADC Technical Report 58-169, 1959.

Baker, A. C. et al., "Project Little Boom," U.S. Air Force, TAC TR-60-18, 1960.

Baker, A. C., et al., "System Operational Test and Evaluation," U.S. Air Force Report TAC-TR-60-18, 1960.

Benham, P. P. and Birks, A. N., "The Response to Concorde's Sonic Boom of Some Historic Buildings in Northern," J. Building Science 8, pp. 137-147.

Berman, A., "Determining Structural Parameters from Dynamic Testing," Shock and Vib. Digest 7(1), pp. 10-17.

Blume and Associates, "Report on the National Sonic Boom Study Structural Reaction Program," Blume and Associates Research Div., SST 65-15, v.1 and 2, 1965.

Blume, J. A. et al., "Effects of Sonic Boom on Structural Behavior - A Supplementary Analysis Report," National Sonic Boom Study Project SST 65-18, John A. Blume & Associates, 1965b.

Blume, J. A., et al., Response of Structures to Sonic Booms, John A. Blume and Associates, 1969.

Blume, J. A. et al., "Response of Structures to Sonic Booms Produced by XB-70, B-58 and F-104 Aircraft, Final Report," (based on Edwards AFB sonic boom experiments), John A. Blume & Associates, National Sonic Boom Evaluation Office, NSBEO-2-67, 1967.

Blume, J. A. et al., "Structural Reaction Program, National Sonic Boom Study Project," SST 65-15 Volumes I and II, John A. Blume & Associates, 1965.

Carden, H. D., et al., "Building Vibrations Due to Aircraft Noise and Sonic Boom Excitation," ASME 69-WA/GT-8, 1969.

Cawthorne, J. M., "Some Sonic Boom Induced Building Responses," J. Acoust. Soc. Am. 35(11), 1963.

Chaumette, A., "Effect of Sonic Booms on Buildings, Report of the Final Synthesis," Royal Aircraft Establishment Library Translation 1663, 1971.

Cook, R., "The Effects of Sonic Boom and Similar Impulsive Noise on Structures," National Bureau of Standards, 1971.

Crawford, R., "Cathedral Vibration and the Sonic Bang," Southampton University ISVR Consultation Report No. 1258 with Addendum, 1969.

Crocker, M. J. and Hudson, R. R., "Structural Response to Sonic Booms," J. Sound Vib. 9, 1969.

De Tricaud, P., "Effect of Sonic Boom on Structures, Third Report, Measurement of Eigenfrequencies of Building Structures Which are Sensitive to the 'Boom,'" NASA TT-F-14057, National Aeronautics and Space Administration Technical Translation, 1971.

De Tricaud, P., "Measurement of the Natural Frequencies of the Walls of Buildings Sensitive to Sonic Boom," Royal Aircraft Establishment Library Translation RAE-Lib-Trans-1589.

Ellis, P., "Effects of Traffic, Vibration on Historic Buildings," The Science of the Total Environment, pp. 37-45, 1987.

Federal Aviation Administration, "Sonic Boom Structural Response Test Program," White Sands Missile Range, New Mexico, FAA, SST 65-4, 1965.

Federal Aviation Administration, "Structural Response Test National Sonic Boom Study Program," FAA, IR-8242, 1964.

Findley, D. S., et al., "Vibration Responses of Test Structure No. 1 During the Edwards Air Force Base Phase of the National Sonic Boom Program," NASA TM-X- 72706, NASA Langley Research Center, 1975.

Findley, D. S., et al., "Vibration Responses of Test Structure No. 2 During the Edwards Air Force Base Phase of the National Sonic Boom Program," NASA TM-X- 72704, NASA Langley Research Center, 1975.

Guild, E., et al., "Sonic Booms Resulting from Extremely Low Altitude Supersonic Flight Measurements and Observations on Houses, Livestock, and People," AMRL-TR-68-52, 1968.

Hart, G. C. and Nelson, R. B. (Eds.), Dynamic Response of Structures, 1968.

Hershey, R. L., et al., "Analysis of the Effects of Concorde Aircraft Noise on Historic Structures," FAA, RD 75-118, 1975.

Higgins, T. H., "A Sonic Boom Index and Structural Reaction to Impulsive Noise," FAA.

Horner, D., "An Investigation into the Response of Building Elements to Simulated Sonic Booms," Institute of Sound and Vibration Research, 1971.

Konon, W. and Sehuring, J. R., "Vibration Criteria for Historic Buildings," J. Construction Engineering Management, pp. 208-215, September 1988.

Koopman, G. and Orris, R. M., "An Improved Method for Assigning a Dynamic Magnification Factor to N-Waves," J. Sound Vib. 19(3), pp. 373-377, 1971.

Lee, L. A., "Additional Sonic Boom Data Related to Tests Conducted at White Sands, New Mexico, and Edwards Air Force Base," FAA-RD-72-114, John A. Blume and Associates, 1972.

Lilley, G. M., "Report in Five Parts on the Sonic Boom. Part 3: Response of Structures to the Sonic Boom," University of Southampton, 1969.

Loftin, L. K., "Building Response to Noise and Sonic Booms," NASA Langley Research Center, LWP-255, 1972.

Lowery, R. L., "Critical Structural Response to the Sonic Boom," NASA CR-66750, 1968.

Lowery, R. L., "Experimental Aids for Predicting Structural Response to Sonic Booms," J. Acous. Soc. Am. 40, p. 1270.

Mayes, W.H. and Edge, P.M. Jr., "Effects of Sonic Boom and Other Shock Waves on Buildings," Materials Research & Standards 4, pp. 588-593, 1964.

Power, J. K., "Some Results of the Oklahoma City Sonic Boom Tests," Materials Research & Standards, 1964.

National Bureau of Standards, "The Effects of Sonic Boom and Similar Impulsive Noise on Structures," U.S. Environmental Protection Agency, NTID300.12, 1971.

National Sonic Boom Evaluation Office, "Sonic Boom Experiments at Edwards Air Force Base," Stanford Research Institute, NSBEO 1-67, 1967.

Newberry, C. W., "Measuring the Sonic Boom and Its Effect on Buildings," Materials Research & Standards 4, pp. 601-611, 1964.

Newberry, C. W., "The Response of Buildings to Sonic Boom," J. Sound Vib 6(3), pp. 406-418, 1967.

Office of Deputy Administer for SST Development, "Final Report, Structural Response to Sonic Booms," FAA, SST 65-1, vol. 1, AD-610822, 1965.

Popplewell, N., "Response of Box-Type Structures to Sonic Boom," Ph.D. Thesis, University of Southampton, Institute of Sound and Vibration Research, NASA CR-66887, 1969.

Rao, B. M., "Analysis of Sonic Boom Waves Incident on Structures," FAA, 1968.

Reddy, N. N., "Response Spectra of Coupled Acoustical Resonators to Transient Excitation," Ph.D. Thesis, Oklahoma State University, 1967.

Seshadri, T. V. and Lowery, R. L., "Low Frequency Damping Mechanisms in Mechano-Acoustical Networks," J. Sound Vib. 29(1), pp. 65-72, 1972.

Sharpe, R. L., "Structural Response to Sonic Booms," J. Structural Division, Proceedings of the ASCE 97 (ST4), pp. 1157-1174, 1971.

Shuman, E. C., "Giant Sonic Boom Causes Only Minor Damage to House," Materials Research & Standards 2, pp. 79-80.

Simpson, J. D., "The Transient Response of a Helmholtz Resonator with Application to Sonic Boom Studies," Ph.D. Thesis, Oklahoma State University, 1966.

Sutherland, L.C. (Ed.), "Sonic Boom," Section 6.3 of Sonic and Vibration Environments for Ground Facilities - A Design Manual, WR 68-2, Wyle Laboratories, pp. 6-39 to 6-45, 1968.

Ting, L. and Pan, Y.S., "Incident of N-Waves on Structures," NASA SP-130, pp. 39-98, 1968.

United States Department of Commerce, "Sonic Boom Experiments at Edwards Air Force Base," NSBEO-1-67, 1967.

Vaidya, P. G., "The Transmission of Sonic Boom Signals Into Rooms Through Open Windows," J. Sound Vib. 25(4), pp. 533-559, 1972.

Web, D. R. B., "A Summary Report of Measurement of Sonic Boom Responses of Structures During Exercise Trafalgar," Royal Aircraft Establishment, YSE/236/08/DRBW.

Webb, D. R. S., "Effects of Sonic-Booms on Buildings in Relation to Environmental Effects," Royal Aeronautical Establishment, RAE TR-78118, 1973.

Webb, D. R. B. and Marner, D. L. S. D., "The Effects of Sonic Booms on Some Buildings in France," Royal Aeronautical Establishment, RAE TR-73188, 1973.

Weber, G., "Sonic Boom Exposure Effect II.1: Structures and Terrain," in Sonic Boom Effects Workshop, (Rhylander (ed.), 1971, pp. 505-509. Also J. Sound Vib. 20, pp. 505-509, February 1972.

White, R. G., "Measurement of Structural Frequency Response by Transient Excitation," Institute of Sound and Vibration Research, ISVR TR-12.

Wiggins, J. H., "The Effect of Sonic Boom on Structural Behavior," SST 65-18, John A. Blume & Assoc. for Federal Aviation Agency, 1965.

Wiggins, J. H., "Effect of Sonic Boom on Structural Behavior," Materials Research & Standards 7(6), pp. 235-245, 1967.

Wiggins, J. H., "Sonic Boom and Natural Deterioration Effects on Buildings: White Sands, N.M. Structure Resurvey," J. H. Wiggins Co., FAA RD-72-25, 1972.

1.1.3.2 Non-Linear Response to Sonic Boom

Adi Murthy, N. K. and Alwar, R. S., "Influence of Large Amplitude on Response to Sonic Booms," AIAA Journal 13, pp. 1549-1550, 1975.

Baker, W. E., "Modeling of Large Elastic and Plastic Deformations of Structures Subjected to Transient Loading," J. Applied Mechanics, pp. 521-527, September 1960.

Knapp, L. J. and Cheng, D. H., "Linear and Nonlinear Response of a Rectangular Plate Subjected to Lateral and In-Plane Sonic Boom Disturbances," NASA CR-66936, 1970.

Nath, Y., "Nonlinear Structural Response to Sonic Booms," AIAA Journal 16(9), pp. 865-866, 1978.

1.1.3.3 Sonic Boom Response of Structural Elements

Al-Aswad, T. M., "Response of Masonry Walls to Blast Loading. A Discrete Element Analysis," Oklahoma State University, 1980.

Benveniste, J. E. and Cheng, D. H., "Sonic Boom Effects on Beams Loosely Bound to Their Supports," J. Aircraft 4, pp. 494-498, 1967.

Benveniste, J. E. and Cheng, D. H., "Dynamic Response of Structural Elements Exposed to Sonic Booms," City College of the City University of New York, NASA CR-1281, 1969.

Bressers, A. J. M., "Pressures Inside Coupled Rooms Subjected to Sonic Boom," University of Toronto Institute for Aerospace Studies TN-241, 1983.

Cheng, D. H., "Some Dynamic Effects of Sonic Booms on Building Structural Elements," NASA Langley Research Center, 1964.

Cheng, D. H. and Benveniste, J. E., "Dynamic Response to Sonic Booms of Structural Elements Loosely Bound to Their Supports," City College of New York, Rept. 2.

Cheng, D. H. and Benveniste, J. E., "Dynamic Response of Structural Elements Exposed to Sonic Booms," NASA CR-1281, 1969.

Cheng, D. H. and Benveniste, J. E., "Transient Response of Structural Elements to Traveling Pressure Waves of Arbitrary Shape," Int. J. Mechanical Sciences 8, pp. 607-618, 1966.

Coleby, J. R. and Mazumdar, J., "Transient Vibrations of Elastic Panels Due to the Impact of Shock Waves," J. Sound Vib. 77, pp. 481-494, 1981.

Craggs, A., "The Response of a Simply Supported Plate to "N" Waves at Oblique Incidence," J. Sound Vib. 16(2), pp. 293-307, 1971.

Craggs, A., "The Response of a Simply Supported Plate to Transient Forces; Part I - The Effect of N Waves at Normal Incidence," NASA CR-1175, 1968.

Craggs, A., "The Response of a Simply Supported Plate to Transient Forces; Part II - The Effect of N-Waves at Oblique Incidence," NASA CR-1176, 1968.

Craggs, A., "The Transient Response of a Coupled Plate-Acoustic System Using Plate and Acoustic Finite Elements," J. Sound Vib. 15(4), pp. 509-528, 1971.

Crandall, S. H. and Kurzweil, L., "On the Rattling of Windows by Sonic Booms," J. Acoust. Soc. Am. 44(2), pp. 464-472, 1968.

Crocker, M. J., "Multimode Response of Panels to Normal and to Traveling Sonic Booms," J. Acous. Soc. Am. 42(5), pp. 1070-1079, 1967.

Johe, C. H., et al., "Damage Threshold for Light Walls Under Single or Repeated Sonic Booms, Part 2," Institute Franco-Allemand De Recherches, ISL-IV73, 1974.

Kunukkasseril, V. X. and Ramakrishnan, R., "Sonic Boom Effects on Circular Bridge Panels," J. Sound Vib. 35(3), pp. 429-440, 1974.

Leigh, B. R., "Lifetime Concept of Plaster Panels Subjected to Sonic Boom," University of Toronto Institute of Aerospace Studies Technical Note No. 191, 1974.

Leigh, B. R., et al., "Aged Plaster Panels Subjected to Sonic Booms," Proceedings of Tenth International Shock Tube Symposium pp. 437-445, Kyoto, Japan, July 1975.

Mayes, W. H. and Newman, J. W., "An Analytical Study of the Response of a Single-Degree of Freedom System to Sonic-Boom-Type Loading," NASA Langley Research Center, LWP-154, 1966.

Mazumdar, J. and Coleby, J. R., "Simplified Approach to the Vibration Analysis of Elastic Plates Due to Sonic Booms," J. Sound Vib. 45(4), pp. 503-512, 1976.

Pretlove, A. J., "Acousto-Elastic Effects in the Response of Large Windows to Sonic Bangs," J. Sound Vib. 9, 1969.

Pretlove, A. J., "Free Vibrations of a Rectangular Panel Backed by a Closed Rectangular Cavity," J. Sound Vib. 2, pp. 197-209, 1965.

McKinley, R. W., "Response of Glass in Windows to Sonic Booms," Materials Research & Standards 4, pp. 601-611, 1964.

Pallant, R. J., "The Response of Some Leaded Windows to Stimulated Sonic Bangs," Technical Report 73111, Royal Aircraft Establishment, England, 1973.

Pavagadhi, L. J. and Yajnik, M. D., "Vibrations of Circular Elastic Plates Due to Sonic Booms," J. Acous. Soc. Am. 52(1) Part 2, pp. 260-269, 1972.

Peschke, W. et al., "Experimental Determination of Acoustic and Structural Behavior of Wall Panel-Cavity Configurations Exposed to Sonic Booms," NASA CR-111925, 1971.

Seaman, L., "Response of Windows to Sonic Booms," Stanford Research Institute for National Sonic Boom Evaluation Office, SRI Project ETU-5897, 1967.

Seshadri, T. V., "Establishing an Upper Bound for Window Response to the Sonic Boom," J. Sound Vib. 21(2), pp. 149-158, 1972.

Slutsky, S. and Arnold, L., "Coupled Elastic and Acoustic Response of Room Interiors to Sonic Booms," Third Conference on Sonic Boom Research, NASA SP-255, pp. 227-240, 1970.

Vaidya, P. G., "The Transmission of Sonic Boom Signals Into Rooms Through Open Windows - Part I: The Steady State Solution," NASA CR-111786, 1970.

Vaidya, P. G., "The Transmission of Sonic Boom Signals Into Rooms Through Open Windows - Part II: The Time Domain Solutions," NASA CR-111787, 1970.

Vaidya, P. G., "The Transmission of Sonic Boom Signals Into Rooms Through Open Windows - Part III: Experimental Work and General Discussions," NASA CR-111788, 1970.

Wahba, N. N., "Effect of Sonic Boom on a Cracked Plaster-Wood Wall Panel," Proceedings of First International Conference on Structural Failure, Product Liability and Technology, pp. 227-233, 1984.

Wahba, N. N., "Pressures Inside a Room Subjected to Sonic Boom," University of Toronto Institute for Aerospace Studies, UTIAS TN-207, 1977.

Wahba, N. N., "Response of a Plaster-Wood Room Subjected to Simulated Sonic Booms," UTIAS RN-276, 1984.

Wahba, N. N., et al., "Response of a Room Subjected to Simulated Sonic Booms," Transport Canada Research, 1981.

Whitehouse, G. D., "Coupled and Uncoupled Panel Response to Sonic Boom Type Inputs," Ph.D. Thesis, Oklahoma State University, 1967.

Zumwalt, G. W., "Computation of the Pressure-Time History of a Sonic Boom Shock Wave Acting on a Window Glass in a Building," NASA CR-66169, 1965.

1.1.3.4 Sonic Boom Response of Liquid Storage Tanks

Haroun, M. A., "Vibration Studies and Tests of Liquid Storage Tanks," Proc. Int. J. Earthquake Eng. and Structural Dynamics 11, pp. 179-206, March 1983.

Haroun, M. A. and Housner, G. W., "Dynamic Characteristics of Liquid Storage Tanks," Proc. J. Eng. Mech. Div., ASCE 108, pp. 783-800, 1982.

Housner, G. W. and Haroun, M. A., "Dynamic Analysis of Liquid Storage Tanks," Proc. 7th World Conference on Earthquake Engineering 8, pp. 431-438, 1980.

1.2 Blast

1.2.1 Blast Response of Ground

Daemen, J. J. K., et al., "Ground and Air Vibrations Caused by Surface Blasting, Volume 1 Executive Summary," University of Arizona, Bureau of Mines. OFR 105(1)-84, 1983.

Stachura, V. J., Siskind, D. E., and Engler, A. J., "Airblast Instrumentation and Measurement Techniques for Surface Mine Blasting," U.S. Department of the Interior, Bureau of Mines, RI-8508, 1981.

Stagg, M. S. and Engler, A. J., "Measurement of Blast-Induced Ground Vibrations and Seismograph Calibration," U.S. Department of the Interior, Bureau of Mines, RI-8506, 1980.

Thoenen, J. R. and Windes, S. L., "Seismic Effects of Quarry Blasting," U.S. Department of the Interior, Bureau of Mines, Bulletin 442.

1.2.2 Blast Response of Structures

Acoustical Society of America, "Estimating Air Blast Characteristics for Single Point Explosions in Air With a Guide to Evaluation of Atmospheric Propagation and Effects," American National Standard S2.20-1983 (ASA 20-1983).

Dickinson, A. A. and Sound, A. R., "Blast Effects on Residential Dwellings," Naval Weapon Center, POR-2117.

Eldred, K., "Noise and Vibration Characteristics of the CERL Low Frequency Blast Response Facility Test House," U.S. Army CERL, KEE Report 85-29.

Gibson, R. G., et al., "Shock Response of Structures Subjected to Blast Loading," University of Southampton Institute for Sound & Vibration Research, 1988.

Harper, M. J., et al., "Explosively Generated Air Pressure Waves for Structural Forcing," J. Sound Vib. 11(2), pp. 217-224, 1970.

Mainstone, R. J., "The Response of Buildings to Accidental Explosions," presented at Conference on the Performance of Building Structures, Glasgow, 1976.

Ray, J. C., Walker, R. E., and Huff, W. L., "Response of Non-Reinforced Masonry Walls to Conventional Weapons," Shock and Vibration Bulletin, pp. 81-88, January 1987.

Siskind, D. E., et al., "Noise and Vibrations in Residential Structures from Quarry Production Blasting - Measurements at Six Sites in Illinois," U.S. Bureau of Mines Report of Investigations RI-8168, 1976.

Stagg, M. S., et al., "Effects of Repeated Blasting on a Wood-Frame House," U.S. Department of the Interior, Bureau of Mines Report of Investigations RI-8168, 1984.

1.3 Aircraft and General Noise

1.3.1 Structural Response to Aircraft and General Noise

Battis, J. C., "Hush House Induced Vibrations at the Arkansas Air National Guard Facility, Fort Smith, Arkansas," Air Force Geophysics Laboratory, TR-87-0320, 1987.

Carden, H. D., and Mayes, W. D., "Measured Vibration Response Characteristics of Four Residential Structures Excited by Mechanical and Acoustical Loadings," NASA TN-D5776, 1970.

Freynik, H. S., "The Nonlinear Responses of Windows to Random Noise," NASA TN-D-2025, 1963.

Koopman, G. H. and Petyt, M., "Building Vibrations and Acoustics," J. Sound Vib. 28(3), pp. 471-485, 1973.

Koopman, G. and Pollard, H., "Model Studies of Helmholtz Resonances in Rooms with Windows and Doorways," NASA CR-1777, 1971.

Langley Research Center, "Concorde Noise-Induced Building Vibrations for Sully Plantation, Chantilly, Virginia," NASA TM-X-73919, 1976.

Langley Research Center, "Concorde Noise-Induced Building Vibrations, International Airport Dulles," Final Report, NASA TM-73083, 1977.

Langley Research Center, "Concorde Noise-Induced Building Vibrations, John F. Kennedy International Airport - Report No.1," NASA TM-78660, 1978.

Langley Research Center, "Concorde Noise-Induced Building Vibrations, John F. Kennedy International Airport - Report No.2," NASA TM-78660, 1978.

Langley Research Center, "Concorde Noise-Induced Building Vibrations, John F. Kennedy International Airport - Report No.3," NASA TM-78660, 1978.

Langley Research Center, "Concorde Noise-Induced Building Vibrations, Montgomery County, Maryland, Report No.3," NASA TM-X-73947, 1976.

Langley Research Center, "Concorde Noise-Induced Building Vibrations, Sully Plantation - Report No.2, Chantilly, Virginia," NASA TM-X-73926, 1976.

Langley Research Center, "Noise-Induced Building Vibrations Caused by Concorde and Conventional Aircraft Operations at Dulles and Kennedy International Airports," Final Report, NASA TM-78769, 1978.

Leyendecker, E. V. and Burnett, E. F., "The Incidence of Abnormal Loading in Residential Buildings," National Bureau of Standards, U.S. Dept. of Commerce, NBS BSS-89, 1976.

Mixson, J. S., et al., "Effects of Aircraft Noise on Flight and Ground Structures," NASA SP-416, 1976.

Norris, C. H., et al., Structural Design for Dynamic Loads, McGraw-Hill, 1959.

Peck, T. P., "Structural Fatigue Due to Acoustical Loading: A Bibliography 1950-1961," General Dynamics Astronautics, San Diego, GDA AE62-0002-1, 1961.

Piersol, A. G., "Extrapolation Techniques for Predicting Structural Responses to Aeroacoustic Loads," J. Acous. Soc. Am. 47, p. 103, 1970.

Popplewell, N., "The Vibration of a Box-Type Structure. I. Natural Frequencies and Normal Modes," J. Sound Vib. 14(3), pp. 357-365, 1971.

Popplewell, N., "The Vibration of a Box-Type Structure. II. Response to a Travelling Pressure Wave," J. Sound Vib. 13(4), pp. 521-531, 1971.

Rickley, E. J., et al., "Noise Emissions and Building Structural Vibration Levels from the Supersonic Concorde and Subsonic Turbojet Aircraft, Final Report," U.S. Department of Transportation, DOT-TSC-OST-74-35, 1975.

Stephens, D. G. and Mayes, W. H., "Aircraft Noise-Induced Building Vibrations," ASTM Special Technical Publication 692, 1979.

Sutherland, L. C., "Low Frequency Response of Structures," Wyle Laboratories Report WR 82-18, 1982.

Sutherland, L. C., et al., "Preliminary Valuation of Low Frequency Noise and Vibration Reducing Retrofit Concepts for Wood Frame Structures," Wyle Research Report WR 83-26, Wyle Laboratories, 1983.

Vaidya, P. G., "The Acoustic Response of Rooms with Open Windows to Airborne Sounds," J. Sound Vib. 25(4), pp. 505-532, 1972.

Vest, G. D., "Plans for Control of the Noise Exposure Produced by Military Aircraft in the 1980's," Inter-Noise 80, Miami, Florida, 1980.

Wesler, J., "Aircraft Noise and Structural Vibration," J. Sound Vib., February 1978.

Wesler, J., "Noise and Induced Vibration Levels from Concorde and Subsonic Aircraft," J. Sound Vib., October 1975.

1.3.2 Response of Primitive Structures to Aircraft and General Noise

Battis, J. C., "Archaeological Monitoring at Long House in Southeast Arizona," draft, 11 July 1988.

Battis, J. C., "The Effect of Low Flying Aircraft on Archaeological Sites, Kayenta, Arizona," Air Force Geophysics Laboratory, TM-146, 1988.

Battis, J. C., "Effects of Low Flying Aircraft on Archaeological Structures," draft, 5 August 1988.

Battis, J. C., "Seismo-Acoustic Effects of Sonic Booms on Archaeological Sites, Valentine Military Operations Area," Air Force Geophysics Laboratory, Environmental Research Paper No. 858, AFGL-TR-83-0304, 1983.

Brumbaugh, D. S., "A Report on the Analysis of the Effect of Helicopter Vibrations on the Pt. Sublime Anasazi Site, Grand Canyon National Park," Northern Arizona University Dept. of Geology.

Haltiwanger, J. D., "Vulnerability Analysis of McDonald Ranch House," Defense Nuclear Agency, Special Studies Report, January 1986.

King, K. W., et al., "Seismic Vibration Hazard Investigation of Chaco Culture National Park," USGS Open-file Report 85-529, 1985.

Nash, P. T., et al., "Dynamic Response of a Soil Covered Arch to Impact and Blast Loadings," Shock and Vibration Bulletin, pt.4, pp. 67-74, 1977.

1.4 Indirect Effects

1.4.1 Effect of Structures on Sonic Boom Signatures

Brooks, J. D., et al., "Laboratory Investigation of Diffraction and Reflection of Sonic Booms by Buildings," NASA Langley Research Center, NASA TN-D-5830, 1970.

Rao, B. M. and Zumwalt, G. W., "Diffraction and Reflection of Sonic Boom Waves," J. de Mechanique 9, pp. 309-324, 1970.

1.4.2 Effect of Ground Motion on Structures

Lee, D.M., "Hazardous Buildings: Some Aspects of the Los Angeles Earthquake Problem," Earthquake Safety Ordinance," Master's Thesis, Department of Engineering, University of California, Irvine, 1982.

Shepherd, R., "High Earthquake Risk Buildings in New England," Earthquake Engineering and Structural Dynamics 6, pp. 383-395, 1978.

1.5 Modeling

1.5.1 Blast, Boom - Prediction, Simulation Codes for Response

Allemang, R. J. and Brown, D. L., "Experimental Model Analysis and Dynamic Component Synthesis - Vol. III Modal Parameter Estimation," AFWAL TR-87-3069, 1987.

Barkley, R. C. and Daemen, J. J. K., "Ground and Air Vibrations Caused by Surface Blasting. Vol. 3 Computer Simulation Predictor of Ground Vibrations Induced by Blasting," Bureau of Mines, OFR 105(3)-84, 1984.

Beason, W. L. and Morgan, J. R., "Glass Failure Prediction Model," J. Struct. Eng., Am. Soc. Civil Eng. 110(2), pp. 197-212.

Craggs, A., "Transient Vibration Analysis of Linear Systems Using Transition Matrices," NASA CR-1237, 1968.

Gloyna, F. L., "Vibroacoustic Response Using the Finite Element Method and Statistical Energy Analysis," Proc. 59th Shock and Vibration Symposium, Vol. 1, pp. 103-118, 1988.

Salzberg, A. A., "Validation of LACE Spacecraft Vibroacoustic Prediction Model," Naval Research Laboratory, 1988.

Slutsky, S. and Arnold, L., "Experimental-Analytic Dynamic Techniques, for Application to Sonic-Boom Structural and Acoustic Response Determination," New York University, NYU AA-70-19, 1970.

Slutsky, S. and Arnold, L., "Numerical Prediction of Interior and Structural Response of Buildings to Sonic Boom Overflights - Final Report Phase I," New York University, FAA-RD-72-116, NYU-AA-72-23, 1972.

Weber, G., "Probability of Aircraft Noise and Sonic Boom Induced Building Damages," Technische Hochschule, Hanover, W. Germany, 1970.

2.0 CONDITION ASSESSMENT

2.1 Assessment of Aircraft Noise Effects

Fidell, S., et al., "Detailed Design Specifications for a Prototype Assessment System for Aircraft Noise (ASAN)," BBN Report 6337, HSD-TR-88-02, 1987.

Hardesty, D. L., "Final Report on the Research Design for Assessing Sonic Boom Damage to Cultural Resources Below the Supersonic Operations Area, Naval Air Station Fallon, Nevada," Office of Community Services Carson City, Nevada, April 1987.

United States Air Force, "Assessing Noise Impact of Air Force Flying Operations," HQ USAF/LEEVX, 1984.

2.2 Methods Available

2.2.1 Photography

Doty Assoc., "Underwater Facilities Inspections and Assessments," U.S. Naval Weapons Station, FPO 1-80(18), 1980.

2.2.2 Mechanical Impedance

Beranek, L. L., Noise and Vibration Control, McGraw-Hill, pp. 348-349, 1971.

Ewing, W. M., et al., Elastic Waves in Layered Media, McGraw-Hill, pp. 64- 71, 1957.

Kendig, M. and Mansfeld, F., "AC Impedance Analysis of Corrosion Fatigue in Naval Aircraft Alloys," Naval Air Development Center, NADC-87183-60, 1987.

Kendig, M. and Mansfeld, F., "Application of Electrochemical and Mechanical Impedance Techniques for Evaluation of SCC and CF," Paper No. 190, NACE, Corrosion/86, 1986.

Morse, P.M., Ingard, K.U., Theoretical Acoustics, McGraw-Hill, pp. 259-267, 370-371, 1968.

2.2.3 Acoustic Methods

Achenbach, J. D., et al., "Mathematical Modeling of Ultrasonic Wave Scattering by Sub-Surface Cracks," Ultrasonics 24, pp. 207-215, 1986.

Kraska, I. R. and Kamm, H. W., "Evaluation of Sonic Methods for Inspecting Adhesive Bonded Honeycomb Structures," AFML, TR-69-283, 1970.

Scandrett, C. L. and Achenbach, J. D., "Time-Domain Finite Difference Calculations for Interaction of an Ultrasonic Wave with a Surface-Breaking Crack," Wave Motion 9, pp. 171-190, 1987.

Zhang, C. and Achenbach, J. D., "Scattering of Body Waves by an Inclined Surface Breaking Crack," Ultrasonic 26, pp. 130-138, 1988.

Zhang, C. and Achenbach, J. D., "Numerical Analysis of Surface-Wave Scattering by the Boundary Element Method," Wave Motion 10, pp. 365-374, 1988.

2.2.4 Visual Observation

Reed, N. L., "Inspection of the Condition of Exterior Paint and Wood of Various Buildings at Watertown Arsenal, April 1931," Watertown Arsenal Laboratories, Mem. Report 361/1, 1931.

2.2.5 Miscellaneous Methods of Condition Assessment

Lester, H. H., "Defects in Metal Arc Fusion Welding that are Shown in Radiographic Negatives," Watertown Arsenal Report 142/27, 1944.

Lester, H. H., "Monel Metal Test Beam Radiographic Report of Conditions Before and After Destructive Test," Watertown Arsenal Report 142/10, 1936.

Lin, A. F. and Dittmer, D. F., "Effect of Multiaxial Loading on Crack Growth Vol. III, Compilation of Interferometry Photographs," AFFDL TR-78-175, 1978.

Rollwitz, W. L., "Magnetoabsorption Techniques for Measuring Material Properties," AFML TR-66-76, 1969.

2.2.6 Evaluation of Methods of Assessment

Andrews, R. J., et al., "Research on Advanced NDE Methods for Aerospace Structures," AFWAL, TR-87-4007, 1987.

Boeing Co., "Detection of Cracks Under Installed Fasteners," AFML TR-78-80, 1974.

Boeing Co., "Practical Sensitivity Limits of Production Nondestructive Testing Methods in Aluminum and Steel," AFML TR-74-241, 1975.

McMaster, R. C. (ed.), Nondestructive Testing Handbook, v. II, Ronald Press Co., New York, 1950.

NASA, "Analytical Techniques - A Compilation. Section 2. Nondestructive Testing," NASA SP-5972(04), pp. 11-21, 1975.

3.0 DAMAGE

3.1 Sonic Boom

3.1.1 Sonic Boom Damage to Structures

Building Research Station, "Examination of Damage Alleged to Have Been Caused by Sonic Boom Produced During Exercise Westminster," BRS Note IC/31/65.

Clark, Buhr and Nexsen, "Studies of Sonic Boom Induced Damage," NASA CR-227, 1962.

Clarkson, B.L. and Mayes, W.H., "Sonic-Boom-Induced Building Structure Responses Including Damage," J. Acous. Soc. Am. 51(2) (Part 2) pp. 742-757, 1969.

Dmitriyenko, S. S., "Empirical Stress-Amplitude Distributions for Calculating Cumulative Damage," Russian Engineering Journal 49(5), pp. 8-10.

Haag Engineering Co., Structural Problems Associated with Sonic Boom Damage Inspections, Haag Engineering Co., February 1968.

Hershey, R. L. and Higgins, T. H., "Prediction of Sonic Boom Structural Damage," Noise Control Engineering, pp. 381-386, 1978.

Hershey, R. L., and Higgins, T. H., "Statistical Model of Sonic Boom Structural Damage, Final Report," FAA-RD-76-87, 1976.

Ramsay, W. A., "Damage to Ottawa Air Terminal Building Produced by a Sonic Boom," Materials Research & Standards 4, pp. 612-616, 1964.

Thybout, J. P., et al., "Damage Threshold Determination of Light Walls Subjected to Single or Repeated Bangs," Pt. 1, Institut Franco-Allemand De Recherches, ISL-35/72-Pt.-1, 1974.

Wiggins, J. H., Sonic Boom Damage to Structures, J. H. Wiggins Co.

Wilhelmsen, A. M. and Larsson, B., "Sonic Booms and Structural Damage," National Swedish Institute for Building Research, D3:1973, 1973.

3.1.2 Sonic Boom Damage to Glass

Hershey, R. L. and Higgins, T. H., "Statistical Prediction Model for Glass Breakage from Nominal Sonic Boom Loads," Booz, Allen Applied Research, FAA-RD-73-79, 1973.

Kao, G. C., "An Experimental Study to Determine the Effects of Repetitive Sonic Booms on Glass Breakage," FAA NO-70-13, 1970.

Lowery, R. L. and Andrews, D. K., "Acoustical and Vibrational Studies Relating to an Occurance of Sonic Boom Induced Damage in a Window Glass in a Store Front," NASA CR-66170, 1966.

Parrott, T. L., "Experimental Studies of Glass Breakage Due to Sonic Booms," Sound—Its Uses and Control, May-June 1962.

Pretlove, A. J., and Bowler, F. F., "An Estimate of Sonic Boom Damage to Large Windows," J. Sound Vib. 22, 1974.

3.1.3 Sonic Boom and Avalanche

Lillard, D. C., Parrott, T. L. and Gallagher, D. G., "Effect of Sonic Booms of Varying Overpressures on Snow Avalanches," SST 65-9, 1965.

3.2 Blast and General Noise

3.2.1 Damage to Structures from Blast and General Noise

Building Research Station, "Cracking in Buildings," BRS Note IC-20/65.

Byrne, K. P., "On the Growth Rate of Bending Induced Edge Cracks in Panels Excited by Convected Random Pressure Fields," J. Sound Vib. 68(2), pp. 161-171, 1980.

Dowding, C. H. and Corser, P. G., "Cracking and Construction Blasting," J. Construction Div. ASCE, v. 107, CO1, pp. 89-106, 1981.

Duvall, W. I. and Fogelson, D. E., "Review of Criteria for Estimating Damages to Residences from Blasting Vibrations," U.S. Bureau of Mines Report of Investigations RI-5968, 1962.

Medearis, K., "The Development of Rational Damage Criteria for Low-Rise Structures Subjected to Blasting Vibrations," Kenneth Medearis Associates, 1976.

Northwood T.D., Crawford, R. and Edwards, A.T., "Blasting Vibrations and Building Damage," The Engineer 215(5601), pp. 973-978, 1963.

Siskind, D. E., "Damage to Residential Structures from Surface Mine Blasting," Soc. Mech. Eng., 1980.

Siskind, D. E. and Stagg, M. S., "Structural Response and Cosmetic Cracking in Residences from Surface Mine Blasting," 59th Shock and Vibration Symposium, 1, pp. 319334, 1988.

Siskind, D. E. and Summers, C. R., "Blast Noise Standards and Instrumentation," Technical Progress Report 78, U.S. Department of the Interior Bureau of Mines, 1974.

Siskind, D. E., et al., "Structure Response and Damage Produced by Airblast from Surface Mining," U.S. Bureau of Mines Report of Investigations, RI-8485, 1980.

Siskind, D. E., et al., "Structure Response and Damage Produced by Ground Vibration from Surface Mine Blasting," U.S. Bureau of Mines Report of Investigations, RI-8507, 1980.

Wiss, J. F. and Nicholls, H. R., "A Study of Damage to a Residential Structural from Blast Vibrations," Am. Soc. Civil Eng. 40(2), pp. 496-498, 1967.

3.2.2 Avalanche from Blast and General Noise

Armstrong, R. L. and Armstrong, B.R., "San Juan Mountains Avalanche Study - Evaluation and Prediction of Avalanche Hazard - Meteorological and Avalanche Observations - Annual Report 1983," National Snow and Ice Data Center, U.S. Department of Commerce, 1983.

Armstrong, R. L. and Armstrong, B. R., "San Juan Mountains Avalanche Study - Evaluation and Prediction of Avalanche Hazard - Meteorological and Avalanche Observations - Annual Report 1984," National Snow and Ice Data Center, U.S. Department of Commerce, 1984.

Armstrong, R. L. and Ives, J. D. (Ed.), "Avalanche Release and Snow Characteristics, San Juan Mountains, Colorado," University of Colorado Institute of Arctic and Alpine Research, INSTAAR-14-06-D-7155-4, 1976.

Gubler, H., "Artificial Release of Avalanches by Explosives," J. Glaciology 19(81) p. 419, 1977.

Perla, R. I., "Avalanche Release, Motion, and Impact," Environment Canada, Canmore, Alberta, Canada.

Terzaghi, K., "Mechanism of Landslides," Geological Society of America, in Engineering Geology, pp. 83-123, 1950.

Toki, K., et al., "Estimation of the Dynamic Stability of a Slope During Strong Earthquake Motion," 1984.

United States Department of Agriculture Forest Service, "Snow Avalanches, A Handbook of Forecasting and Control Measures," FSH 2309.14, Agriculture Handbook No. 194, 1968.

World Data Center for Glaciology (Snow and Ice), "Glaciological Data Report GD-16 - Soviet Avalanche Research - Avalanche Bibliography Update: 1977-1983," 1984.

3.3 Environmental Impact

Hubbard, H.H., "Noise Induced House Vibrations and Human Perception," Noise Control Eng. 19, pp. 49-55, 1982.

3.3.1 Claims Analysis

Acoustical Society of America, "Method for Assessment of High-Energy Impulsive Sounds with Respect to Residential Communities," American National Standards Institute ANSI S12.4-1986 (ASA 63-1986), 1986.

Borsky, P. N., "Community Reactions to Sonic Booms in the Oklahoma City Area," National Opinion Research Center, AMRL-TR-65-37, 1965.

Grubb, C. A. et al., "Report on Data Retrieval and Analysis of USAF Sonic Booms Claim Files," SRI Technical Report 4, Stanford Research Institute, 1967.

Guest, S. H. and Slone, R. M., "Structural Damage Claims Resulting from Acoustic Environments Developed During Static Test Firing of Rocket Engines," NASA TM-X-2570, pp. 45-69, 1972.

Guest, S. H., and Slone, R. M., "Structural Damage Claims Resulting from Acoustic Environments Developed During Static Test Firing of Rocket Engines," NASA TN D-6823, 1972.

Hilton, D. A., et al., "Sonic-Boom Exposures During FAA Community-Response Studies Over a 6-Month Period in the Oklahoma City Area," NASA Langley Research Center, NASA TN-D-2539, 1964.

National Research Council, "Assessment of Community Response to High-Energy Impulsive Sounds," Committee on Hearing, Bioacoustics, and Biomechanics, 1981.

Nixon, C. W., and Hubbard, H. H., "Results of USAF-NASA-FAA Flight Program to Study Community Responses to Sonic Boom in the Greater St. Louis Area," NASA TN-D-2705, 1965.

United States Environmental Protection Agency, "Information on Levels of Environmental Noise Requisite to Protect Public Health and Welfare with an Adequate Margin of Safety," U.S. Environmental Protection Agency Report EPA 550/9-74-004, 1974.

3.3.2 Environmental Impact Analysis

United States Air Force, "Environmental Impact Statement, Supersonic Flight Operations in the Reserve Military Operations Area, Holloman Air Force Base, New Mexico, Final," Department of the Air Force, Tactical Air Command, Washington, D.C., 1979.

United States Air Force, "Environmental Impact Statement, Supersonic Flight Operations in the Valentine Military Operations Area, Holloman Air Force Base," U.S. Department of the Air Force, Tactical Air Command, Washington, D.C., 1979.

United States Navy, "Draft Comprehensive Environmental Impact Statement for the Proposed Supersonic Operations Area and Other Proposed Actions at Naval Air Station Fallon, Nevada," 1985.

APPENDIX B

Metric Conversion Tables and
Physical Properties of Various Basic Building Construction Materials

Abstracted from
Sonic and Vibration Environments for Ground Facilities - A Design Manual
Louis C. Sutherland (Ed.)
Wyle Laboratories Report WR 68-2
1968

Table of Contents

	Page
B.1 Metric Conversion Chart	B-2
B.2 Physical Properties of Materials	B-4
References for Section B.2.....	B-15

METRIC CONVERSION CHART

1 ft	=	0.3048 m
1 in	=	2.54 cm = 0.0254 m
1 ft ²	=	0.0929 m ²
1 in ²	=	0.0006452 m ²
1 lb/ft ³	=	16.02 kg/m ³
1 lb/in ³	=	27,683 kg/m ³
1 lb	=	4.448 N
1 psi	=	6895 Pa (N/m ²)
1 psf	=	47.88 Pa(N/m ²)

B.2 PHYSICAL PROPERTIES OF MATERIALS

TABLE B.2-1

PHYSICAL PROPERTIES OF VARIOUS BASIC BUILDING CONSTRUCTION MATERIALS

Building Material	Ultimate strength, psi Allowable Strength, psi			Modulus of Rupture, psi	Endurance Limit	Young's Modulus Mod of Rigidity, $\times 10^{-9}$ psi	Poisson's Ratio	Loss Factor	Density, pcf	Thermal Expansion
	Comp.	Tension	Shear							
ASBESTOS-CEMENT										
Corrugated Sheet										
Type A (Std.) 3/8"				3,000					3.7-4.0	
Type B (Light Wt.) 3/16"				5,300					3.7-4.0	
Flat Sheet and Fiberboard Insulating Panel										
Type F (Flexible)				9,000 -						
1/8" to 5/8"				10,000						
Type U (Utility)				7,000						
3/16" to 5/8"										
BOARD										
Beaverboard, 1/2"						0.175		0.027	0.31	13
Cellulose Insulation Board, 1/2"		145-270							0.7-1.7	39
Masonite, 3/16"						0.61		0.017	0.91	13
Paper Board										3
Asbestos Board, 3/16"		1,250		3,000					1.361	
Asphalt-Saturated Sheathing, 25/32"		185		38						
Cellulose Insulation Building Board, 1/2"		650		1,100					1.01	
Under Floor Insulation Board, 25/32"		650		1,100					1.331	
Sheathing Insulation Board, 25/32"		200		300					1.401	
Wallboard, Panel Board		930-2,030							0.951	
Hardboard, 11/32"										
Plasterboard, 27/32"						0.035		0.009	0.91	3
Sheetrock, 1/2"						0.31		0.008	2.31	13
Transite, 1/4"						0.68		0.007	2.31	13
BRICK										
70% of U.S. made Clay, Shale, and Sand-Lime Bricks	2,500 - 15,000	500 - 9,000		450 - 1,500		0.75-1.8 [0.3-0.6]		0.01	110-130	2.5 5.0 28.29
25% of U.S. made Clay, Shale, and Sand-Lime Bricks	15,000 - 22,500			1,500 - 3,500		0.75-1.8 [0.3-0.6]		0.01	110-130	
Brick						0.75-1.8		0.01	100-130	
Grade SW	2,500 - 3,000 M									
MW	2,000 - 1,500 M									
NW	1,250 - 2,500 M									
Concrete Building Brick	1,250 - 2,500 M					0.75-1.8		0.01	100-125	
SCR Brick (Manufactured by Structural Clay Product Research Foundation)	11,140			458					106	10
BLOCK CONCRETE										
Load Bearing, Hollow	600 - 1,000 M							0.005	30-70	18
Load Bearing, Solid	1,000 - 1,300 M							0.012	70-120	18
Non-Load Bearing, Hollow	300 - 350 M							0.005	30-70	

TABLE B.2-1 (CONTINUED)
PHYSICAL PROPERTIES OF VARIOUS BASIC BUILDING CONSTRUCTION MATERIALS

Building Material	Ultimate Strength, psi ① Allowable Strength, psi			Modulus of Rupture psi ②	Endurance Limit ③	Young's Modulus Mod. of Rigidity $\times 10^{-6}$ psi ④	Poisson's Ratio μ	Loss Factor η ⑤	Density lb/cu ft (lb/sq ft)	Reference	
	Comp.	Tension	Shear								
CONCRETE (28 Day Strength)											
	Add 20 to 30% for Dynamic Strength.										1, 7, 5, 16, 27, 43
Plain Concrete	(750-900)	(80-160)	(80-160)		0.5-0.6	2.0-2.2 (0.07-0.1) 4.0-4.2D ⑥	0.07-0.1	0.06-0.12	145-160	14	
Am. Concrete Institute (Command Building):											
Type I	2,800 - 3,500	350									
Type II	2,800 - 3,500	325									
Type III	2,300 - 3,000	325									
Type IV	2,000	300									
Type V	3,000	325									
U.S. Military Spec.										24	
Class AAA	5,000				0.5-0.55		0.07-0.1	0.06-0.1			
AA	3,750										
A	3,000										
B	2,500										
C	1,500										
Lightweight Aggregate Concretes:											
Expanded Slag	350 - 2,100			120-600		0.8-2.5			90-130		
Haydite	1,500 - 7,000			250-600		1.8-3.0			90-125		
Vermiculite and Perlite	90 - 1,100			20-70		0.8-2.9			35-80		
Precast Concrete											
Floor Slab	1,500 - 7,000	(2-7)							50-120		
Insulating Roof Tile (Reinforced)	400 - 600								35-55		
Roof Slab	1,500 - 2,500	(2-3)							50-70		
Reinforced Concrete (Ordinary 1 to 2% of Tensile Reinforcement)	2,500 - 7,500 (750 - 1,000) 3,000 - 9,000D ⑥	1,500 - 3,000 M (500 - 750)	1,500 - 3,000 M (500 - 750)		0.45-0.55	2.3-3.4	0.07-0.1	0.06 - 0.12	155-170		
GLASS											
										2, 3, 25	
Annealed Plate Glass and Window Glass	34,000 (1,000) ⑧	6,500 (1,000) ⑦ ⑧		6,500 ⑦	0.45-0.50 ⑧	10 12.5 D 3.6	0.17 - 0.27	0.002 - 0.03	120-180		
Laminated Glass				3,500					120-180		
Tempered Plate Glass	90,000 - 180,000	20,000 - 30,000		20,000 - 30,000					120-180		
Glass Block Panel with 100 psi Bond Strength	400 - 600	0.4 ⑨		10							

TABLE B.2-1 (CONTINUED)
PHYSICAL PROPERTIES OF VARIOUS BASIC BUILDING CONSTRUCTION MATERIALS

Building Material	Ultimate strength, psi Allowable Strength, psi			Modulus of Rupture psi	Endurance Limit	Young's Modulus Mod. of Rigidity psi	Poisson's Ratio	Loss Factor	Density p.c.f. lb./cu. ft.	Refer- ence
	Comp.	Tension	Shear							
GYPSUM PRODUCTS										
Lath 3/8" to 1/2"				700- 750 (10) 280- 335 (11)		1.0		0.005	60-80	2, 4, 7, 26, 28
Ready Mixed Plaster	400 M							108		
Plaster (Neat, Wood-Fibered, Bond, and Ganging)	1,200 - 2,200	50 - 2,200						50		
Wallboard 1/4" to 3/8"				990 - 1,400 (10) 420 - 670 (11)			0.035	0.01-0.03		43-62
1/2" to 5/8"				670 - 770 (10) 270 - 350 (11)						70-85
Sheathing Board				770 (10) 350 (11)						
Formboard, 1/2"				1,120 (10) 420 (11)						
Gypsum-Concrete Class A	500 M (125)	[100]	[10]			1.2-1.8 0.2 D				55-65
Class B	1,000 M (220)	[165]	[20]			1.2-1.8 0.6 D				
Gypsum-Cement	5,000 - 9,000	600 - 1,000		700 - 2,400		1.2-1.8			80-115	
Gypsum Hollow Tile	75 M									
METALS										
Commonly Used in Building Structures										
Aluminum Alloys										
Annealed 1100-O, 2014-O, 3003-O, 3004-O, 5052-O, 5154-O, and 6061-O	3,500 11,000	11,000 - 30,000	8,000 - 19,000		0.6 (12)	10 3.81	0.33	0.003	165	30, 44 49
Heat Treated 2014-T3, T4, T6 6061-T4, T6, T62	32,000 - 58,000 14,000 - 26,000	55,000 - 60,000 26,000 - 35,000	34,000 - 40,000 16,000 - 22,000		0.5 (12) 0.5 (12)	10.6 4.01 10 3.81	0.33	0.003	165	
Brass	25,000 (12,000)	65,000 (12,000)	15,000 (7,000)		0.35 - 5	13.5 4.81	0.33		525	32, 49

TABLE B.2-1 (CONTINUED)

PHYSICAL PROPERTIES OF VARIOUS BASIC BUILDING CONSTRUCTION MATERIALS

Building Material	Ultimate strength, psi (1) Allowable Strength, psi			Modulus of Rupture psi (2)	Endurance Limit (3)	Young's Modulus Mod. of Rigidity $\times 10^{-6}$ psi (4)	Poisson's Ratio μ	Loss Factor η (5)	Density lb/cu ft b/m ³	Refer- ence
	Comp.	Tension	Shear							
METALS (Continued)										
Copper					0.35-0.5	13-17 (6.4)	0.33	0.103	555	32, 49
Annealed	30,000	33,000 36,700 D	23,000							
Cold Rolled	38,000 (19,000)	45,000 - 53,000 60,000 D (19,000)	23,000 - 28,000 (11,000)							
Gray Cast Iron					0.35-0.5		0.25		450	50
# 20	75,000 (10,000)	20,000 (3,000)	(3,000)			12 (5)				
# 40		40,000				18 (7)				
Structural Steel	30,000 - 41,000 (21,000)	52,000 - 75,000 (21,000) 33,000 46,000 (13)	37,000 - 52,000 (14,000)		0.65	29 (12)	0.33	0.001 - 0.003	490	31
MORTAR										
General Mix (Cement:Lime:Sand) By Volume 1:1:6	900 - 2,800 100 - 750 M	165 - 350	45 - 70			0.8-1.3 2.3 (9)			45-70	9, 29
1:1/2 to 1: 4-1/2	2,100 - 3,600 1,800 M	270 - 400	55 - 70							
1:1 4-2-1/4 to 3.0 (Type A-1)	4,800 - 5,500 2,500 M	420 - 460								
1:1 4 to 1:2: 2-1/4 to 3.0 (Type A-2)	2,100 - 2,300 1,800 M	260 - 300								
High Bond Mortar 1:0.2-1: 2 to 3.0 (with 15% to 20% Saron Polymer)	5,000 - 10,000	460 - 1,100	140 - 260			10 - 1.8				
Stucco 1:1/4:3-1/4	1,500 - 2,800									
STONE, Building										
Granite	7,700 - 60,000	600 - 1,000	2,000 - 4,800	1,400 - 5,200		5.7-8.2			160-190	2, 5
Limestone	2,600 - 28,000	280 - 900	800 - 4,600	500 - 2,300		7.5 - 12.4			150-170	
Marble	8,000 - 50,000	150 - 2,300	1,300 - 6,500	600 - 5,000		7.2 - 14.5			160-180	
Sandstone	5,000 - 20,000	280 - 500	300 - 3,000	700 - 2,300		1.9-7.7			135-160	
Slate		3,000 - 4,300	2,000 - 3,600	6,000 - 15,000		9.8-18			170-180	
SYNTHETIC MATERIAL										
Acrylic (Plexiglass)	18,000	10,500		16,000		3.45		0.002	75	48, 18

TABLE B.2-1 (CONTINUED)

PHYSICAL PROPERTIES OF VARIOUS BASIC BUILDING CONSTRUCTION MATERIALS

Building Material	Ultimate and Allowable Strength				Endurance Limit	Young's Modulus Mod. of Rigidity $\times 10^{-6}$ psi	Poisson's Ratio μ	Loss Factor n	Density p/cu ft lb/sq ft	Reference
	Comp. (14)	Trans. (15)	Backing (16)	Impact (17)						
<u>WALL (Continued)</u>										
10" Brick-Brick Cavity Wall	520 (30-110)	0.17	50 51	2.8					671	36
10" Brick-Tile Cavity Wall	238	0.20	53	3.0					621	37
10" Block-Block Cavity Wall	315	0.35	50	3.0					441	34
Solid Concrete Unit Masonry, with Ordinary Mortar	(100-140)		61				0.1	0.012		2
Hollow Concrete Unit Masonry, with Ordinary Mortar	(70)		51				0.1	0.007		2
Reinforced Solid Concrete Unit Masonry	(250-300)		30-50)			0.3-0.4 0.75-0.90	0.1	0.012		7, 20
Reinforced Hollowed Concrete Unit Masonry	(225)		30-50)							7
Wood Frame Wall, or Partition, 8 Ft. High Conventional Construction:										
- Wall Using 2x4 Studs; 16" o.c., 5/16" Plywood Sheathing; 1/4" Plywood or 1/4" to 1/2" Wall-board Inside Face; with Siding or Shingle; Total Wall Thickness 5-1/4" to 5-7/8"	92-140	1.5-2	20-38	10					(4.5-5.5)	39, 40 41, 44 45
- Wall Using 2x4 Studs; 16" o.c., 25/32" Sheathing Board, Level Siding or Shingle Outside Face; Lath and Plaster Inside Face; Total Thickness 6" to 7"	90-157	2.1-2.4 0.4-0.6 (15)	19-24						(9-10.5)	45, 39
- Wall Using 2x4 Studs; 16" o.c., 25/32" Sheathing Board and Brick Veneer Outside Face; Lath and Plaster Inside Face; Total Thickness 10-1/4"	52.5	2.2 0.83 (18) 0.52 (19)	51	6.5					50.5)	45
- Wall Using 2x4 Studs; 16" o.c., 25/32" Sheathing Board; Metal Lath and Stucco Outside Face; Lath and Plaster Inside Face; Total Thickness 6-3/4"	83.5	2-36 0.6 (18)	26	5.7					20)	45
- Wall, or Partition, Using 2x4 Studs; 16" o.c., Fiberboard Sheen Both Faces; Total Thickness 4-1/2"	116	2.5	10.5	6.5					(3.6)	47
- Same as above Except Sidelings are Added to the Outside Face; Total Thickness 5-1/2"	68-78	1.7-2.3	11.4-2.1	10					4.5)	39, 47

TABLE B.2-1 (CONTINUED)

PHYSICAL PROPERTIES OF VARIOUS BASIC BUILDING CONSTRUCTION MATERIALS

Building Material	Ultimate Load Allowable Strengths				Endurance Limit	Young's Modulus Mod. of Rigidity	Poisson's Ratio	Stress Factor	Density lb./cu. ft.	Reference
	Allowable Strengths									
	Comp. (1)	Trans. (2)	Racking (3)	Impact (4)						
WALL (Continued)										
- Partition, Using 2x4 Studs; 10" a.c., Wall Board on Both Faces; Total Thickness 4-5/8"	38	0.95	13	5.8					5.41	40
- Wall Using 1x3 Studs; 15" a.c., 3/8" Outside and 1/4" Inside Plywood Faces; Total Thickness 3-1/8"	280	2.1	5.0	10					3.21	41
- Partition, Same Construction as Above Except 1/4" Plywood Faces on Both Faces; Total Thickness 3"	250	1.9	48	7.0					2.91	41
Metal Panel Wall-										
- Sheet-Steel Wall, Using 3" Steel Channel Studs; 10" a.c., Sheet-Steel on Both Faces; 18 gage Steel; Total Thickness 3"	225	1.7	37	7.0					7.51	23
- Sheet-Steel Wall, Using 16" Wide Outside Channel Shaped Sheet Steel Panel; 16" Wide Inside Sheet Steel Panel; Wood Strip and Key Construction in Joining Panels; 18 Gage Steel; Total Thickness 3"	230	1.2	21	10					6.31	42
- Sheet-Steel Partition, Using 3" Steel Channel Studs; 16" a.c., or Using 16" Inside Channel Shaped Steel Panel; Wallboard on Both Faces				13-17					4.21	22, 42
ROOF										
Steel Roof Deck; 18 to 22 Gage Steel	18,000								1.2-31	9
Sheet-Steel Roof with Joist, Angle, Zee, Insulation Board, and Built-up Roofing		1.1-1.3							10.5-121	23
Wood Frame Roof; 1x4 Joist, 11-1/4" a.c., Bridging, 25" a.c., 3/8" Plywood Sheathing; 1/4" Plywood Ceiling		1.0-1.5							7.21	41

TABLE B.2-1 (CONTINUED)

PHYSICAL PROPERTIES OF VARIOUS BASIC BUILDING CONSTRUCTION MATERIALS

Building Material	Density $\frac{b}{ft^3}$	Fiber Strength at Proportion Limits, $\times 10^{-3}$ psi Allowable Strength in Brackets						Ultimate Static Bending $\times 10^{-3}$ psi		Max. Compression Crushing Strength $\times 10^{-3}$ psi		Endurance Limit (3)
		Compression		Tension		Bending Tension Parallel to grain		Max. Shear	Mod. of Rupture Parallel to Grain	Young's Modulus		
		Par. to Grain	Perp. to Grain	Par. to Grain	Perp. to Grain	Static	Impact			Par. to Grain	Perp. to Grain	
		(1)	(2)	(3)	(4)	(5)	(6)	(7)	(8)	(9)	(10)	
References: 1, 2, 3, 4, 5, 7, 17, 18, 21, 22, 23, 54												
WOOD, TIMBER AND PLYWOOD (20)												
Douglas Fir	26-30	4.6 - 5.45 0.95 - 1.01	0.32 - 0.28 0.25 - 0.28	(22)	(23)	6.3 - 8.1 1.6 - 2.6	11.8 - 12.7	0.12 - 0.15	6.8 - 9.6	1,400 - 1,900	6.56 - 7.42	1.07 - 1.19
See Legend (24) for Poisson's Ratio, Elastic Ratio, Rigidity Ratio and Material Loss Factor of Douglas Fir.)												
Balsam Fir and White Fir	22-24	3.87 - 3.97 0.95 - 1.01	0.38 - 0.22 0.61 - 0.22	(22)	(23)	5.2 - 6.3 1.3 - 1.6	7.8 - 11.2	0.11 - 0.12	7.6 - 9.3	1,230 - 1,470	4.53 - 5.38	0.71 - 0.93
Hemlock (Eastern and Western)	25-26	4.02 - 5.34 0.95 - 1.20	0.68 - 0.22 0.8 - 0.22	(22)	(23)	6.1 - 6.8 1.6 - 1.9	10.7 - 12.4	0.10 - 0.11	8.9 - 10.1	1,200 - 1,450	5.41 - 6.21	1.06 - 1.17
Pine (Lodgepole, Northern White, Western White and Ponderosa)	22-25	3.68 - 4.48 0.95 - 1.05	0.54 - 0.75 0.16 - 0.19	(22)	(23)	6.0 - 6.7 1.3 - 1.6	9.5 - 11.9	0.09 - 0.12	9.2 - 9.5	1,260 - 1,510	4.84 - 5.62	0.8 - 1.16
Pine (Southern Yellow and Norwegian)	30-32	4.82 - 6.15 1.05 - 1.20	0.83 - 1.19 0.16 - 0.28	(22)	(23)	7.7 - 9.4 1.6 - 2.6	12.1 - 15.9	0.16 - 0.19	12.5 - 14.7	1,760 - 1,990	7.08 - 8.44	1.23 - 1.50
Spruce (Eastern)	25	4.16 - 4.05 1.05	0.59 - 0.19 0.19	(22)	(23)	6.5 - 11.6 1.6	11.4	0.12	10.1	1,440	5.59	1.07 - 0.3
Plywood (Douglas Fir)	30	1.8 - 2.51	1.94 - 0.35 0.41	6.18	3.91	9.34 - 2.0 3.01		0.15 - 0.17		1,530	126	
Plywood (White Fir)	25		1.81 - 5.67	3.70		9.2				1,580	100	
Plywood (White Pine)	26	1.3 - 1.45	2.05 - 0.24 0.28	5.72	3.34	10.13 - 1.6 2.01		0.1 - 0.14		1,570	111	
Plywood (Southern Pine)		2.0 - 2.35	0.35 - 0.41			2.75 - 3.20		0.18 - 0.22		1,800		
Plywood (Hemlock)	29	1.65 - 2.31	1.96 - 0.33 0.35	6.8	4.58	9.25 - 2.3 2.41		0.13 - 0.15		1,580	112	

LEGEND FOR TABLE B.2-1

- (1) Strength in lb/in^2 on gross area if applicable. Values may be given as average values or as ranges. Values followed by letter "M" indicate minimum strength as approved by American Standards Association. Values followed by letter "D" indicate dynamic strength. Values in square brackets indicate allowable strength commonly recommended.
- (2) Modulus of Rupture is defined as the stress given by the formula M/I , where M is the maximum bending moment in a beam specimen loaded to rupture, I is the distance from the neutral axis to extreme fiber, and I is the area moment of inertia. It is also known as flexural tensile strength.
- (3) Fraction of ultimate tensile strength at 10^3 cycles of loading. The S-N curves of some common materials are shown in Figure B.2-6.
- (4) Both Young's Modulus of elasticity and modulus of rigidity are determined by static tests, except those values followed by a letter "D", which indicates from dynamic tests. Values of modulus of rigidity are given in square brackets.
- (5) This material damping term is defined as $\eta = 1/Q = 2\xi$, where Q is the dynamic magnification factor at resonance, and ξ is the critical damping ratio. C/C_c . Values of η are given for a frequency range of 100 to 1000 cps.
- (6) Determined by shock wave propagation method, a very fast rate of loading.
- (7) Strength also depends on size of glass plate.
- (8) Strength also depends on load duration, test period, aspect-ratio and nature of loading. See Figures B.2-1 through B.2-5 for various service conditions.
- (9) Lateral loading for glass block; or perpendicular loading for the case of mortar.
- (10) Bending parallel to fiber of surfacing.
- (11) Bending across fiber of surfacing.
- (12) Based on 10^3 cycles of loading.
- (13) Yield strength of structural steel.
- (14) Vertical compression load on wall sample. Values in psi.
- (15) Transverse load, lb/in^2 of surface area, based on equivalent uniform lateral loading on outside face.
- (16) A measurement of diagonal tension and shear strength, lb/in^2 , based on cross-sectional area of wall.
- (17) Maximum drop height, in feet, of a 60 lb sandbag that causes specimen failure. Wall span 7'-1 2/3' supported along top and bottom edges of interior face. Drop-load on exterior face.
- (18) Plaster cracks on interior side of wall.
- (19) Mortar cracks on exterior brick veneer.
- (20) Small clear specimen, free of defect, average moisture 12 percent for wood and timber, or 9 percent for plywood. For various service conditions, see Table B.2-2.
- (21) For clear material under long-time service at maximum design load and dry condition use.
- (22) Strength much higher than the corresponding compressive strength.
- (23) Approximately three times the corresponding values of the compressive strength.
- (24) Douglas fir:

Poisson's Ratio	Elasticity Ratio	Rigidity Ratio
$\mu_{LR} = 0.229$	$E_T/E_L = 0.050$	$G_{LR}/E_L = 0.064$
$\mu_{LT} = 0.450$	$E_R/E_L = 0.068$	$G_{LT}/E_L = 0.078$
$\mu_{RT} = 0.390$		$G_{RT}/E_L = 0.007$
$\mu_{RL} = 0.036$		
$\mu_{TL} = 0.029$	Loss Factor	
$\mu_{TR} = 0.374$	$\eta = 0.006 -$ $= 0.013$	

where subscripts L, R, and T indicate longitudinal, radial, and tangential respectively.

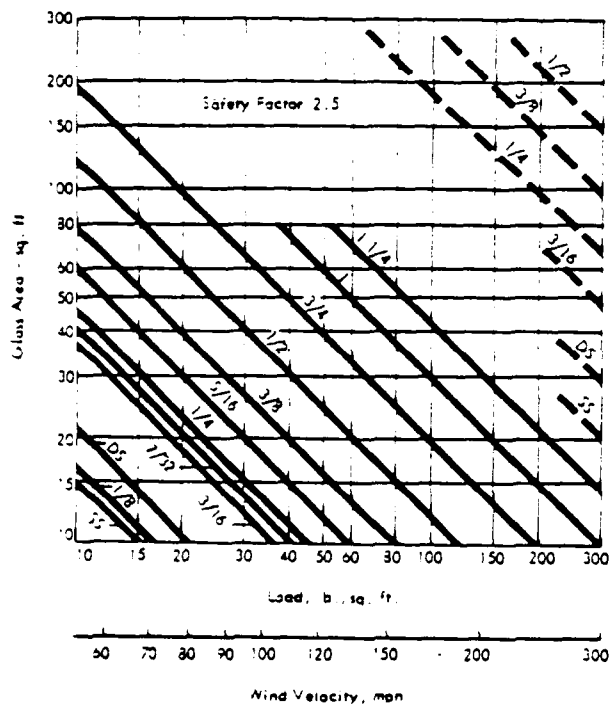


FIGURE B.2-1 Allowable Loads for Minimum Thickness of Rectangular Plate and Window Glass, Four Sides Supported, Subjected to Wind Load (Solid Lines) and Sonic Boom (Dashed Lines), or their Equivalents. One Minute Uniform Loading, Representative of "Fastest Mile Wind." Where Short Side/Long Side $\leq 1/3$, Adjust Glass Area By Using Figure 12.2.

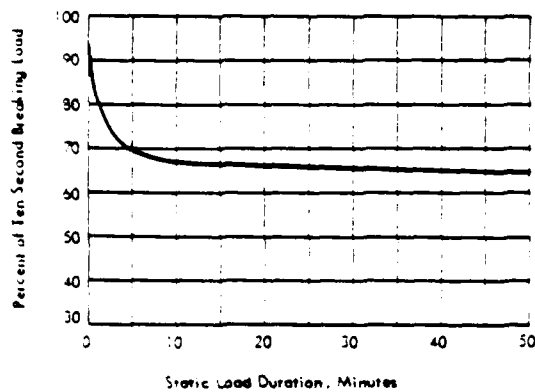


FIGURE B.2-3 Strength of Glass as Function of Load Duration

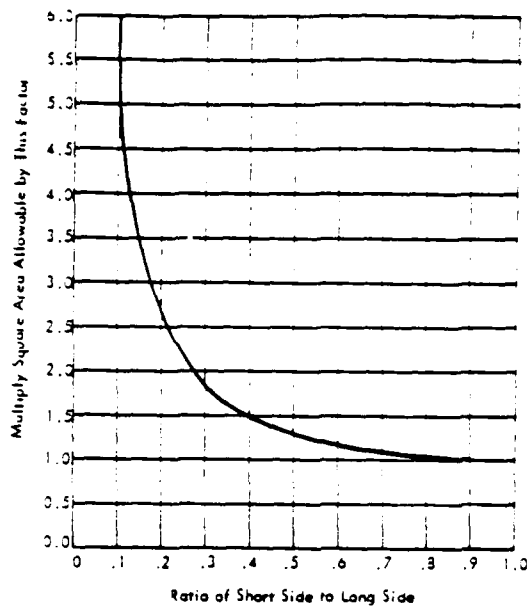


FIGURE B.2-2 Aspect-Ratio (Short Side/Long Side) Correction Factors for Rectangular Glass Panels.

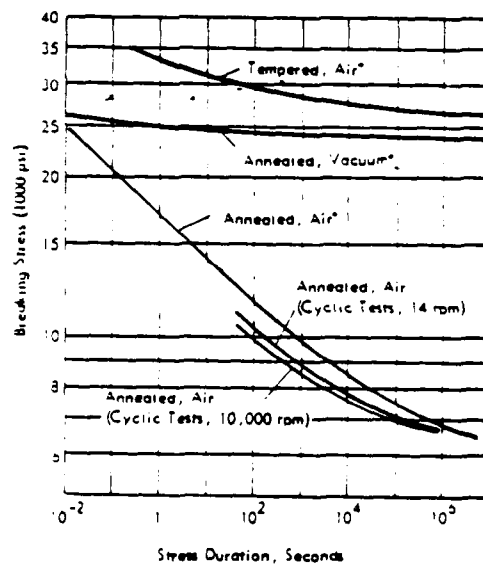


FIGURE B.2-4 Stress-Time Characteristics and Dynamic-Fatigue Characteristics of Glass at Room Temperature.

• Indicates Static Test.

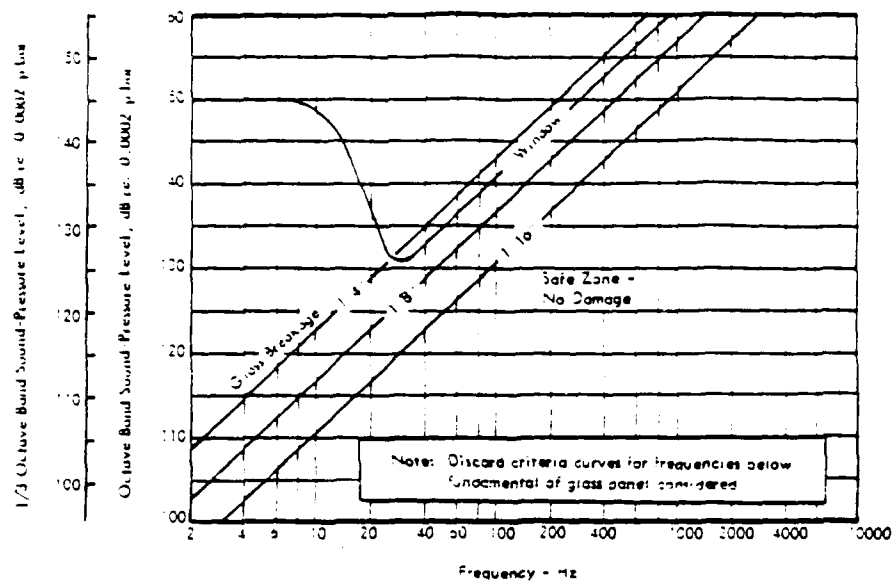


FIGURE B.2-5 Tentative Damage Criteria for Glass Panes of Various Thicknesses and Window Exposed to Random Acoustic Noise. Adopted from Regier, et al., "Noise Control," 4, 13-19, 1959.

TABLE B.2-2 Strength Variations of Wood and Lumber Under Various Service Conditions.

Strength Variations of Wood and Lumber Under Various Service Conditions, in Percentage Increase (+), or Decrease (-) from Small Clear Test Specimen as Defined in (20)	Density $\frac{b}{f}$	Fiber Strength at Proportion Limit Allowable Strength in Bracket				Ultimate Static Bending		Maximum Compression Crushing Strength	
		Compression		Bending		Max. Horiz. Shear	Mod. of Rupture		
		Par. to Grain	Perp. to Grain	Static	Impact		Parallel to Grain	Par. to Grain	Perp. to Grain
Slope of Grain with Respect to Straight Grain Load Application Slope = 1:5	1:40 1:20 1:10			0 -21 -48 -68	0 -10 -38 -64		0 -7 -9 -45	0 -4 -11 -33	
Full Size Common Grade Lumber with Ordinary Defects		0 to -40	0 to -50	0 to -50	0 to -50		0 to -60	0 to -50	0 to -50
Increase of Specimen's Moisture Content by 1%		-5	-5.5	-5	-3		-4	-2	-5
Possible Variation of an Individual Piece from Species Average	-8	-18	-21	-16	-13		-12	-16	-13
Temperature Effect, °F Douglas Fir	-20 0 40 70 100 140	-32 -25 -01 01 -11 -25		-25 -51 -81 -101 -25			15 to 40 0 to 35 5 to 15 0 -7 to -15 -4 to -38	3 to 18 3 to 15 1 to 10 0 -3 to -8 -8 to -28	20 to 50 10 to 40 5 to 51 0 -5 to -18 -10 to -40
Effect of Use Under Continuously Wet Condition or when Moisture Exceeds 16%		0 to -201	0 to -201	0 to -201		01			
Effect of Load Duration, in Days Douglas Fir	10 ⁻⁴ 10 ⁻² 1 10 ² 10 ⁴						-3 -6 -13 -31 -42		

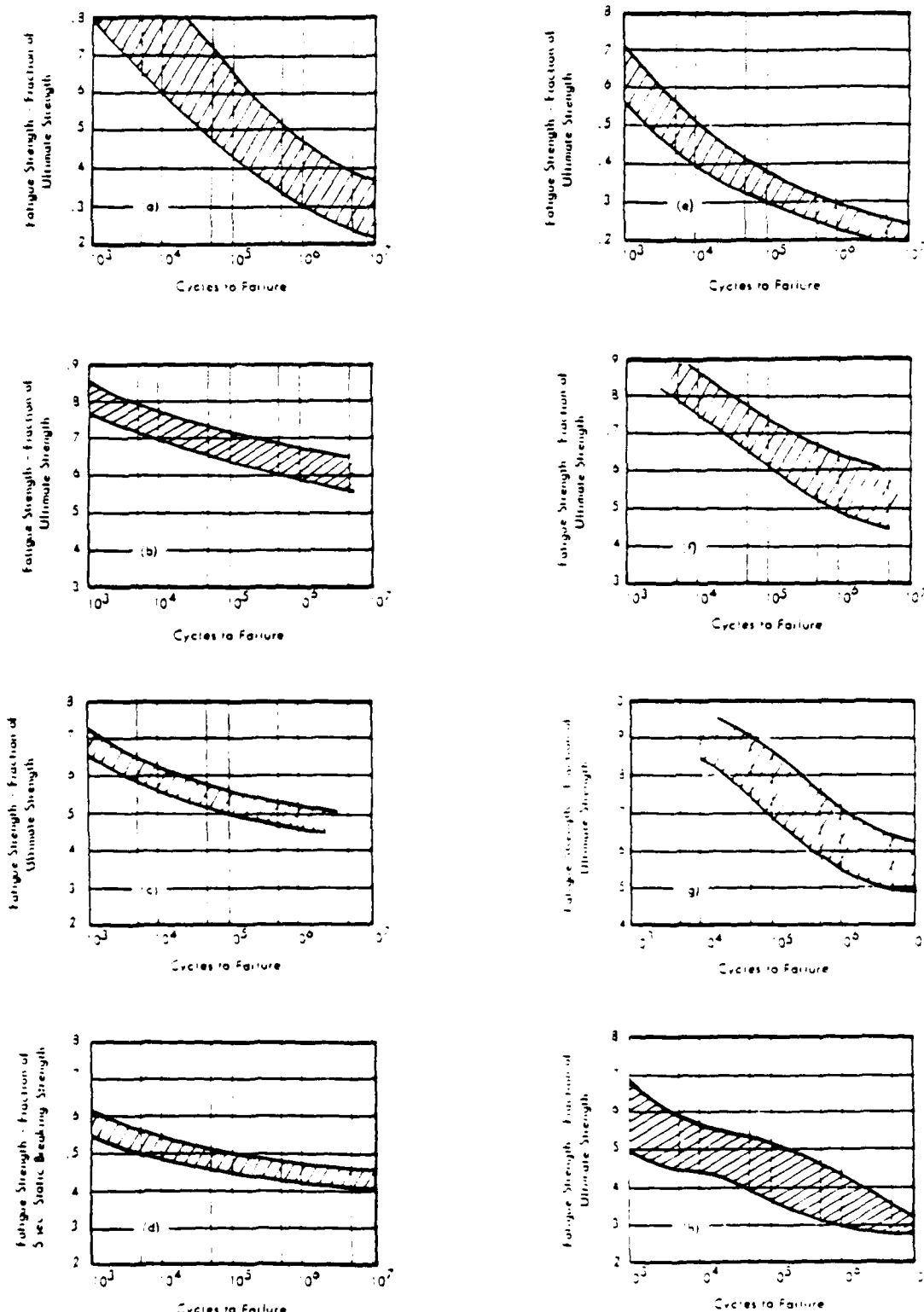


FIGURE B.2-6

Composite Stress-Cycle (S-N) Curves for Some Building Construction Materials, Subjected to Complete-Reversal-Repeated Loads Except Indicated. (a) Aluminum Alloys, Ref. 52, (b) Plain Concrete, Ref. 16, 27, (c) Reinforced Concrete, Ref. 16, 27, (d) Annealed Glass, Ref. 25, (e) Glass-Fiber Reinforced Plastic Laminates, Ref. 25, 54, (f) Wrought Steels, Ref. 51, 54, (g) High-Strength Low-Alloy Steels, Ref. 53, 54, and (h) Natural and Laminated Woods, (Solid Sinker, Spruce and Douglas Fir, and 5-Ply Yellow Birch and Yellow Poplar) (a) and (c) are Subjected to Zero-To-Maximum Repeated Loads.

REFERENCES FOR APPENDIX B

REFERENCES FOR SECTION B.2

1. Abbebt, R. W., "American Civil Engineering Practice," Vol. III, Wiley and Sons, 1957.
2. Merritt, F. S. Ed., "Building Construction Handbook," McGraw-Hill, 1958.
3. Miner, D. F. and Seastone, J. B., Editors, "Handbook of Engineering Materials," Wiley and Sons, 1955.
4. Mills, G. C. and Hayward, H. W., "Materials of Construction," 3rd Edition, Wiley and Sons, 1926.
5. Moor, H. F., "Materials of Engineering," 7th Edition, McGraw-Hill, 1947.
6. Davidson Brick Co., "Steeltyd and Modular Grouted Reinforced Brick Masonary Structural Design Manual," Los Angeles 22, Calif., 1956.
7. International Conference of Building Offices, California, "Uniform Building Code," Vols. I and III, 1964.
8. Whittemore, H. L., Ambrose, H. S. and Parsons, D. E., "Structural Properties of Six Masonry Wall Constructions," Building Materials and Structures Report BMS 5, National Bureau of Standards, 1938.
9. Monk, C. B., Jr., "Testing High Bond Clay Masonry Assemblages," from the Symposium on Masonry Testing Special Technical Publication, Number, 3201, Am. Soc. for Testing and Materials, 1962.
10. Monk, C. B., Jr., "SCR Brick Wall Tests," A Research Report by Structural Clay Products Research Foundation, 1965.
11. Chi, S. H., "Bibliography and Tabulation of Damping Properties of Non-Metallic Materials," University of Minnesota, 1962.
12. Parrott, T. L., "Experimental Studies of Glass Breakage due to Sonic Booms," Sound, Its Uses and Control, Vol. I, Number 3, pp. 18-21, Acoustical Soc. of Am., 1962.
13. Clary, R. R. and Leadbette, S. A., "Experimental Investigation of the Vibratory Responses and Structural Characteristics of Some Simulated Wall Panels," NASA Langley Working Paper 41, 1964.
14. Goldsmith, W., Polivka, M. and Yang, T., "Dynamic Behavior of Concrete," J. of Soc. for Experimental Stress Analysis, Vol. 6, Number 2, 1966.
15. "Significance of Tests and Properties of Concrete and Concrete Aggregates," ASTM Special Technical Publication, Number 169, 1956.
16. Am. Concrete Institute, "Fatigue of Concrete," ACI Bibliography 3, 1960.
17. Brady, G. S., "Material Handbook," 9th Edition, McGraw Hill, 1963.
18. Beranek, L. L., "Noise Reduction," McGraw-Hill, 1960.
19. F. W. Dodge Corp., "Sweet's Catalog Service," New York.
20. Norris, C. H., Hansen, R. J., Holly, M. J., Jr., Biggs, J. M., Namyet, S. and Minami, J. K., "Structural Design for Dynamic Loads," McGraw-Hill, 1959.
21. Dietz, A. G. H., "Materials of Construction, Wood, Plastics, Fabrics," Van Nostrand, 1949.
22. Forest Products Laboratory, "Forest Products Journal," Vol. XI, Number 9, U. S. Government Printing Offices, 1961.
23. Forest Products Laboratory, "Wood Handbook," Agriculture Handbook, Number 72, U. S. Government Printing Offices, 1955.
24. Engineering Manuals for Military Construction.
25. Shand, E. B., "Glass Engineering Handbook," McGraw-Hill, 1958.
26. A. S. T. M., "Cement; Lime; Gypsum," Part 9, ASTM Standards, Am. Soc. for Testing and Materials, 1965.
27. A. S. T. M., "Cement and Concrete," Am. Soc. for Testing and Materials, 1956.
28. A. S. T. M., "Mortars, Clay and Concrete Pipe and Tile; Masonry Units; Asbestos-Cement Products," Part 12, ASTM Standards, Am. Soc. for Testing and Materials, 1965.
29. Plummer, H. C. and Blume, J. A., "Reinforced Brick Masonry Lateral Force Design," Structural Clay Product Institute, Washington D. C., 1953.
30. ALCOA Structural Handbook, Al. Co. of Am.
31. A. I. S. C., "Steel Construction Manual," Am. Inst. of Steel Construction, 6th Edition.
32. Rothbart, H. A., Ed., "Mechanical Design and Systems Handbook," McGraw-Hill, 1964.
33. Whittemore, Stang, and Phelan, Building Materials and Structures Report BMS 9, National Bureau of Standards, 1938.

REFERENCES FOR APPENDIX B (CONTINUED)

34. Whittemore, Ambrose, and Parsons, Building Materials and Structures Report BMS 21, National Bureau of Standards, 1939.
35. Whittemore, Stang, and Parsons, Building Materials and Structures Report BMS 22, National Bureau of Standards, 1939.
36. Whittemore, Stang, and Parsons, Building Materials and Structures Report BMS 23, National Bureau of Standards, 1939.
37. Whittemore, Stang, Fishburn, Building Materials and Structures Report BMS 24, National Bureau of Standards, 1939.
38. Whittemore, Stang, and Parsons, Building Materials and Structures Report BMS 32, National Bureau of Standards, 1939.
39. Whittemore, Stang, and Wilson, Building Materials and Structures Report BMS 42, National Bureau of Standards, 1940.
40. Whittemore, Stang, and Wilson, Building Materials and Structures Report BMS 47, National Bureau of Standards, 1940.
41. Whittemore, Stang, and Luxford, Building Materials and Structures Report BMS 104, National Bureau of Standards, 1945.
42. Whittemore, Stang, and Phelan, Building Materials and Structures Report BMS 46, National Bureau of Standards, 1940.
43. Chan, G. C., "Fatigue of Reinforced Concrete Due to Sinusoidal and Random Loadings," Wyle Laboratories Report WR 66-40, Huntsville, Alabama, 1966.
44. Grover, H. J. and Gordon, S. A., "Fatigue of Metals and Structures," U.S. Government Printing Offices, 1960.
45. Whittemore, Stang, and Wilson, Building Materials and Structures Report BMS 31, National Bureau of Standards, 1939.
46. Whittemore, Stang, and Wilson, Building Materials and Structures Report BMS 30, National Bureau of Standards, 1939.
47. Whittemore, Stang, and Wilson, Building Materials and Structures Report BMS 48, National Bureau of Standards, 1940.
48. Machine Design, Vol. 38, Number 14, "Plastics," A Penton Publication, Cleveland, June 16, 1966.
49. Machine Design, Vol. 35, Number 22, "Non-ferrous Metals Book," A Penton Publication, Cleveland, 1963.
50. Machine Design, Vol. 37, Number 21, "Metals," A Penton Publication, Cleveland, 1965.
51. Lipson, C. and Juvinall, R. C., "Application of Stress Analysis to Design and Metallurgy," Handbook of Stress and Strength, MacMillan, 1963.
52. Grover, H. J., Gordon, S. A. and Jackson, L. R., "Fatigue of Metals and Structures," U.S. Government Printing Offices, 1960.
53. Information from McLouth Steel Corp., Detroit, Michigan.
54. Cummings, H. N., "Some Quantitative Aspects of Fatigue of Materials," WADD Technical Report 60-42, 1960.

APPENDIX C

Analytical Background

- C.1 Relationship Between Various Spectral Measures of Sonic Booms
- C.2 Multimodal Response of Simply Supported Panel to Normally Incident Sonic Boom

Appendix C – Analytical Background

C.1 Relationship Between Various Spectral Measures of Sonic Boom

For a finite pressure pulse $P(t)$ starting at time 0 and ending at time T , the Fourier Spectra $P(f)$, or, for simplicity in notation, $P(f)$, is:

$$P(f) = \int_0^T P(t) e^{-j2\pi ft} dt, \quad \text{psf} \cdot \text{sec} \quad (1)$$

The Energy Spectral Density $E(f)$ is, by definition (Kryter, et al., 1966):

$$E(f) = |P(f)|^2 \quad (\text{psf} \cdot \text{sec})^2 \quad (2)$$

$$\text{The mean square pressure } \overline{P^2} \text{ is } \left(\frac{1}{T}\right) \int_0^T P(t) \cdot P(t) dt = SE/T \quad (3)$$

where SE is the sound exposure for the event over its duration T .

But, from the inverse Fourier transform, $P(f) = \int_{-\infty}^{+\infty} P(f) e^{j2\pi ft} df$, then

$$\overline{P^2} = \left(\frac{1}{T}\right) \int_0^T P(t) \left[\int_{-\infty}^{+\infty} P(f) e^{j2\pi ft} df \right] dt, \quad (\text{psf})^2 \quad (4)$$

Since the complex conjugate $P^*(f)$ of $P(f) = \int_0^T P(t) e^{-j2\pi ft} dt$ and changing the order of integration in Eq. (4) and since the complex Fourier spectrum is symmetrical about a zero frequency:

$$\overline{P^2} = \left(\frac{1}{T}\right) \int_{-\infty}^{+\infty} P^*(f) \cdot P(f) df = \frac{2}{T} \int_0^{\infty} |P(f)|^2 df \quad (5)$$

Now, define the Sound Exposure Spectral Density $SE(f)$, such that the integral of this spectrum from 0 to infinite frequency is the sound exposure SE , or:

$$SE = \int_0^{\infty} SE(f) df \quad (\text{psf})^2 \cdot \text{sec} \quad (6)$$

Combining Eq. (3) and Eq. (5), $SE = 2 \int_0^{\infty} |P(f)|^2 df$ so, equating the integrands,

$$SE(f) = 2|P(f)|^2 \quad (\text{psf})^2(\text{sec})^2 \quad (7)$$

Therefore, from Eq. (2) $SE(f) = 2 E(f)$ (8)

To evaluate the dynamic transient response of undamped systems to a transient pressure pulse, the Residual Shock Spectrum $D_R(f)$ is useful since it defines the envelope of peak responses versus natural frequency f_0 of the system when the peak response occurs after the end of the transient pulse. It can be shown that $D_R(f)$ is related to $P(f)$ by (Ayre, 1961):

$$D_R(f) = (2\pi f_0) |P(f)| \text{ psf} \quad (9)$$

where f_0 = natural frequency of the responding system. Thus, from Eq. (7):

$$D_R(f) = 2\pi f_0 \left[\frac{1}{2} SE(f) \right]^{1/2} \quad (10)$$

As shown in Section 4 of the main body of this report, the most useful response parameter is peak velocity V_{pk} . For a single degree of freedom system it is shown in the next section that this response can be expressed as a Residual Velocity Shock Spectrum $V_R(f_0)$ in a dimensionless form as:

$$\frac{V_R(f)(2\pi f_0)}{g} = \frac{D_R(f)}{w} \quad (11)$$

where f_0 = resonance frequency of SDOF system, Hz

$D_R(f)$ = Residual Pressure Shock Spectrum, psf

w = surface weight of responding system in psf

g = acceleration of gravity, 386 in/sec²

Thus, from Eqs. (7) and (9) to (11),

$$V_R(f) = \frac{g}{2\pi f_0} \cdot \frac{2\pi f_0}{w} |P(f)| = \frac{g}{w} |P(f)|, \text{ or} \quad (12)$$

$$V_R(f) = \frac{g}{w} \sqrt{\frac{1}{2} SE(f)} \text{ in/sec} \quad (13)$$

where the peak velocity $V_R(f)$ ($= V_{pk}$) is understood to occur at the natural resonance frequency $f = f_0$ of a single degree of freedom (i.e., undamped mass-spring) system.

Thus, a simple expression is established relating the Sound Exposure Spectrum $SE(f)$ of a sonic boom to the Residual Velocity Shock Spectrum $V_R(f)$ for the response of an undamped SDOF system, both being evaluated at the natural resonance frequency $f = f_0$ of the system. In reality, of course, any structure will have many natural frequencies, one for each vibration mode, and Eqs. (12) and (13) simply provide one way to estimate the envelope of these peak velocity responses. Consider, now, what is the expected form of this velocity response spectrum. The absolute value of the Fourier Spectrum $|P(f)|$ for an ideal N-wave with a peak free field (pressure doubling included) pressure P_f is given by (Sutherland, 1968a):

$$|P(f)| = \frac{P_f}{\pi f} \left| \frac{\sin(\pi f T)}{\pi f T} - \cos(\pi f T) \right| \quad (14)$$

where T = full duration of N-wave. Then from Eq. (9) and for $f = f_0$:

$$D_R(f_0) = 2 P_f \left| \frac{\sin(\pi f_0 T)}{\pi f_0 T} - \cos(\pi f_0 T) \right| = P_f DAF(f) \quad (15)$$

where, in this case, $DAF(f)$ is the dynamic amplification factor for an ideal N-wave sonic boom. Finally, from Eq. (11), the Residual Velocity Shock Spectrum, $V_R(f)$ as a function of the fundamental resonance frequency f_0 , is:

$$V_R(f) = \frac{g D_R(f)}{2 \pi f_0 w} = \frac{2 g P_f}{2 \pi f_0 w} \left| \frac{\sin(\pi f_0 T)}{\pi f_0 T} - \cos(\pi f_0 T) \right|, \text{ in/sec} \quad (16)$$

The product of the Residual Shock Spectrum $V_R(f)$ and w/P_f is plotted in Figure C-1 as a function of resonance frequency f_0 for an N-wave, duration T , of 0.10. Also shown is the envelope for $T = 0.1$ and 0.2 sec. The lower duration value is essentially the same as the value derived from the average Sound Exposure Spectrum Levels for the ACM sonic boom measurements obtained in this program (see Figure 3-14b).

For design purposes, it is desirable to establish an envelope for the upper bound of this velocity shock response.

For low frequencies, as $fT \rightarrow 0$, expanding the sin and cos terms,

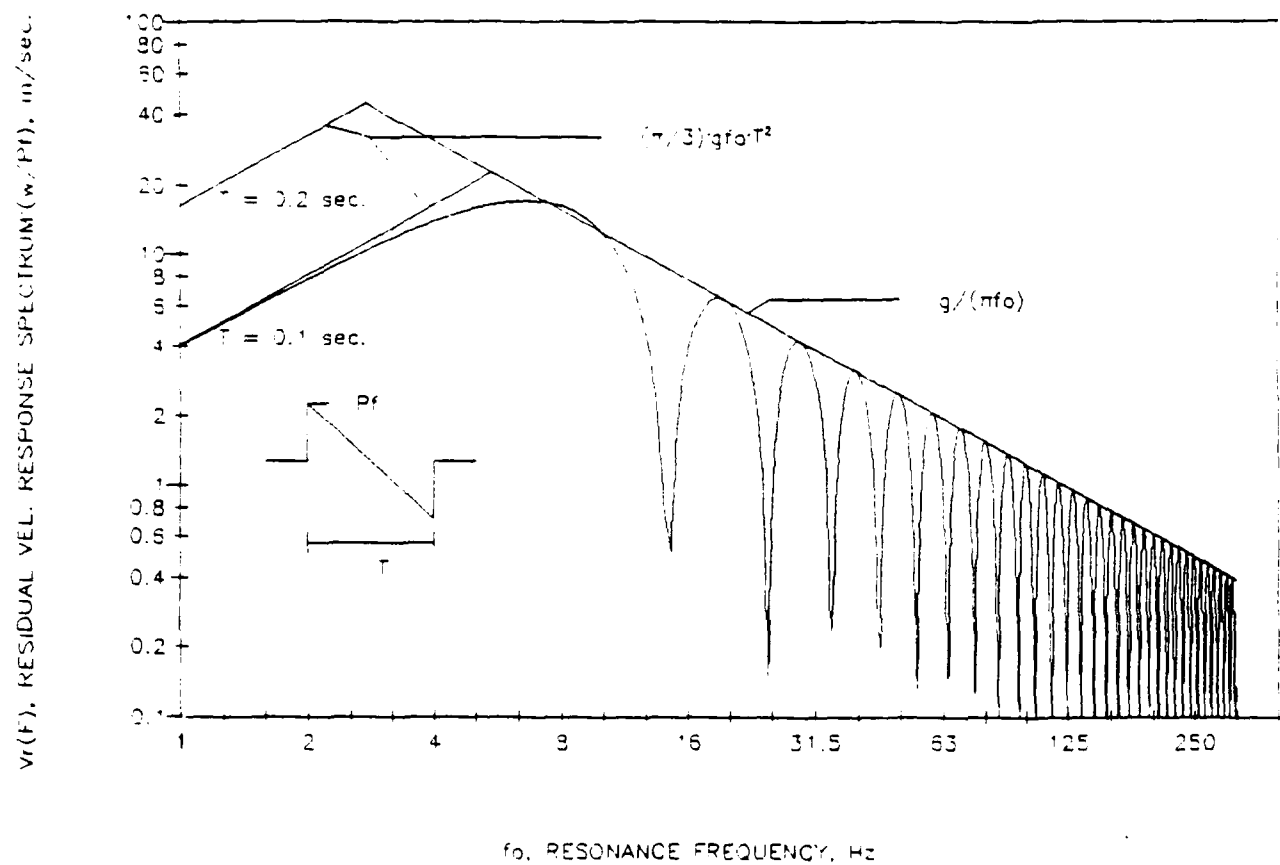


Figure C-1. Residual Velocity Shock Spectrum for Response of Undamped SDOF System to Ideal N-Wave.

$$\frac{\sin \pi f T}{\pi f T} \rightarrow 1 - \frac{(\pi f T)^2}{6} \text{ for } f T \rightarrow 0$$

and

$$\cos \pi f T \rightarrow 1 - \frac{(\pi f T)^2}{2} \text{ for } f T \rightarrow 0$$

so the low frequency asymptote for $V_R(f)$ is:

$$\begin{aligned} V_R(f) &\rightarrow \frac{2gP_f}{2\pi f_0 w} \left| 1 - \frac{1}{6}(\pi f_0 T)^2 - 1 + \frac{1}{2}(\pi f_0 T)^2 \right| \\ &\rightarrow \frac{gP_f}{\pi f_0 w} \left(\frac{1}{3}\pi^2 f_0^2 T^2 \right) = \frac{\pi}{3} \frac{gP_f}{w} f_0 T^2 \end{aligned} \quad (17)$$

For high frequencies, the envelope of $\left| \frac{\sin x}{x} - \cos x \right| \rightarrow 1$ for $x \rightarrow \infty$, so:

$$V_R(f) \rightarrow \frac{2gP_f}{2\pi f_0 w}, \quad f_0 \rightarrow \infty \quad (18)$$

These two asymptote trends meet at a frequency f_{\max} given by:

$$f_{\max} = \sqrt{3}/\pi T \quad (19)$$

C.2 Response of a Simply Supported Panel to a Normally Incident Sonic Boom

It has been shown in Crocker, 1967, that the multimodal displacement response $G(X,Y,t)$ at any position X,Y and time t on a panel to a sonic boom with a pressure time history $P(t)$ acting normal to the panel is given by the summation over all modes of the product of the generalized displacement $\epsilon_{mn}(t)$ for the m,n th modal response and the shape $g_{mn}(X,Y)$ of this mode, or:

$$G(X,Y,t) = \sum_m \sum_n \epsilon_{mn}(t) g_{mn}(X,Y) \quad (20)$$

for a simply supported plate,

$$g_{mn} = \sin(\pi m X/a) \sin(\pi n Y/b) \quad (21)$$

where m and n are mode numbers (i.e., number of one-half bending wavelengths) along the panel sides a and b respectively.

The generalized displacement $\epsilon_{mn}(t)$ is the maximum displacement amplitude in each mode which occurs at panel positions $X = a/2m$ and $Y = b/2n$ for the m,n th mode. For example, for the 1,1 fundamental panel mode, the maximum displacement occurs at the middle of the panel (i.e., $X = a/2$, $Y = b/2$).

For transient excitation by a normally incident sonic boom of peak free field pressure P_f (including pressure doubling) and duration T , the generalized displacement response $\epsilon_{mn}(t)$ following cessation of the sonic boom, that is, the residual response, can be shown to be (Crocker, 1987):

$$\epsilon_{mn}(t) \Big|_{t > T} = \frac{4abP_f}{mn\pi^2 M_{mn}\omega^2} \left[2 \left(\frac{\sin \omega T/2}{\omega T/2} - \cos \omega T/2 \right) \cos \omega(T/2 - t) \right] \quad (23)$$

where P_f = Peak free field pressure of N-wave

m,n,a,b = Odd mode numbers and panel sides as defined above

ω = $2\pi f_{mn}$ = Angular resonance frequency for m,n th mode, radians/sec

For this case of a normally incident sonic boom, the response is zero if either mode number m or n is even.

The generalized mass of M_{mn} of any uniform panel vibrating in its m,n th mode is given by:

$$M_{mn} = \frac{w}{g} \int_0^a \int_0^b g_{mn}^2(X,Y) dx dy \quad (24)$$

where w = the uniform surface weight of the panel with a total weight wA and area $A = ab$, and

g = acceleration of gravity.

For a simply supported panel, with $g_{mn}(X,Y)$ given by Eq. (22), this reduces to:

$$M_{mn} = \frac{1}{4} wab/g \quad (25)$$

The m,nth resonance frequency f_{mn} for a simply supported panel with sides a,b can be conveniently given by:

$$f_{mn} = f_0 [(mb/a)^2 + n^2] / [(b/a)^2 + 1] \quad (26)$$

where f_0 = the fundamental resonance frequency for the m,n = 1,1 mode of the panel (see Section 4.3.1.2 in main body of text)

Since Eq. (23) is for the free (unforced) undamped vibration response of the panel after the cessation of the N-wave, the velocity response $V_{mn}(t)$ for the m,nth mode is simply equal to $2\pi f_{mn}$ times the displacement response or with Eq. (25):

$$V_{mn}(t) = \frac{16P_f g}{\pi^2 mn (2\pi f_{mn}) w} \left[2 \left(\frac{\sin(\pi f_{mn} T)}{\pi f_{mn} T} - \cos(\pi f_{mn} T) \right) \cos(2\pi f_{mn}(T/2 - t)) \right] \quad (27)$$

Comparing this expression with Eq. (16) in Section C.1, it can be shown that Eq. (27) can be expressed as:

$$V_{mn}(t) \Big|_{t > T} = \frac{16}{\pi^2 mn} [V_R(f_{mn})] \cos[2\pi f_{mn}(T/2 - t)] \quad (28)$$

Thus, the time history of the multimodal residual velocity response of a panel in its m,nth mode following excitation by a normally incident N-wave is simply equal to the peak velocity response $V_R(f_{mn})$, predicted for a simple, mass-spring system given by Eq. (16), at a frequency f_{mn} multiplied by: a modal constant $16/\pi^2 mn$ (with m,n odd), and the cosine time function.

To find the total multimodal response, it is necessary to sum these time histories over odd mode numbers m and n and determine the peak envelope of this time history as a function of a non-dimensional parameter $f_0 T$ for several aspect ratios a/b of a simply supported panel. For this evaluation, it is convenient to divide Eq. (27) by the dimensionless ratio of the free field sonic boom pressure P_f to the surface weight w. In this form, the total multimodal velocity responses $V_T(t)$ can be expressed as the double summation:

$$\begin{aligned} \frac{V_T(t)}{(P_f/w)} = \sum_m \sum_n \frac{16g}{\pi^3 mn f_{mn}} & \left[\frac{\sin(\pi f_0 T \cdot (f_{mn}/f_0))}{(\pi f_0 T)(f_{mn}/f_0)} \right. \\ & \left. - \cos(\pi f_0 T (f_{mn}/f_0)) \right] \cos[2\pi f_0 T (f_m/f_0) (\frac{1}{2} - t/T)] \end{aligned} \quad (29)$$

The envelope of the absolute value of the peaks of this total modal (residual) response time history becomes the multimodal Residual Velocity Response Spectrum for an undamped simply supported panel. This can be compared then with the comparable velocity response spectrum envelope for the simple mass-spring SDOF model defined by Eqs. (17) and (18).

For example, for the response of just the first mode of a panel, with $f_{mn} = f_0$, the envelope of the first term in Eq. (29) (with $m,n = 1$) would simply be $16g/\pi^3 f_0$. This can be compared to the expected value from Eq. (18) (for the usual case where $f_0 T > \sqrt{3}/\pi$) for the SDOF model which is simply $g/\pi f_0$. The ratio of these two factors is $16/\pi^2 \sim 1.62$ as expected according to Eq. (28). This is simply the adjustment to the SDOF response model to account for the effective mass and load, for normal incidence of a sonic boom, of a simply supported panel.

Figures C.2 a to d show the normalized velocity response spectrum given by Eq. (29) as function of frequency for $T = 0.1$ and 0.2 seconds and for an aspect ratio (a/b) of a simply supported panel of 1.0 and 0.2 which encompasses the basic range of interest for this report. The summation was carried for the first five odd modes in each direction ($m,n = 1, 3, 5, 7$ and 9). This was found to be adequate to define the total multimodal response within an average error of $\pm 1.5\%$. Also shown are the Residual Velocity Response spectrum envelope for the SDOF model from Eq. (17) and (18) and the corresponding envelope for the multimodal response spectrum. This latter envelope turns out to be closely approximated by simply increasing the response spectrum envelope from Eq. (17) and (18) by a factor of 2.

In summary, a proper model for velocity response of a simply supported panel has a Residual Velocity Response Spectrum envelope for the first panel mode which is 1.62 times the value for a mass-spring SDOF model and approximately 2 times the SDOF value when higher modes are included. This factor of 2 increase is included in Section 4.1.1 as an approximate correction for multimodal response of walls and ceilings of built-up structures.

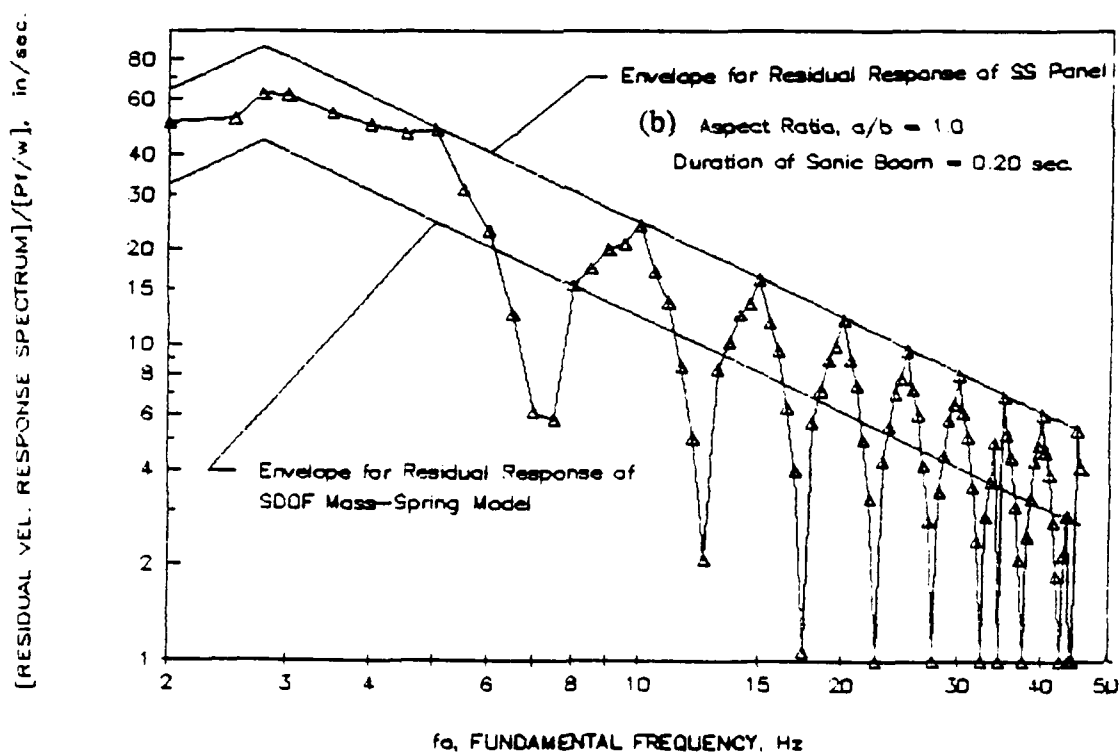
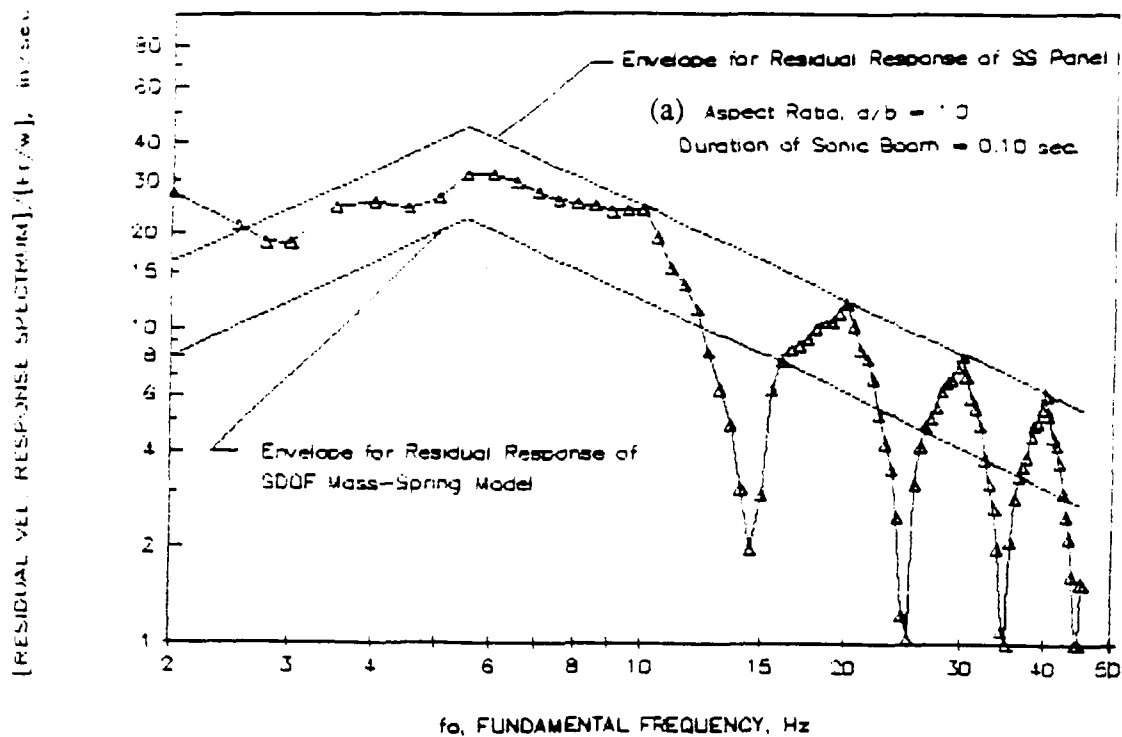
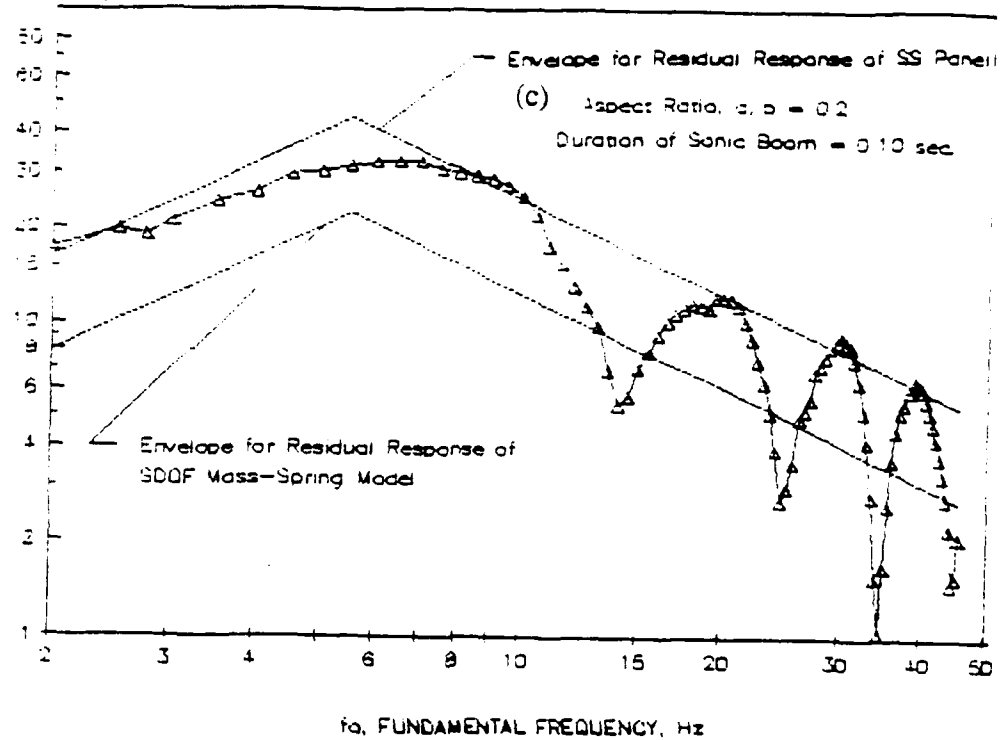


Figure C-2. Residual Multimodal Velocity Response Spectrum for an Undamped Simply Supported Panel with Aspect Ratio = 1.0 (a,b) and 0.2 (c,d) Driven by a Normally Incident Sonic Boom with Durations of 0.1 and 0.2 Seconds Compared to Envelopes for this Spectrum and Envelope, Lower by a Factor of 2, for the Comparable Response Spectrum for a SDOF System.

[RESIDUAL VEL. RESPONSE SPECTRUM]/[P1/w], in./sec.



[RESIDUAL VEL. RESPONSE SPECTRUM]/[P1/w], in./sec.

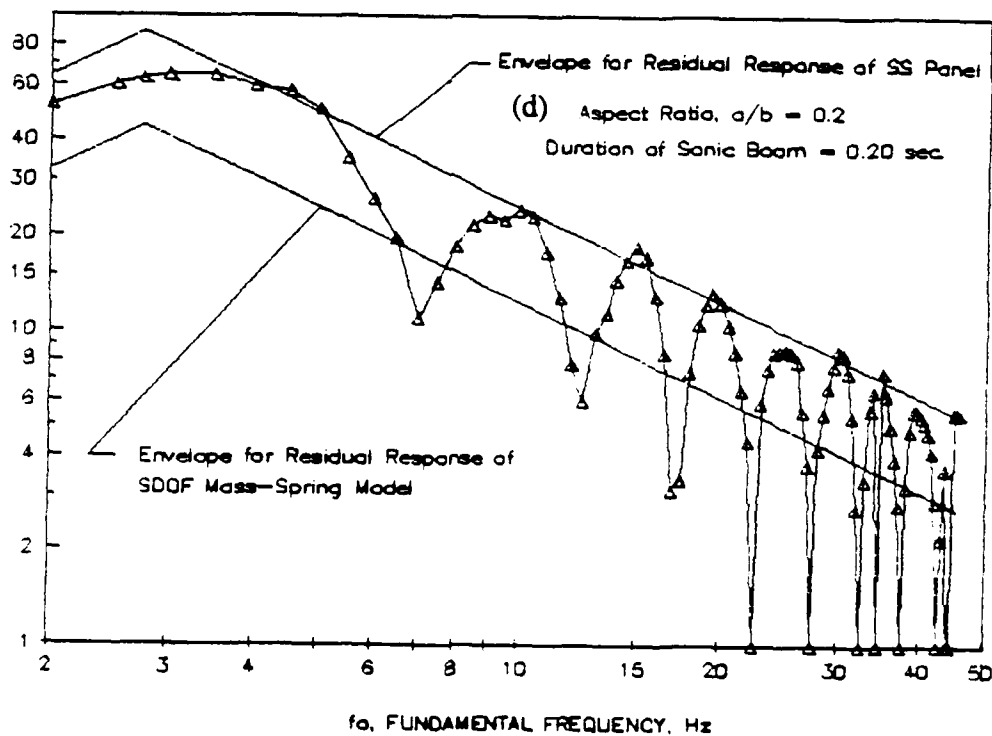
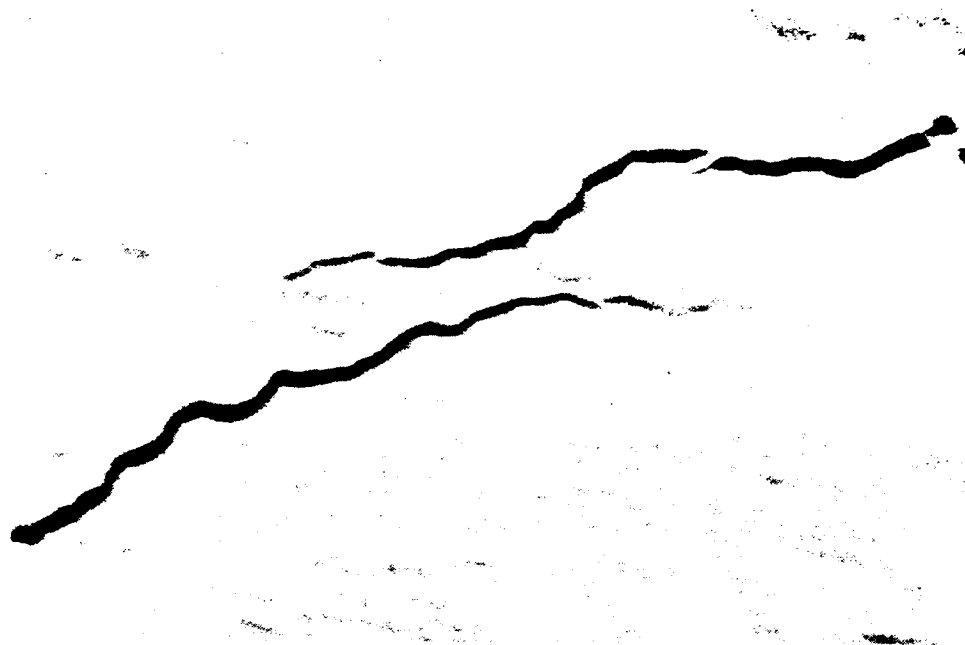


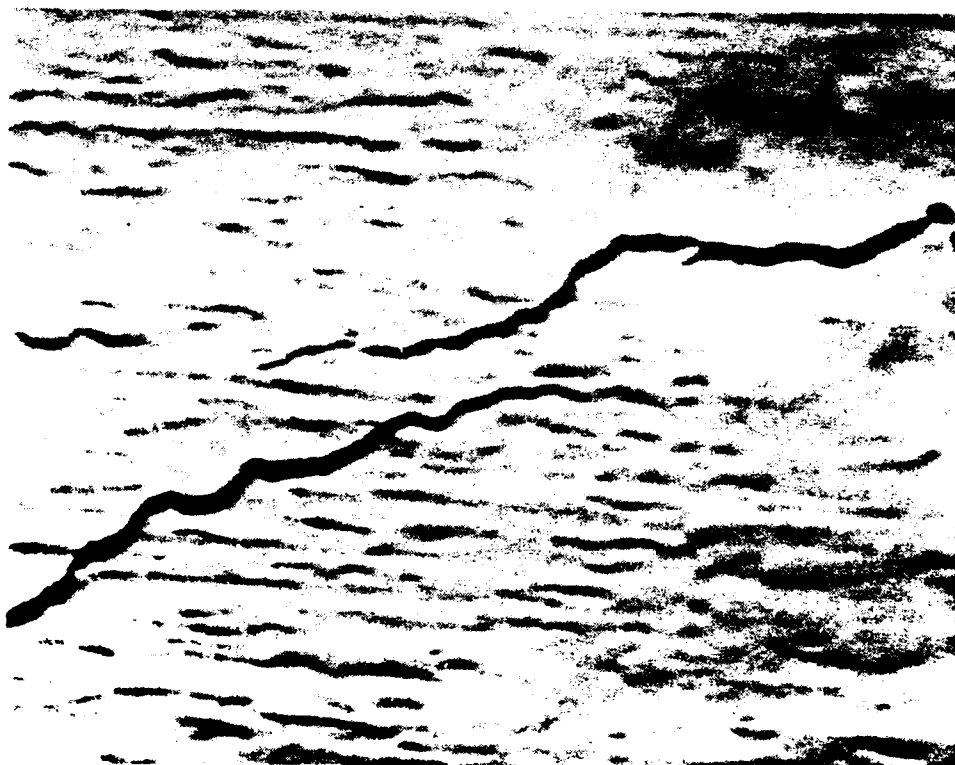
Figure C-2. (Continued)

APPENDIX D

Photographs of Structure A Walls Before and After Tests



(a) Pre-Test Photograph

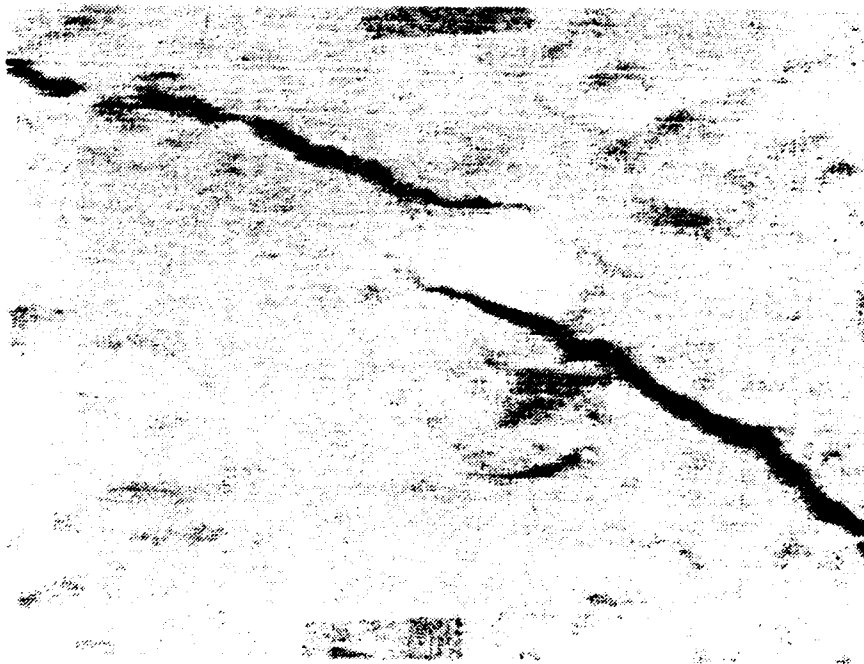


(b) Post-Test Photograph

Figure D-1. Room 102 North Wall, Main Wall Crack

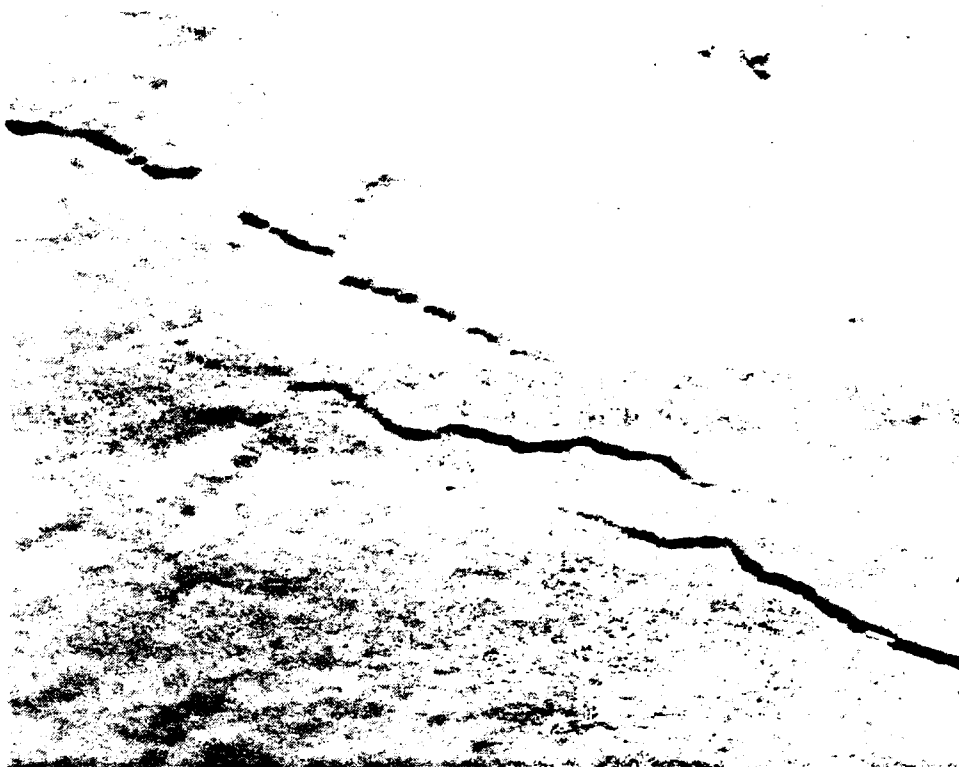


(a) Pre-Test Photograph



(b) Post-Test Photograph

Figure D-2. Room 101 South Wall, Middle of Wall



(a) Pre-Test Photograph



(b) Post-Test Photograph

Figure D-3. Room 101 South Wall, Cracks Up to Trim

APPENDIX E

Time Histories of Sonic Boom Pressure and Structural Response of Structures A and B

Amplitudes of the events shown in the time history plots in this Appendix are contained in Table 5-3. Notable features of these plots are as follows:

- For Structure A, Channel 0 (Figures E-1, E-2 and E-3) is acoustic pressure, Channel 8 is displacement, and all other channels are acceleration. For Structure B (Figure E-4), Channel 0 is acoustic pressure, Channels 6 and 7 are displacement, and all other channels are acceleration.
- Plots of the acoustic pressure of the sonic booms are distorted by the limited low frequency response of the acoustic channel. The low frequency cut-off of approximately 2 Hz causes the decaying ramp of the N-wave to be curved upward. Many of the booms were truly U-shaped and there were several multiple boom events caused by more than one aircraft.
- For each event, the position of the boom pressure in its plot indicates the approximate time the structural response should begin in the other plots.
- For some events, particularly at Structure B, very low frequency interference is apparent for some plots that could not be explained but may be due to shifts in the transducer fixity to the wall resulting from the necessary nonrigid accelerometer attachment method employed for these historic structures (see discussion in Section 5.2.3 of the main body of this report).

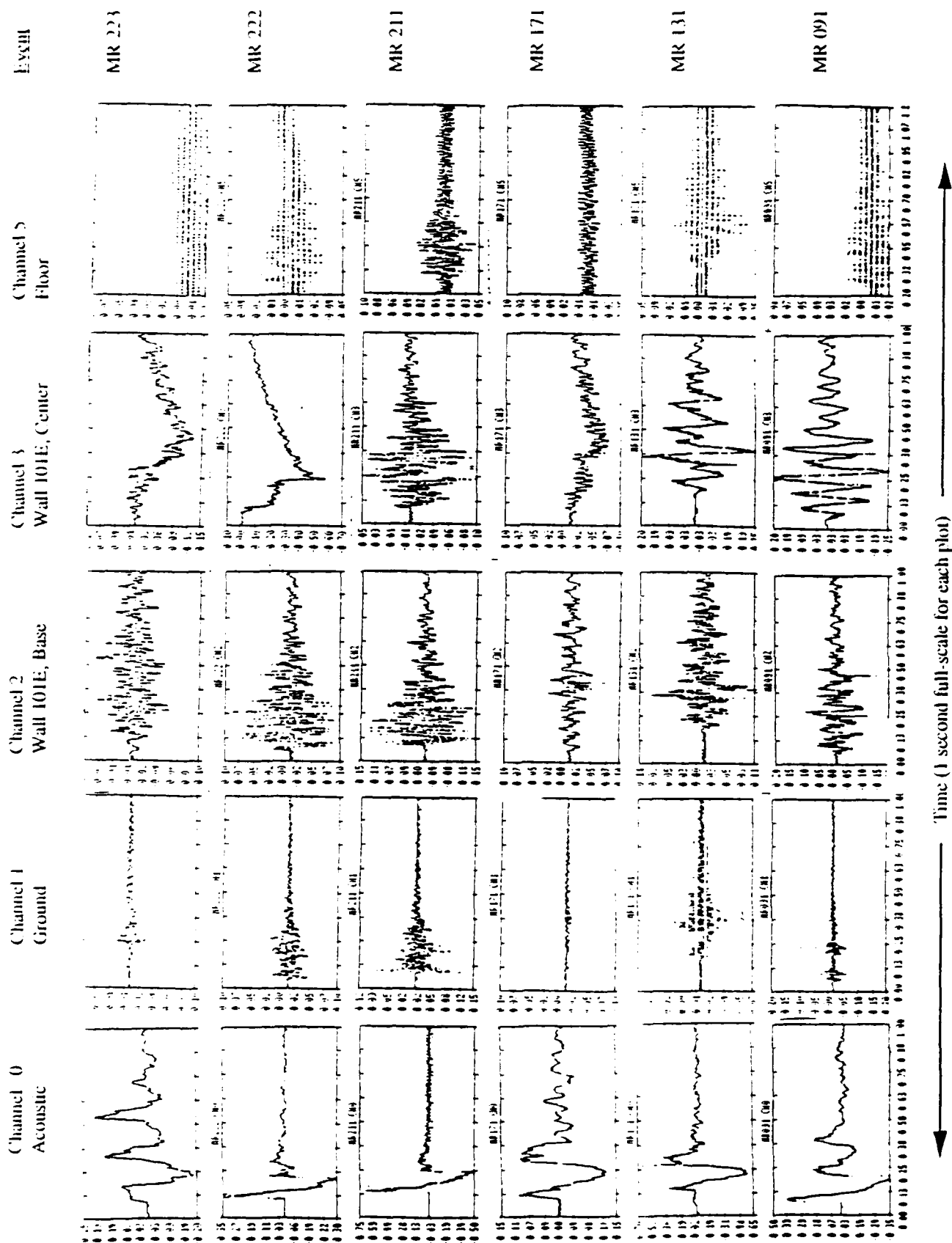


Figure E-1a. Matrix of Time History of Sonic Boom Pressure and Structural Response for Events at Structure A

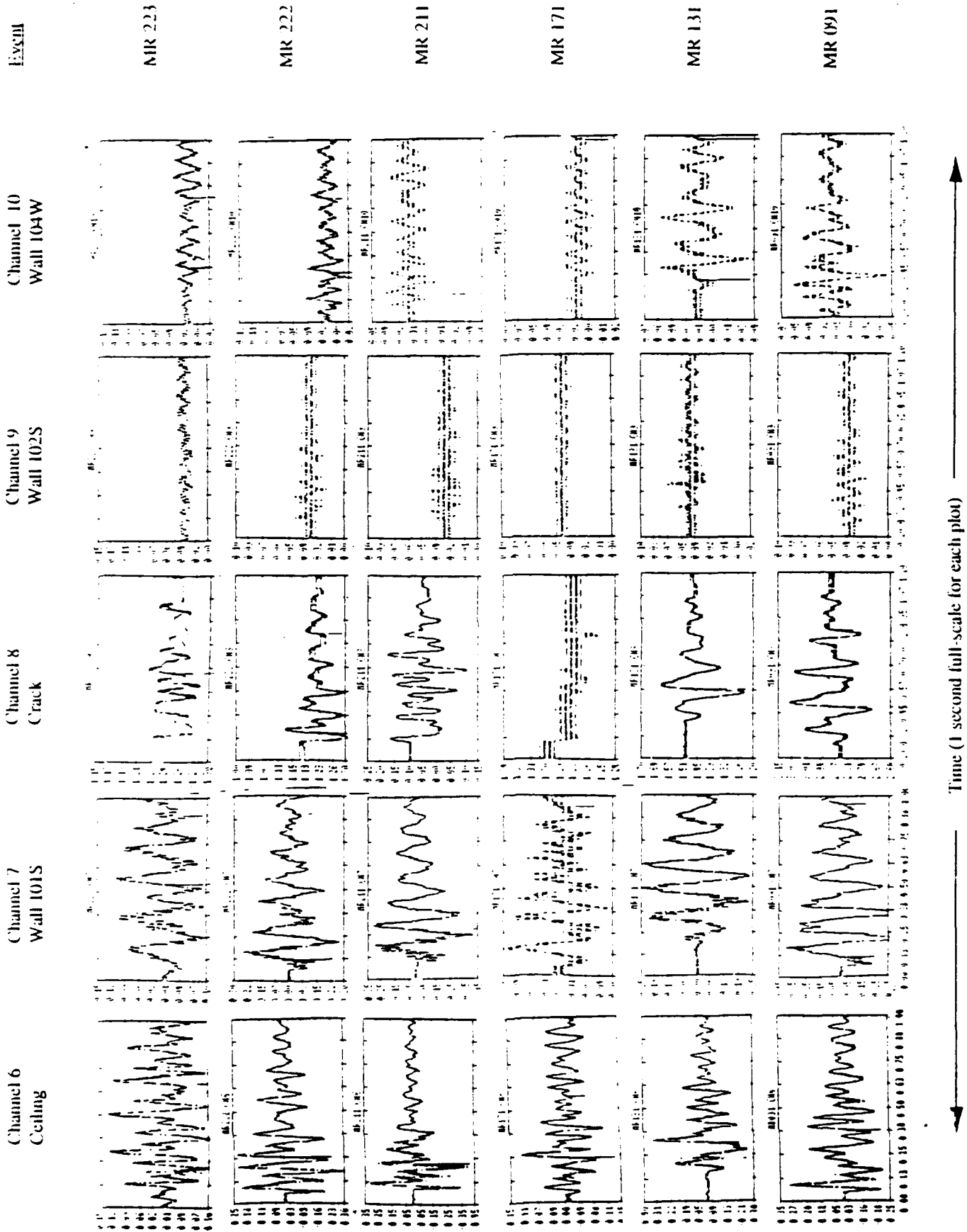


Figure E-1b. Matrix of Time History of Sonic Boom Pressure and Structural Response for Events at Structure A

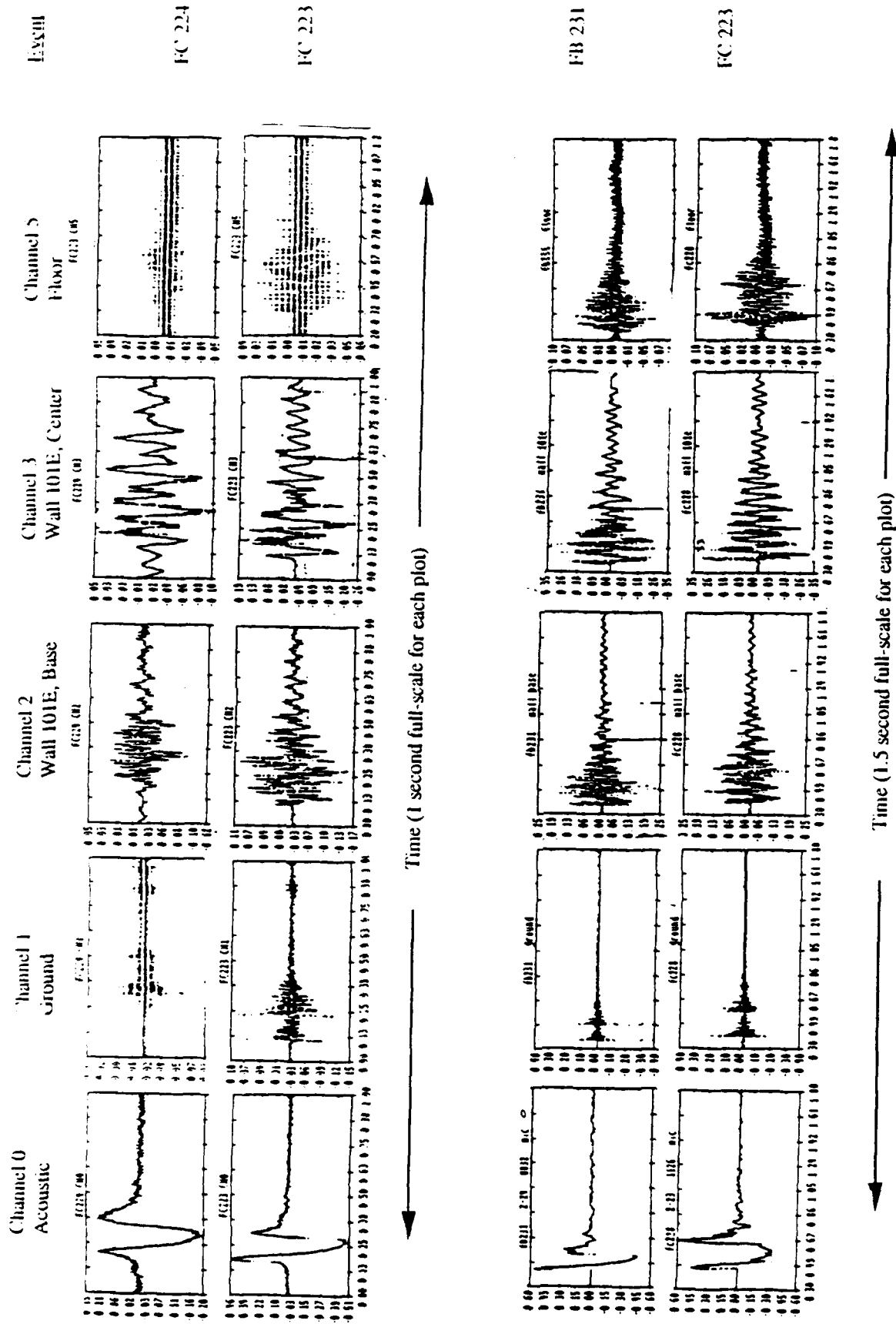


Figure E-2a. Matrix of Time History of Sonic Boom Pressure and Structural Response for Events at Structure A

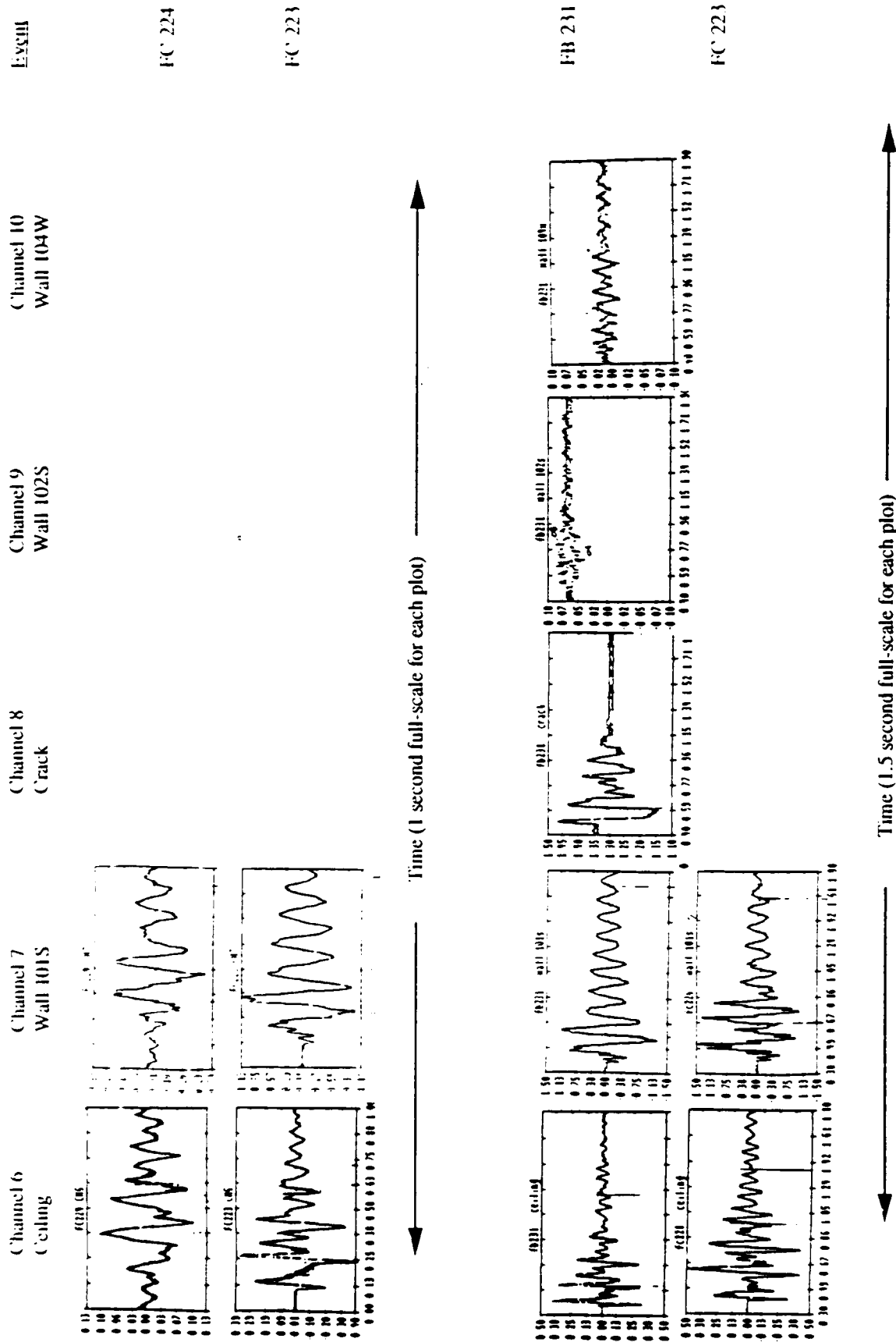


Figure E-2b. Matrix of Time History of Sonic Boom Pressure and Structural Response for Events at Structure A

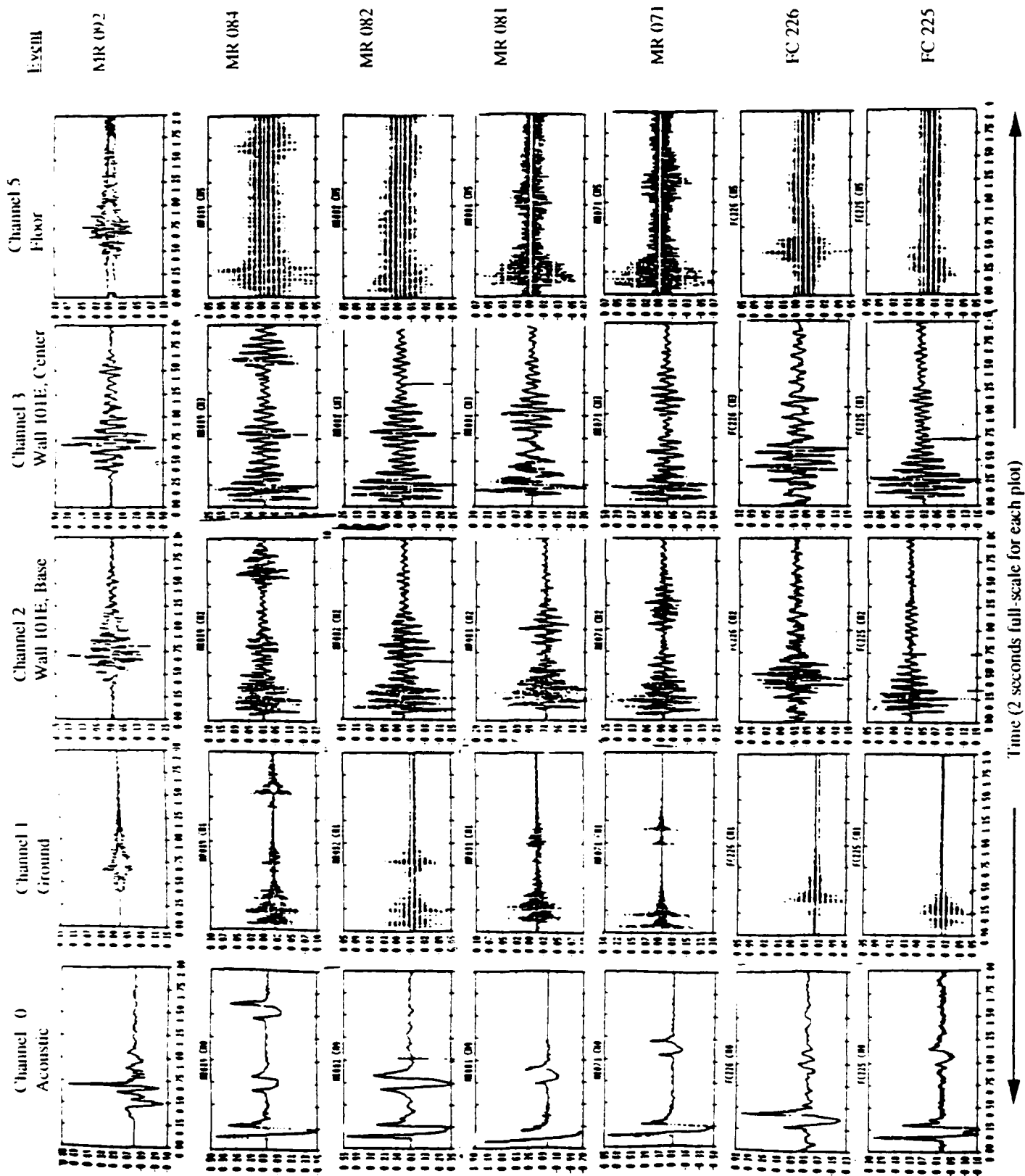
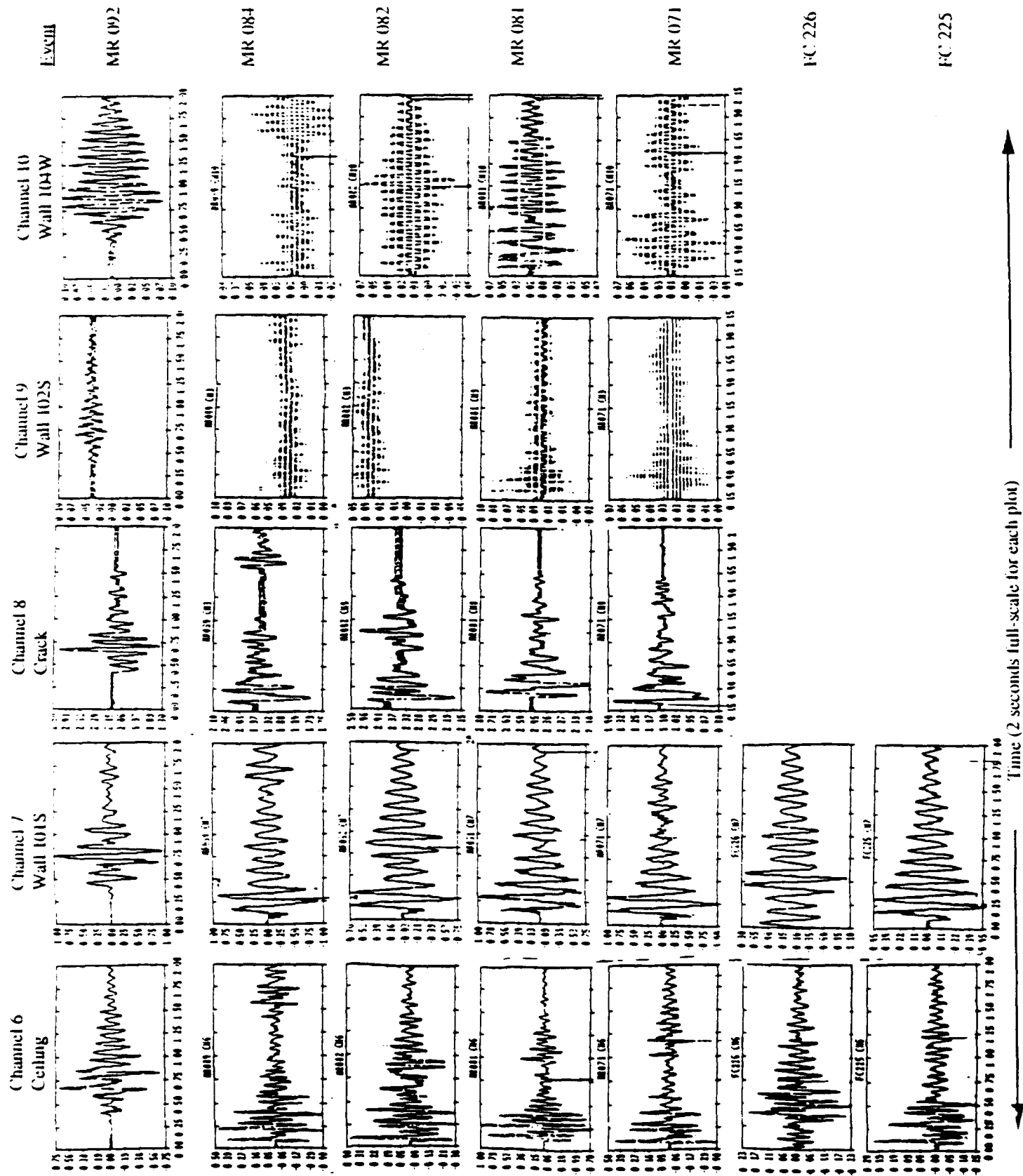


Figure E-3a. Matrix of Time History of Sonic Boom Pressure and Structural Response for Events at Structure A



Time (2 seconds full-scale for each plot)

Figure E-3b. Matrix of Time History of Sonic Boom Pressure and Structural Response for Events at Structure A

EXCIII

AP 051

AP 053

MR 302

AP 052

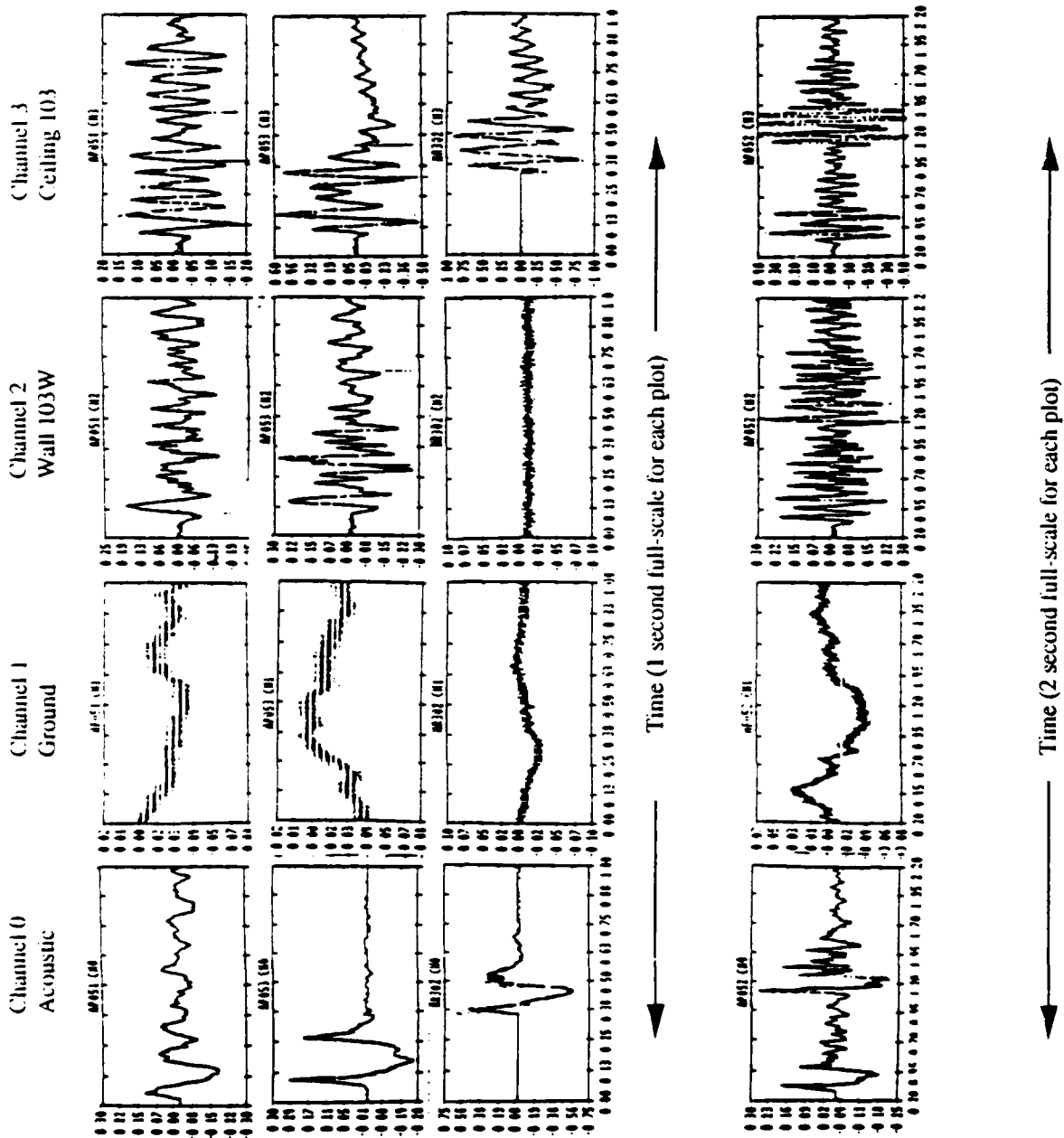


Figure E-4a. Matrix of Time History of Sonic Boom Pressure and Structural Response for Events at Structure B

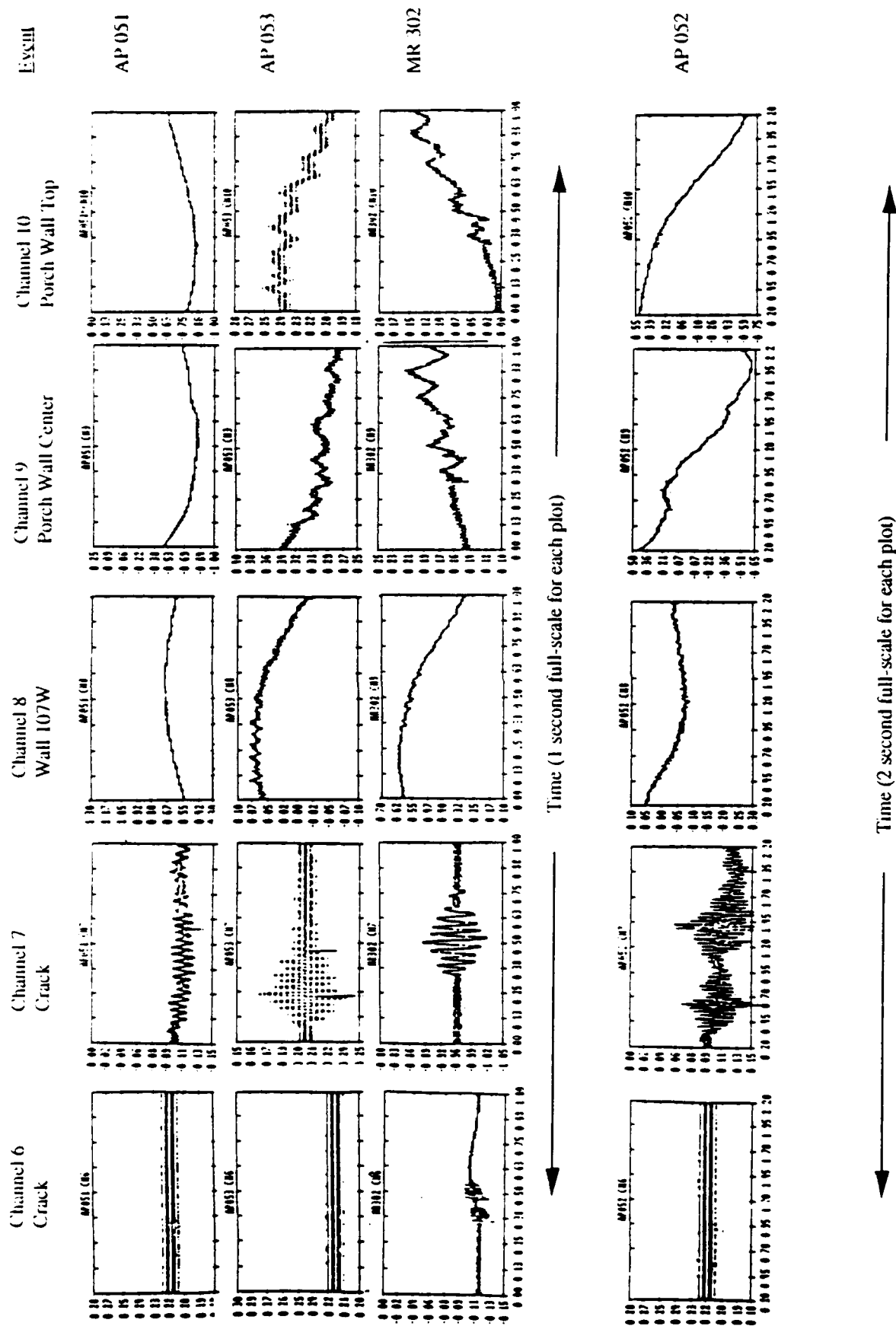


Figure E-4b. Matrix of Time History of Sonic Boom Pressure and Structural Response for Events at Structure B

Appendix F

Compilation of Weather Data from White Sands Missile Range (Zurf Site)* for the
Period of February 20, 1989 to April 12, 1989

Date	Time	Temp (°F)	RH (%)	Wind Speed (kts)	Date	Time	Temp (°F)	RH (%)	Wind Speed (kts)
2-20	0000	35	41	3	3-3	0000	49	18	12
	0600	34	42	7		0600	41	26	10
	1200	55	16	20		1200	57	16	22
	1800	52	17	16		1800	52	17	15
2-21	0000	34	21	4	3-4	0000	32	60	4
	0600	27	23	9		0600	30	59	9
	1200	49	18	15		1200	31	24	18
	1800	53	17	8		1800	37	20	5
2-22	0000	28	22	5	3-5	0000	22	31	5
	0600	16	34	3		0600	21	47	3
	1200	54	17	3		1200	39	20	4
	1800	60	15	0		1800	46	18	3
2-23	0000	30	22	7	3-6	0000	21	29	5
	0600	22	26	7		0600	15	42	52
	1200	60	16	8		1200	50	18	6
	1800	63	15	9		1800	57	16	5
2-24	0000	35	21	8	3-7	0000	29	22	6
	0600	26	23	6		0600	25	24	7
	1200	66	14	2		1200	62	15	3
	1800	69	14	5		1800	64	15	13
2-25	0000	36	20	7	3-8	0000	43	19	4
	0600	32	22	6		0600	31	22	7
	1200	70	14	4		1200	71	13	2
	1800	71	13	6		1800	76	12	1
2-26	0000	39	20	5	3-9	0000	41	19	7
	0600	32	21	7		0600	33	21	2
	1200	70	13	5		1200	76	12	4
	1800	73	13	12		1800	79	12	5
2-27	0000	50	18	2	3-10	0000	43	19	8
	0600	47	18	4		0600	35	21	6
	1200	66	14	24		1200	77	12	7
	1800	65	14	18		1800	80	12	1
2-28	0000	44	19	11	3-11	0000	42	19	6
	0600	28	22	2		0600	36	20	7
	1200	59	16	3		1200	79	12	2
	1800	61	15	13		1800	78	12	4
3-1	0000	36	20	2	3-12	0000	46	18	5
	0600	32	21	5		0600	35	21	6
	1200	64	15	6		1200	79	12	4
	1800	64	15	6		1800	79	12	10
3-2	0000	41	19	1					
	0600	26	23	3					
	1200	58	16	14					
	1800	58	16	7					

* Weather site located 8 miles northwest of
Structure A (see Figure 5-2)

Appendix F (Continued)

Date	Time	Temp (°F)	RH (%)	Wind Speed (kts)	Date	Time	Temp (°F)	RH (%)	Wind Speed (kts)
3-13	0000	53	17	6	3-25	0000	44	19	3
	0600	39	20	2		0600	30	22	5
	1200	74	12	10		1200	69	14	5
	1800	74	13	18		1800	70	13	10
3-14	0000	53	17	5	3-26	0000	43	19	1
	0600	36	20	7		0600	43	19	8
3-15	0600	28	22	6		1200	66	14	20
	1200	68	14	3		1800	57	16	19
	1800	70	14	8	3-27	0000	47	18	6
	0000	44	19	6		0600	42	54	4
3-16	0600	31	21	7		1200	56	19	4
	1200	71	13	9		1800	56	17	5
	1800	73	13	12	3-28	0000	34	52	4
	0000	44	19	6		0600	26	56	2
3-17	0600	40	20	4		1200	64	15	13
	1200	74	13	10		1800	69	14	8
	1800	76	12	12	3-29	0000	41	19	5
	0000	47	18	8		0600	33	21	4
3-18	0600	33	21	7		1200	72	13	4
	1200	75	13	4		1800	75	13	9
	1800	75	12	10	3-30	0000	54	17	5
	0000	51	17	4		0600	35	22	8
3-19	0600	34	21	7		1200	66	14	6
	1200	73	13	8		1800	73	13	11
	1800	74	13	12	3-31	0000	44	19	8
	0000	60	16	12		0600	38	20	15
3-20	0600	40	19	3		1200	66	14	5
	1200	63	15	6		1800	70	14	12
	1800	45	21	21	4-1	0000	44	19	2
	0000	27	38	19		0600	32	21	4
3-21	0600	23	51	10		1200	75	13	10
	1200	43	20	6		1800	74	13	20
	1800	54	17	2	4-2	0000	54	17	8
	0000	27	47	1		0600	32	21	3
3-22	0600	21	53	6		1200	71	13	5
	1200	60	15	5		1800	76	12	14
	1800	66	14	12	4-3	0000	63	15	15
	0000	47	18	6		0600	54	17	5
3-23	0600	28	25	6		1200	74	13	11
	1200	70	14	8		1800	77	12	14
	1800	69	14	12	4-4	0000	48	18	4
	0000	48	18	7		0600	36	20	7
3-24	0600	29	22	2		1200	70	13	11
	1200	70	13	3		1800	74	13	8
	1800	71	13	7	4-5	0000	53	17	9
						0600	36	20	4
						1200	68	14	7
						1800	75	12	4

Appendix F (Continued)

Date	Time	Temp (°F)	RH (%)	Wind Speed (kts)
4-6	0000	48	18	7
	0600	34	21	4
	1200	75	13	18
	1800	80	12	12
4-7	0000	52	17	5
	0600	34	21	1
	1200	79	12	9
	1800	85	10	12
4-8	0000	49	18	3
	0600	37	20	6
	1200	81	11	9
	1800	86	10	7
4-9	0000	54	17	6
	0600	48	18	5
	1200	83	11	5
	1800	78	12	15
4-10	0000	52	17	12
	0600	30	22	23
	1200	52	17	6
	1800	56	16	17
4-11	0000	40	20	14
	0600	36	21	9
	1200	61	15	13
	1800	69	14	16
4-12	0000	56	16	17
	0600	42	19	16
	1200	71	13	7
	1800	68	14	13
	1800	73	13	23